THE INFLUENCE OF TIME, ROCK PROPERTIES, AND CLIMATE ON MECHANICAL WEATHERING

by

Monica Rasmussen

A dissertation submitted to the faculty of
The University of North Carolina at Charlotte
in partial fulfillment of the requirements
for the degree of Doctor of Philosophy in
Infrastructure and Environmental Systems

Charlotte

2024

Approved by:

_____
Dr. Martha Cary Eppes

_____
Dr. Russell Keanini

_____
Dr. Brian Magi

_____
Dr. Philip G. Meredith

_____
Dr. Ronald Smelser

ABSTRACT

MONICA RASMUSSEN. The Influence of Time, Rock Properties, and Climate on Mechanical Weathering. (Under the direction of DR. MARTHA CARY EPPES)

Rock weathering, or the mechanical and chemical breakdown of rock over time, creates the landscape on which all terrestrial life is built. Weathering produces sediment, allows the carbon cycle to proceed, and provides a rich soil substrate on which organisms can grow, die, and decompose. The cyclicity of Earth processes is a function of weathering at all scales.

The primary purpose of this Dissertation is to quantify the rates and controls over mechanical weathering [rock cracking/fracturing] of surficial boulder deposits in Eastern California using field data collection, laboratory analysis, and simple mathematical modeling. I collected rock and crack field measurements, clast size distribution data from the field, and rock elastic properties through laboratory testing. I used a chronosequence or space-for-time approach, a method often employed by soil scientists [Jenny, Hans, 1948; Birkeland, Peter W., 1999], whereby data are collected from rocks or sediments that have been exposed to natural weathering conditions for a range of times, using the properties of the stable deposits to represent the amount of weathering that occurs over the time span of exposure. I studied rocks at three sites, within which each site's climate and rock types are the same, but rocks have been deposited starting 148,000 years ago and continuing into the present with active channels and washes.

In the field, I manually measured 8763 crack lengths, widths, and orientations from 2221 *in situ* boulders on Earth's surface. These data were processed in JMP and Excel software, with some interpretation of data performed using Python and MATLAB. In Chapter 2, the data show that rock cracking is initially fastest when rocks are exposed to Earth's surface conditions and begin to weather, with rocks accumulating

cracks at a rate of 9-1502 mm of cracks per m^2 rock surface over a thousand years, or 0.1-36 individual cracks per m^2 rock surface over a thousand years. After this point, rocks continue to crack, but the rate of crack growth slows down. After about 30,000 years [30 ka], the growth rate is <36 mm of cracks/m^2 of rock surface per ka, or <1 individual cracks/m^2 of rock surface per ka. From two of these sites, I also collected a single granitic boulder from each dated deposit, and performed standard rock mechanics testing [Chapter 3]. These data show that rock compliance increases over time while mechanical weathering leads to an increase in microscale cracks, which do not lead to the rock breaking into pieces, but effectively alter its strength and elastic strain response under stress.

Using the laboratory analyses and local weather station data, I implemented a simple daily stress model that uses Paris' law of subcritical crack growth to predict single crack growth after each day of weather conditions. I extrapolated the weather data out to 5000 years to determine whether this simple model can predict the cracking observed in the field. The magnitude of cracking itself was the slowest at the coolest, semi-arid site, then was faster at the two warmer sites to the south. Cracking occurred over only a limited number of unusually intense weather days [Ch. 4] when the daily range of air temperatures [air temperature flux] was the largest. In the two semi-arid sites, these cracking days were hot, dry summer days; in the arid site, the day when the most crack growth was predicted coincided with summer monsoonal rains. The model is highly sensitive to rock elastic properties, which supports the theory that a gradual increase in bulk compliance [Ch. 3] allows rocks to withstand stress without cracking over thousands of years [Ch. 2].

To better understand the drivers of cracking I performed statistical comparisons among rock and crack field data [Ch. 5], and determined that age itself has the most consistent, positive, statistically significant correlation with the number of fractures per rock surface area [fracture number density] and the total length of fractures

measured per rock surface area [fracture intensity]. This suggests that counting cracks on rocks is another simple and reliable metric for relative age dating in the field. Other factors like lichen growth and varnish development increased with rock exposure age and generally acted to infill and decrease the number or length of measurable cracks on the rock. Lithology was also an important factor, but even with this large dataset, more advanced bulk rock modeling and/or more precise compositional and grain size data than the categorical indices employed herein, are required.

Finally, I present clast size data to show that rocks decrease in overall size with time, and that the fastest cracking upon initial exposure [Ch. 2] corresponds with the abrupt increase in small clasts that has long been recognized in the context of the development of desert pavements. For volcanic and carbonate rocks, there is a correlation between the geometry of cracking observed on the rocks and the shape of sediments on older deposits: when many cracks are parallel to the rock surface, older deposits tend to have more flattened rocks on them. This shows that cracking rates and crack geometries can play a strong role in clast size and shape evolution over geologic time, and mechanical weathering should be considered when interpreting sediments in the geologic record.

Overall, I find that rock cracking rates decrease over time [Ch. 2], during which time rock mechanical properties like porosity and permeability increase, and rock density, strength, and Young's modulus [incompressibility] decrease [Ch. 3]. These findings are directly applicable to geoscientists attempting to understand sediment production from larger pieces of rock, and help constrain the geochemical reaction rates that drive the carbon cycle. Rock fall and landslide hazards can also be better assessed through this understanding of progressive rock cracking, its controls, and its environmental drivers.

More broadly, the decreasing rock cracking rates that accompany slow mechanical property changes represent a real-world example of material fatigue vs. material

failure. Engineers and geologists concerned about present-day Earth conditions must understand that what they see now is not necessarily what exists underground, and that rock properties are evolving over timescales beyond direct human observation. As geologists commonly employ a uniformitarianism approach [Hutton, James, 1899] whereby what we see happening now is presumably representative of what has happened in the past, it is critical that all geologists understand how dramatically rock physical properties can change once the rock reaches the Critical Zone. This Dissertation offers an analysis of the slow, but critical, process of Earth surface mechanical evolution.

DEDICATION

For my friends and family and their endless support, and willingness to feign interest in geology (and providing access to their pool). For the Coffee House in Antarctica (RIP) where I met a fellow kooky geologist – and for Missy, who encourages my wild ideas and bold moves. And of course, for my husband Warren, the #1 rock in my life.

ACKNOWLEDGEMENTS

I would never have even applied for graduate school if not for the never-ending support of my husband Warren, the long-time mentorship and encouragement of Dr. Scotty Mildren, and the enthusiasm and hard work of Dr. Missy Eppes. Missy has been a constant source of inspiration, energy, and conversation, and I've delighted in our times discussing rocks, cracks, and life.

My committee was instrumental in the conceptualization and execution of this Dissertation, and I owe all of you more credit than I can give. Dr. Keanini has provided me a wonderful outlet for my wacky physics ideas, and somehow translates them into meaningful and sound models. Russ is also one of the kindest and most supportive mentors I have ever met. Dr. Magi has greatly assisted with my ability to code and understand statistics, and Dr. Smelser effectively gave me a frenzied and long-overdue proper introduction to linear elasticity, and the engineering research behind it. Finally, Dr. Meredith has always been able to take the swirling ideas I have in my mind and distill them into a simple, elegant sentence that ties it all together. Phil, your understanding of rock physics has helped bring together so many concepts for me, and I cannot thank you enough for hosting me in London, providing your continued mentorship, and serving on this committee post-retirement.

This Dissertation was funded in part by the UNC Charlotte Graduate School, UNC Charlotte Graduate and Professional Student Government, the UNC Charlotte departments of Geography and Earth Sciences, and Infrastructure and Environmental Systems, the National Science Foundation, the Israel Binational Science Foundation, the American Geophysical Union EPSP Division, the Geological Society of America including the Southeastern Section and the QG&G Division, and the U.S. National Committee for Quaternary Research at the National Academy of Sciences. Thank you to the indigenous landowners of North Carolina and California for allowing us to perform scientific work on your lands.

I must thank the UNC Charlotte Center for Graduate Life and Learning for their support, inspiration, and free coffee; the Mono Committee for housing and technical support; the Sweeney Granite Mountains Desert Research Center for housing and technical support, and specifically Jim and Tasha for turning a research base into a home; and the University College London Rock and Ice Physics Laboratory. Dr. Tom Mitchell provided amazing laboratory support and training, and Jim Davy and Karin Hofer Apostolidis were the best lab mates I could ask for. Dr. Nicolas Brantut put up with me using his space and equipment and kindly showed me the art of affixing strain gauges. Dr. Amit Mushkin and Dr. Uri Shaanan brought me into the Negev Desert in Israel for a magical geological adventure which I will never forget. The Bureau of Land Management, Inyo Forest Service, and Mojave National Park provided permitting, direction, and technical support.

I must thank my field assistants Warren Baker and Samantha Berberich for carrying heavy things, maintaining a good attitude despite multiple years of record-breaking heat, and supporting my dogged approach to field work. Dr. Alex Rinehart and the entire 'Crackergentsia' provided the perfect sounding board for explaining ideas to a critical audience, and always went above and beyond to share ideas, encouragement, and journal articles. Anne Voigtländer has always and continues to blow my mind with her insights into the fundamental physics of rocks, and I cherish our insightful conversations. I hope we all continue this collaboration in the future.

Finally, thank you to Dr. Providence Adu for unintentionally competing with me to finish our PhDs, Patrick Webb for helping with data analysis and allowing me to turn him into a rock cracking enthusiast, Dr. Jenn Aldred for the warm friendship and guidance and donuts, and the CZ+ reading group for pulling me away from cracking to think about the world around us. And thanks to you, for reading this; without an audience, my tireless efforts would be meaningless.

TABLE OF CONTENTS

LIST OF TABLES

LIST OF FIGURES

LIST OF SYMBOLS

α	thermal expansion differential between mineral grains, $^{\circ}C^{-1}$
ϵ	strain, MPa
κ	permeability
ν	Poisson's ratio
Φ	porosity, %
ρ	density, grams/centimeter^2
σ	stress, MPa
^{10}Be	beryllium-10 radioactive dating
^{14}C	carbon-14 radioactive dating
AE	acoustic emissions
A	Paris' law equivalent of the Charles' Law C parameter
a	crack length
CIA	Chemical Index of Alteration
CIW	Chemical Index of Weathering
C	Charles' Law C parameter
d_g	grain diameter
dT	diurnal temperature change, °C
E	Young's modulus, GPa
GD	granular disintegration/disaggregation

$IRPL$ Infrared Photoluminescence dating

$IRSL$ Infrared Stimulated Luminescence dating

K_{IC} mode-I fracture toughness

K_I mode-I stress intensity

ka age date in thousands of years

kyr time interval in thousands of years

MAP mean annual precipitation, mm

MAT mean annual temperature, °C

m Paris' law equivalent of the subcritical crack growth index

N number of stress cycles in Paris' law

n subcritical crack growth index

RH relative humidity, %

r grain radius

T_{max} maximum daily air temperature

T_{min} minimum daily air temperature

$Temp$ temperature, °C

T tensile strength, MPa

UCS uniaxial compressive strength, MPa

VP vapor pressure, hPa

Vp compressional [P-wave] velocity, meters/second

Vs shear [S-wave] velocity, meters/second

CHAPTER 1: INTRODUCTION

1.1 Background

Rocks mechanically weather, or crack, due to exposure to the sun and wind, tectonic and gravitational forces, the freezing of water, biological activity, impacts with other objects, and expansion and contraction due to chemical reactions. Chemical and mechanical weathering are often studied separately but proceed in tandem and are interdependent. Mechanical weathering exposes fresh surfaces on which chemical weathering can begin anew [Brantley, Susan L., Evans, Brian, Hickman, Stephen H. and Crerar, David A., 1990; Riebe, Clifford S., Kirchner, James W. and Finkel, Robert C., 2003]. Chemical weathering changes the chemical composition and porosity of rocks through mineral alteration, leaching, and reprecipitation; all of which, in turn, alter the rock's mechanical properties [resistance to cracking] and can alter the stress distribution within the rock [Laubach, Stephen E., Lander, R. H., Criscenti, Louise J., Anovitz, Lawrence M., Urai, J. L., Pollyea, R. M., Hooker, John N., Narr, Wayne, Evans, Mark A. and Kerisit, Sebastien N., 2019].

Many geologic processes predicated on rock cracking proceed far too slowly to be directly observed, so researchers [e.g., Atkinson, Barry Kean, 1982; Nara, Yoshitaka, Yamanaka, Hiroshi, Oe, Yuma and Kaneko, Katsuhiko, 2013] have turned to theoretical and laboratory methods to understand cracking processes overall. Classical fracture mechanics theory considers the "strength" of an elastic object [rock] to be the stress load at which the object critically fails [cracks] in compression [compressive strength] or tension [tensile strength] [Griffith, Alan Arnold, 1921]. Cracking is often conceptualized as a large force being applied which exceeds this critical strength, causing a rock to break apart nearly instantaneously.

However, Charles, R. J. [1958] showed that an elastic object under low but persistent stress can slowly crack through subcritical cracking [i.e., cracking can proceed when the stress at the crack tip is lower than the object's critical tensile strength]. Subcritical cracking also occurs under low-stress cyclic loading [Paris, P. C. and Erdogan, Fazil, 1963]. Modeling [Eppes, Martha-Cary and Keanini, Russell, 2017] has shown that subcritical cracking can occur in response to low stress magnitudes that rocks can encounter under a large range of Earth surface conditions. Subcritical rock cracking at Earth's surface may therefore be far more ubiquitous than previously considered.

Yet, it is vastly understudied. Recent studies [e.g., Moon, S., Perron, J. T., Martel, S. J., Holbrook, W. S. and St. Clair, J., 2017; Riebe, Clifford S., Callahan, Russell P., Granke, Sarah B. M., Carr, Bradley J., Hayes, Jorden L., Schell, Marlie S. and Sklar, Leonard S., 2021; St. Clair, J., Moon, S., Holbrook, W. S., Perron, J. T., Riebe, C. S., Martel, S. J., Carr, B., Harman, C., Singha, K. and Richter, D. deB., 2015] aim to link tectonic stresses to weathering rates, but do not specifically address how slow, low-magnitude tectonic stresses lead to landscape-scale mechanical weathering. Direct analysis of rock cracking itself has been limited to short-term laboratory and field studies [e.g., Eppes, Martha Cary, Magi, Brian, Hallet, Bernard, Delmelle, Eric, Mackenzie-Helnwein, Peter, Warren, Kimberly and Swami, Suraj, 2016; Nara, Yoshitaka, Morimoto, Kazuya, Yoneda, Tetsuro, Hiroyoshi, Naoki and Kaneko, Katsuhiko, 2011] spanning hours to years. Beyond thin section analysis [e.g., Mazurier, Arnaud, Sardini, Paul, Rossi, Ann M., Graham, Robert C., Hellmuth, Karl-Heinz, Parneix, Jean-Claude, Siitari-Kauppi, Marja, Voutilainen, Mikko and Caner, Laurent, 2016] limited to microscale cracks, quantitative knowledge about cracking rates over geologic time in natural settings is generally lacking.

1.2 Cracking mechanisms

Experimental and theoretical work on subcritical single crack growth [e.g., Atkinson, Barry Kean, 1984; Nara, Yoshitaka. Kashiwaya, Koki. Nishida, Yuki and Ii, Toshinori, 2017; Nara, Yoshitaka, Yamanaka, Hiroshi, Oe, Yuma and Kaneko, Katsuhiko, 2013] suggest that four primary factors control mechanical weathering:

1. stress magnitude and orientation,
2. time,
3. material properties, and
4. environmental conditions.

Field study using acoustic emissions as a proxy for crack growth [Eppes, Martha Cary, Magi, Brian, Hallet, Bernard, Delmelle, Eric, Mackenzie-Helnwein, Peter, Warren, Kimberly and Swami, Suraj, 2016] correlated instances of granitic boulder cracking with times of maximum diurnal thermal expansion, while modeling [Eppes, Martha-Cary and Keanini, Russell, 2017] has shown that the low stresses to which rocks are regularly exposed likely require too many cycles for direct human observation of cracking. Further, strain rate is an important factor in a material's mechanical response [e.g., Lajtai, E. Z., Duncan, E. J. Scott and Carter, B. J., 1991], so we do not know whether cracking proceeding over geologic time behaves in accordance with the higher stress and strain rate experimental data we have available.

Multiple studies have recorded crack occurrence and/or orientation on the surface of rocks for understanding the impact of thermal stress [Aldred, Jennifer, Eppes, Martha Cary, Aquino, Kimberly, Deal, Rebecca, Garbini, Jacob,, 2016; Eppes, Martha Cary, McFadden, Leslie D., Wegmann, Karl W. and Scuderi, Louis A., 2010; McFadden, L. D., Eppes, M. C., Gillespie, A. R. and Hallet, B., 2005], fracture spacing [e.g., Dühnforth, Miriam, Anderson, Robert S., Ward, Dylan and Stock, Greg M., 2010],

mechanical weathering rates at a single site [Berberich, Samantha, 2020], engineering properties [e.g., Ündül, Ömer and Tuğrul, Atiye, 2011], and the influences of cracking on erodibility [e.g., Shobe, Charles M., Hancock, Gregory S., Eppes, Martha C. and Small, Eric E., 2017]. However, further evidence is needed to understand the influence of different climates and lithologies on cracking rates over geologic time.

1.2.1 Sources of stress and stress distribution

For rocks lying on Earth's surface, the dominant stresses acting on them are local; that is, the stresses are a function of the conditions of their immediate surroundings. Tectonic stresses within the Earth result from the combination of far-field regional horizontal stresses and gravitational stress perpendicular to the surface of the planet. However, this study will focus mainly on loose clasts not attached to the crust that are $\leq$50 cm maximum diameter, and gravitational stresses will be considered negligible. Therefore, the dominant sources of stress acting on a surficial rock are its external environmental stresses, which can be grouped as

1. thermal,
2. frost weathering,
3. biological, and
4. chemical.

These will define the stress magnitude, which is critical for understanding how our laboratory analysis [higher stress, shorter time] may scale to natural processes [lower stress, longer time].

1.2.1.1 Thermal stress

Thermal radiation from the sun [insolation] is a ubiquitous source of stress for rocks on and near Earth's surface [Aldred, Jennifer, Eppes, Martha Cary, Aquino, Kimberly, Deal, Rebecca, Garbini, Jacob,, 2016; Collins, Brian D. and Stock, Greg

M., 2016; Collins, Brian D., Stock, Greg M., Eppes, Martha-Cary, Lewis, Scott W., Corbett, Skye C. and Smith, Joel B., 2018; Eppes, Martha Cary and Griffing, David, 2010; Eppes, Martha Cary, Magi, Brian, Hallet, Bernard, Delmelle, Eric, Mackenzie-Helnwein, Peter, Warren, Kimberly and Swami, Suraj, 2016; Freire-Lista, David Martín, Fort, Rafael and Varas-Muriel, María José, 2015; Lamp, J. L., Marchant, D. R., Mackay, S. L. and Head, J. W., 2017; Vasile, Mirela and Vespremeanu-Stroe, Alfred, 2017] and other terrestrial bodies [Delbo, Marco, Libourel, Guy, Wilkerson, Justin, Murdoch, Naomi, Michel, Patrick, Ramesh, K. T., Ganino, Clément, Verati, Chrystele and Marchi, Simone, 2014; Eppes, Martha-Cary, Willis, Andrew, Molaro, Jamie, Abernathy, Stephen and Zhou, Beibei, 2015; Molaro, J. L., Hergenrother, C. W., Chesley, S. R., Walsh, K. J., Hanna, R. D., Haberle, C. W., Schwartz, S. R., Ballouz, R. L., Bottke, W. F., Campins, H. J. and Lauretta, D. S., 2020; Tesson, P. A., Conway, S. J., Mangold, N., Ciazela, J., Lewis, S. R. and Mège, D., 2020]. Thermal stresses lead to anisotropic expansion of individual mineral grains [Eppes, Martha-Cary, Willis, Andrew, Molaro, Jamie, Abernathy, Stephen and Zhou, Beibei, 2015; Molaro, Jamie L., Byrne, Shane and Langer, Stephen A., 2015; Vázquez, Patricia, Shushakova, Victoria and Gómez-Heras, Miguel, 2015] as well as bulk rock expansion and contraction due to a radial thermal gradient perpendicular to the outer surface of the rock [e.g., Collins, Brian D. and Stock, Greg M., 2016]. These stresses are generally low and persistent, leading to rock degradation through what is often termed "thermal fatigue", altering the rock's fracture toughness [e.g., Chandler, Mike, Meredith, Philip, Brantut, Nicolas and Crawford, Brian, 2017].

Bulk rock thermal conductivity varies as a function of porosity, mineralogy, albedo, and grain size [Janio de Castro Lima, José and Paraguassú, Antenor Braga, 2004; Vosteen, Hans-Dieter and Schellschmidt, Rüdiger, 2003], with the size of the rock and the rate of heating and cooling controlling the intensity and location of tension induced by variations in the thermal stress field [Gunzburger, Yann and Merrien-Soukatchoff,

Véronique, 2011]. The magnitude of these stresses can be additive, with granular expansion and contraction acting on a grain-boundary scale and bulk expansion and contraction acting on an unconstrained whole-rock scale. Modeling [Eppes, Martha-Cary and Keanini, Russell, 2017] has shown that just daily thermal stresses can lead to grain boundary cracking when repeated daily over geologic timescales. This has not yet been verified in the field.

1.2.1.2 Frost weathering

When pore space is at least 91% saturated and water cannot escape the pores, water that freezes from its liquid to solid form expands 9% volumetrically [Hirschwald, Julius, 1908]. This phase transition can exert up to 207 MPa of pressure on the rock [Tsytovich, Nikolai Aleksandrovich, 1975]. However, this varies with pore geometry and connectivity, and requires that water can saturate the rock, but not escape it. When saturation is below 91% or water can flow in and out of pores, the 9% volumetric expansion during freezing can be accommodated by air, exerting a negligible stress on the surrounding medium [Hirschwald, Julius, 1908].

For clasts resting on Earth's surface, a more prevalent cause of cracking is frost weathering through ice segregation [Walder, Joseph and Hallet, Bernard, 1985]. Ice segregation occurs when local temperatures vacillate just below the freezing temperature of water [-15 to -3 °C] [see summary in Matsuoka, Norikazu and Murton, Julian, 2008]. As ice freezes in a porous medium, the temperature gradient between frozen and unfrozen water causes suction to develop, pulling water towards the freezing zone. The suction itself is estimated to exert a ∼1.2 MPa pressure differential per 1 °C of temperature drop [Matsuoka, Norikazu and Murton, Julian, 2008].

Despite prior research, disentangling the impacts of gradual cracking from daily insolation cycles, sudden thermal shock cracking from lightning or fire, high-stress freeze/thaw cycles, and gradual ice segregation cracking remains difficult, given that in most environments, some or all of these sources of stress act upon rocks over geologic

timescales. Here, I acknowledge this complexity and do not attempt to disentangle the complex drivers of mechanical weathering,

1.2.1.3 Biological stresses

Adding to the stresses from abiotic processes [bulk rock and grain scale expansion and contraction, water phase transitions], all rocks on Earth are exposed to the forces exerted by living things as they move, grow, and consume rocks on the surface and subsurface. Macroscale biological stresses are commonly imposed by plants and trees. Tree root growth varies with microclimate and species, and once roots are emplaced, they exert force on surrounding rock through swelling during water uptake and movement due to wind gusts [e.g., Marshall, Jill A., 2018]. The forces exerted by tree roots have been shown to correlate with diurnal and stochastic weather events through the impact of precipitation on water uptake and vapor pressure deficit on tree respiration. Elasticity of wood and the depth of root penetration vary with plant species and determine how surficial forces translate to subsurface root movement [Jimerson, Cole Robert, 2020]. Jimerson, Cole Robert [2020] suggested that measured tree root forces were capable of instigating subcritical crack growth in rocks, and while the ∼0.5-2 MPa radial pressure exerted by tree roots may be insufficient to crack rocks on its own [Pawlik, Łukasz, Phillips, Jonathan D. and Šamonil, Pavel, 2016], due to the additive nature of stress, these values should not be ignored.

One of the most ubiquitous organisms growing on rocks is lichen. Lichen modify rock surfaces, including crack surfaces through chemical alteration and leaching, and release acids into their environment which can aid in further chemical weathering of the rock. Physically, lichen exert forces through burrowing into existing cracks [Burford, E. P. and Fomina, M. and Gadd, G. M., 2003]. While lichen have been shown to directly weather rocks both physically [e.g., Scarciglia, Fabio, Saporito, Natalina, La Russa, Mauro F., Le Pera, Emilia, Macchione, Maria, Puntillo, Domenico, Crisci, Gino M. and Pezzino, Antonino, 2012] and chemically [e.g., Song, J. F., Ru, J. X.,

Liu, X. P. and Cui, X. Y., 2019], their contribution to cracking is unclear, given that they can also hold cracked rock in place by attaching their filaments to opposing crack faces or can precipitate minerals within and atop rocks [Burford, E. P. and Fomina, M. and Gadd, G. M., 2003], both of which may counteract stresses and in turn make the rock more resistant to weathering. Varnish development on a rock's surface is a microbially-mediated process that occurs from the outside inwards, and can strengthen rock while also enhancing the likelihood of rock cracking [e.g., Lamp, J. L., Marchant, D. R., Mackay, S. L. and Head, J. W., 2017; Thomachot, Céline and Jeannette, Daniel, 2004].

1.2.1.4 Chemical stresses

Chemistry defines mineralogy and thus rock properties, but additionally, chemical processes themselves can exert stresses on the surrounding rock. These processes may be continuous and scale with the availability of a given mineral or may occur episodically under specific conditions.

For example, biotite, a common rock forming mineral, expands during oxidation to exert an anisotropic stress on surrounding minerals which can lead to reaction-induced cracking, and has been proposed as the mechanism by which rounded corestone morphology is created [Buss, Heather L., Sak, Peter B., Webb, Samuel M. and Brantley, Susan L., 2008]. Mineralogical changes can occur through in situ alteration or dissolution and precipitation. The new mineral composition will affect thermal and mechanical properties of the bulk rock, and the reactions themselves exert stress during mineral formation.

During chemical weathering, feldspar hydrolysis can occur as water is incorporated into the new mineral's crystal structure, increasing the grain size. Like the expansive force from mineral precipitation, the new crystal can exert stress on surrounding mineral grains. If non-expansive minerals weather into expansive clays like smectite, they can expand when wetted and contract when dried. Water molecules are elec-

trostatically attracted to the very thin charged layers between clay molecules, and because the spacing between clay layers is so thin, water intrusion can expand the space by as much as 30% during hydration [Scherer, George W., 2006]. This can occur in saturated or humid conditions within continuous, macroscopically layered clay deposits, or within rocks containing small amounts of clay surrounding other mineral grains.

Like clay minerals, salts can shrink and swell and are easily transported in water. In natural settings, salt weathering generally occurs when chlorides and other salts are dissolved in rainwater and transported both onto the surface and into pores in rocks, where the water evaporates and salt precipitates; or solutions become supersaturated as temperature drops, initiating mineral crystallization [Sousa, Luís, Siegesmund, Siegfried and Wedekind, Wanja, 2018]. During the crystallization process, pressure on the pore wall can reach substantial levels. For example, theoretical and experimental studies of crystallization of mirabilite [a sodium sulfate mineral] provide a crystallization stress range between 13-19 MPa at 20 °C [Espinosa-Marzal, Rosa M., Hamilton, Andrea, McNall, Megan, Whitaker, Kathryn and Scherer, George W., 2011; Flatt, Robert J., 2002], well within the range of stresses required to initiate critical tensile cracking.

In the absence of liquid water, salts can still crystallize, hydrate, and dissolve due to variations in humidity, e.g., cracking sandstone during experimental oscillations between 20-98% relative humidity at 20 °C [Sato, Masato and Hattanji, Tsuyoshi, 2018]. Note that, like all chemical processes, the pressure exerted during these processes is highly dependent on temperature and the specific salt composition [Menéndez, Beatriz and Petráňová, 2016]. The impacts of different types of salts can also vary based on their chemical characteristics like solubility and phase change behavior [Warke, P. A., 2007].

1.2.2 Strain response

Regardless of the sources of stress acting on the rock, which likely act in concert, the total stress applied to the rock results in elastic strain. This strain is the ultimate cause of cracking [brittle failure] and is the focus of this Dissertation. The ability for an applied stress to crack a rock [or any elastic body] is a function of

1. the magnitude and the orientation of the stress field;
2. the strength of the material;
3. the speed at which stress is applied [strain rate]; and
4. the temperature, fluid pressure, fluid chemistry, and moisture level of the environment.

The magnitudes of stresses were discussed in previous sections, and the orientations and material strength are discussed below. Strain rate and the influence of temperature and moisture will be discussed in Chapter 4.

Rocks are natural materials which contain some microscopic flaws [cracks and/or pores] as a function of their imperfect formation conditions. Therefore, to understand how rocks crack, we must understand not what initiates a crack, but what causes existing cracks to grow. When the stress acting on a body is resolved in three dimensions, different areas within the body will be subjected to different magnitudes of tensile, shear, and compressive stresses [see Hoek, E. and Martin, C. D., 2014]. Griffith, Alan Arnold [1921] linked the tensile strength T of a material to its ability to absorb strain before it critically fractures in tension [fracture toughness]. If there exists a place in the body where the tensile stress exceeds the tensile strength σ_{T} of the material, the strain [deformation] has exceeded the body's fracture toughness, and it will critically fail through brittle cracking relatively quickly. This is how tensile strength is determined, e.g., through a Brazilian disk test, where a spherical disk is

stressed until tensile failure initiates internally, and the magnitude of stress required for failure is measured to estimate the body's tensile strength [T]. Since T of a material is its weakest strength – compressive strength can be 8-28 times higher than T [e.g., Goodman, Richard E., 1989] – in unconfined bodies like boulders, tensile failure is likely to occur before other modes of failure.

1.3 Griffith's criterion

Once T is established, further experiments can determine the fracture toughness. Fracture toughness is a material property that correlates with tensile strength and can be determined through laboratory experiments [e.g., methods in Meredith, P. G. and Atkinson, B. K., 1985]. Griffith's criterion [Griffith, Alan Arnold, 1921, Eq. 1.1] mathematically relates the tensile strength of a material to the crack length and fracture toughness:

$$T = C * [K_{\mathrm{IC}}/a^{0.5}] \tag{1.1}$$

where T is the tensile strength, C is a geometrical constant, K_{IC} is mode I [tensile] fracture toughness, and a is the crack length or diameter.

Experimentally, an initial flaw with a known length a is created in the material, then a tensile stress is applied to the material and its crack extension is measured. Through multiple iterations of loading and unloading the stress on the sample, and measuring the crack propagation velocity, the fracture toughness can be derived [see review by Ouchterlony, Finn, 1982]. The geometrical constant C is related to lithology and will be discussed regarding Chapter 4.

1.3.1 Faster or slower cracking?

Subcritical crack growth rates are non-linear even if the stress does not change, because longer cracks experience higher stresses at the crack tip, leading to faster cracking as the crack grows [Griffith, Alan Arnold, 1921]. Similarly, under constant

magnitude cyclical stresses, the longer the crack grows, the higher the stress concentrates at its tip, and the faster it grows [Paris, P. C. and Erdogan, Fazil, 1963].

These observations address single-crack behavior, assuming that one crack is growing in an isotropic, intact elastic medium. Yet there are other fracture mechanics theories that are in seeming contrast with the Griffith model of single-crack growth.

When a rock is cracked, its bulk material compliance [Poisson's ratio divided by Young's modulus] increases, which means that a cracked rock can accommodate more strain energy than a solid rock [e.g., Bažant, Zdenek P., Le, Jia-Liang and Salviato, Marco, 2021; Lyakhovsky, Vladimir, Reches, Ze'ev, Weinberger, Ram and Scott, Thurman E., 1997]. By behaving like a sponge, the cracked rock can deform elastically without failing, while the same stress applied to a less compressible rock can cause cracks to propagate in response. This means that instead of the rate of cracking increasing over time as a function of the crack lengthening [Griffith's crack behavior], the cracking rate will decrease over time as a function of enhanced compliance. We do not know which concept dominates - or how these two mechanisms interact - over geologic timescales. By collecting data from rocks that have cracked over thousands of years, this study begins to test the veracity and application of decades of cracking experiments and theoretical models in the context of mechanical weathering.

Subcritical cracking is a reasonable mechanism explaining rock breakdown in nature, yet these stresses lead to extremely slow crack velocities. The intergranular stress model of Eppes, Martha-Cary and Keanini, Russell [2017] estimated that subcritical crack velocities reach a reasonable maximum on Earth's surface at $3\text{x}10^{-11}$ m/s, or just under one mm/year. A simple estimate of crack velocity using the fracture toughness of recently failed granodiorite in the Sierra Nevada [0.7 MPa$\sqrt{m}$; Collins, Brian D. and Stock, Greg M., 2016] and laboratory estimates of long-term cracking rates in stronger granites [Nara, Yoshitaka, Yamanaka, Hiroshi, Oe, Yuma and Kaneko, Katsuhiko, 2013] provide crack velocity estimates of $<10^{-11}$ m/s. These

estimates are likely on the high end of single-process driven cracking, and it is difficult to estimate how the combination of natural stresses with natural heterogeneities will translate these estimates to natural rock cracking rates.

The rate of subcritical crack growth of a single crack in a homogeneous material is most accurately determined through double torsion testing whereby a rock is cut into a simple geometric shape, pre-cracked at a specific location, then a known force is applied to observe tensile propagation of that crack [e.g., work by Nara, Yoshitaka, Yamanaka, Hiroshi, Oe, Yuma and Kaneko, Katsuhiko, 2013]. However, rocks in nature are often irregularly shaped, have multiple pre-existing cracks, and many different forces are applied to them throughout regularly changing environmental conditions. These elements of randomness can cause cracking rates in natural settings to vary from controlled settings, possibly resulting from both single-crack growth acceleration and whole-rock compliance increase. Field-based estimates of cracking rates are extremely limited. Berberich, Samantha [2020] collected cracking data for a chronosequence of granites, and those data will be leveraged in my work. Otherwise, to my knowledge this Dissertation will provide some of the first data testing whether cracking rates calculated in laboratory settings and models are valid in real-world settings.

1.4 Relevance to Earth sciences

The rock property analysis here presents a first-of-its-kind combination of detailed rock physics, rock mechanics, and thermal properties derived in the laboratory; and field measurements of rocks in natural settings. Combining these data will be directly useful for any field geoscientist, because they explain how the properties of rocks at the surface may not represent the current state of rocks at depth.

Subsurface models depend on rock properties derived at Earth's surface, and these are often derived from quarried rocks, like the infamous Carrara marble and Westerly granite. Yet the data presented here show that the properties of these rocks can

change dramatically within a few thousand years of exposure to environmental conditions. In geology, this rate is remarkably rapid, and just this knowledge may greatly alter how surface rocks are used to interpret and model their subsurface counterparts.

Landscapes evolve through erosion and deposition. Erosion is constrained by the material properties of rocks and soils, which are not static, because rocks are altered through chemical and mechanical weathering. A fundamental understanding of cracking processes is lacking in most geomorphology literature, and may explain why lithology [as defined by a geologist] does not necessarily explain erosion rate [Young, Holly H. and Hilley, George E., 2018], why chemical weathering does not proceed at rates predicted in laboratory settings [Riebe, Clifford S., Kirchner, James W. and Finkel, Robert C., 2004], or what causes the "intangible fatigue effect" observed during laboratory and field experiments on rock weathering [Warke, P. A., 2007, , p. 46].

Irregular weathering rates have puzzled planetary geologists observing crack-related features like surface roughness on lunar craters, but they have not necessarily attributed these to changes in rock cracking rates [Wang, Juntao, Kreslavsky, Mikhail A., Liu, Jianzhong, Head, James W., Zhang, Ke, Kolenkina, Maria M. and Zhang, Li, 2020]. Instead, they do not provide any specific constraints on how quickly these features form. In the case of Martian geology, fractures are recognized, but only used to delineate mapping units [Apuzzo, A., Frigeri, A., Salvini, F., Brossier, J., De Sanctis, M. C, Schmidt, G. W. and Ma MISS Team, 2022], and their rate and mode of formation has not been studied. Studies of clast size degradation over time at Earth's surface simply consider the residence time in the "weathering zone" to scale with clast size degradation [Neely, Alexander B. and DiBiase, Roman A., 2020]. The field measurements in this Dissertation provide a necessary link among geomorphology, fracture mechanics, material science, planetary geology, and structural geology.

Given that cracking may be the main mechanism by which fresh rock is supplied for

chemical weathering [e.g., Baynes, J. and Dearman, W, 1978], chemical weathering rates can be improved with better estimates of mechanical weathering rates. Since erosion and sediment production start with cracking, we cannot fully understand how lithology regulates landscape evolution until we understand the controls of material properties, and time, on cracking.

While erosion rates are important for understanding landscape evolution, cosmogenic dating is used widely in Quaternary geology, and unknowns in erosion rates can lead to systematic underestimation of cosmogenic dating uncertainty [Phillips, Fred M. and Argento, David C. and Balco, Greg and Caffee, Marc W. and Clem, John and Dunai, Tibor J. and Finkel, Robert and Goehring, Brent and Gosse, John C. and Hudson, Adam M. and Jull, A. J. Timothy and Kelly, Meredith A. and Kurz, Mark and Lal, Devendra and Lifton, Nathaniel and Marrero, Shasta M. and Nishiizumi, Kunihiko and Reedy, Robert C. and Schaefer, Joerg and Stone, John O. H., 2016]. One case study by Kelly, Meredith A., Lowell, Thomas V., Applegate, Patrick J., Phillips, Fred M., Schaefer, Joerg M., Smith, Colby A., Kim, Hanul, Leonard, Katherine C. and Hudson, Adam M. [2015] showed that erosion rates between boulders on one surface could be anywhere between $1x10^{-4}$ to $5x10^{-4}$ cm/year, and that these values are minimum erosion rates that are only due to subaerial erosion [Kelly, Meredith A., Lowell, Thomas V., Applegate, Patrick J., Phillips, Fred M., Schaefer, Joerg M., Smith, Colby A., Kim, Hanul, Leonard, Katherine C. and Hudson, Adam M., 2015]. Their mathematical erosion rate corrections were performed on a per-rock basis.

During most cosmogenic nuclide calculations, an average erosion rate is assumed for a surface, as chosen by the researcher. Numerical modeling for ages <100 ka suggests that climate variations in, e.g., moraine settings can lead to significant variation in erosion rates and therefore rock exposure [Madoff, Risa D. and Putkonen, Jaakko, 2016]. The erosion of grains or large pieces of rock from the boulder surface [due to

cracks propagating through the rock] is not considered.

Finally, and certainly broadly applicable for Earth surface processes, mean climate [mean annual temperature, precipitation] values are the standard representatives for "environmental conditions", yet surface process models depend on both slow and punctuated events. The debate between the importance of long-term climate vs. short-term weather is ongoing, and Chapter 4 will show the impact of these two approaches on rock cracking. The weather/climate analysis here will aid in our understanding of the importance of climate change, and the potential implications for geologic hazards, hydrology, river erosion, sediment production, and natural CO_2 sequestration.

1.5 Dissertation goals

This Dissertation uses field data, laboratory analysis, and single-crack modeling to address three critical drivers of mechanical weathering:

1. Time: understanding whether cracking rates increase, decrease, or remain constant over timescales of 10^3 to 10^5 years. This is primarily addressed in Chapter 2, and rock properties changing over time are presented and investigated in Chapter 3.

2. Rock properties: assessing the sensitivity of trends to different rock types. This is addressed in Chapters 3, 5, and 6.

3. Climate: quantifying the impact of different climatic variables [vapor pressure, temperature] on rock cracking behavior. This is addressed in Chapter 4.

CHAPTER 2: WHAT DOESN'T BREAK ROCK MAKES IT TOUGHER

AUTHORS:

Monica Rasmussen, Martha Cary Eppes, Amit Mushkin, Philip G. Meredith, Thomas M. Mitchell, Yang Yuan, Russell Keanini, Jennifer Aldred, Pavao Andričević, Samantha Berberich, Maxwell P. Dahlquist, Sarah Evans, Mayank Jain, Mehdi Morovati, Anthony Layzell, Yoshitaka Nara, Alex Rinehart, Elaine Sellwood, Uri Shaanan

2.1 Abstract

Rock fracturing drives and limits the evolution of Earth's topography, the global carbon cycle, geologic hazards, and the stability of the built environment. Yet there remains a paucity of constraints on long-term fracturing behavior. Here we use field observations to show that fracturing rates in natural surface rocks decrease exponentially over time. We present experimentally-derived Young's modulus measurements showing that these results are consistent with rock mechanics experimental data and theory linking progressive fracturing to decreasing brittle strain response to stress. We characterize fracture evolution over periods of $1-100$ kyr for three different field sites and three rock types. For rocks with less than 5 kyr of exposure, fractures grow at rates on the order of 10^1-10^2 mm/kyr, then after $10-15$ kyr, fractures grow by less than 2 mm/kyr. Over similar timescales, the 'appearance' of visible fractures also decreases, dropping from 36 new fractures per m^2/kyr to < 2 per m^2/kyr. We independently document similar fracturing deceleration trends using microfracture analyses, plus a novel application of infrared photoluminescence [IRPL] dating for three in situ fractures in a single clast. Our results contrast significantly with current landscape-scale conceptual models that assume fracturing rates and characteristics

are invariant over time and are controlled by short term rock strength and external stress magnitudes alone. Instead, our findings indicate that, over geologic time, rock's fracturing increases its toughness.

2.2 Introduction

Rock fractures are ubiquitous on Earth [Eppes, Martha Cary and Griffing, David, 2010; Lamp, J. L., Marchant, D. R., Mackay, S. L. and Head, J. W., 2017] and other terrestrial bodies [Eppes, Martha-Cary, Willis, Andrew, Molaro, Jamie, Abernathy, Stephen and Zhou, Beibei, 2015], and fracturing is the most pervasive deformation mechanism in Earth's upper crust[Gudmundsson, Agust and Brenner, Sonja L., 2001]. Fractures control rock strength and erodibility [DiBiase, Roman A., Rossi, Matthew W. and Neely, Alexander B., 2018], so fracturing contributes to the pace of volcanism [Caricchi, Luca, Townsend, Meredith, Rivalta, Eleonora and Namiki, Atsuko, 2021], rockfalls and landslides [Collins, Brian D. and Stock, Greg M., 2016], soil production [Heimsath, Arjun M., Dietrich, William E., Nishiizumi, Kunihiko and Finkel, Robert C., 1997], anthropogenically induced earthquakes [Kang, Jian-Qi, Zhu, Jian-Bo and Zhao, Jian, 2019], and building stone decay [Viles, Heather A., 2005]. Rock fracturing increases water infiltration, impacting feedbacks between erosion and weathering rates [Brantley, S. L., Shaughnessy, Andrew, Lebedeva, Marina I. and Balashov, Victor N., 2023], hydrology and drought tolerance of trees [Klos, P. Zion, Goulden, Michael L., Riebe, Clifford S., Tague, Christina L., O'Geen, A. Toby, Flinchum, Brady A., Safeeq, Mohammad, Conklin, Martha H., Hart, Stephen C., Berhe, Asmeret Asefaw, Hartsough, Peter C., Holbrook, W. Steven and Bales, Roger C., 2018], nutrient availability [Goodfellow, Bradley W., Hilley, George E., Webb, Samuel M., Sklar, Leonard S., Moon, Seulgi and Olson, Christopher A., 2016], and carbon sequestration [Penman, Donald E., Caves Rugenstein, Jeremy K., Ibarra, Daniel E. and Winnick, Matthew J., 2020]. Drawing clear linkages between rock fracture and these processes requires a full understanding of the factors that control fracturing rates themselves.

Rock fracturing comprises the brittle accommodation of a rock mass to stress. Fracture mechanics dictates that fractures commonly propagate under stresses much lower than their short-term strength due to chemo-physical feedbacks in the damage zone, in a process known as subcritical cracking. Field data [Shaanan, Uri, Mushkin, Amit, Rasmussen, Monica, Sagy, Amir, Meredith, Philip, Nara, Yoshitaka, Keanini, Russell and Eppes, Martha-Cary, 2023] and modeling [Eppes, Martha-Cary and Keanini, Russell, 2017] suggest that subcritical cracking is a fundamental mechanism of progressive fracturing at and near [$<$ 500 m] Earth's surface. As with all fracturing, rock subcritical cracking rates are dependent upon external stress-loading magnitude and on environment, which can influence fracture tip chemo-physical processes [Atkinson, Barry Kean and Meredith, Philip George, 1981].

Subcritical cracking rates are also, however, strongly dependent on fracture geometry. Experimental and theoretical rock mechanics data provide well-established descriptions of different internal feedbacks between subcritical cracking and time-dependent rock behavior [Atkinson, Barry Kean and Meredith, Philip George, 1981]. A single fracture under active loading that is accommodating a majority of the stresses within a rock accelerates as it lengthens due to enhanced stress concentration at the fracture tip [Charles, R. J., 1958]. Conversely, if multiple fractures accommodate stresses by lengthening simultaneously, this can result in an increase in rock 'toughness', that is, its ability to absorb energy without further fracture. This reduction in stiffness is accompanied by a reduction in stress intensity experienced throughout the rock mass, and thus an overall deceleration in the aggregate subcritical cracking rate for a given stress magnitude [Brantut, Nicolas and Baud, Patrick and Heap, M. J. and Meredith, P. G., 2012]. Fractures interact and accommodate stresses to the point where, even under constant stress, the rate of fracturing slows down as rock compliance increases.

Despite ample laboratory and experimental data exposing both of these contrary

short-term behaviors, most landscape-scale conceptual and numerical models of fracture dependent geologic processes either explicitly or implicitly assume that brittle damage over geologic time accelerates or remains constant; and that short-term rock failure strength is the primary control on fracturing, leading to 'triggering' of catastrophic failure by large external stresses.

Practical constraints preclude experimental testing of realistic, complex long-term scenarios that could challenge these assumptions. Thus, field data for in situ rock fracturing rates over geologic timescales never before collected are required to reconcile experimental and theoretical observations with those of complex natural systems.

2.2.1 Methods and site selection

Here we document decelerating natural rock fracturing over timescales of 10^3-10^4 years. Three study sites in eastern California, USA span different climatic conditions [Table 2.1. Fig. 2.1A] and contain granitoid, volcanic and/or carbonate [Fig. 2.1B] rock types. The sites were previously mapped [Rood, Dylan H., Burbank, Douglas W. and Finkel, Robert C., 2011; D'Arcy, Mitch. Roda Boluda, Duna C.. Whittaker, Alexander C. and Carpineti, Alfredo, 2015; Dühnforth, Miriam, Anderson, Robert S., Ward, Dylan and Stock, Greg M., 2010; Blisniuk, Kimberly Diem Chi, 2011; McDonald, Eric V., McFadden, Leslie D., Wells, Stephen G., Enzel, Y. and Lancaster, N., 2003; Wang, Yang, McDonald, Eric, Amundson, Ronald, McFadden, Leslie and Chadwick, Oliver, 1996; Stone, Paul, Miller, David M., Stevens, Calvin H., Rosario, Jose, Vazquez, Jorge A., Wan, Elmira, Priest, Susan S. and Valin, Zenon C., 2017] and dated using ^{10}Be [Rood, Dylan H., Burbank, Douglas W. and Finkel, Robert C., 2011; D'Arcy, Mitch. Roda Boluda, Duna C.. Whittaker, Alexander C. and Carpineti, Alfredo, 2015; Blisniuk, Kimberly Diem Chi, 2011; Dühnforth, Miriam, Anderson, Robert S., Ward, Dylan and Stock, Greg M., 2010], ^{14}C and IRSL [McDonald, Eric V., McFadden, Leslie D., Wells, Stephen G., Enzel, Y. and Lancaster, N., 2003], as well as surface geomorphological and soil development features. In the field, the

location of specific dated boulders and soils were located, and data collection sites were selected based on surface continuity, geomorphological character relative to the mapped surface descriptions, and availability of appropriately sized clasts.

To best isolate time as the primary controlling variable on fracturing, we minimized variations in erosion, external environment, and stresses between individual rock exposures by making measurements on subaerially exposed loose clasts [15 - 50 cm diameter; Fig. 2.2; Methods]. This size range is large enough to ensure stability on the low-sloping [$< 5°$] surfaces, but small enough that a statistically significant number of clasts could be sampled in full. Fracture propagation in the observed rocks is inferred to have been primarily driven by low-magnitude thermal stresses based on past work and field data [crack orientation example in Fig. 2.3], and we assume that other factors that might have contributed to these stresses [climate, biota, surface stability] do not vary within the relatively small geographical area and consistent elevation [Table 2.1] of each study site.

Following the pioneering work of Shaanan, Uri, Mushkin, Amit, Rasmussen, Monica, Sagy, Amir, Meredith, Philip, Nara, Yoshitaka, Keanini, Russell and Eppes, Martha-Cary [2023] we apply a 'space for time' [chronosequence] approach and assume each clast's exposure age correlates with the age of the depositional surface on which it is found [Birkeland, Peter W., 1999]. For the purposes of this macrofracture analysis, we first analyzed clasts found within dry, ephemeral channels or flowing modern stream channels [Figs. 2.1B; 2.2]. These clasts experience periodic removal of any preexisting major fractures or heterogeneities through saltation, tumbling, and abrasion within the active channels [Olsen, Telemak, Borella, Josh and Stahl, Timothy, 2020]. Given that the abandoned surfaces which frequently contain m-scale boulders were formed through high-energy alluvial and glacial outwash deposits, the modern creek clasts provide the baseline of relatively fracture-free rocks, hereafter 'time 0'. Older, abandoned geologic surfaces of known depositional age [Rood, Dylan

H., Burbank, Douglas W. and Finkel, Robert C., 2011; D'Arcy, Mitch. Roda Boluda, Duna C.. Whittaker, Alexander C. and Carpineti, Alfredo, 2015; McDonald, Eric V., McFadden, Leslie D., Wells, Stephen G., Enzel, Y. and Lancaster, N., 2003] [Fig. 2.4] provide numerous 'snapshots' of fracturing after varying years of exposure.

To study fracture evolution since clast deposition, we measured all visible $\geq$20 mm long open, planar discontinuities [hereafter fractures] in 50 - 150 randomly selected clasts on each geologic surface. To ensure a statistically representative number of fractures for each surface, we collected data until the dataset exhibited a statistically significant power-law distribution - a recognized inherent feature of fracture sets. We report three statistical metrics of fracturing averaged for each studied surface:

1. number density [total numbers of fractures per area; $\#/m^2$],
2. fracture intensity [sum length of all fractures per area; mm/m^2], and
3. maximum-length [lengths of the single longest fractures on individual clasts; mm]

[Fig. 2.5; Methods]. Maximum-length fracture growth rate is calculated using the median of all fracture lengths on the modern deposit [0 kyr] and the maximum-length fracture per rock on each dated surface, averaged per surface and rock type. This estimation is based on the mechanics of a body of fractures, whereby the stress intensity of the longest fracture is high enough that it effectively dissipates the stress intensity on other fracture tips. Therefore, the longest fracture is most likely to continue to grow. Additionally, this is the most conservative estimate of fracture growth, given that no fracture can be measured once it has fully propagated through the rock.

We calculated fracturing rates as time-averaged millennial changes relative to the time 0 surfaces for each metric [Fig. 2.1C-E; Methods]. We observe negative power law trends in the rates of change of the three fracture metrics regardless of rock type

or climate of the site [Fig. 2.1; Table 2.1; 2.2; 2.3; Supplemental Data S2.1]. We document similar trends using an independent means of calculating fracturing rates from the measured duration of light exposure of fractures [Fig. 2.6; Methods]. Power law fits are provided due to the scale-invariant nature of the fit [Bonnet, Eric, Bour, Olivier, Odling, Noelle E., Davy, Philippe, Main, Ian, Cowie, Patience and Berkowitz, Brian, 2001] and the observation that power law fits are the most robust fits when compared with exponential or log-normal distributions for, e.g., sandstone formations [Hooker, J. N., Laubach, S. E. and Marrett, R., 2014].

We attribute fracture deceleration to mechanisms innate to all rock, involving internal feedbacks between fracture growth and its influence on material properties that toughen the rock. We test this idea by measuring Young's modulus for a select set of samples [Methods] and observe increasing compliance over time [Fig. 2.7]. We infer that among other elastic changes, the increased compressibility reduces sensitivity to the stresses that caused the initial fracturing.

Thus, our results indicate that the majority of natural fractures spend most of their lifetimes growing slowly, even decreasing in growth rate through time unless

1. fractures sufficiently grow such that they begin to coalesce and thus accelerate [Bažant, Zdenek P., Le, Jia-Liang and Salviato, Marco, 2021];

2. the rock is exposed to significant new, higher magnitudes of external stress-loading, or similar stress-loading under more favorable fracture-tip environmental conditions [hotter and/or wetter [Eppes, M. C., Magi, B., Scheff, J., Warren, K., Ching, S. and Feng, T., 2020]]; or

3. the rock is sufficiently eroded as to expose more brittle rock.

Because erosion rates – the rate at which upper portions of a rock surface are removed – determine the extent to which fracturing is 'reset' to time 0, these results help to explain observations of strong linkages between rock erosion rates and

weathering rates that influence a broad array of geologic processes, including Earth's temperature modulation [Brantley, S. L., Shaughnessy, Andrew, Lebedeva, Marina I. and Balashov, Victor N., 2023].

2.3 Decelerating fracturing

Initially, observed rocks exhibit relatively few, small fractures, with number densities of $2/m^2$ - $36/m^2$ and fracture intensities of 55 - 1369 mm/m^2 [Figs. 2.5A-B; Methods; Supplemental Data S2.1]. At time 0, median fracture lengths range from 6 - 23 mm, and average maximum-lengths range from 6 - 50 mm [Fig. 2.5C]. Rocks observed on the next-youngest studied surfaces are markedly more fractured, with number densities and fracture intensities 51 - 343 percent and 63 - 82 percent higher than those of the modern channel, respectively [Fig. 2.5A-B; Supplemental Data S2.1].

Although fractures generally continue to increase in length and number over the exposure timescales of the studied rocks [10^4 kyr], rates of fracturing decrease substantially within the first ∼10 kyr [Fig. 2.1]. Before ∼0 kyr, maximum-length growth rates range from 2.0 - 28.0 mm/kyr [Supplemental Data S2.1] across rock types and sites, noting that no $<$ ∼15 kyr data is available for the Northernmost site. After ∼10 - 20 kyr, these rates hold steady at ∼0 - 7.6 mm/kyr. Time-averaged increase-rates for number density and fracture intensity decrease over time by negative power law functions [Fig. 2.1; Table 2.2], slowing to, at most, $3.6/m^2$ per kyr and 131.9 mm/m^2 per kyr beyond ∼10 kyr, respectively [Supplemental Data S2.1].

After ∼20 - 30 kyr, number density and maximum-lengths decrease slightly [Fig. 2.5], likely due to fracture coalescence and/or 'loss' of fractures due to rock comminution. Thus, to analyze portions of rock that have unambiguously not been disaggregated, we also measured microcracks visible in thin sections of selected granitoid clasts from the Middle site [Methods]. These data [Fig. 2.8], the scale and rock interior location of which preclude observational biases associated with erosion [Sadler,

Peter M. and Jerolmack, Douglas J., 2015], exhibit similar trends as the macroscale data [Fig. 2.5].

To provide another independent measure of fracturing rates over time within a single rock mass, a novel application of infrared photoluminescence [IRPL] was used [Prasad, Amit Kumar, Poolton, Nigel R. J., Kook, Myungho, Jain, Mayank, 2017]. This technique allowed measurement of the light-exposure age of three decimeter-scale fractures observed in situ on one naturally fractured granitoid clast found on the Northernmost site's ∼18 kyr surface [Andričević, P., Sellwood, E. L., Freiesleben, T., Hidy, A. J., Kook, M., Eppes, M. C. and Jain, M., 2023] [Fig. 2.6; Methods]. IRPL emissions were measured at 880 nm peak [$IRPL_{880}$; after [Kumar, R., Kook, M., Murray, A. S. and Jain, M., 2018]] and 955 nm peak [$IRPL_{955}$; Fig. 2.6B-C]. Resetting of IRPL in rock due to light exposure results in measurable bleaching fronts [blue and green regions in the $IRPL_{955}$ ratio maps, Fig. 2.6B] within an otherwise unbleached rock [red region, Fig. 2.6B]; in absence of any bleaching the image would be only red. The bleaching front progresses deeper into the rock as a function of the light exposure duration and light flux. Regarding the latter, recent research [Andričević, Pavao, Sellwood, Elaine L., Eppes, Martha-Cary, Kook, Myungho and Jain, Mayank, 2023] shows that luminescence behavior is governed by diffused light, independent of width for above-millimeter sized fractures. Therefore, the bleaching front at the top surface, of known exposure age, can be used as calibration for estimating the time required to develop the bleaching fronts across the fracture surfaces. As shown in Fig. 2.6C, the surface has the deepest bleaching front, followed by fractures A, B, and C, respectively. The gradual change in luminescence signature relative to depth within the rock [2.6C] show that the fracture has gradually opened to the surface; if the fracture had cracked instantaneously either recently or in the past, the signal would be uniform across the fracture face.

This calibration approach has been used to measure quantitative exposure ages of

these fractures using the $IRPL_{880}$ signal [Andričević, P., Sellwood, E. L., Freiesleben, T., Hidy, A. J., Kook, M., Eppes, M. C. and Jain, M., 2023], which when combined with the surface exposure lengths [this study] yields a time-averaged, long-term fracturing rate per fracture [Methods; Fig. 2.6D]. Applying this technique, the calculated fracturing rates are consistent with decelerating fracturing on this single clast. The first, longest fracture A breached the rock surface very quickly after the rock was deposited [similar maximum IRPL signals as the rock surface], followed increasingly later by the two subsequent fractures [i.e., fractures B and C]. We acknowledge that we have no means of verifying when fractures began to grow in the rock interior, and that absolute fracturing rates of individual fractures may have been rapid compared to their time-averaged rates, e.g., all three fractures could have grown dynamically and much faster than their entire exposure history. Nevertheless, the significantly younger light-exposure ages of fractures B and C definitively point to decelerating fracturing of the entire rock body over time. Notably, the fracturing rate magnitudes calculated with this independent method are on the order of the changing rates measured for hundreds of clasts when extrapolated back to very young exposure ages [Fig. 2.1C]. For example, the IRPL-calculated fracturing rate for fracture A [$\sim$550 mm/kyr] is on the order of rates projected by best fit curves for the field-based dataset [Table 2.1] for the same time period [686 mm/kyr at 200 years after deposition; 63 mm/kyr at 1 kyr after deposition].

2.4 Universality of results [Testing the Limitations]

Although this study focused on individual surface clasts, we predict that subcritically cracking bedrock across all environments and rock types will behave similarly, even under constant tectonic or gravitational stresses, because the decelerating mechanisms understood from experimental data still apply. Several basic and well-established rock and fracture-mechanics concepts predict that fracturing should decelerate - barring exposure of fresh rock - regardless of the source of stress or the

rock type.

When rocks are first exposed to new stresses in a relatively non-fractured state, the longest fractures most favorably aligned with principal stresses are the most susceptible to 'everyday' low stresses and propagate rapidly. Over time, however, fracturing itself toughens the rock [Kachanov, Mark L., 1982] whereby a fractured rock is more compliant [less stiff] and thus better able to accommodate stress, limiting further brittle damage. In laboratory brittle creep experiments, for example, where rocks are subjected to a constant externally applied stress, subcritical cracking rates decelerate in a phenomenon commonly known as 'primary creep' [Brantut, Nicolas and Baud, Patrick and Heap, M. J. and Meredith, P. G., 2012]. This deceleration is explained by a decrease in the effective 'global' stress intensity factor for the total array of fractures within the rock, due to the progressive fracturing itself [Kachanov, Mark L., 1982]. Decelerating fracturing is also predicted by, for example, the 'Kaiser effect' observed from acoustic emissions research [Daoud, Ali, Browning, John, Meredith, Philip G. and Mitchell, Thomas M., 2020], 'fatigue limit' studies in material sciences [Schijve, Jaap, 2003], or 'damage precursors' assessed for construction integrity [Dexing, Li, Enyuan, Wang, Xiangguo, Kong, Haishan, Jia, Dongming, Wang and Muhammad, Ali, 2019].

We find evidence for this predicted rock toughening in measurements of compliance for a subset of samples with identical lithologies collected at the Middle site. The measured elastic moduli for these samples also decrease by a power law function over time [Fig. 2.7; see Rasmussen et al., Ch. 3]. Thus, a key implication of our results is that common approaches of understanding fracture through stress and geometric metrics such as fracture toughness should be replaced by metrics that reflect the energy required to propagate individual fractures. Appropriate metrics might include material toughness, the R-curve, or the J-integral, all of which reflect the strain energy of the fracturing process, integrating stress history, fracture geometry, and damage-

dependent rock stiffness [Atkinson, Barry Kean and Meredith, Philip George, 1987b].

Numerous additional well-studied fracture mechanics mechanisms may also contribute to toughening and fracturing deceleration. For example, growing fractures are increasingly likely to encounter barriers such as large phenocrysts that inhibit their further propagation [Gudmundsson, Agust and Brenner, Sonja L., 2001]. Additionally, chemically precipitated varnish or the growth of lichens commonly develop on exposed rock surfaces, which may chemically toughen the rock surface, lower thermal stresses, and/or infill pre-existing fractures [Carter, N. E. A. and Viles, H. A., 2005].

2.5 Runaway versus decelerating fracture

To our knowledge, our dataset represents the first field documentation of long-term fracturing rates that reflect a balance of runaway and stabilization behaviors, previously recognized in short-term subcritical cracking brittle creep tests [Atkinson, Barry Kean and Meredith, Philip George, 1987b], and in the context of human-time scale applications like building stone decay [Viles, Heather A., 2005], mining excavations [Leith, Kerry, Moore, Jeffrey R., Amann, Florian and Loew, Simon, 2014], and concrete structures [Bažant, Zdenek P., Le, Jia-Liang and Salviato, Marco, 2021]. Even this short-term understanding was hard-won. For example, the 'size-effect' driving abrupt failure in rock and concrete structures is intimately related to constant or accelerating fracture and took decades to understand [Bažant, Zdenek P., Le, Jia-Liang and Salviato, Marco, 2021].

Here, initially high fracturing rates [Fig. 2.1] likely reflect, in part, dynamic growth rates for a few large, favorably oriented fractures that achieve critical or close to critical lengths. The IRPL data from a single clast [Fig. 2.6] support this inference. Further, clasts at all sites - and those of other studies [Shaanan, Uri, Mushkin, Amit, Rasmussen, Monica, Sagy, Amir, Meredith, Philip, Nara, Yoshitaka, Keanini, Russell and Eppes, Martha-Cary, 2023] - commonly exhibit one or two 'dominant' fractures

similar to that visible in Fig. 2.6A. Unlike a laboratory test, however, which ends after these errant fractures cause lab specimens to 'break', our 'experiments' continue naturally, and we observe that brittle fracturing subsequently slows down in the remaining rock mass [Fig. 2.1] as it becomes elastically compliant, i.e., tougher [Fig. 2.7]. In brittle creep experiments there is a similar long period of extremely slow fracturing, frequently interpreted as 'arrested'. As understood for underground excavations and for natural exhumation [Leith, Kerry, Moore, Jeffrey R., Amann, Florian and Loew, Simon, 2014], the fracture toughness and initial microcrack distribution and density likely determine the point at which fracture propagation rates reach these minimums. Prior modeling suggests that when subcritical cracking is slower and/or initial fracture density is lower, higher number densities and fracture intensities can arise before stabilization occurs [Olson, Jon E., 2004]. Thus, although number density might be a strong proxy for short-term rock strength, it does not necessarily positively correlate with fracturing rates. On the contrary, more slowly fracturing rocks may be the most fractured because they have been able to slowly reach a highly fractured stabilization state. The toughened rock supports longer and more fractures through its very damage, as observed through 'pre-stressed' UCS testing [de Vilder, S. J. and Brain, M. J. and Rosser, N. J., 2019]. We believe this phenomenon explains why observed number densities are highest for the driest site [Fig. 2.5A]. This is further supported by number densities for carbonate clasts in a hyper-arid climate that are almost twice as high over similar timescales as carbonate rock densities in our data collected at a semi-arid site [Fig. 2.5A].

Following fracture deceleration, in subcritical cracking experiments fracture interactions eventually become dominant, leading to an increase in effective stress intensity. In turn, fracturing accelerates until critical lengths are reached and the specimen 'fails'. In nature, any change in fracturing response to stresses - from decelerating to accelerating - requires the rock to either pass through this internal threshold in

fracture intensity [Brantut, Nicolas and Baud, Patrick and Heap, M. J. and Meredith, P. G., 2012] or be subject to overall higher stresses or more conducive environmental conditions. For example, changing climatic conditions could reinvigorate subcritical cracking rates from higher stresses due to 'frost cracking' [Marshall, Jill A., Roering, Joshua J., Bartlein, Patrick J., Gavin, Daniel G., Granger, Darryl E., Rempel, Alan W., Praskievicz, Sarah J. and Hales, Tristram C., 2015] or more favorable environments that accelerate chemo-physical fracture-tip bond breaking [Eppes, M. C., Magi, B., Scheff, J., Warren, K., Ching, S. and Feng, T., 2020].

If the rock surface becomes 'reset' through erosion, the fracturing life cycle starts over. In our data, such resetting is precluded, because thermal stresses impact the entire rock for clasts in the size range examined [Molaro, J. L., Byrne, S. and Le, J. L., 2017]. Thus, even if a clast splits into two pieces, those pieces have already sufficiently fractured such that fracturing continues to decelerate. Similarly, while non-cyclic forces like gravity may be maintained in a bedrock mass such that stress intensity continuously increases for one or more large fractures until they accelerate in runaway behavior [Collins, Brian D. and Stock, Greg M., 2016], we predict that fracturing slows down for the rest of the rock mass. In bedrock, tectonics also induces sustained stresses but, as for earthquakes, after fractures grow, time and appropriate boundary conditions are required to rebuild stress to a level exceeding that which the fractures themselves can accommodate.

2.6 Feedbacks between fracturing rates and rock weathering and erosion

The presented data are from rocks in relatively arid climates that are not experiencing tectonic or gravitational stresses, so the observed magnitudes of fracturing – particularly initially – likely represent minimums for surface rocks in other locations. Although we likely 'missed' maximum rates for the northernmost site due to the lack of young surfaces, our reported rates are $\sim$2 - 3 orders of magnitude lower than rates commonly measured in laboratory experiments conducted at $\sim$60 - 80% of the critical

stress intensity [fracture toughness], consistent with the idea that the stresses causing our observed fractures were low in magnitude. Notably, our overall measured ranges of rates are on the same order of magnitude [10^0 - 10^1 m/My] as bare rock erosion rates averaged over ∼85 kyr and measured across the Sierra Nevada for similar granites [Stock, Greg M., Anderson, Robert S. and Finkel, Robert C., 2005], and to rock weathering rates measured for carbonate alluvial clasts in a semi-arid environment over similar timescales [Mushkin, Amit, Sagy, Amir, Trabelci, Eran, Amit, Rivka and Porat, Naomi, 2014]. These similarities are expected since both bedrock and clast erosion and breakdown are limited by the growth and coalescence of fractures that allows sediment to be produced and eroded from the rock surface.

Our results thus provide new insight into relationships between fracturing, erosion, and by inference, chemical weathering. Our data suggest that the supply of fresh mineral surfaces through fracturing may be a function of the ratio of fracture 'resetting' by erosion relative to the timescales of fracture deceleration that are dependent on rock type and environment. When erosion rates are sufficiently fast to remove the upper portions of fractured rock, positive feedbacks may develop whereby fracturing rates can always keep up with erosion rates. For rock types that are subject to relatively fast fracturing rates, this positive feedback could explain the conundrum of the apparent lack of sediment production 'speed limits' observed in some fast eroding landscapes [Heimsath, Arjun M. and DiBiase, Roman A. and Whipple, Kelin X., 2012].

Conversely, if fracturing rates outpace erosion rates, soils will begin to form. In this scenario, chemical weathering will be limited by fracture propagation rates, which themselves are limited by erosion. Such interplay between fracture, erosion, and weathering has been proposed to possibly explain why, in large watersheds, chemical weathering rates correlate with erosion rates, but do not correlate with temperature [Brantley, S. L., Shaughnessy, Andrew, Lebedeva, Marina I. and Balashov, Victor N.,

2023]; or why there are discrepancies between higher chemical weathering rates observed in laboratory settings vs. natural settings [Moore, Oliver W., Buss, Heather L. and Dosseto, Anthony, 2019]. Our results provide a mechanistic explanation for how these feedbacks might operate. Such insight is critical for interpreting and modeling what is one of the few negative feedback mechanisms proposed to slow down ongoing global climate warming - that of temperature and weathering.

In sum, our results provide a mechanism to explain or better understand any geological phenomena that are impacted by changing rock strength, damage, or hydrology; all of which are strongly dependent on fractures. For example, they have implications for those seeking to document long-term strength of rock for applications like nuclear waste repositories [Damjanac, Branko and Fairhurst, Charles, 2010] and rockfall hazards [Collins, Brian D. and Stock, Greg M., 2016]. Decreasing fracturing rates may explain why we have outcrops at all [even in locations with known high stress-loading], and how clasts and bedrock tors can persist on old landscapes [Fink, David, McKelvey, Barrie, Hambrey, Michael J., Fabel, Derek and Brown, Roderick, 2006] or other planets [Delbo, Marco, Walsh, Kevin J., Matonti, Christophe, Wilkerson, Justin, Pajola, Maurizio, Al Asad, Manar M., Avdellidou, Chrysa, Ballouz, Ronald-Louis, Bennett, Carina A., Connolly Jr., Harold C. and others, 2022]. Our results could also help to explain commonly observed discrepancies between basin-averaged and outcrop erosion rates, where calculations derived from concentrations of cosmogenic radionuclides like ^{10}Be typically assume constant erosion.

2.7 Tables

Table 2.1: PRISM database values extracted from 30-year mean maps at the approximate location listed below [PRISM Climate Group, Oregon State University, 2024]. Climate and vegetation interpreted from field observation at each site.

Site	WGS84 Approx. center	Elevation [m]	Climate; Vegetation	Mean annual temperature [°C] [PRISM, 1990-2020]	Mean annual precipitation [mm] [PRISM, 1990-2020]
Northernmost	38.0288, -119.1778	2150-2500	Semi-arid; sagebrush scrub to piñon or juniper	7.3	407
Middle	36.7189, -118.2408	1400-1800	Semi-arid; sagebrush scrub	12.7	265
Southern most	34.9375, -115.6180	735-980	Arid; Creosote bush scrub	18.6	160

Table 2.2: Power-law trend fits and statistics for fracture metrics over time, for maximum-length fracture growth rate [mm/kyr]. For tables 2.2, 2.3, and 2.4, the power law equation format is $y = Ax^k$.

Site	Rock type	A	K	R^2	Two-tailed p-value
Northernmost	granitoid	63.4	-1.48	0.86	0.0
Middle	granitoid	48.5	-1.09	0.99	0.00
Southernmost	granitoid	31.9	-0.88	1.00	0.00
Southernmost	volcanic	24.0	-0.83	0.60	0.12
Southernmost	carbonate	5.5	-0.38	0.03	0.79

Table 2.3: Power-law trend fits and statistics for fracture metrics over time, for fracture number density increase rate [fractures/m^2 per kyr]. Dashes [-] indicate insufficient data for calculating a trend.

Site	Rock type	A	K	R^2	Two-tailed p-value
Northernmost	granitoid	-	-	-	-
Middle	granitoid	25.11	-0.95	0.99	0.00
Southernmost	granitoid	40.95	-0.97	0.99	0.00
Southernmost	volcanic	42.81	-1.12	0.95	0.01
Southernmost	carbonate	32.35	-0.68	0.29	0.36

Table 2.4: Power-law trend fits and statistics for fracture metrics over time, for fracture intensity increase rate [mm/m^2 per kyr]. Dashes [-] indicate insufficient data for calculating a trend.

Site	Rock type	A	K	R^2	Two-tailed p-value
Northernmost	granitoid	-	-	-	-
Middle	granitoid	990.47	-0.96	0.98	0.00
Southernmost	granitoid	1655.30	-0.95	0.99	0.00
Southernmost	volcanic	1717.90	-1.04	0.78	0.05
Southernmost	carbonate	1014.10	-0.62	0.19	0.47

2.8 Figures

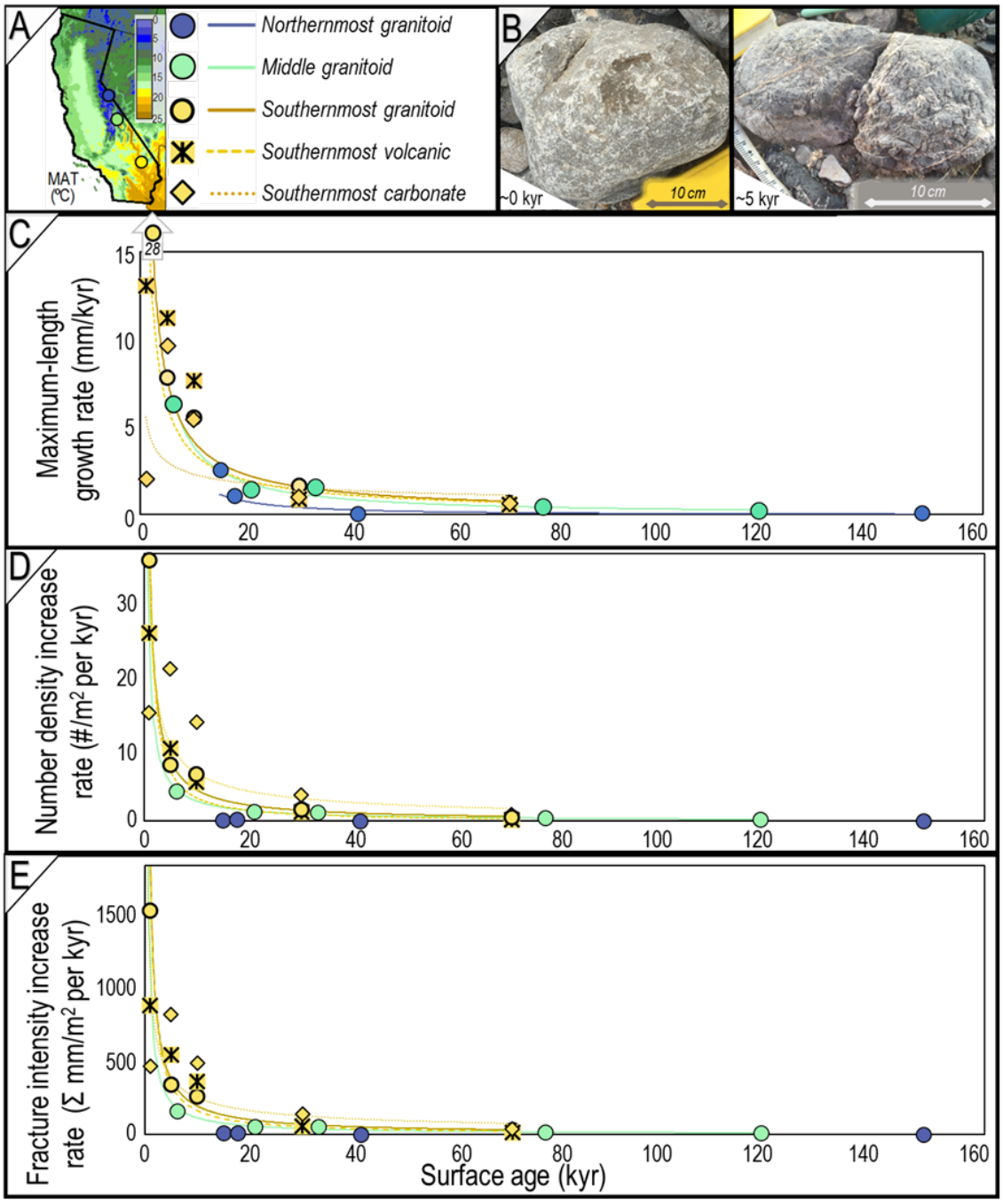

Figure 2.1: A. Field sites in California, USA colored by approximate modern mean annual temperature [MAT, °C], California map copyright [PRISM Climate Group, Oregon State University, 2024]. B. Representative carbonate rocks from the Southernmost site measured on the modern wash surface [time 0, left] and the ∼5 kyr surface [right]. C - E] mean-to-mean rate of change values for all rocks per surface [Methods], for C. maximum-length, D. number density, and E. fracture intensity.

Figure 2.2: A. Northernmost site modern creek deposit with measurement boulders on a small unvegetated bar adjacent to the active channel. B. typical Middle site modern boulder bar with measuring tape indicating transect measurement location. C. Southernmost site modern boulder bar exhibiting impact marks and minimal varnish, lichen, and fractures.

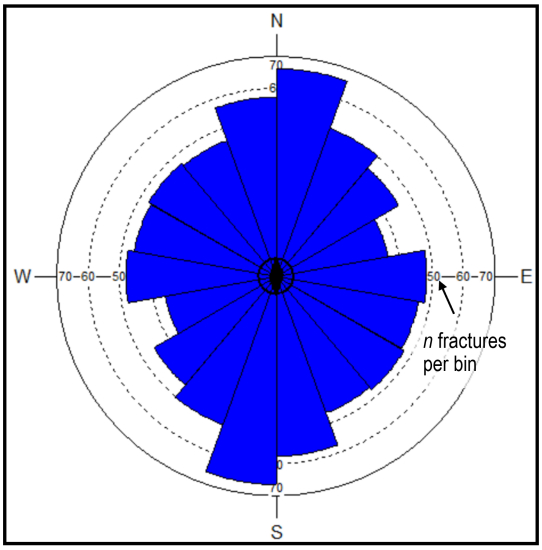

Figure 2.3: All fracture plane strikes measured on granitoid rocks on the ∼76 kyr exposure age surface at the Middle site. Data are plotted biaxially. Note statistically significant orientations, suggesting a thermal stress origin due to the natural directionality of diurnal solar heating [Stone, Paul, Miller, David M., Stevens, Calvin H., Rosario, Jose, Vazquez, Jorge A., Wan, Elmira, Priest, Susan S. and Valin, Zenon C., 2017].
N fractures = 441; vector mean = 179 °; median = 5 °; circular std. dev. = 64 °; Rayleigh p-value = 0.05; Rao's spacing p-value = <0.01

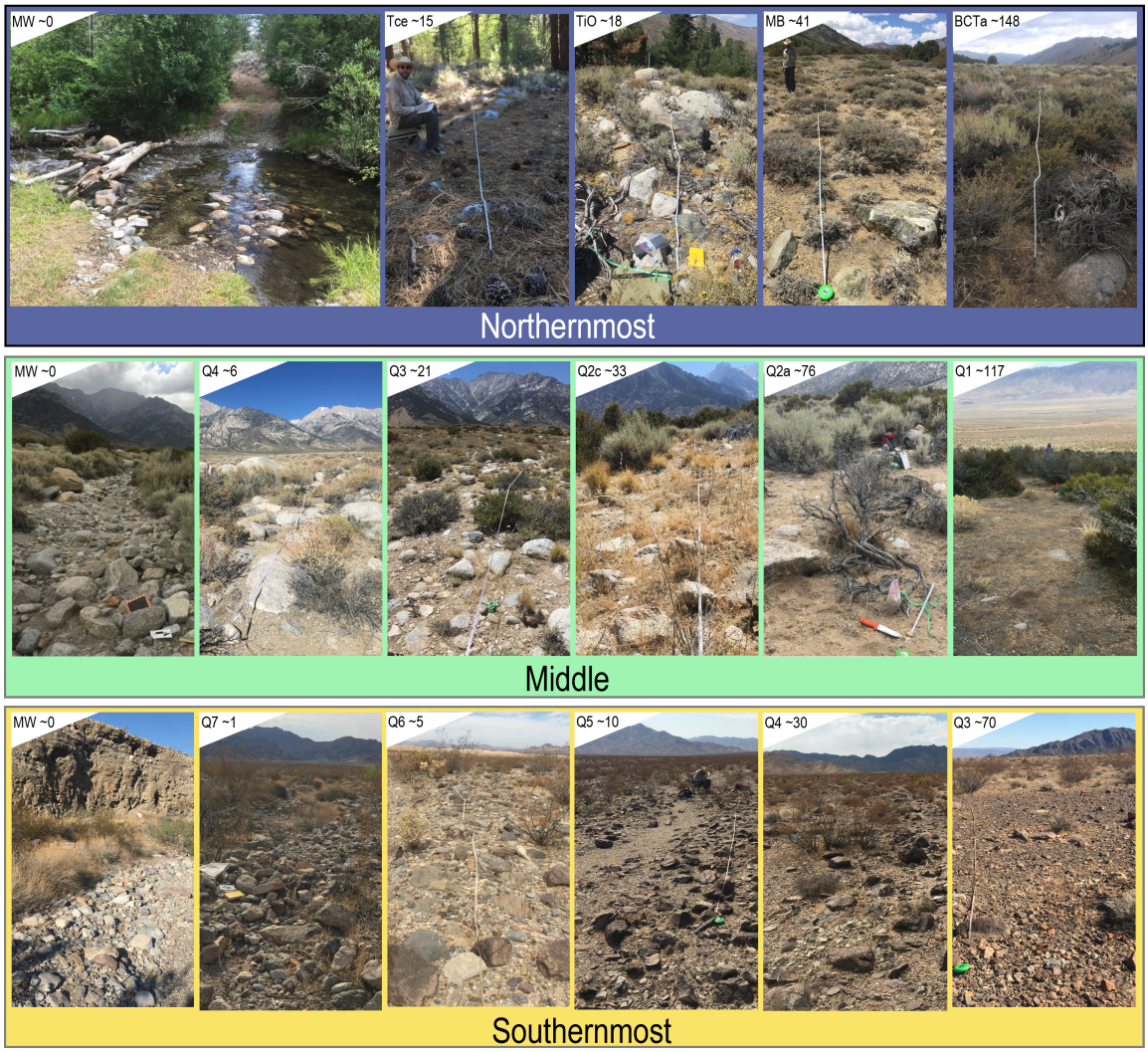

Figure 2.4: Depositional surfaces on which boulders were measured, with ages in kyr before present. Notice difference in abundance and type of vegetation at Northernmost [coolest, present day semi-arid], Middle [warmer, semi-arid], and Southernmost [hot, arid] sites, reflecting increasing aridity from North to South.

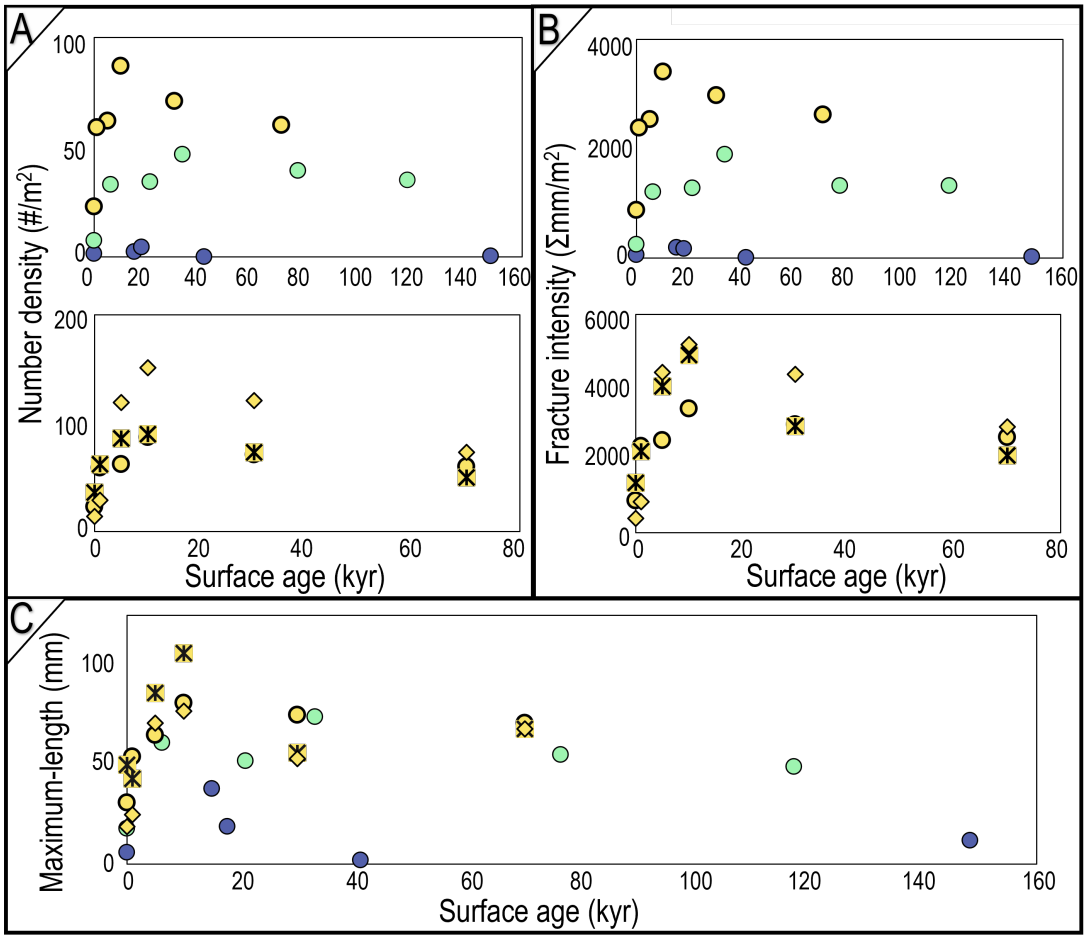

Figure 2.5: Chronofunctions by climate [top] and rock type [bottom] of the mean values for all measured rocks per surface for A. number density B. fracture intensity and for all sites and rock types for C. maximum-length. Key in Fig. 2.1.

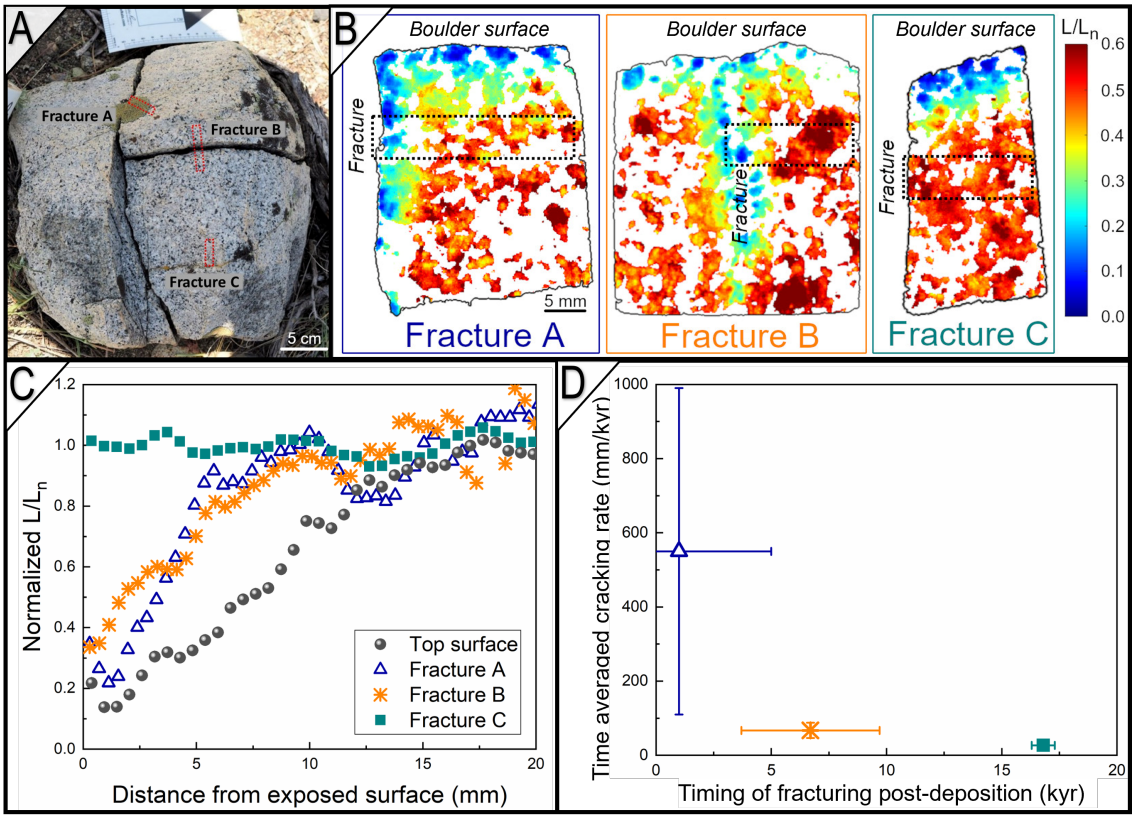

Figure 2.6: IRPL measurements of fracture surfaces in a single boulder. A. Image of the sampled boulder in situ on the ∼18 kyr surface at the Northernmost site. The red dashed rectangles indicate slices from where IRPL images were taken. B. $IRPL_{955}$ luminescence ratio maps $[L/L_n]$ of the slices across the three fractures shown in A, where L is the natural luminescence signal and Ln is the signal after giving a 2 kGy saturation gamma dose; normalization is done to account for spatial variations in luminescence sensitivity. C. $IRPL[L/L]_{955}$ vs. depth profiles perpendicular to the exposed fracture surfaces [blue triangles = Fracture A, orange stars = Fracture B, and teal squares = Fracture C] and the exposed top surface of the rock [grey circles]. The profiles for the fracture surfaces were derived at a depth of 10 mm below the top surface of the rock [black rectangles in B]. D. Time-averaged fracturing rates calculated using the field-measured fracture lengths. The timing of the fractures [x-axis] is calculated relative to the time when the rock was first deposited on the surface [Methods]. Error bars are projections of OSL calculation error.

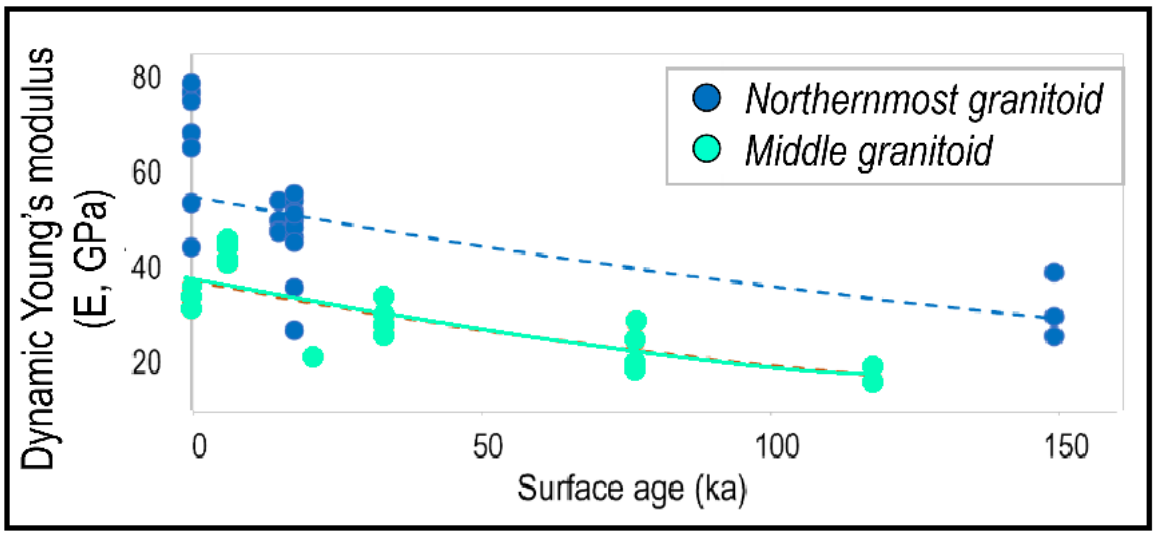

Figure 2.7: Chronofunctions of static Young's modulus of representative rocks at the Northernmost and Middle sites.

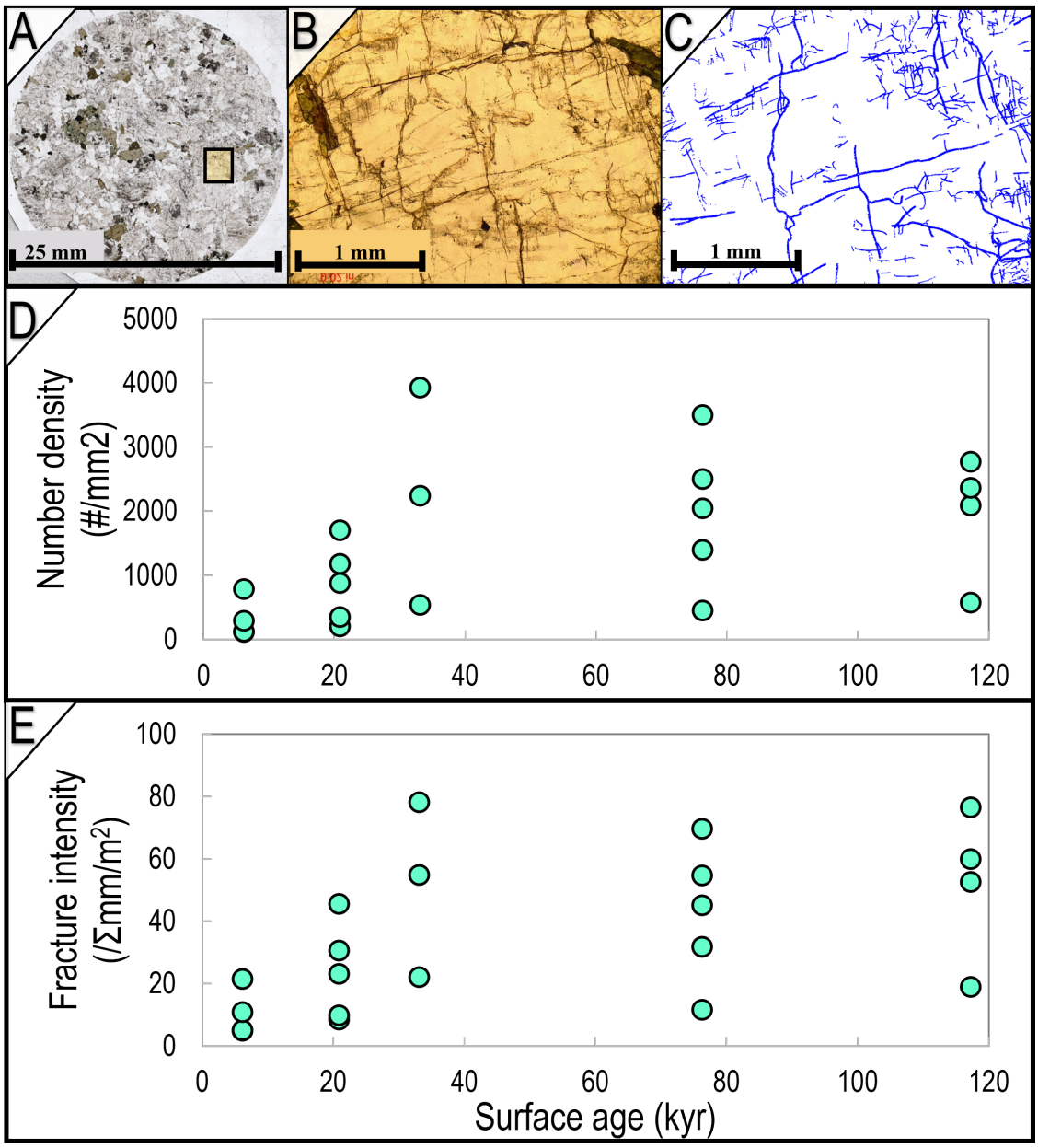

Figure 2.8: Thin section analyses from select samples of the Middle site. A. Thin section of a granite sample. B. Microstructure scanned by microscopy and C. the same sample as B, showing the mapped fractures isolated for import into FracPaQ [Healy, David, Rizzo, Roberto E., Cornwell, David G., Farrell, Natalie J. C., Watkins, Hannah, Timms, Nick E., Gomez-Rivas, Enrique and Smith, Michael, 2017] analyze fracture properties. Microcracking chronofunctions of D. number density and E. intensity derived from 3-5 locations within thin sections of selected rocks of identical lithology from the Intermediate site.

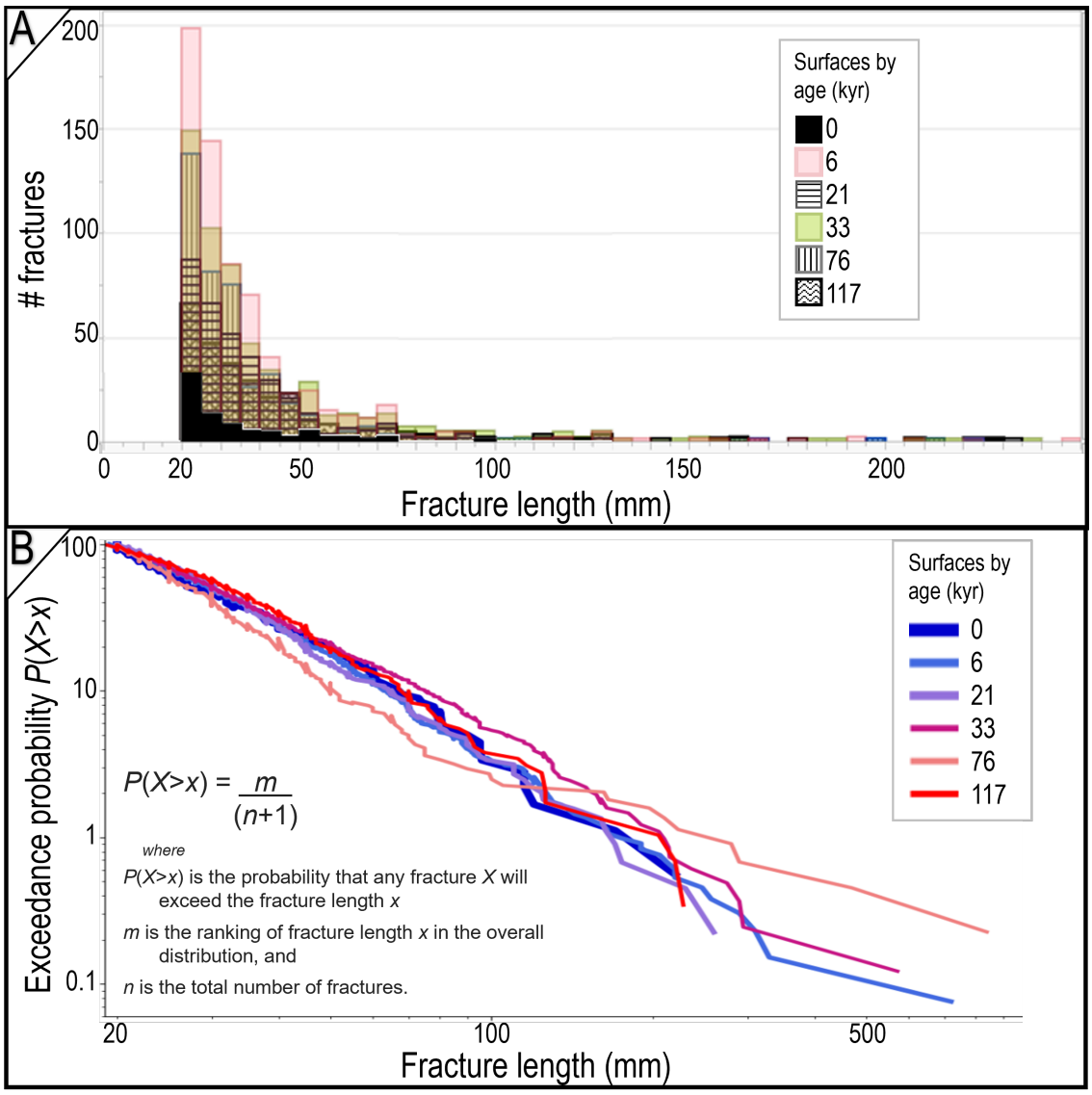

Figure 2.9: A. Exponential distribution of fractures [length vs. count] from 90 randomly selected granitoid clasts per surface at the Middle site. Y-axis displays the number of all cracks counted within a given 5mm bin on each surface. Surface bars are non-normalized and overlapped, indicating that the modern surface [0 ka] has the least cracks overall. B. Probability that a rock will contain fractures of a given length or longer, calculated using the inset equation and all fractures on all rocks measured at the Middle site. The exceedance probability function exhibits similar distributions for the 0, 6, and 21 kyr surfaces; then higher probabilities of longer fractures on the next older 33 and 76 kyr surfaces. The 117 kyr surface data [the oldest rocks] indicate that fracture length probabilities have 'reset' to initial values, although the histogram [A] shows that these rocks still have a higher number of fractures than the modern [0 kyr] rocks.

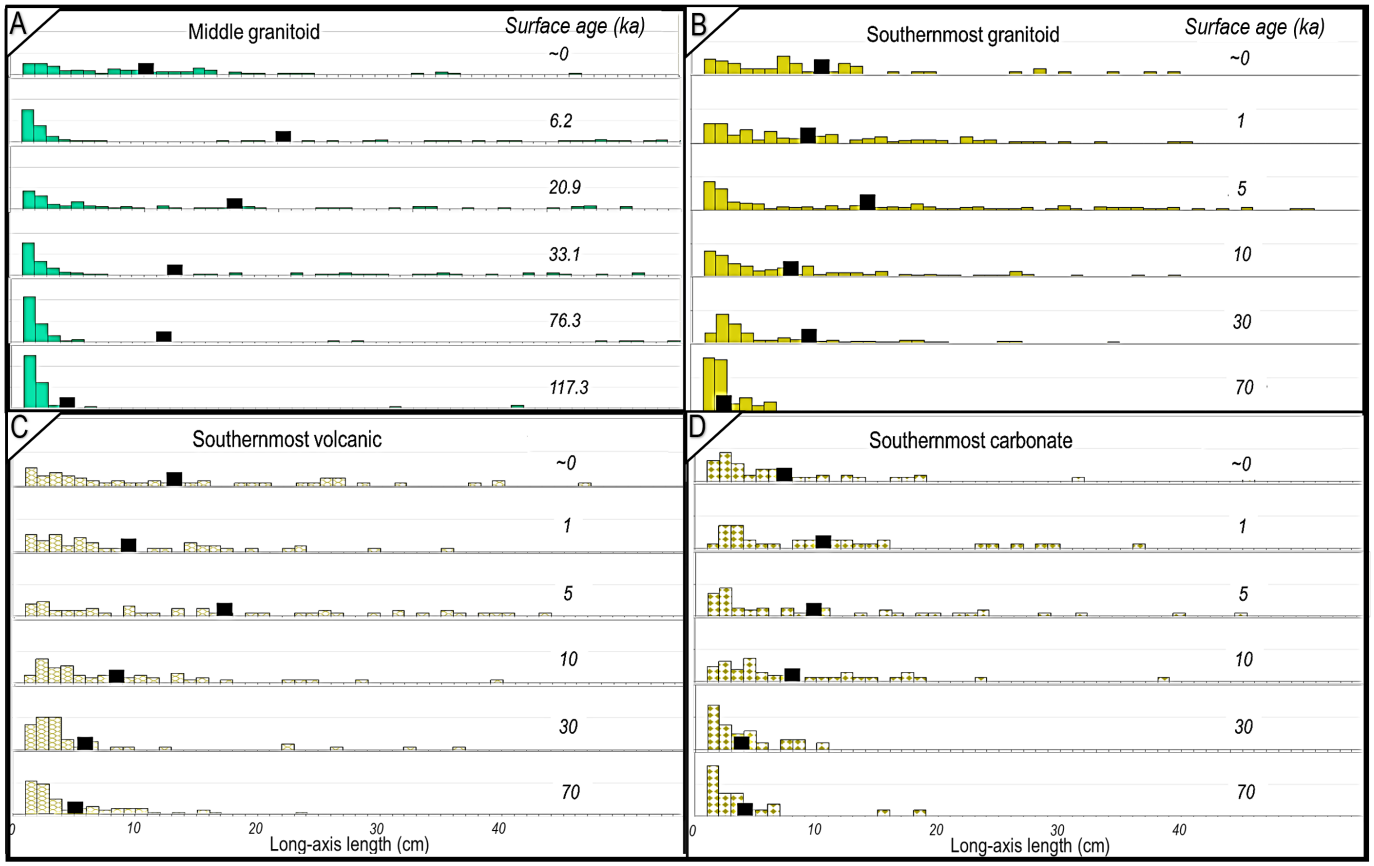

Figure 2.10: Wolman pebble counts collected at regular intervals along each bar surface, represented as normalized histograms of the relative count of each rock size bin, with surface ages in kyr overlain to the right of each distribution. Three primary axes were measured on every $\geq$10 mm intermediate axis length granitoid clast encountered at the A. Middle site, granitoid rocks, and B - D. Southernmost site granitoid, volcanic, and carbonate rocks. Displayed data are 10 mm bins of intermediate-axis length of clasts. Dark bars represent means.

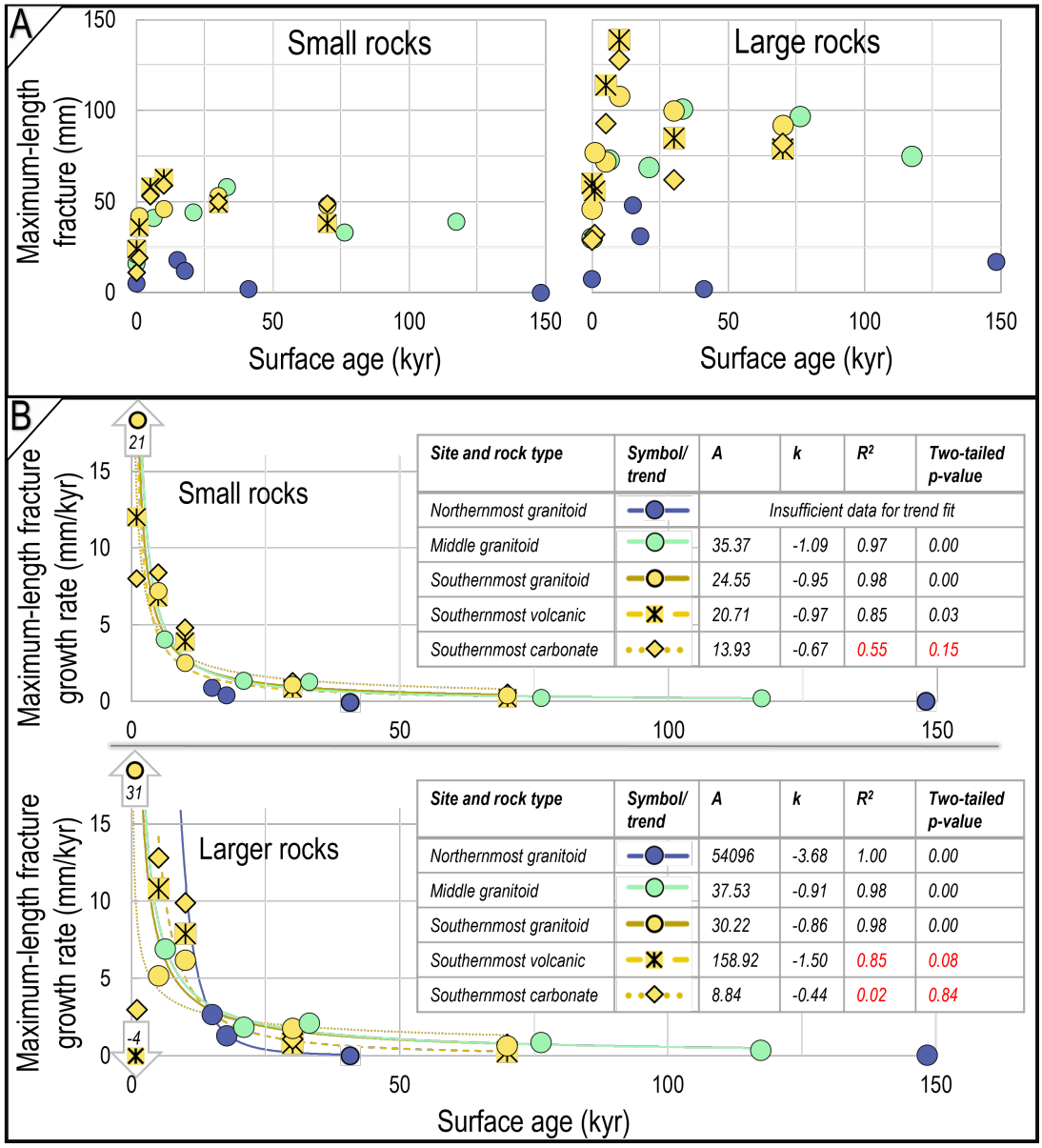

Figure 2.11: A. Maximum-length fractures and B. maximum-length fracture growth rates for smaller rocks [left] vs. rates for larger rocks [right]. Cut-off of rock sizes was 30 cm long-axis length for the Northernmost and Middle site and 20 cm long-axis length at the Southernmost site, where rocks were smaller overall. Negative points exist where 1] large volcanic rocks at the Southernmost site are estimated to decrease in length by -4 mm/kyr on the 1 kyr surface; and 2] large and small granitoid rocks at the Northernmost site are near-zero and/or negative on the two oldest surfaces. Negative points were not included in trendline fitting.

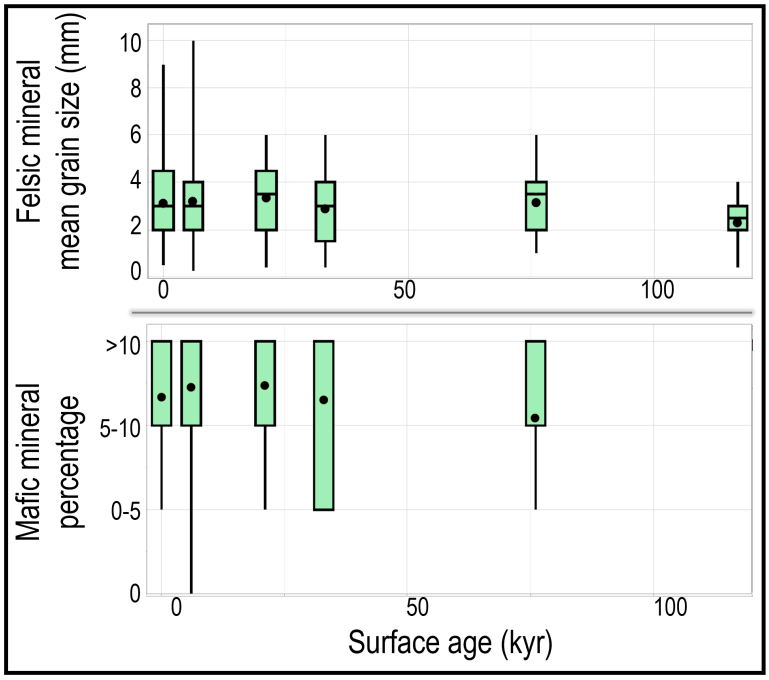

Figure 2.12: A. Grain size and B. mafic mineral percentages of Middle site granitoid rocks. Solid circles represent mean value and horizontal lines of boxes indicate p25, p50, and p75 percentiles. Whiskers represent outlier extents. The Middle site contains the highest number of boulders measured and therefore the most statistically robust subsets of data. The lack of time trends suggest that the observed and calculated fracture metrics are not artifacts of 'survivor's bias' due to exceptional rocks remaining on older surfaces.

CHAPTER 3: QUANTIFYING THE EVOLUTION OF ROCK POROSITY, PERMEABILITY, STRENGTH, AND COMPLIANCE IN THE CRITICAL ZONE

AUTHORS:

Monica Rasmussen, Yang Yuan, Karin Hofer-Apostolidis, Martha Cary Eppes, Alan Hidy, Philip Meredith, Thomas Mitchell, Ami Mushkin, Valerie Reynolds, Patrick Webb, Russell Keanini, Alex Rinehart, and Maxwell P. Dahlquist

3.1 Abstract

Geologists study and sample rocks at Earth's surface, assuming that their physical characteristics are static. Yet as rocks are exhumed and adjust to their new and complex environmental conditions within Earth's Critical Zone [from the tree canopy through the water table], physical and chemical changes damage the rock. Short-term field and laboratory experiments are typically employed to quantify the rates and magnitudes of that damage [e.g., Turowski, J. M., Pruß, G., Voigtländer, A., Ludwig, A., Landgraf, A., Kober, F. and Bonnelye, A., 2023; Heap, M. J., Vinciguerra, S. and Meredith, P. G., 2009; de Vilder, S. J. and Brain, M. J. and Rosser, N. J., 2019; Eppes, Martha Cary, Magi, Brian, Hallet, Bernard, Delmelle, Eric, Mackenzie-Helnwein, Peter, Warren, Kimberly and Swami, Suraj, 2016], but these processes proceed and interact over geologic timescales. Here we employ ASTM standard rock testing to quantify the changing mechanical properties of granitoid clasts due to in situ environmental exposure over 105 years. At two "warm-summer Mediterranean" [Beck, Hylke E., Zimmermann, Niklaus E., McVicar, Tim R., Vergopolan, Noemi, Berg, Alexis and Wood, Eric F., 2018] sites in Eastern California, different magnitudes, but similar trends were observed. Although trends are similar between sites, rocks of all ages at the site with lower mean annual temperature and higher mean annual precipitation exhibit overall lower porosity [Φ] and permeability [κ], and higher compressive strength [UCS] and tensile strength [T] than rocks of similar ages at

the warmer, more arid site. By comparing freshly deposited clasts with the oldest weathered clasts, we find that mean Φ increases by 337-437% and mean κ increases by one to two orders of magnitude. These increases mirror decreases in compressional [29-33%] and shear [22-32%] velocities [Vp/Vs], UCS [31-67%] and T [35-63%], static Young's modulus [E_{stat}, 19-59%], and rock density [ρ, 4-5%]. Geochemical indices do not systematically change over time, so we conclude that the mechanical property changes are predominantly driven by progressive rock fracture.

3.2 Introduction

Surface exposures of rocks have long served as critical analogs of subsurface rocks, providing rock property data, informing our understanding of the subsurface, and providing abundant materials for testing structural integrity [Saunders, M. K. and Fookes, P. G., 1970], carbon sequestration potential [Brantley, S. L., Shaughnessy, Andrew, Lebedeva, Marina I. and Balashov, Victor N., 2023], and tectonic behavior [Leith, Kerry, Moore, Jeffrey R., Amann, Florian and Loew, Simon, 2014]. Yet shallow rocks undergo a decrease in confining stress and pore pressure as they approach the surface, and once within hundreds of meters of the surface [e.g., Moon, Seulgi, Perron, J. Taylor, Martel, Stephen J., Goodfellow, Bradley W., Mas Ivars, Diego, Hall, Adrian, Heyman, Jakob, Munier, Raymond, Näslund, Jens-Ove, Simeonov, Assen and Stroeven, Arjen P., 2020], moisture, temperature, and biological factors continue to produce mechanical and chemical changes that are typically considered together as 'weathering' processes.

For engineering purposes, mechanical property changes that accompany weathering have been investigated relative to overall weathering proxies like Rock Durability Indicator [Fookes, P. G., Gourley, C. S. and Ohikere, C., 1988] or Weathering Degree [Flandes, Nicol E., Villalobos, Felipe A. and King, Robert, 2023]. In geosciences, the notion that weathering impacts rock properties is widely observed and accepted [e.g., Heimsath, Arjun M., Dietrich, William E., Nishiizumi, Kunihiko and Finkel,

Robert C., 1997; Montgomery, David R., 2004; Moore, Jeffrey R., Sanders, Johnny W., Dietrich, William E. and Glaser, Steven D., 2009; Brantley, Susan L., Buss, H. and Lebedeva, M., Fletcher, R. C. and Ma, Lin, 2011; Brantley, S. L., Shaughnessy, Andrew, Lebedeva, Marina I. and Balashov, Victor N., 2023; Holbrook, W. Steven, Marcon, Virginia, Bacon, Allan R., Brantley, Susan L., Carr, Bradley J., Flinchum, Brady A., Richter, Daniel D. and Riebe, Clifford S., 2019; Neely, Alexander B. and DiBiase, Roman A., 2020], with the degree of chemical weathering quantified through metrics like the Chemical Index of Alteration [CIA; Nesbitt, H. W. and Young, G. M., 1982] or Chemical Index of Weathering [CIW; Harnois, Luc, 1988], and the degree of mechanical fracturing quantified through metrics like Rock Mass Strength [e.g., Moore, Jeffrey R., Sanders, Johnny W., Dietrich, William E. and Glaser, Steven D., 2009; DiBiase, Roman A., Rossi, Matthew W. and Neely, Alexander B., 2018]. Both physical and chemical weathering of surface rocks have been studied through controlled field simulation [de Vilder, S. J. and Brain, M. J. and Rosser, N. J., 2019], natural field experiments spanning years [Eppes, Martha Cary, Magi, Brian, Hallet, Bernard, Delmelle, Eric, Mackenzie-Helnwein, Peter, Warren, Kimberly and Swami, Suraj, 2016], and *in situ* bedrock testing [Riebe, Clifford S., Callahan, Russell P., Granke, Sarah B. M., Carr, Bradley J., Hayes, Jorden L., Schell, Marlie S. and Sklar, Leonard S., 2021]. However, in both engineering and geoscience, these studies capture single points in time, or very short timescales, and the full physical and chemical weathering history of rocks over 10^5 years is poorly constrained. These weathering-induced changes will dictate how surface and subsurface rocks respond to tectonic stress [e.g., Moon, S., Perron, J. T., Martel, S. J., Holbrook, W. S. and St. Clair, J., 2017], human structures [e.g., Ündül, Ömer and Tuğrul, Atiye, 2011], climate change [Eppes, M. C., Magi, B., Scheff, J., Warren, K., Ching, S. and Feng, T., 2020], and river incision [e.g., Shobe, Charles M., Hancock, Gregory S., Eppes, Martha C. and Small, Eric E., 2017], all of which are of critical importance throughout

the geosciences.

Here we use a "space-for-time" chronosequence approach [e.g., Birkeland, Peter W., 1999] at two Eastern California sites to quantify changes in mechanical properties of granitoid clasts due to their exposure to natural conditions over timescales up to 10^5 years. Employing ASTM standard testing methods, we find that at both sites, porosity [Φ], permeability [κ], and elastic compliance [inverse of E_{stat}] increase over exposure time, while rock compressive strength [UCS], tensile strength [T], and P- and S-wave velocities [Vp and Vs] decrease. To test if chemical alteration alone could explain these results, we calculated both the CIA and CIW for each of the clasts and determined that chemical weathering is insufficient for explaining the physical changes observed. We therefore attribute rock property changes primarily to mechanical weathering [cracking/fracturing] progressing throughout clast exposure. These data represent the first quantified rock property changes tied directly to natural rock weathering relative to a specific exposure time. Our results have interesting implications for how surface clasts may or may not reflect their subsurface counterparts.

3.3 Methods

3.3.1 Study design and field areas

We studied clasts of similar Half Dome, Cathedral Peak, Eagle Creek, Dragon Pluton, and Bullfrog Pluton granitoids [Bateman, P. C., 1992; Dohrenwend, J. C., 1982; Keith, W. J. and Seitz, J. F., 1981; Moore, J. G., 1981; Stone, Paul, Dunne, George C., Moore, James G. and Smith, George I., 2000] at two eastern Sierra Nevada sites characterized by differing current climates [PRISM Climate Group, Oregon State University, 2024, , Fig. 3.1A]. We collected modern creek deposits as well as clasts deposited atop alluvial fans and fluvial terraces issuing from the Lundy Canyon, CA region [0-148 ka] and the Shepherd Creek, CA drainage basin [0-117 ka; Fig. 3.1B]. It is understood that these intermittently glaciated catchments experience significant bedrock erosion, exposing relatively unweathered bedrock during deglaciation [e.g.,

Simon H. Brocklehurst and Kelin X. Whipple, 2002]. Once eroded from bedrock, the energetic transport of these alluvial sediments presumably removes major pre-existing rock fractures [Olsen, Lars, 1983], effectively 'resetting' the fracture properties of the rocks. Having this baseline of relatively fresh rock allows us to isolate the impacts of subsequent subaerial exposure and associated weathering on rock mechanical and chemical properties.

To construct chronosequences of weathering, we leveraged robust ^{10}Be rock dating [this study, see Appendix; D'Arcy, Mitch. Roda Boluda, Duna C.. Whittaker, Alexander C. and Carpineti, Alfredo, 2015; Rood, Dylan H., Burbank, Douglas W. and Finkel, Robert C., 2011] combined with detailed surficial mapping of geomorphically distinct alluvial surfaces [Blisniuk, Kimberly Diem Chi, 2011; D'Arcy, Mitch. Roda Boluda, Duna C.. Whittaker, Alexander C. and Carpineti, Alfredo, 2015; Dühnforth, Miriam, Anderson, Robert S., Ward, Dylan and Stock, Greg M., 2010; Rood, Dylan H., Burbank, Douglas W. and Finkel, Robert C., 2011]. We infer, as have past chronosequence studies [e.g., Rasmussen et al., Ch. 2; Shaanan, Uri, Mushkin, Amit, Rasmussen, Monica, Sagy, Amir, Meredith, Philip, Nara, Yoshitaka, Keanini, Russell and Eppes, Martha-Cary, 2023; McFadden, Leslie D., McDonald, Eric V., Wells, Stephen G., Anderson, Kirk, Quade, Jay and Forman, Steven L., 1998] that the current properties of clasts found on the surface of what is interpreted to be a stable, non-eroding landform are a proxy for the degree of weathering that occurs over the timespan of the surfaces' depositional ages [10^3-10^5 ka]. A single ∼30 cm diameter spheroidal granitoid clast was collected from each dated depositional surface [Fig. 3.2]. Following Phillips, Jonathan D. [2005], clasts were collected from stable portions of geomorphic surfaces away from sloping edges [examples in Fig. 3.1B], best ensuring their exposure age was consistent with that of the dated surface. We also collected clasts within active channels at both sites to represent time-zero [initial] properties. We employed a lithological reference cobble at each site to visu-

ally ensure we sampled similar clasts, matching as closely as possible exterior grain size, color, and approximate mafic percentages. Coordinates and photographs were recorded and *in situ* horizontal and north orientations were marked on the clasts to allow preparation of similarly oriented samples for testing [Fig. 3.2A].

3.4 Laboratory Analysis

Based on prior work showing that directional diurnal insolation drives north-south trending fractures to preferentially grow over geologic time [Adelsberger, Katherine A. and Smith, Jennifer R., 2009; Aldred, Jennifer, Eppes, Martha Cary, Aquino, Kimberly, Deal, Rebecca, Garbini, Jacob,, 2016; Eppes, Martha-Cary, Willis, Andrew, Molaro, Jamie, Abernathy, Stephen and Zhou, Beibei, 2015; Eppes, Martha Cary, Magi, Brian, Hallet, Bernard, Delmelle, Eric, Mackenzie-Helnwein, Peter, Warren, Kimberly and Swami, Suraj, 2016; McFadden, L. D., Eppes, M. C., Gillespie, A. R. and Hallet, B., 2005], clasts were prepared relative to their in situ clast field orientations, simulating a north-south trending vertical fracture propagating during strength testing. Where sufficient rock mass was available, we avoided sampling the outer 1-2 cm of the clast, minimizing the impacts of chemical weathering rinds which were visible on older clasts [see bisected clasts, Figs. 3.2E, and bisected rocks, Figs. 3.2B and 3.2C]. Cores with visible planar fractures were discarded due to test instability. Between 1-11 samples were prepared per clast per sample type. The number of samples tested for each analysis are shown in Table 3.1. Supplement S3.1 contains the data acquired from all tests.

3.4.1 Sample Preparation

Brazil disk samples [19 mm axial length, 38 mm diameter] for tensile strength [T] testing were prepared from cylindrical cores, with the core's long axis oriented approximately horizontal to the ground surface in a north-south orientation. Cores for uniaxial compressive strength [UCS] testing [62.5 mm axial length, 25 mm diameter]

were aligned vertically relative to the clast's natural position on the ground surface [Fig. 3.2E, blue cores]. Core samples were ground to length then baked at 80 °C for a minimum of 36 hours to remove unbound water, then mass [g], length [mm] and diameter [mm] were measured.

Vp and *Vs* were measured from the 25 mm diameter cores before *UCS* testing. Bulk porosity [Φ] and permeability [κ] were measured from randomly oriented cylindrical samples, generally comprised of the ends of cores [volumes ∼6-28 cm^3]. For mineralogical and microfracture analysis, one 2.7 x 4.6 cm thin section was prepared per clast, oriented parallel to the clast's natural upward facing surface and ∼1.5 cm depth into the clast [Fig. 3.2E, pink rectangle].

3.4.2 Rock property measurements

Density [ρ] was calculated as mass/volume for cylindrical samples. P- and s-wave ultrasonic transducers measured ultrasonic emissions JSR Ultrasonic's DPR300 Pulser-Receiver, then waveform arrivals were manually picked from the long-axis travel time through *UCS* cores. *Vp* and *Vs* were calculated by dividing sample length by waveform travel time. Φ was measured using a Micromeritics AccuPyc II 1340 He pycnometer. Distilled water κ was measured following Mitchell, T. M. and Faulkner, D. R. [2008], calculating κ during steady state flow conditions at confining pressure steps ranging from 5-50 MPa. Rock strength tests were conducted at constant displacement rates of 0.00062 mm/s [*UCS*] and 0.005 mm/s [*T*]. Vertical and horizontal strain gauges with 0.2% sensitivity [Tokyo Sokki Kenkyujo F-series general use strain gauges] were affixed to the long axes of selected *UCS* cores before testing. Static Young's modulus [E_{stat}] was derived from linear stress-strain relationships measured during *UCS* tests, and static Poisson's ratio [ν_{stat}] was calculated from vertical and horizontal strains during *UCS* tests.

Dynamic Young's modulus [E_{dyn}] and dynamic Poisson's ratio [ν_{dyn}] were calculated from *Vp*, *Vs*, and ρ following [Mavko, Gary, Mukerji, Tapan and Dvorkin, Jack, 2020,

Eq. 3.1 and 3.2].

$$E_{dyn} = [\rho Vs^2 * [3Vp^2 - 4Vs^2]]/[Vp^2 - Vs^2] \tag{3.1}$$

$$\nu_{dyn} = [Vp^2 - 2Vs^2]/[2 * [Vp^2 - Vs^2]] \tag{3.2}$$

3.5 Rock property changes

All measurements are shown in Figs. 3.3, 3.4, 3.5, and 3.6. The data are presented in terms of the change over time at each site, calculated as the percentage change from the mean value of the freshly deposited 'modern' clasts, to the mean values of the clasts atop older, abandoned surfaces. Permeability [κ] is shown for 5 MPa confining pressure test conditions [Fig. 3.3] and all data are available in Supplement S3.1. Uniaxial compressive strength [UCS] and tensile strength [T] are presented as Mohr Coulomb plots [Fig. 3.4] with constant failure envelope slopes of 0.6.

At both sites, clasts become more permeable [κ increasing one to two orders of magnitude] and porous [Φ increasing 337-437%], mirroring decreasing ρ [by 4-5%] over the time of exposure [between 117-148 ka; Fig. 3.3]. Rock strength decreases over exposure time [UCS decreasing 31-67%, T by 35-63%; Fig. 3.4]. Velocities generally decrease with exposure age [Vp by 29-33%, Vs by 22-32%, Fig. 3.5]. Linear elastic behavior observed before failure during UCS testing shows that clasts are more compliant over time [E_{stat} decreasing 19-59%], consistent with decreasing E_{dyn} values calculated from Vp, Vs, and ρ [E_{dyn} decreasing 47-53%, Fig. 3.6].

At Shepherd Creek, static Poisson's ratio [ν_{stat}] decreases 7% and ν_{dyn} decreases 78% [Fig. 3.6]. By contrast, Lundy Canyon clasts exhibited an increase in ν_{dyn} of 30% [Fig. 3.6], and ν_{stat} data were unavailable. These inconsistencies may be due to the highly interpretive nature of Vs measurements. Given the uncertainties in picking shear velocity arrivals, we test the validity of our E_{stat} results by calculating E_{stat}

from E_{dyn} using a standard dynamic-static correction [Canady, Wyatt, 2011]. The prediction from E_{dyn} fits remarkably well with the measured E_{stat} data at Shepherd Creek, whereas the prediction at Lundy Canyon deviates significantly from measured E_{stat} [Fig. 3.7].

3.6 Geochemical indicators do not explain mechanical property changes

The commonly employed geochemical indices of *CIA* [Nesbitt, H. W. and Young, G. M., 1982] and *CIW* [Harnois, Luc, 1988], both of which are designed to show chemical weathering trends, do not exhibit any consistent trends with surface age [Fig. 3.2D]. We assess the sampled clasts using modal mineralogy, plotting the granitoid clasts on an International Union of Geological Sciences quartz-alkali feldspar-plagioclase diagram [IUGS QAP diagram, Fig. 3.8]. This shows that the clasts we collected included quartz syenite, monzonite, granite, and granodiorite. Granitic rock standards [e.g., Westerly Granite] are considered "similar" based on their orthoclase/plagioclase ratios [Fairbairn, H. W., 1951]; 4/5 Shepherd Creek and 3/4 Lundy Canyon clasts show remarkably similar A/P percentages [$\sim$50-60% and 35-50% respectively], within the expected variability of Westerly Granite. The outlier clasts are of various ages [0 ka at Lundy Canyon and 76 ka at Shepherd Creek] and do not appear to explain slight outliers calculated of different time trends.

3.7 Discussion

This study provides evidence that rock compliance and porosity [Φ] increase following statistically significant trends over 10^5 years in natural subaerial conditions, while rock strength decreases. We conclude that progressive rock fracturing in response to environmental stresses [i.e., mechanical weathering] predominantly drives these changes. These results are broadly similar to rock property changes resulting from weathering experiments [de Vilder, S. J. and Brain, M. J. and Rosser, N. J., 2019; Riebe, Clifford S., Callahan, Russell P., Granke, Sarah B. M., Carr, Bradley

J., Hayes, Jorden L., Schell, Marlie S. and Sklar, Leonard S., 2021; Shobe, Charles M., Hancock, Gregory S., Eppes, Martha C. and Small, Eric E., 2017] which show decreased *UCS* and ρ, and increasing Φ after weathering. Here we begin to quantify the time periods over which these changes operate, demonstrating that measurable changes occur after less than 15 kyr in two different climates, and continue to occur after 76 kyr of exposure.

Neither *CIA* nor *CIW* vary consistently across depositional age at either site [p-values 0.22-0.62; Fig. 3.2D], suggesting that chemical weathering likely plays a minimal role in the mechanical property trends we observe. However, differences in the magnitude of physical properties between the two sites may be related to bulk mineralogical differences [Fig. 3.8], where Lundy Canyon clasts contain more quartz overall and, as might be expected [e.g., Cowie, S. and Walton, G., 2018], are stronger, less porous, and less compliant.

We test for evidence that differences in petrology are responsible for these trends [see Supplement S3.2]. If mineralogical or grain size differences were driving fracture behavior, past experimental results suggest that larger overall grain sizes would correlate with lower T and *UCS* [e.g., review in Lindqvist, J. E., Åkesson, U. and Malaga, K., 2007; Yu, Miao, Wei, Chenhui, Niu, Leilei, Li, Shaohua and Yu, Yongjun, 2018]. Although quartz content increases with older clasts at Shepherd Creek, it is statistically insignificant [p-value 0.28] and at Lundy Canyon quartz content remains constant. Grain size decreases slightly on older clasts [p-value 0.05] at Shepherd Creek, which could increase T and *UCS* [Lindqvist, J. E., Åkesson, U. and Malaga, K., 2007], but also increase [Janio de Castro Lima, José and Paraguassú, Antenor Braga, 2004] or decrease [Yin, Weitao, Feng, Zijun and Zhao, Yangsheng, 2021] thermal expansion. At Lundy Canyon, grain size remains relatively constant. Neither quartz content nor mean grain size cause statistically significant changes to *UCS* or T at Shepherd Creek or Lundy Canyon [$R^2 < 0.02$ and/or insignificant p-value].

3.7.1 Comparison to fracture data

At these exact sites and depositional surfaces, Rasmussen et al. [in preparation, Ch. 2] collected macrofracture data for 3699 visible fractures ≥2 cm in length from 1308 15-50 cm diameter granitoid clasts [Fig. 2.5]. At both sites, microfracture intensity increased dramatically upon initial exposure, then levelled off beyond ∼30 ka of exposure. Thus, the increase in measured macroscale cracks [Rasmussen et al., Ch. 2] and laboratory elasticity [this study] initially correlate, but laboratory elasticity of the clasts beyond ∼30 ka increases while visible field macrofractures do not.

To further investigate the source of our observed rock property changes, manual thin section fractography was performed on 5/6 of the middle site clasts. Consistent with macrocracks measured in the field [Rasmussen et al., in prep, Ch. 2; presented modified as Fig. 3.9A] microfracture intensity [sum fracture length normalized to area] increased after exposure [Fig. 3.9B]. The microfracture intensity continues to increase at a slower rate, following the macrofracture data. As microfractures increase, E_{stat} decreases linearly [Fig. 3.9C]. The micro and macrofracture metrics support the key conclusion of Rasmussen et al. [Ch. 2] which are verified by our laboratory measurements: that an increase in bulk rock compliance due to microfracturing allows the clasts to better accommodate stress, thus allowing the rate of macroscale fracturing to steadily decrease over exposure time .

A detailed look at rock property trends [Figs. 3.3, 3.4, 3.5, and 3.6] shows that outliers deviate from the trends for the 6 ka exposure age at Shepherd Creek [unusually low ρ but high Vp and thus E_{dyn}], the 21 ka exposure age clast at Shepherd Creek [high κ and Φ, low E_{stat} and E_{dyn}], and the 15 ka exposure age at Lundy Canyon [low κ, high ρ and UCS]. Geochemistry [Fig. 3.8] shows that the outlier clasts at Shepherd Creek contain less quartz than all other clasts at this site, and typical grain sizes. The Lundy Canyon 15 ka clast does not exhibit any grain size or mineralogical differences. The

outlier behavior may be due to microfracture alignments within individual samples, which can vary with core orientation and location within the boulder and impact elastic properties and strength. The samples may have had fractures internally which were not visible from the outside, so samples were not discarded. Despite these slight outliers, most rock property age trends are statistically significant, with 15 out of 21 age vs. property trends having best fit line p-values of <0.05, and R^2 of 0.34-0.99. These strong correlations support our conclusion that observed trends in rock mechanical properties are due to progressive rock cracking.

3.7.2 Limitations

Here we do not account for possible variability in paleoclimate conditions over time. Viles, Heather, Messenzehl, Karoline, Mayaud, Jerome, Coombes, Martin and Bourke, Mary [2018] and Warke, P. A. [2007] suggests that the stress that has been applied to a rock throughout its exposure history is critical to determining how the rock will weather in the future. Significant glacial/interglacial cycles are expected to have moderated weathering behavior at these sites, and clasts at both sites experienced similar relative changes in paleoclimate throughout the Quaternary [e.g., Bacon, Steven N., Jayko, Angela S., Owen, Lewis A., Lindvall, Scott C., Rhodes, Edward J., Schumer, Rina A. and Decker, David L., 2020]. However, the clasts studied here were deposited at different times at each site. If the conditions at the time of deposition were dictating how the clast subsequently weathered, the different sites where the clasts were deposited at different times would show different trends, yet they are similar.

Rock mineralogical and geochemical composition heterogeneity, even within a single rock formation, is unavoidable in field studies. Presumably, such variability could mediate evolving fracture growth and modify associated rock material properties. Such variability could also possibly lead to "survivor's bias" whereby clasts available for sampling only represent the "strongest" clasts in the assemblage. However, our

observed lack of age-related geochemical and mineralogical variability suggests that such a bias is not occurring for these granitoid rocks. Further, robust rock property trends exist at both sites, and the slopes of the trends are similar.

Finally, this study has focused only on loose clasts exposed at Earth's surface, significantly decreasing the potential impact of tectonic and topographic stresses on rock property evolution. In the near-surface, tectonic stresses act on rocks, and also result in stress concentrations due to topography [e.g., St. Clair, J., Moon, S., Holbrook, W. S., Perron, J. T., Riebe, C. S., Martel, S. J., Carr, B., Harman, C., Singha, K. and Richter, D. deB., 2015; Moon, S., Perron, J. T., Martel, S. J., Holbrook, W. S. and St. Clair, J., 2017]. As bedrock is exhumed by surface erosion, damage from the deep subsurface is expressed within rock through joint spacing and modifications to elasticity [e.g., Molnar, Peter, Anderson, Robert S., Anderson, Suzanne Prestrud, 2007]. Further, confining stresses are released as the rock is exhumed and can lead to fracture opening hundreds of meters in the subsurface [Moon, Seulgi, Perron, J. Taylor, Martel, Stephen J., Goodfellow, Bradley W., Mas Ivars, Diego, Hall, Adrian, Heyman, Jakob, Munier, Raymond, Näslund, Jens-Ove, Simeonov, Assen and Stroeven, Arjen P., 2020]. Although the data presented here are not measured from bedrock, weathering processes impact all rocks exposed at Earth's surface. It is therefore possible, if not likely, that the addition of tectonic stresses could enhance progressive rock fracture and thus the progressive change of rock properties.

3.7.3 Implications

These rock property trends provide quantifiable corrections of elastic properties for modeling and predicting rock behavior at Earth's surface. The implications of property changes must be considered when attempting to use surface-exposed rocks as proxies for subsurface behavior and can be considered a practical shift in the way we analyze and utilize laboratory data. These data are critical for near-surface geophysics and landscape evolution models, given their dependency on rock elastic

behavior, and thus geophysical response. This study focused on geologic timescales, but archaeological and restoration studies on granitoid rocks over hundreds of years [e.g., Fort, Rafael, Alvarez de Buergo, Monica and Perez-Monserrat, Elena M., 2013] provide abundant data for testing these trends over human timescales. Similar studies in different climates and/or lithologies, or using these younger data, would greatly help elucidate the drivers of weathering trends, and how universal our observations may be on and near Earth's surface.

The trends observed here are not a product of chemical weathering. Chemical and mechanical weathering proceed in tandem; however, in this study, mechanical weathering outpaces chemical weathering. Therefore, chemical weathering must in turn occur after cracking, making the connectivity of cracks, surface area of fresh rock exposed by cracks, and the likelihood of continued cracking a fundamental limiting factor of chemical weathering. Cracking studies must be considered when attempting to understand the rates of chemical weathering, and thus how Earth's carbon cycle proceeds [Brantley, S. L., Shaughnessy, Andrew, Lebedeva, Marina I. and Balashov, Victor N., 2023].

For landscape evolution, few studies consider mechanical and chemical processes with equal weight. One such study by Riebe, Clifford S., Callahan, Russell P., Granke, Sarah B. M., Carr, Bradley J., Hayes, Jorden L., Schell, Marlie S. and Sklar, Leonard S. [2021] attempts to disentangle chemical and mechanical weathering as the drivers of increasing bedrock porosity, and like our study, attributes a significant amount of porosity development to mechanical processes. However, the authors treat climate as a lever which shifts the balance of weathering towards chemically-dominated (warmer and/or wetter) or mechanically-dominated (cooler and/or drier). Instead, we suggest that climate is first considered as a fundamental driver of rapid mechanical weathering, as seen at these sites [Rasmussen et al., Ch. 2], which allows chemical weathering to follow.

This approach furthers our understanding of how low magnitude stresses operate beyond human timescales, providing geologists, material scientists, rock physicists, and engineers a more practical understanding of material fatigue and low-stress fracture mechanics. The theoretical concepts proposed as explanations for these trends should apply to all rock at and near Earth's surface, including bedrock. Therefore, bedrock fracture analysis, especially using near-surface rocks with known erosion and exhumation histories, is necessary for future work to connect this analysis to a wider range of geological applications.

3.8 Tables

Table 3.1: Number of samples per test for the Northern [N] site, Lundy Canyon, and the Southern [S] site, Shepherd Creek. Samples tested twice are indicated as duplicates by parenthesis []. *The age of the sample N_15 was calculated using ^{10}Be. Other samples were dated by previous researchers using ^{10}Be dating of large boulders along the same geomorphic surface [Rood, Dylan H., Burbank, Douglas W. and Finkel, Robert C., 2011; D'Arcy, Mitch. Roda Boluda, Duna C.. Whittaker, Alexander C. and Carpineti, Alfredo, 2015; Blisniuk, Kimberly Diem Chi, 2011; Dühnforth, Miriam, Anderson, Robert S., Ward, Dylan and Stock, Greg M., 2010].

Site age [ka]*	Permeability [κ]	Porosity [Φ]	Density [ρ]	Tensile strength [T]	Compressive strength [UCS]	Velocity [Vp, Vs]	Bulk geo-chemistry	Thin section mineralogy
N_0	1	11	4	9	3	6 [1]	2	2
N_15*	2 [1 no flow]	7	6	6	2	4	2	2
N_18	1	9	5	6	3	11 [3]	2	2
N_148	1	4	7	3	2	2 [1]	1	3
S_0	1	3	2	11	6	9 [1]	0	2
S_6	1	2 [1]	7	7	3	6	1	1
S_21	2	3	3	4	2	1	1	1
S_33	1	3 [1]	9	8	3	8	0	1
S_76	1	2 [1]	6	8	2	5	1	1
S_117	1	4 [1]	3	5	2	2	2	1

Table 3.2: Power-law trend fits and statistics for rock properties over time, equation format y = Ax^k. P-values shown are two-tailed p-values.

Site	Indep. variable	Dep. variable	A	K	R^2	p-value
Northern	surface age	*CIW*	70.10	$6*10^{-5}$	0.04	0.81
Southern	surface age	*CIW*	69.57	$3*10^{-4}$	0.20	0.55
Northern	surface age	*CIA*	58.86	$-1*10^{-4}$	00.23	0.52
Southern	surface age	*CIA*	58.88	$-3*10^{-4}$	0.60	0.23
Northern	surface age	κ	$1*10^{-19}$	0.01	00.23	0.00
Southern	surface age	κ	$3*10^{-18}$	0.04	0.05	0.78
Northern	surface age	Φ	0.40	0.01	00.79	0.00
Southern	surface age	Φ	0.87	0.01	0.67	0.00
Northern	surface age	ρ	02.68	$-3*10^{-4}$	00.71	0.00
Southern	surface age	ρ	2.65	$-3*10^{-4}$	0.60	0.00
Northern	surface age	*UCS*	119	$-6*10^{-3}$	0.03	0.00
Southern	surface age	*UCS*	163	$-2*10^{-3}$	0.29	0.11
Northern	surface age	*T*	14.63	$1*10^{-3}$	0.14	0.12
Southern	surface age	*T*	9.26	$-4*10^{-3}$	0.35	0.00
Northern	surface age	*Vp*	4984	$-2*10^{-3}$	0.71	0.00
Southern	surface age	*Vp*	4112	$-3*10^{-3}$	0.63	0.00
Northern	surface age	*Vs*	2957	$-3*10^{-3}$	0.36	0.00
Southern	surface age	*Vs*	2349	$-3*10^{-3}$	0.44	0.00
Northern	surface age	E_{stat}	23.16	$-2*10^{-3}$	0.72	0.01
Southern	surface age	E_{stat}	31.58	$-1*10^{-2}$	0.45	0.03
Northern	surface age	E_{dyn}	55.00	$-4*10^{-3}$	0.41	0.00
Southern	surface age	E_{dyn}	37.21	$-7*10^{-3}$	0.65	0.00
Southern	surface age	ν_{stat}	0.30	$-8*10^{-3}$	0.42	0.08
Northern	surface age	ν_{dyn}	0.18	$3.6*10^{-3}$	0.03	0.46
Southern	surface age	ν_{dyn}	0.20	$2.2*10^{-3}$	0.05	0.32

3.9 Figures

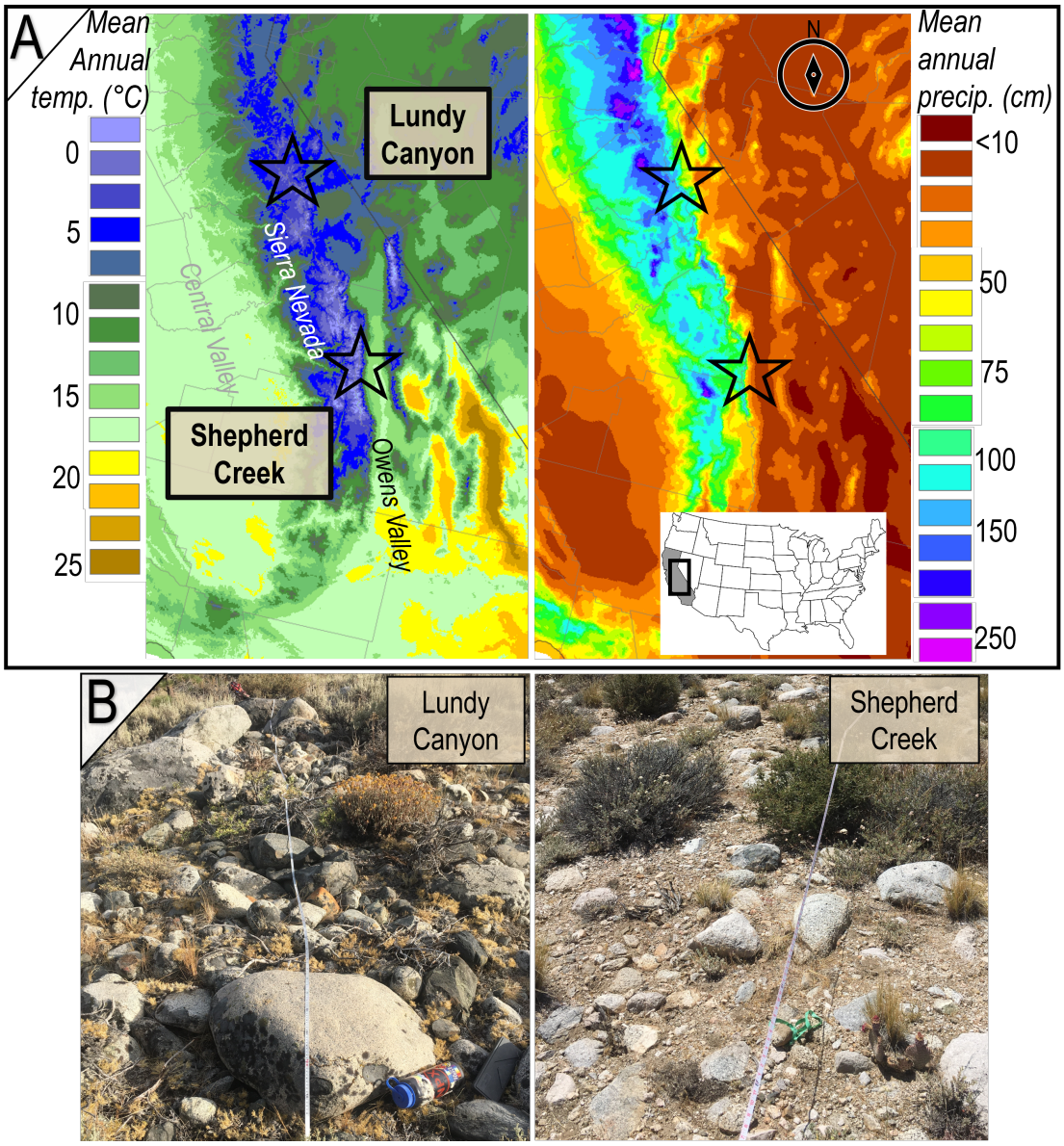

Figure 3.1: A. Mean annual temperature [left] and precipitation [right] for 1990-2020 with Lundy Canyon and Shepherd Creek sites starred. Center of open circles represents site locations. Maps modified from PRISM Climate Group, Oregon State University [2024]. B. Visual examples of boulder bar formations on ∼18 ka surface [left, Lundy Canyon] and ∼33ka surface [right, Shepherd Creek].

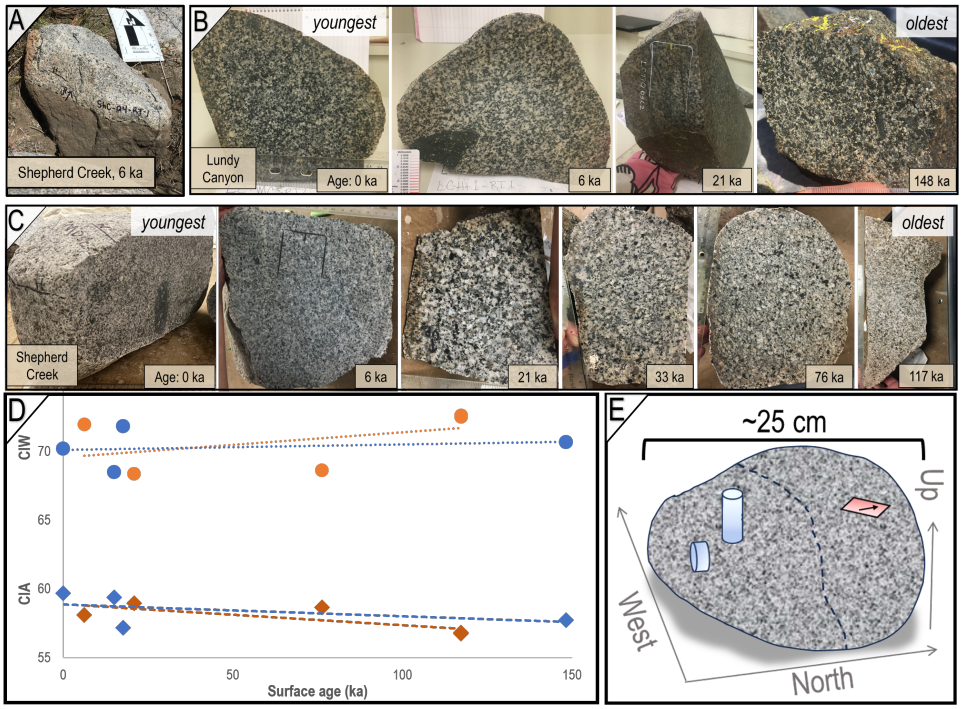

Figure 3.2: A. In situ boulder with field markup and North arrow; note arrow is 20cm long. Boulder was partially buried and soil stain is still visible where the base of the boulder has been exposed through digging. B. Lundy Canyon and C. Shepherd Creek boulder interiors shown after cutting in half, with increasing exposure age from left to right. Boulders are air dry. Note the slightly increased grain size in the Shepherd Creek ~21 ka boulder, and weathering rind development in, e.g., the outer edges of the Shepherd Creek ~76 ka boulder. D. Ternary diagram from bulk geochemistry showing the range of boulders sampled, identical to those visualized in B-C. E. Cartoon schematic of sample preparation per boulder. Dashed line indicated a common initial cutting plane, with the result visualized in B-C. Blue cores represent Brazil disk samples [horizontal] and *Vp*, *Vs*, and *UCS* samples [vertical]. Red rectangle represents surface-parallel thin section at 1.5cm depth into the rock. All samples were prepared inside the boulder, avoiding the outer weathering rind.

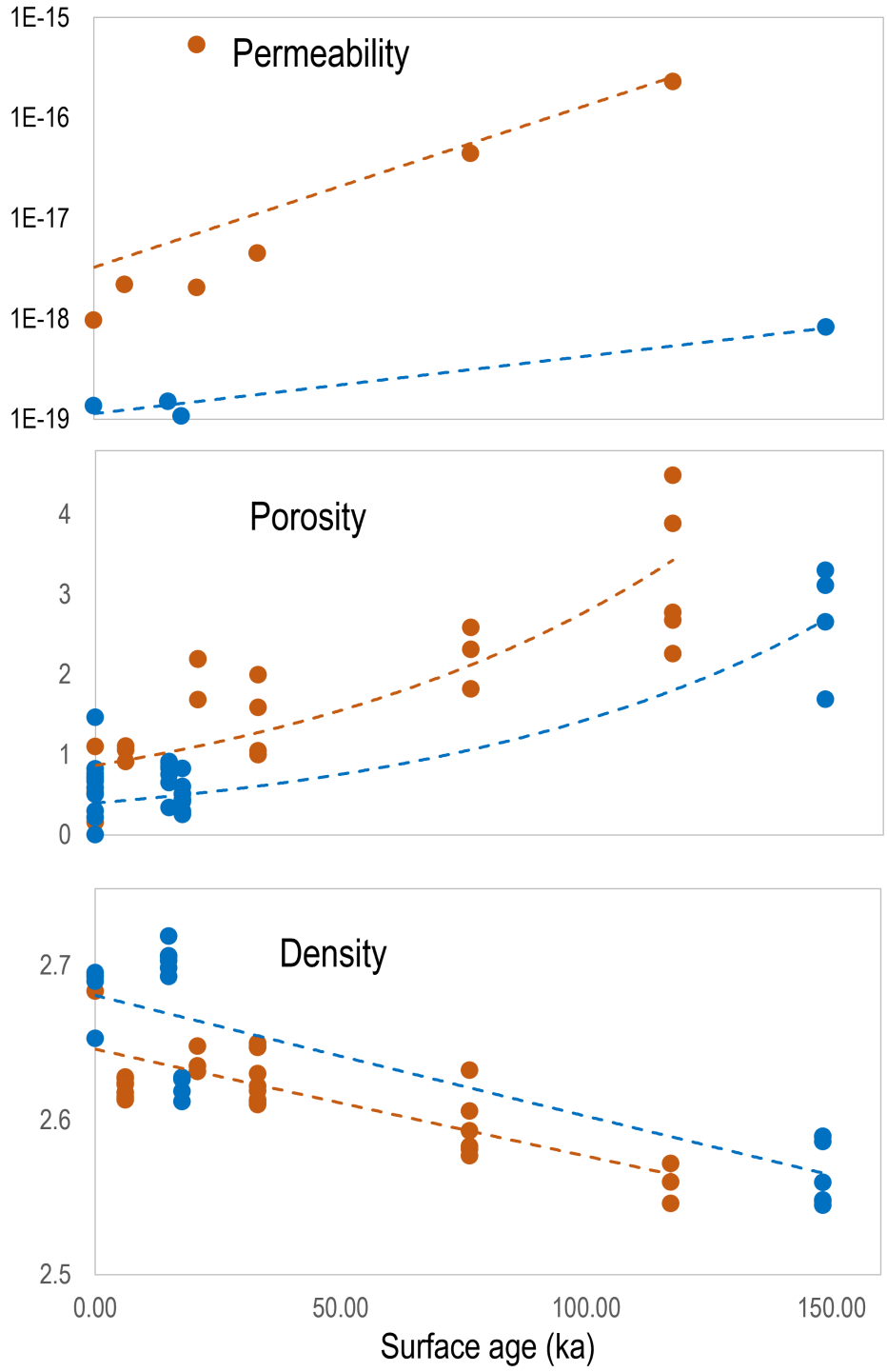

Figure 3.3: All permeability, porosity, and density measurements plotted as a function of rock exposure age, with exponential best-fit curves displayed as dashed lines; their equations are described in Table 3.2. Lundy Canyon data are shown in blue and Shepherd Creek are shown in orange.

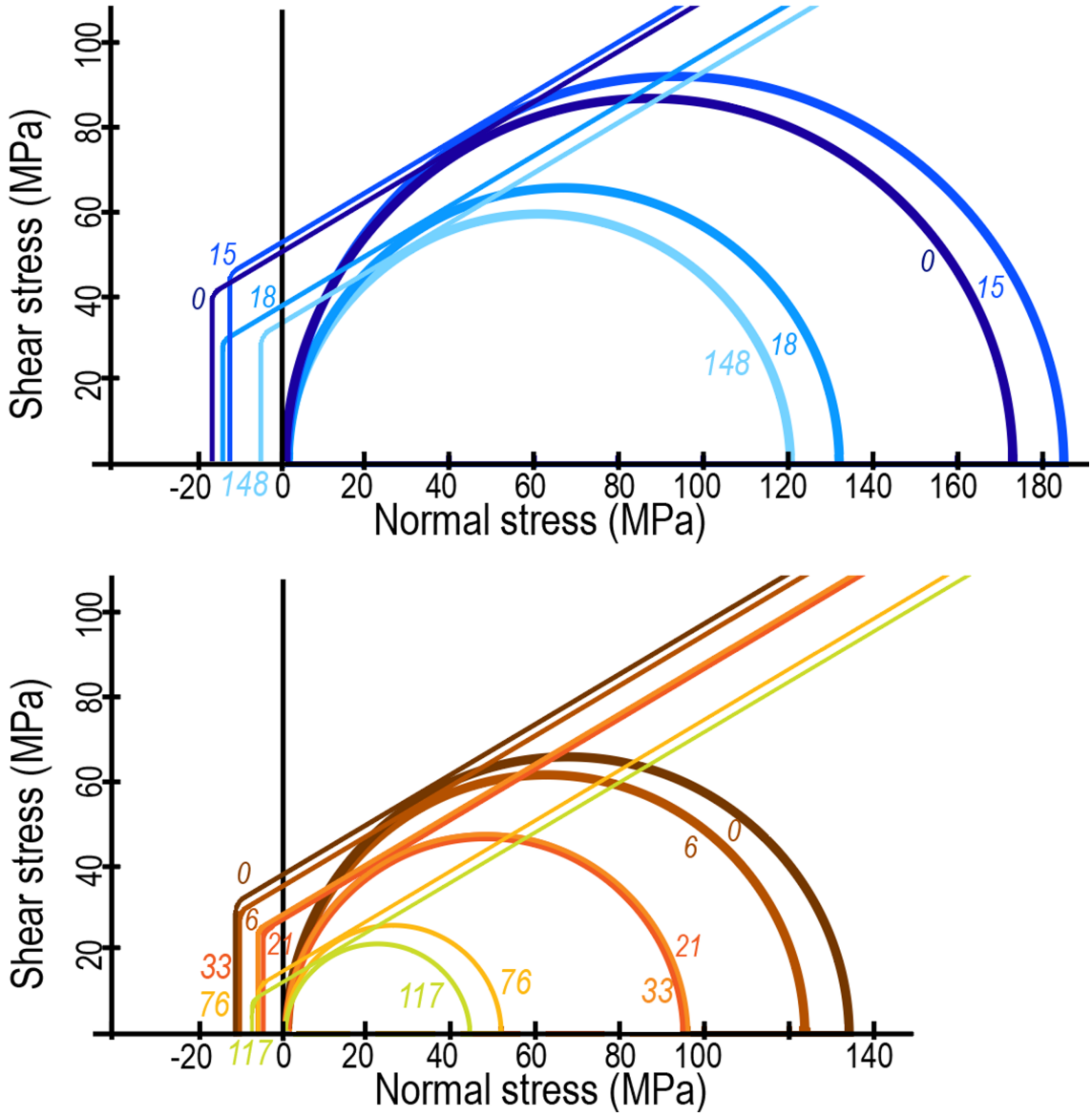

Figure 3.4: Mohr Coulomb plot of normal stress [x-axis] vs. shear stress [y-axis] plotted using a failure envelope slope of 0.6, with positive stress for compression. The mean UCS values from all tests per boulder are plotted as σ_1, and mean T is plotted as the tensile strength [negative stress]. Surface ages in kyr are indicated as color-coordinated labels next to circles and failure envelopes, with the darkest colors representing the youngest rocks.

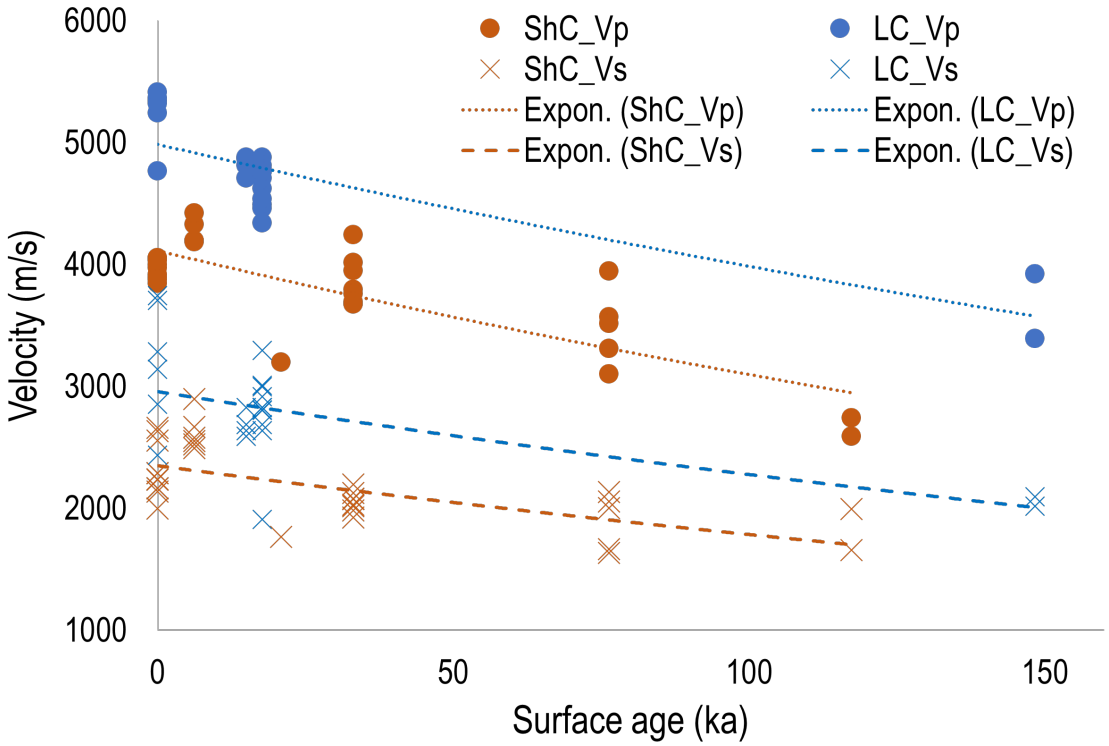

Figure 3.5: Compressional [Vp] and shear [Vs] velocities of all samples at both sites plotted relative to the surface or rock exposure age [ka]. Exponential fits are shown as dashed lines, and equation variables are included in Table 3.2.

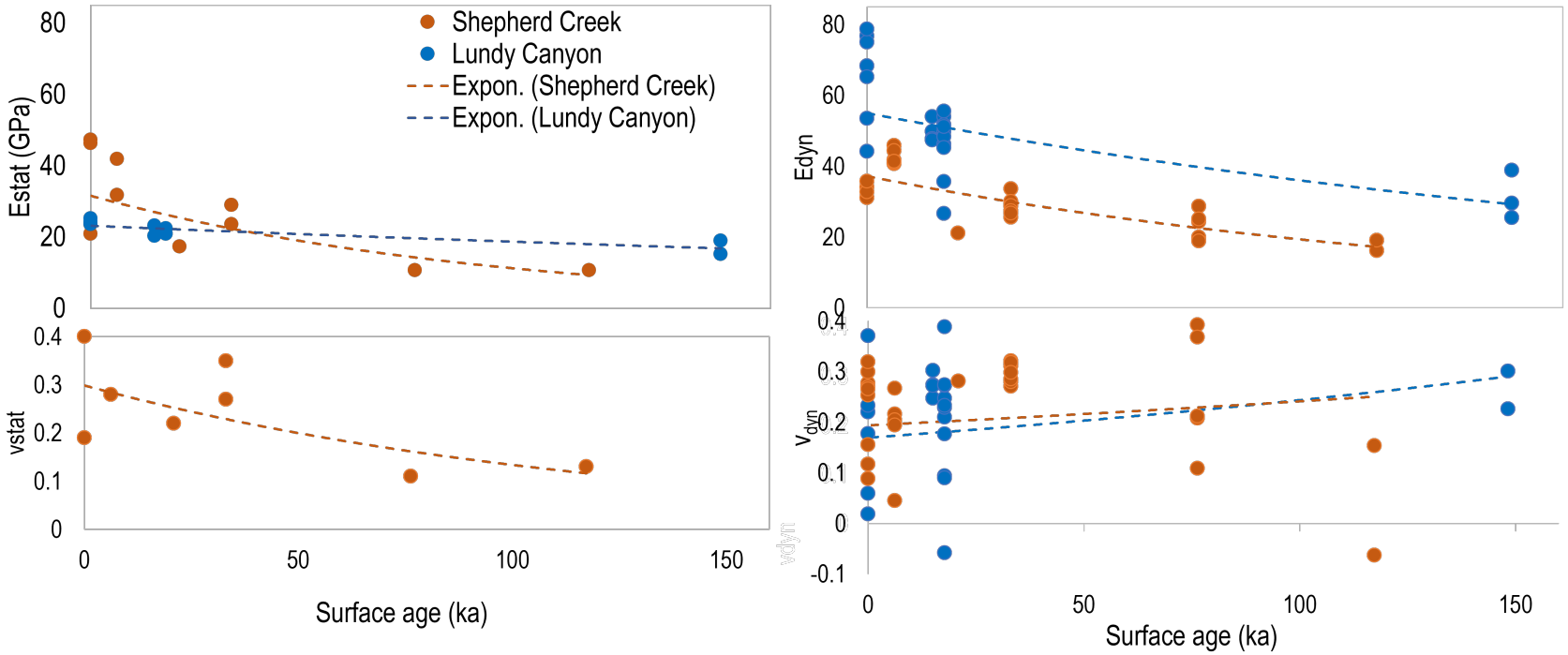

Figure 3.6: All E_{stat}, ν_{stat}, E_{dyn}, and ν_{dyn} data from both sites, plotted as a function of rock exposure age, with exponential best-fit curves displayed as dashed lines; their equations are described in Table 3.2. Lundy Canyon data are shown in blue and Shepherd Creek are shown in orange.

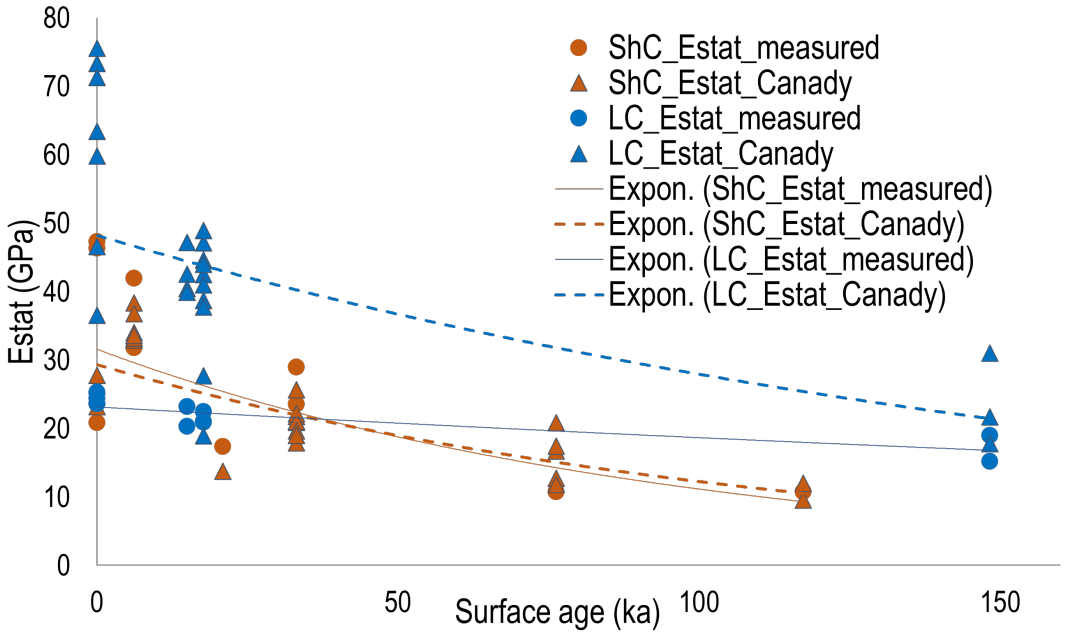

Figure 3.7: E_{stat} for both sites, with measured values [circles] calculated before failure during *UCS* testing, from the linear stress-strain relationship as loading increased. Lundy Canyon data are shown in blues and Shepherd Creek are shown in oranges and yellows. Exponential best-fit curves are displayed as dashed lines; their equations are described in Table 3.2. The triangles are calculated values using an established relationship by Canady, Wyatt [2011], deriving E_{stat} from E_{dyn}.

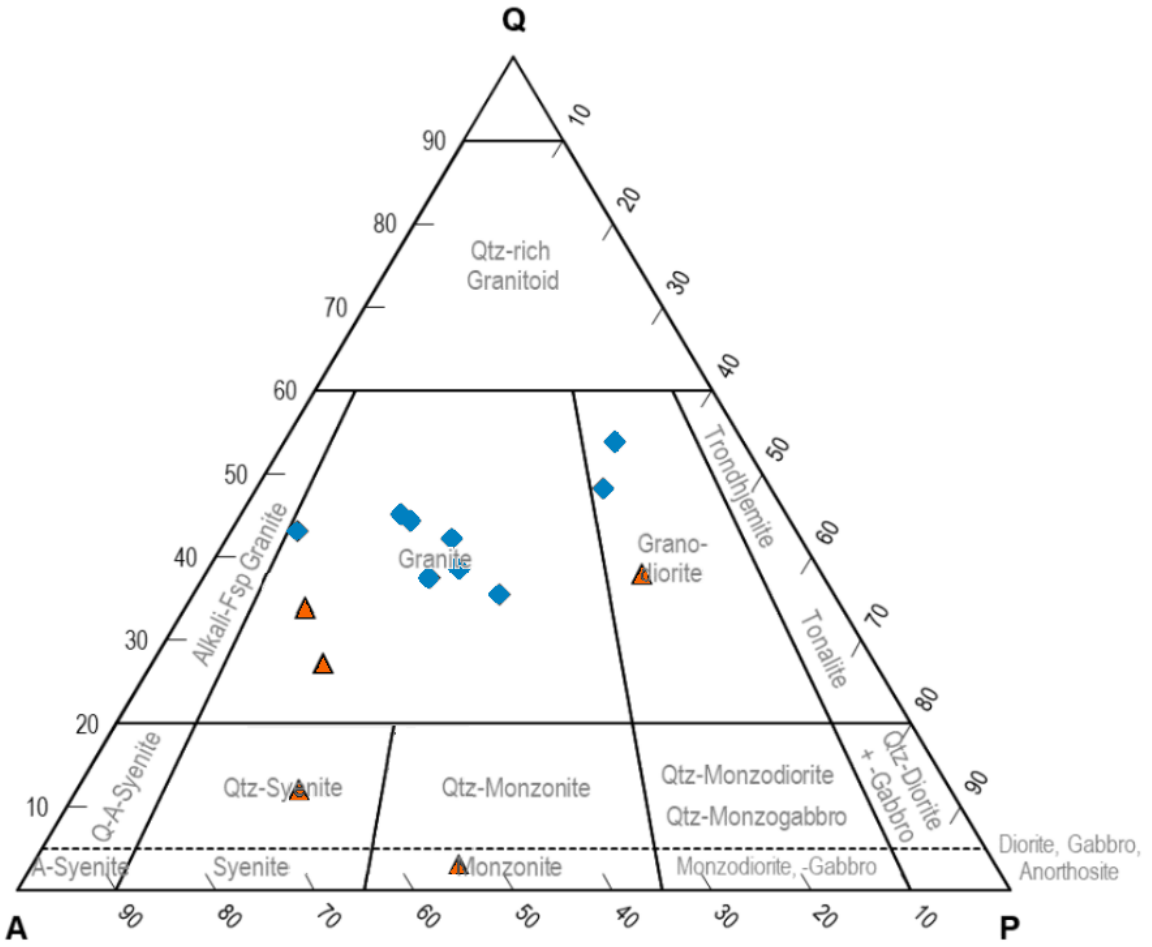

Figure 3.8: IUGS classification [ternary diagram] from bulk geochemical analysis showing the range of boulders sampled, with the boulder age displayede with each point. Orange triangles are from Shepherd Creek and blue diamonds are from Lundy Canyon.

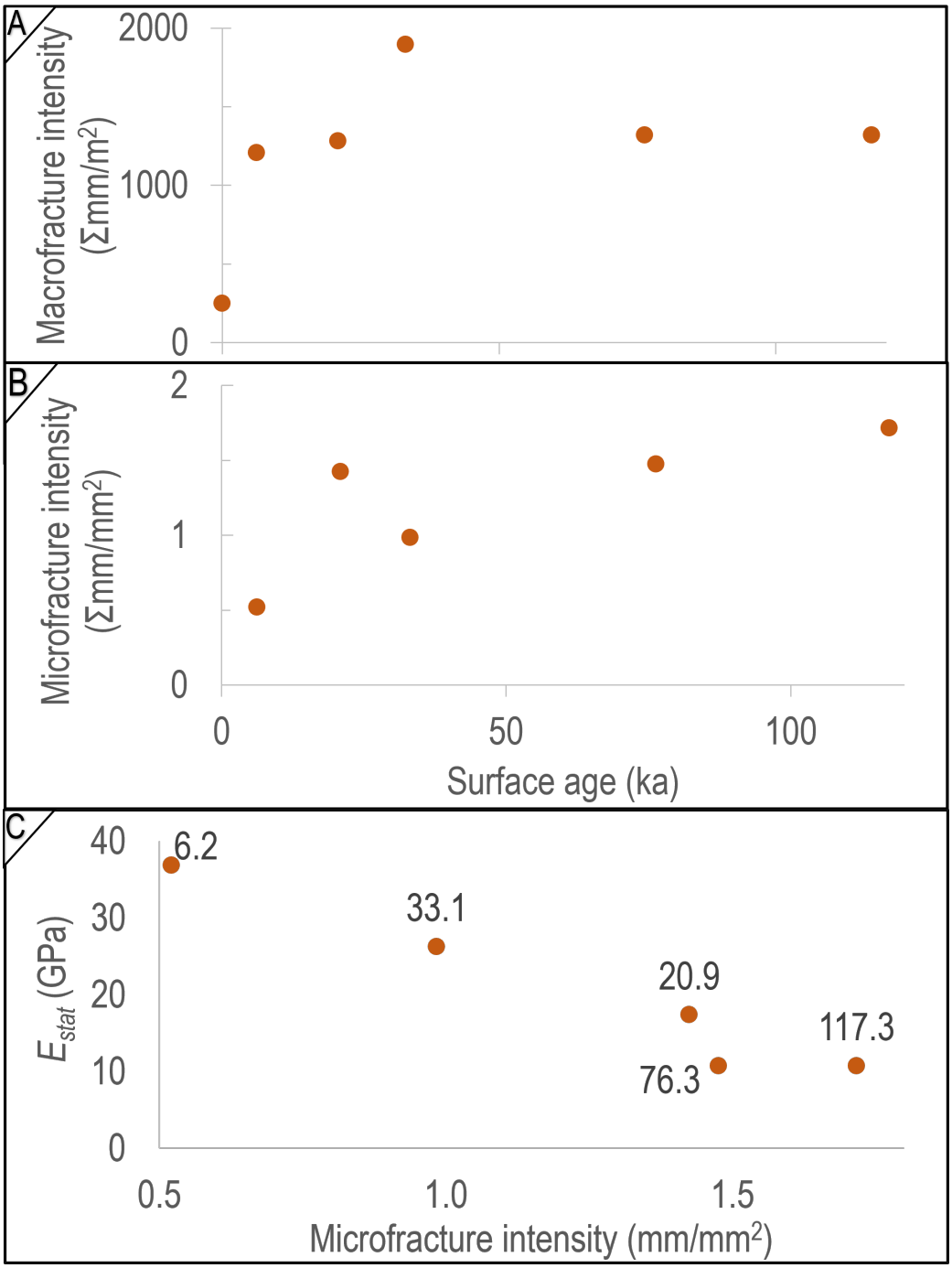

Figure 3.9: Macrofracture intensity average from multiple clasts measured in the field at the Shepherd Creek site [modified from Rasmussen et al., in prep, Ch. 2], compared with B: microfracture intensity from manually mapped fractures in thin section from clasts collected from the same Shepherd Creek surfaces [this study]. C: Microfracture intensity plotted relative to the mean E_{stat} values from all measurements of those clasts. Points are annotated with surface ages [ka].

CHAPTER 4: EXPLORING THE IMPACTS OF WEATHER ON CLIMOSEQUENCES OF ROCK CRACKING

AUTHORS:

Monica Rasmussen, Brian Magi, Philip G. Meredith, Yoshitaka Nara, and Martha Cary Eppes

4.1 Abstract

Rocks and landscapes can respond catastrophically to extreme weather events, leading to landslides, cliff failures, and other rapid erosional events. Yet long-term, gradual processes are also responsible for major geologic features and events like the formation of sinkholes, carving steep-sided canyons, and development of aeolian dune fields. As a precursor to these erosive and sedimentary events, intact bedrock must be converted into disconnected, mobile regolith. This occurs through mechanical weathering [rock cracking], and erosion from the solid bedrock mass. Rock cracking can occur in response to large magnitude stochastic stress events, e.g., an unusually warm [Leith, Kerry, Perras, Matthew, Siren, Topias, Rantanen, Tuomas, Heinonen, Suvi and Loew, Simon, 2017] or wet day [Delonca, A., Gunzburger, Y. and Verdel, T., 2014], or more frequent low magnitude stresses like diurnal heating and cooling [e.g., Collins, Brian D. and Stock, Greg M., 2016; Eppes, Martha Cary, Magi, Brian, Hallet, Bernard, Delmelle, Eric, Mackenzie-Helnwein, Peter, Warren, Kimberly and Swami, Suraj, 2016].

When geoscientists conceptualize the impact of climate on weathering, long-term processes are frequently the focus, with mean annual temperature and precipitation being used as the primary climate variables. Using field data, Eppes, Martha Cary, Magi, Brian, Hallet, Bernard, Delmelle, Eric, Mackenzie-Helnwein, Peter, Warren, Kimberly and Swami, Suraj [2016] show that daily weather events like rainfall and temperature flux [the daily range of air temperatures] can drive rock cracking events,

as indicated by acoustic emissions measured from boulders left on Earth's surface throughout the year. However, modeling by Eppes, Martha-Cary and Keanini, Russell [2017] show that long-term rock cracking can be highly variable, with cracking rates varying by multiple orders of magnitude based on changes in daily average conditions. Given that many Earth surface processes proceed over geologic timescales and cannot be directly observed, our understanding of the balance between these two drivers of rock fracture is poorly constrained, and difficult to disentangle in the geologic record.

Here I use single-crack growth modeling to estimate the dependence of granitoid rock cracking on daily weather events. I calibrate an existing intergranular thermal stress model [Eppes, Martha-Cary and Keanini, Russell, 2017] with rock properties from boulders in Eastern California [Rasmussen et al., Ch. 3] using environmental conditions measured by local weather stations at these same locations. I then model daily crack growth using available modern records of daily temperature flux and moisture conditions that vary with the weather. As a comparison, I also model the crack growth that would occur if the variability of weather was ignored, and instead the temperature flux and moisture were representative of the average daily conditions [i.e., climate].

I find that repeating the average daily temperature flux - an approach following the typical geologic assumption that climate is represented by long-term mean annual conditions - only results in substantial crack growth when the stiffest, or least compressible, rock properties are used. Only by adding daily variability, including the most extreme events recorded by hourly weather station data, can I use more representative rock properties to simulate crack growth that results in pieces of rock breaking off of boulders. Comparing these models with field crack length measurements [Rasmussen et al., Ch. 2] and clast size data [Rasmussen et al. Ch. 6] that show that substantial cracking does indeed disaggregate pieces of rock over similar timescales, indicates that stochastic daily weather events should be considered in

order to produce the amount of cracking and rock erosion observed.

4.2 Introduction and Background

The debate between catastrophism and uniformitarianism is one of the oldest in the history of Geology, starting with biologist and paleontologist Georges Cuvier's arguments for catastrophism in the natural world [Ouchterlony, Finn, 1982] and countered by the now widespread notion of uniformitarianism presented by James Hutton, James [1899]. Modern interpretations are more nuanced, recognizing a balance between 'catastrophic' natural events that have dramatically altered landscapes before human observation, and the gradual, 'uniform' daily conditions that modify the environment [e.g., Baker, Victor R., 1998]. Given the difficulty of predicting the magnitude and timing of catastrophic events, it is unsurprising that in the absence of evidence of such events, geologists apply uniformitarianism principles.

However, storm events are known to drive a disproportionate amount of geomorphological change, whether it is through increased sediment supply to rivers [e.g., Page, M. J., Trustrum, N. A. and DeRose, R. C., 1994], mass wasting [e.g., Yellen, Brian, Woodruff, Jonathan D., Cook, Timothy L., Newton, Robert M., 2016], rockfalls [e.g., Westoby, Matthew, Lim, Michael, Hogg, Michelle, Dunlop, Lesley, Pound, Matthew, Strzelecki, Mateusz and Woodward, John, 2020; Collins, Brian D. and Stock, Greg M., 2016], fan aggradation [e.g., Miller, David M., Schmidt, Kevin M., Mahan, Shannon A., McGeehin, John P., Owen, Lewis A., Barron, John A., Lehmkuhl, Frank and Löhrer, Rene, 2010], river incision [e.g., Watanabe, Masaru, Saito, Masashi, Toda, Kenichiro and Shirasawa, Hiroaki, 2023], and landslides or debris flows [e.g., DeGraff, Jerome, Wagner, David L., Gallegos, Alan J., DeRose, Margie, Shannon, Casey and Ellsworth, Todd, 2011]. Such storm events can be so efficacious in landscape modification that they overwhelm the geologic record and daily, incremental changes due to 'gradual' conditions are unnoticeable and catastrophism dominates [Stephen G. Smith, Karl W. Wegmann, Elana L. Leithold and Delwayne R. Bohnenstiehl, 2019].

Other dramatic environmental events like fire, lightning, and freezing cause geomorphic change through fast, critical cracking [fracturing], where the stress caused by such events exceeds the tensile strength of the rock [Blackwelder, Eliot, 1925]. When considering the effect of moisture on rock cracking, pore pressure is a substantial driver that has been widely shown to cause rock slope failure due to its ability to decrease overall stress conditions and intensify stress differential along a failure plane [Hillis, Richard R., 2003; Terzaghi, Karl, 1943; Mohr, Otto, 1900, 1928]. Even under conditions where the rock is not fully saturated, slow, subcritical rock cracking can dominate mechanical weathering of rocks over geologic timescales [Eppes, Martha-Cary and Keanini, Russell, 2017; Stock, Greg M., Collins, Brian D., Santaniello, David J., Zimmer, Valerie L., Wieczorek, Gerald F. and Snyder, James B., 2013] and is dependent on environmental conditions like temperature, moisture, and water chemistry [Atkinson, Barry Kean and Meredith, Philip George, 1987a]. Few field studies have directly tied environmental conditions to rock failure in wet but not fully saturated rocks [Eppes, Martha Cary, Magi, Brian, Hallet, Bernard, Delmelle, Eric, Mackenzie-Helnwein, Peter, Warren, Kimberly and Swami, Suraj, 2016; Collins, Brian D. and Stock, Greg M., 2016; Collins, Brian D. and Sitar, Nicholas, 2008], and most studies focus only on the impact of rain events on bedrock failure [e.g., Young, Adam P., Guza, R. T., Flick, R. E., O'Reilly, W. C. and Gutierrez, R., 2009; Jones, E.C. Vann, Rosser, N. J., Brain, M. J. and Petley, D. N., 2015].

In laboratory studies [e.g., Nara, Yoshitaka, Yamanaka, Hiroshi, Oe, Yuma and Kaneko, Katsuhiko, 2013; Nara, Y., 2015; Nara, Yoshitaka. Harui, Tomoki and Kashiwaya, Koki, 2018, and data compiled by Atkinson and Meredith, 1987] of various lithologies, increasing the relative humidity and/or temperature conditions during subcritical crack growth tests decreases the stress required to propagate a crack. In other words, when stresses are below the critical strength of a rock, crack growth is faster in warmer and wetter conditions. To test if this impacts rocks in natural

environments, Eppes, Martha Cary, Magi, Brian, Hallet, Bernard, Delmelle, Eric, Mackenzie-Helnwein, Peter, Warren, Kimberly and Swami, Suraj [2016] conducted a years-long study measuring acoustic emissions, a proxy for rock cracking, emitted from loose boulders resting on the ground surface in New Mexico and North Carolina. In addition to acoustic emissions, they collected weather data adjacent to the boulder at one-minute intervals. An updated analysis of these data by Eppes, M. C., Magi, B., Scheff, J., Warren, K., Ching, S. and Feng, T. [2020] showed that the most significant cracking events correlated with times of rapid air temperature change [dT] and high vapor pressure [VP] conditions. While relative humidity [RH] is typically employed to represent 'moisture' in laboratory studies, the correlation with cracking was stronger when considering VP, which is influenced by both RH and temperature. While the importance of air temperature flux is a known variable impacting weathering due to its ability to induce stress within a rock mass [Sumner, P. D., Nel, W. and Hedding, D. W., 2004], the impact of 'moisture' in field studies is generally represented through precipitation, thus missing a critical variable impacting rock cracking. The most ubiquitous daily stressor is diurnal heating and cooling due to this insolation. In addition to cooling or heating the rock, as shown in laboratory analysis by [Nara, Yoshitaka, Yamanaka, Hiroshi, Oe, Yuma and Kaneko, Katsuhiko, 2013, and others,], increasing 'moisture' itself can also decrease the rock's resistance to breaking.

Surface process geoscientists and soil scientists can approximate the impact of temperature and moisture on Earth surface processes using climosequences [Jenny, Hans, 1948; Birkeland, Peter W., 1999], a series of different sites where the most significantly different site variable is the climate. The most widely available climate variables are mean annual temperature [MAT] and mean annual precipitation [MAP], which can be easily calculated with historical weather data collected over decades [e.g., 30 year means calculated by PRISM Climate Group, Oregon State University, 2024], and

thus represent reasonable estimates of long-term conditions. Therefore, MAT and MAP are the de facto variables used for understanding the climate of a given study site. However, based on the aforementioned field data collected from boulders [Eppes, Martha Cary, Magi, Brian, Hallet, Bernard, Delmelle, Eric, Mackenzie-Helnwein, Peter, Warren, Kimberly and Swami, Suraj, 2016], MAT and MAP may not be the most relevant variables when studying any given Earth surface process, particularly those that, like rock fracture, are non-linearly dependent on temperature flux dT and vapor pressure VP at the crack tip.

MAT and MAP are frequently employed partially because estimating the likelihood and magnitude of rare weather events remains challenging even with the best climate models, and the geomorphic impact of such events is further complicated by climate-dependent events like fires [see review in East, Amy E. and Sankey, Joel B., 2020]. Approaches for understanding the frequency of extreme events include paleotempestology [e.g., Page, M. J., Trustrum, N. A. and DeRose, R. C., 1994], mapping and dating of geologic materials deposited during energetic transport events [e.g., Miller, David M., Schmidt, Kevin M., Mahan, Shannon A., McGeehin, John P., Owen, Lewis A., Barron, John A., Lehmkuhl, Frank and Löhrer, Rene, 2010], paleolake sedimentology and coring [e.g., Reheis, Marith C., Adams, Kenneth D., Oviatt, Charles G. and Bacon, Steven N., 2014], and statistical extreme event analysis [e.g., Bellprat, Omar, Guemas, Virginie, Doblas-Reyes, Francisco and Donat, Markus G., 2019]. Here, as a simple first-look analysis, I use historical weather station data to investigate the impacts of yearly to decadal weather events on one type of subcritical rock cracking: grain disaggregation from the rock surface resulting from stresses imposed by grain-grain thermal expansion and contraction. Weather station data capture both decadal-scale 'extreme' storms, and also represent the uniformitarianism principle that we can use the present data to interpret how climate impacted rock cracking in the past.

I model rock cracking over geologic time at three sites of different climates using real weather data to derive dT and VP, where the impact of temperature on stress is calculated using daily dT and the impact of temperature and RH on crack propagation is captured by VP. If rare weather events drive subcritical rock failure over timescales beyond human observation, then our understanding of the impact of climate on rock mechanical weathering must consider not only historical daily dT and VP, but also the daily weather conditions that have occurred over thousands of years and are reflected in the current geologic record. This represents a realistic combination of uniformitarianism and catastrophism that will help inform our interpretation of 'climate' as a variable in rock mechanical weathering.

4.3 Modeling methods

Any stress applied to a rock can cause cracking, regardless of the cause or causes. Broadly, rock cracking can be conceptualized as two different processes: whole-rock fracture due to bulk stresses within the entire rock mass [e.g., stresses modeled by Molaro, J. L., Byrne, S. and Le, J. L., 2017, and Collins and Stock, 2016], and grain-scale fracture resulting from grain-grain stresses arising due to a differential strain response between two grains of differing mineralogy and/or orientation [e.g., Vázquez, Patricia, Shushakova, Victoria and Gómez-Heras, Miguel, 2015]. Bulk rock stresses can result from daily temperature cycles, with the solar angle changing throughout the day and warming the rock from different directions at different times [Eppes, Martha Cary, McFadden, Leslie D., Wegmann, Karl W. and Scuderi, Louis A., 2010]. This complex warming and cooling is dictated by rock size, shape, and thermal properties [Molaro, J. L., Byrne, S. and Le, J. L., 2017], and leads to expansion and contraction that changes throughout the day.

As a first approach to assessing the impact of dT and VP on rock cracking over geologic time, a simpler grain-grain stress model developed by Eppes, Martha-Cary and Keanini, Russell [2017] is applied here. Grain-grain stresses result from expansion

and contraction of mineral grains due to temperature or moisture changes. Because nearly all rocks on Earth's surface are exposed to solar radiation on a daily basis, the most ubiquitous daily stressor is diurnal heating and cooling due to this insolation. Therefore, this model estimates a grain-grain stress that results from daily temperature flux. This model does not consider bulk rock expansion and contraction, therefore it is most applicable for understanding the disaggregation of grain-scale pieces of rock off of a larger rock mass.

4.3.1 Site selection

I test the impact of weather on crack growth of granitoid rocks at three field sites in Eastern California that represent a traditional 'climosequence' [Jenny, Hans, 1948] that is used to understand the impact of climate on rock weathering and soil development. At these sites, rock mechanical properties, microscale rock cracking, and macroscale rock cracking were previously studied as they changed over geologic timescales up to 148 kyr [Rasmussen et al., Ch. 2 and 3]. All sites contain granitoid rocks, so for site comparison, the modeling here considers only granitoid rock types. The Northernmost site represents the coolest [lowest MAT], the Middle site is warmer, and the Southernmost site is the warmest. The sites also follow a precipitation gradient with the coolest Northernmost site being the wettest [highest MAT], the Middle site being drier, and the Southernmost site being the driest [see Table 4.1]. After modeling is performed at these sites, I compare the model results with the real cracking [Rasmussen et al., Ch. 2] and clast size trends [Rasmussen et al., Ch. 6] of granitoid rocks, validating model outputs.

4.3.2 Crack growth modeling due to grain-grain stresses

Crack growth [Δa] can be modeled using Charles' law for a single crack experiencing static stresses [Eq. 4.1; Charles, R. J., 1958] and/or Paris' law for crack growth over

a number N of stress cycles [$\Delta a/N$] [Eq. 4.2; Paris, P. C. and Erdogan, Fazil, 1963].

$$\Delta a = A * {K_\mathrm{I}}^n \tag{4.1}$$

$$\Delta a/N = C * {\Delta K_\mathrm{I}}^m \tag{4.2}$$

Here, A and C are climate- and lithology-dependent parameters, K_I is the mode-I [tensile crack] stress intensity at the crack tip, ΔK_I is the magnitude of stress intensity change over each stress cycle N, n is the climate- and lithology-dependent subcritical cracking index, and the exponent m can be regarded as a similar subcritical cracking index to n [see equivalence proposed in Eppes, Martha-Cary and Keanini, Russell, 2017, and shown experimentally by Ko and Lee, 2020]. Diurnal thermal stresses most closely align with cyclical crack growth, therefore Paris' law [Eq. 4.2] is employed here. I follow the workflow shown in Fig. 4.1, first calculating stress from rock and weather data, then crack stress intensity as a function of initial crack length, then crack growth with Paris' law [Eq. 4.2] due to the calculated daily stress, then repeating the process the next day with the new stress and crack length.

Diurnal temperature flux [dT, °C] is derived from the hourly weather data, and bulk Young's modulus [E] and Poisson's ratio [ν] values are derived from *UCS* laboratory testing previously performed by Rasmussen et al. [Ch. 3]. Specific parameters are presented in section 4.4.2 and Table 4.2. Following Eq. 4.3 from Eppes, Martha-Cary and Keanini, Russell [2017], I calculate the diurnal intergranular stress magnitude for each day of crack growth, using the full range of potential thermal expansion differentials [α] between quartz and feldspar, daily dT, and various elastic properties from real rocks, using Eq. 4.3. The derivation of this equation is provided in Appendix C of Eppes, Martha-Cary and Keanini, Russell [2017].

$$\sigma = [dT * E * \alpha]/[1 - \nu] \tag{4.3}$$

Here, I use air temperature as a proxy for the temperature of the rock surface. While rock surface temperature is a more relevant variable for estimating stress within the rock, air temperature is a more commonly available metric and is thus more useful for broad application. Implications of this and other assumptions are addressed in the Discussion.

The calculated σ is next converted into a crack-tip stress intensity K_{I} [MPa $\sqrt{m}$] following the work of Irwin, George R. [1957] [Eq. 4.4].

$$K_{\mathrm{I}} = \sigma \sqrt{\pi [0.5 * a]} \tag{4.4}$$

As shown above, stress intensity – and thus crack growth – is dependent not just on the stress magnitude itself, but also on the crack length. For this model, the initial crack [flaw] length is estimated following the Ashby, M. F. and Sammis, C. G. [1990] model extended by Chandler, Michael R., Mecklenburgh, Julian, Rutter, Ernest and Lee, Peter [2019], using uniaxial compressive strength [UCS] from Rasmussen et al. [Ch. 3] and fracture toughness [K_{IC}] tests performed on the same rocks. Fracture toughness data and crack length derivation is described in section 4.4.3.

4.4 Modeling variables

4.4.1 Meteorological data

I use the closest weather stations available to the exact study sites from both public [Western Regional Climate Center: WRCC, 2023] and private sources [Kelson and Amundson, 2023; Miller, 2020]. Raw private weather station records are available as Supplemental data S4.1, S4.2, and S4.3. The Northernmost site weather station was located atop the ∼15 kyr surface. Data were recorded nearly continuously from 2005-2020 at 10 min. intervals, with about 12 total months of data missing at sporadic intervals throughout the record, for a total of 13.9 years of data [Table 4.1]. At the Middle site, the public Oak Creek weather station lies about 12 km north, at a

similar elevation [∼1500 m] to the field site from which Rasmussen, et al. [Ch. 2, 3] collected data. Weather data were recorded between 1994-2023 at hourly intervals for a total of 27.8 years of data. The Southernmost site weather station is located atop the ∼5 kyr surface. Data were recorded from 2017-2019 and 2021-2023 at 5 or 10 min. intervals, for a total of 4.9 years of data. All weather station data included precipitation, relative humidity, and air temperature.

Weather station data were processed to hourly timesteps using the values of temperature [*Temp*, °C], dewpoint, °C] and relative humidity [*RH*, %] that were measured on the hour [e.g., at times #:00:00]. This removed measurements from the datasets acquired at finer temporal resolutions like 5 or 10 minutes; however, this data resolution is used because it is the most typical data resolution available from public weather stations.

For each hourly data entry, *VP* was calculated using Eq. 4.5 [Brice, Tim and Hall, Todd, 2024].

$$VP[hPa] = RH[\%]/100 * 6.11 * 10^{[7.5*Temp[^\circ C]]/[237.3+Temp[^\circ C]]} \tag{4.5}$$

For each day of available data at each site, the daily temperature change [dT] was calculated as $T_{\max} - T_{\min}$ from the 24 entries from the entire 24 hour period, i.e., from 12:00 a.m. to 11:00 p.m. For each day, the hour with the maximum calculated *VP* is used for this analysis, given that diurnal heating and cooling of mineral grains occurs over an extended period of time, and brief moments of high vapor pressure can effectively impact crack-tip processes, as shown by Eppes, M. C., Magi, B., Scheff, J., Warren, K., Ching, S. and Feng, T. [2020], where cracking that results from stress due to heating and cooling occurs at times of high *VP*.

To calculate long-term 'average' daily conditions that are most aligned with a uniformitarianism approach to understanding climate, all of the daily dT and *VP*

values are averaged together, resulting in a simple estimate of one value of dT and its corresponding VP for an average day over the entire weather record.

4.4.2 Rock property data

All rock property values used in modeling are shown in Table 4.2. Since historical weather data are recent, the rock mechanical properties of clasts that were collected within active creek or wash deposits are used to represent 'fresh' rock that is unweathered. At this exact site, these data and data from clasts atop older deposits were collected by Rasmussen et al. [Ch. 3] for granitoid clasts at the Northernmost and Middle sites, but not the Southernmost site due to the wide variability of granitoid bedrock lithologies in the catchment [Stone, Paul, Miller, David M., Stevens, Calvin H., Rosario, Jose, Vazquez, Jorge A., Wan, Elmira, Priest, Susan S. and Valin, Zenon C., 2017]. To calculate stresses following [Eq. 4.3], the rock mechanical properties E and ν are required, plus the thermal expansion differential [α] between grains. For 'average compliance' model runs, the average experimentally-derived values of E and ν per rock are calculated from multiple samples that were prepared and tested from a single freshly deposited rock at the Northernmost site [24.4 GPa and 0.2, respectively] and the Middle site [32.34 GPa and 0.295, respectively]. The 'most compliant' model runs use the E and ν values of the single sample with the lowest E, and thus highest compliance, on the freshly deposited rock at the Northernmost site [23.6 GPa and 0.2, respectively] and the Middle site [20.88 GPa and 0.2, respectively]. Similarly, the 'least compliant' models use the sample with the highest E, and its corresponding ν, at the Northernmost site [25.3 GPa and 0.2, respectively] and Middle site [47.28 GPa and 0.4, respectively].

Like Eppes, Martha-Cary and Keanini, Russell [2017], I use the thermal expansion differential between two granite-forming minerals quartz and feldspar. Given the thermal anisotropy inherent in both minerals, the thermal expansion differential between the two, [α], can be a range of values depending on the grain orientations.

Eppes, Martha-Cary and Keanini, Russell [2017] used both the low endmember value [i.e., the lowest thermal expansion difference between the two minerals, 2.75 * 10^{-5} per °C] and the high endmember value [i.e., the highest possible thermal expansion difference, 5.06 * 10^{-5} per °C] to produce a realistic range of model outputs. Here, I apply the maximum differential [α of 5.06 * 10^{-5} per °C] for the 'least compliant' scenarios resulting in the least compliant rock also experiencing the highest expected thermal stress; the average of the two values [3.905 * 10^{-5} per °C] for 'average compliance' scenarios; and the minimum differential [2.75 * 10^{-5} per °C] for the 'most compliant' scenario, resulting in the rock that is most easily compressed also having the lowest estimated thermal stress. These variables result in average, maximum, and minimum reasonable estimate of stress, given the mathematical relationship among parameters in Eq. 4.3.

Since elastic properties change over rock exposure time, a phenomenon quantified by Rasmussen, et al. [Ch. 3], I also run the model using the properties of clasts that were collected from stable, flat-lying portions of the youngest dated geomorphic surface at the Northernmost [15 ka] and Middle [6 ka] sites ['weathered rocks'] and the next older dated surfaces at the Northernmost [18 ka] and Middle [21 ka] sites ['most weathered rocks']. These rocks exhibit lower E values overall due to weathering, and are thus less likely to crack under a given subcritical stress load. Therefore, to instigate some cracking during the model runs, I apply the highest thermal expansion differential [α] alongside the 'least compliant' elastic properties measured from all samples of these clasts, providing the highest possible estimate of crack growth. Values for all scenarios are shown in Table 4.2.

4.4.3 Initial crack length

Crack growth rates under low stress loads are dictated not just by the magnitude of stress σ, but also by the length of the crack itself [see Eq. 4.4], with longer cracks experiencing higher crack tip stress intensity K_{IC} than shorter cracks. Therefore, the

initial crack length of the model is a critical factor for understanding how cracks grow in response to daily stresses. Here, I follow the work of Chandler, Michael R., Mecklenburgh, Julian, Rutter, Ernest and Lee, Peter [2019] to calculate an initial characteristic flaw size.

The required *UCS* data are available from Rasmussen et al. [Ch. 3] for the modern, 6 ka, 15ka, 18 ka, and 21 ka rocks from which I derive E and ν for all cases. However, fracture toughness [K_{IC}] data are only available via double torsion testing, which was not performed on all samples. Employing the K_{IC} [Fig. 4.2] and *UCS* [Rasmussen et al., Ch. 3] of the 6 ka rock from the Middle site, and a commonly employed coefficient of internal friction for granitic materials of $\sim$0.6 [e.g., Byerlee, James D., 1967], results in a characteristic flaw size of 0.7 mm. Given the grain sizes of various minerals range from 0.5-3 mm in these rocks, this is an appropriate starting point for crack growth, making the characteristic flaw size smaller than the characteristic grain size used in the model. This initial crack length is used for all modeling scenarios.

4.4.4 Subcritical cracking parameters C and m for crack growth

Crack growth modeling following Paris, P. C. and Erdogan, Fazil [1963] [see 4.2] requires the environment- and lithology-controlled subcritical cracking parameters C and m. The value of the subcritical cracking index n can vary widely, between, e.g., 8 - 179 [Atkinson, Barry Kean and Meredith, Philip George, 1987b]. To calculate m I follow the assumption that the Charles' law subcritical cracking index n [also called the stress corrosion index] is approximately equivalent to the Paris' law parameter m; this has been shown mathematically by Eppes, Martha-Cary and Keanini, Russell [2017] and experimentally by Ko, Tae Young and Lee, Sean Seungwon [2020]. Like n, m depends on environmental conditions, lithology, rock fabric, and strain rate. I control for everything except environment by comparing presumably isotropic granitoid rocks tested using the same methodology under different *Temp* and *RH* conditions [this study combined with data from Nara, Yoshitaka, Yamanaka, Hiroshi,

Oe, Yuma and Kaneko, Katsuhiko, 2013; Nara, Y., 2015; Nara, Yoshitaka. Harui, Tomoki and Kashiwaya, Koki, 2018]. With these data, I convert *Temp* and *RH* of testing conditions to *VP*. Then, using data including the 15 kyr surface boulder from the Northernmost site; the modern, 21 ka, 33 ka, 76 ka, and 117 ka surface boulders from the Middle site; one 30 ka boulder from the Southernmost site; and prior experimental data from granitic boulders [Nara, Yoshitaka, Yamanaka, Hiroshi, Oe, Yuma and Kaneko, Katsuhiko, 2013; Nara, Y., 2015; Nara, Yoshitaka. Harui, Tomoki and Kashiwaya, Koki, 2018]; I derive a best-fit power-law relationship to predict n from *VP* in hPa [Fig. 4.3; Eq. 4.6, R^2 0.21, p-value 0.02].

$$m \approx n = 85.929 * [VP]^{-0.151} \tag{4.6}$$

From those five sources, n varies between 29.6-85 when predicted from *VP*. Applying Eq. 4.6 to calculate $m \approx n$ from weather data results in significantly less variability than laboratory results, likely because the testing conditions in laboratory studies were sometimes outside the range of Earth surface conditions encountered at the three sites; in some experiments, environmental conditions were >50 °C and samples were fully saturated with water.

Due to the minimal availability of K_{IC} with corresponding C/m values, I follow Eppes, Martha-Cary and Keanini, Russell [2017] and utilize the standard K_{IC} value of 1.7 MPa$\sqrt{meter}$ from averages calculated using values of multiple granitoid rocks in Atkinson, Barry Kean and Meredith, Philip George [1987b]. This value is confirmed by double torsion testing performed on the 6 ka rock at the Middle site which yields a K_{IC} of 1.72 [Fig. 4.2]. These results are from the same experiment that is also used to calculate the characteristic flaw size for initial crack length.

I employ the relationship established by Eppes, Martha-Cary and Keanini, Russell [2017] for calculating C [Eq. 4.7], where d_g is the characteristic grain size, which is typically ∼0.002 m for granitic rocks, and m is calculated from *VP* as described

above.

$$C = d_{\mathrm{g}} * {K_{\mathrm{IC}}}^{-m} \tag{4.7}$$

4.4.5 Modeling scenarios

For each site, six scenarios were modeled using a combination of weather station and laboratory testing inputs and approximations, and a seventh scenario was modeled at the Northernmost and Middle sites where the m prediction from VP is adjusted to match the available laboratory data. As the exposure age of these rocks increases, E decreases, representing an increase in overall compliance with surface age [see Rasmussen et al., Ch. 3]. When more time has passed and the bulk compliance of rocks has changed more significantly, crack growth is theoretically predicted to slow down; this is consistent with the mathematical prediction of stress applied here [Eq. 4.3]. Therefore, all initial model runs were performed using 'fresh' or unweathered rock, then another series of model runs applied the elastic properties of weathered rocks.

Since clast laboratory data are unavailable for the Southernmost site, data from the Middle site were used for the elastic parameters of the modern [scenarios 1-4], weathered [scenario 5], and most weathered [scenario 6] rocks. Below, the 'most/least compliant' and 'average compliance' signify the magnitudes of E and ν, and correlate with low/high/average α values, respectively.

At each site, the nearby weather station was unique to that location and located within $\sim$12 km from where the laboratory samples were collected. I completed a single model run with each of the following parameters and conditions:

1. "Average compliance, average weather conditions": crack growth modeled using average values of E, ν, and α, using the average of all daily dT and VP conditions being applied equally every day.

2. "Average compliance, daily weather conditions": crack growth modeled using

average values of E, ν, and α, using daily variable weather conditions from the nearby weather station.

3. "Most compliant, daily weather conditions": crack growth modeled using the lowest values of E, ν, and lowest α, using daily variable weather conditions from the nearby weather station.

4. "Least compliant, daily weather conditions": crack growth modeled using the highest values of E, ν, and α, using daily variable weather conditions from the nearby weather station.

5. "Least compliant weathered rock, daily weather conditions": crack growth modeled using the highest E and ν values tested per clast, using the clast sitting atop the 15 ka surface at the Northernmost site and the 6 ka surface at the Middle site, along with the highest value of α, using daily variable weather conditions from the nearby weather station.

6. "Least compliant, most weathered rock, daily weather conditions": crack growth modeled using the highest values of E and ν for the clast sitting atop the 18 ka surface at the Northernmost site, and the 21 ka surface at the Middle site, and the highest value of α, using daily variable weather conditions from the nearby weather station.

7. "Most compliant, daily weather conditions, shifted m": the same properties are used as the "3. Most compliant, daily weather conditions" model, where the VP to m prediction is shifted vertically to better fit the laboratory-derived relationships for the Northernmost and Middle site clasts, as opposed to fitting the entire dataset of laboratory derived VP to $m \approx n$ relationship.

Each scenario was calculated for a total of 1,826,250 days, or 5 kyr. When weather station data were used, the entire weather dataset was repeated back-to-back for a

total of 5 kyr worth of data. When the crack length reached the length required to fully disaggregate a grain, approximately equivalent to the characteristic grain size circumference [$2 * \pi * r = 2 * \pi * 1mm = 6.3mm$], the calculation was halted, with the assumption that a grain-scale piece of rock breaks off.

4.5 Results

For the most compliant rock, which is the most elastically deformed under stress and therefore the least likely to crack, daily weather conditions do not initiate any crack growth ['Most compliant, daily weather']. For the least compliant rock in which elastic deformation is the lowest, and thus the likelihood of cracking under a given stress magnitude is the highest, daily weather conditions always initiate some crack growth ['Least compliant, daily weather']. At the Northernmost site the growth is near-zero at around 0.0006 mm after 5000 years. At the Middle and Southernmost sites, grains can break off after only one or two days, respectively.

Crack growth resulting from model scenarios is depicted in Fig. 4.4. By applying the rock properties of the least compliant sample alongside average daily weather data ['Least compliant, average weather'], the model predicts that no crack growth will occur at the Nothernnmost site. Using the stiffest sample from the Middle site to model the same 'Least compliant, average weather' conditions, growth exceeding the characteristic grain size circumference, thus predicting that a grain-size clast could break off of the larger rock through clast disaggregation, occurs after just two days at the Middle site and four days at the Southernmost site. When only altering the elastic properties E, ν, and α to represent the average compliance properties of each modern rock, and still using average weather conditions ['Average compliance, average weather'], the conditions most equivalent to long-term mean 'climate' conditions, no crack growth is predicted at any site. By contrast, using the average rock parameters but instead using the variable daily weather conditions ['Average compliance, daily weather'] leads to grain disaggregation at the Middle and Northernmost site after 12.5

and 8.0 years, respectively. At the Northernmost site, the daily weather conditions with average compliance do not cause any crack growth.

Based on these results in this modeling approach, rock elastic properties are the most significant variable predicting rock cracking. If rock compliance is the highest – that is, the rock deforms elastically and cracking is least likely – even variable weather conditions ['Most compliant, daily weather'] cannot predict any rock cracking after 5000 years. By using the least compliant rock and thermal expansion properties, cracking is predicted in all but one scenario ['Least compliant, average weather' at the Northernmost site]. Still, with least compliant rocks, when comparing the daily variable weather ['Least compliant, daily weather'] with the average weather conditions ['Least compliance, average weather'], weather conditions can result in rock disaggregation in half the time at the Middle and Southernmost sites.

4.5.1 The impact of different climate zones on daily rock cracking behavior

To better understand why daily variables are impacting cracking, I analyze the sites in terms of a common, climate classification: the Köppen-Geiger climate classification [Köppen, 2011], updated using PRISM data in [PRISM Climate Group, Oregon State University, 2024] by Peel, M. C., Finlayson, B. L. and McMahon, T. A. [2007] [Fig. 4.5]. This classification includes not only mean conditions, but also seasonal trends in precipitation and temperature. By processing our weather data into seasonal trends [Fig. 4.6] and comparing it with the site classifications [shown in Fig. 4.5] I confirm that the sites represent warm and dry summer mediterranean continental [Dsb; Lundy Canyon], hot and dry summer mediterranean temperate [Csa; Shepherd Creek], and hot, dry desert [Bwh, Providence Mountains].

Figure 4.6 shows the raw weather data from each site processed as monthly precipitation [top] and monthly averages of daily dT [bottom], colored by the average of each day's highest VP value. All data shown in the upper plots correspond to the full data range used in the lower plots. The seasonal trends at the Northern-

most and Middle site are similar, with winter months representing the wettest time and summer representing the driest. At the Northernmost and Middle [semi-arid] sites the months with the highest precipitation do not correlate with the months of highest *VP*, indicating that *MAP* is a poor metric for rock cracking analysis at these sites. At the Southernmost [arid] site, overall precipitation is very low and the two highest precipitation months [July/August] do correlate with the highest *VP* months. Interestingly, August also contains the largest *dT* outlier for that site.

I identify the days with the most significant crack growth throughout the entire weather record [Supplement S4.1, S4.2, and S4.3]. The high growth days are highlighted with arrows identifying their timing and conditions on Fig. 4.6. At the Middle and Southernmost site, all crack growth occurred on one day. The five highest days at the Northernmost site and the single highest day at the Middle site correlate with both high daily *dT* and relatively high *VP*, but not high precipitation. At the Southernmost site [arid, desert] where monsoonal summer storms are expected to explain the slight increase in summer precipitation, the highest single growth day correlates with the highest daily *dT*, exceptionally high *VP*, and 29 mm of precipitation [see Supplemental S4.3]. This suggests that *MAP/MAT* classifications may be appropriate for understanding the influence of climate on cracking in California desert sites, but clearly are insufficient for explaining rock cracking behavior at the semi-arid Eastern Sierra sites. Additionally, since two sites exhibit different drivers in cracking when compared with the third site, this does not accurately represent the gradual change in climatic parameters that was predicted by *MAP* and *MAT* trends, with the most arid site experiencing cracking on a rainy day, while the other two sites do not. This also shows that *MAP* is not a relevant predictor of cracking in the Northernmost and Middle sites, where there is no precipitation on the highest cracking days.

4.5.2 Sensitivity to rock exposure age [weathering]

The compliance change over time at the Northernmost site is minimal relative to the other sites, with the 'most weathered' ∼18 kyr exposed rock having an 11% lower average E [21.5± 1 std. dev. of 0.9, vs. 24.4±0.9 GPa]. At the Middle site the difference between the modern rock and 'most weathered' ∼21 kyr exposed rock is more substantial, having a 63% lower average E [20.4±4.2 vs. 30.9±12.4 GPa].

At all three sites, when the rock properties used in the model are derived from least compliant [stiffest] cores measured from individual rocks that have experienced either 6 or 15 kyr of exposure to natural conditions, variable daily weather conditions lead to crack growth ['Least compliant weathered rock, daily weather']. At the Northernmost site, the ∼15 kyr exposed rock has an 8% lower E and 25% higher ν than the 'fresh' rock. At the Middle site, the ∼6 kyr exposed rock has an 11% lower E and 30% lower ν than the 'fresh' rock [Rasmussen et al., Ch. 3, Fig. 3.6].

When compared with the 'fresh' or least weathered rock's properties, using the properties of weathered rocks decreases the crack growth rate. For the Northernmost site, the crack growth is about 4x lower using the weathered rock properties than when using the 'fresh' rock properties. Similarly, at the Southernmost site, the weathered rock properties result in a 4x decrease in time-to cracking when compared with the 'fresh' rock. By contrast, at the Middle site, clast disaggregation takes 111 days using weathered rock properties, instead of a single day when using the 'fresh' rock.

Using the next most weathered measured clast from Rasmussen et al. [Ch. 3] ['Least compliant, most weathered rock, daily weather'], crack growth still occurs at all three sites, but at a fraction of a millimeter over 5000 years. At the Northernmost site, the ∼18 kyr exposed rock has an 11% lower E and 25% higher ν than the 'fresh' rock, and at the Middle site, the ∼21 kyr exposed rock has a 63% lower E and 45% lower ν than the 'fresh' rock [Rasmussen et al., Ch. 3, Fig. 3.6].

4.5.2.1 Prediction of m from VP

Subcritical crack growth is also sensitive to the C/m values which directly moderate ΔK_I via Eq. 4.2. While C is very poorly constrained in the literature, the prediction of m can be easily modified, thus altering C through Eq. 4.7 and crack growth directly through Eq. 4.2.

For sensitivity analysis, I therefore modify the m prediction by shifting the best-fit line vertically to match the average VP-m relationship at the Northernmost site [shifted up by 12.9 as shown by Fig. 4.3, 'Most compliant, daily weather, shifted m prediction'] and from the Middle site [shifted down by 21.9 as shown by Fig. 4.3, 'Most compliant, daily weather, shifted m prediction']. Given that the 'Least compliant, daily weather' model results in clast disaggregation at the Middle site after only one day, any decrease in m – which will enhance cracking rates – will similarly break off a clast in one day. As expected, an increase in m – which decreases the stress intensity in the model and thus diminishes cracking – at the Northernmost site results in no crack growth. At the Middle site, crack growth is non-zero, but nearly zero.

4.6 Discussion and summary

Modeled crack growth at these sites only occurs when applying [1] daily variable weather conditions, or [2] rock properties of the least compliant sample available. This means that a traditional 'climosequence' approach, whereby model inputs are derived from averages of long-term mean climate records and for all rock samples per site, would result in no crack growth. When compared with the rock cracking data of Rasmussen et al. [Ch. 2] which suggests that rock cracking at the Northernmost site conservatively reaches 2.5 mm/kyr by 15 ka, the Middle site reaches 6.3 mm/kyr by 6 ka, and the Southernmost site reaches 28.0 mm/kyr by 1 ka. By averaging long-term climate and applying average rock properties per sample, this level of crack growth is not predicted. Only model scenarios that use the least compliant elasticity

measurements available, or weather conditions, predict growth of this magnitude at any site.

The model is highly sensitive to thermal and elastic parameters. While the stress calculation is linearly dependent on weather data for each day [dT], it is also linearly dependent both on Young's modulus E and the thermal expansion differential α. I covary E and α because I assume that the trends observed by Rasmussen et al. [Ch. 3] apply here, where lower E [increased elastic compliance] correlates with higher porosity, and thus a decrease in the amount of stress that will result from thermal expansion [lowest α]. Therefore, the simultaneous decrease in E and α together leads to a stronger impact of elastic properties on cracking, when compared with the effect of diurnal dT.

The rock properties of the fresh rock at the Middle site, which are applied in the Southernmost site models as well, represent a rock with very low compliance [E = 47.28 GPa]. This is nearly double the most compliant rock at the Northernmost site [E = 25.3 GPa] and will thus almost double the stress prediction, even if weather conditions are identical. However, over just 6 kyr of rock exposure, this compliance increases by 11%, increasing the time-to-disaggregation by 4-111 fold. By the time rocks have been exposed to weathering conditions for 18-21 kyr ['most weathered rock'], their compliance has increased enough that the modeled crack growth for the next 5000 years is negligible. This implies that grain disaggregation would occur rapidly, then due to the enhanced compliance of weathered rocks, it would decrease once rocks have weathered. This is consistent with the abundance of grain-scale clasts present on the youngest dated surface at the Northernmost, Middle, and Southernmost sites [Rasmussen et al., see Ch. 6].

If I ignored the modeling run using the highest measured value of E of any sample tested from the modern rock at the Middle site ['Least compliant'] and instead focus on the crack growth events that occurred using average sample parameters, the impact

of daily weather vs. average climate is clear. All crack growth occurs on just 1-5 days per site. If a longer timespan of weather data were available, even the most compliant rocks may be able to crack within the modeled 5 kyr, given that rare, high-magnitude weather events will be encountered more frequently. Since long-term climate data are averaged throughout the entire weather record, the longest weather record [Middle site] is the most likely to encounter such events, resulting in the shortest time required to break off a piece of rock [Fig 4.4] when these events can be repeated for thousands of years.

Even with the short weather record [4.9 years total] of the hot, arid Southernmost site, one high dT day is capable of breaking a piece of rock [Fig. 4.6]. While high temperatures during crack propagation will enhance subcritical crack growth through bond weakening, temperature is only considered in the m prediction in this model. Based on laboratory correlations of VP predicting m, higher temperatures have a negligible impact on this intergranular rock cracking model. Therefore, the unusually high daily dT at this Southernmost site is interpreted to be the most impactful climate factor. This is partially a result of a rare rain event on that day, which occurs in the monsoonal climate of southern California and can accompany a drop in temperature. Here, combining an understanding of seasonality with MAP may indeed help elucidate rock cracking over geologic time, because precipitation during warm seasons can rapidly cool rocks, resulting in enhanced thermal stresses.

Using either daily weather or long-term averages, there is a climate signature evident within the modeling, with the hottest Southernmost site experiencing the fastest crack growth in most cases, and the coolest, more temperate Northernmost site experience the slowest crack growth. Since the model is driven more by dT than absolute daily temperature, the increase in cracking is more dependent on the likelihood of daily temperature swings, and is thus amplified in arid conditions where temperature can rapidly change.

This is inconsistent with the theory posited by Rasmussen et al. [Ch. 2] who suggest that the more gradual, diffuse accumulation of cracks allows the Southernmost site rocks to express such high cracking metrics (both fracture intensity anfd fracture number density) without fully breaking the rock. This discrepancy may be explained by bulk vs. intergranular cracking behavior, or the elastic property data. The modeling here is focused on intergranular cracking, while Rasmussen et al. [Ch. 2] measured $\geq$2.0 cm cracks. These longer cracks may take longer to grow, and are more dependent on the stress field of the bulk rock. This modeling does not address these stresses in any way. Critically, the elastic property data used for modeling in the Southernmost site is borrowed from the sampled clasts at the Middle site because no laboratory data were collected for the Southernmost site rocks. As shown here, the modeling exercise is highly dependent on elastic properties, so the discrepancy between field and laboratory data may be a result of improper model calibration.

This modeling exercise shows that climosequences for rock cracking should first be constructed by considering the seasonal effects of weather per site, like the Köppen Climate Classification. For example, in these Eastern California sites [Fig. 4.6], areas where summer rains are dominant experience the maximum annual VP during the summer when MAP and MAT are also at their maximum, and when it is likely that a precipitation event will increase the likelihood of a high dT day. Where winter rains are dominant, like in the Northernmost and Middle site, MAP does not accurately reflect the relevant moisture conditions. Instead, VP is most dependent on temperature, so unusually high dT days – which do coincide well with peak summer temperatures – are the main drivers of rock cracking.

4.6.1 Model assumptions and limitations

When using naturally variable daily weather data for modeling crack growth, disaggregation from the rock surface can occur in as little as one daily stress cycle. However, the model is highly sensitive to rock elasticity and the magnitude of tem-

perature flux on a given day. An accurate understanding of rock elastic properties at any given site is essential for this modeling because lithological variability between sites may result in significant differences in elasticity. This is seen when comparing the nearly 100% difference in Young's modulus between the modern rock at the Northernmost and Middle sites where both granitic boulders were visually similar in mineralogical composition and grain size. Other minimally constrained parameters which our modeling suggests can strongly influence crack growth include K_{IC} and the C/m parameters in Paris' law; while the m parameter does not vary significantly within the weather conditions of these study sites, the C parameter is mathematically estimated and not calibrated to any laboratory analysis. Given that C linearly impacts crack growth [see Eq. 4.2], any change to this parameter could have significant impacts on model results.

Here, I use air surface temperature instead of rock temperature due to its ubiquitous availability from weather stations. The rock surface temperature will likely exceed air surface temperature by multiple °C [e.g., rock surface vs. air temperatures across seasons show by Eppes, Martha Cary, Magi, Brian, Hallet, Bernard, Delmelle, Eric, Mackenzie-Helnwein, Peter, Warren, Kimberly and Swami, Suraj, 2016; Moore, Jeffrey R., Gischig, Valentin, Katterbach, Maren and Loew, Simon, 2011; Fiorucci, Matteo, Marmoni, Gian Marco, Martino, Salvatore and Mazzanti, Paolo, 2018]. Rock surface temperature cannot be estimated without direct measurement because it is modified by albedo and porosity, both of which may change from rock to rock and will be modified over time by weathering itself, including chemical and biological modification. Thermal diffusivity through the rock will also be dictated by rock fabric and mineralogy and is porosity dependent. Generally the increase in porosity over time is paralleled by a decrease in E over time [Rasmussen et al., Ch. 3], so here I assume that the porosity difference is accounted for in the model through the lower E of the weathered rock cases. Thermal diffusivity is not considered in the model, and grain

disaggregation is presumably only occurring at the outer surface of the rock.

This model only considers intergranular stress at the rock's surface due to diurnal temperature flux. Therefore, this model may reasonably assess the time-to-failure of single or multi-crystal grus disaggregating from granitoid rocks. However, this is only one source of stress and mode of fracture in a bulk rock mass. Other sources of stress could include chemical reactions, biological growth, or frost weathering. Stress is additive, so these weather- and climate-dependent processes could increase, decrease, or modify the location of cracking within the rock. Even when just considering dT as a primary driver of rock cracking, the bulk rock mass experiences radial stress concentrations that are dictated by mineralogy, rock size, and bulk thermal conductivity [see modeling in Shi, Jian, 2011]. To fully understand rock cracking behavior, all stress sources would need to be integrated into a bulk rock stress model, e.g., a modification of such models presented by Molaro, J. L., Hergenrother, C. W., Chesley, S. R., Walsh, K. J., Hanna, R. D., Haberle, C. W., Schwartz, S. R., Ballouz, R. L., Bottke, W. F., Campins, H. J. and Lauretta, D. S. [2020] or the simplified version by Ravaji, Babak, Alí-Lagoa, Víctor, Delbo, Marco and Wilkerson, Justin W. [2019]. I propose that the current model presented here is an excellent starting point for understanding the importance of weather variables and rock elastic properties in modulating rates of cracking for rocks on Earth's surface.

4.6.2 Capturing extreme events

The weather data temporal resolution and length of record both dictate the likelihood and magnitude of "extreme" events being captured. The 27.8 years of recorded weather data at the Middle site will capture rarer events than the 4.9 years of data at the Southernmost site, but even the 27.8 year record would not capture the rare events that will surely occur over the 5 kyr record I attempt to simulate. The field of paleotempestology could provide some insights into the likelihood, seasonality, and magnitude of rare weather events in the paleoweather record, but such work is beyond

the scope of this study. Advancements in this area are needed for various geoscience applications [see summary in East, Amy E. and Sankey, Joel B., 2020] and are actively being developed.

4.6.3 Comparison to prior study

Within my hourly model data, the dT/dt values are incomparable to the per-minute weather station data collected alongside *in situ* acoustic emission data presented in Eppes, Martha Cary, Magi, Brian, Hallet, Bernard, Delmelle, Eric, Mackenzie-Helnwein, Peter, Warren, Kimberly and Swami, Suraj [2016]; Eppes, M. C., Magi, B., Scheff, J., Warren, K., Ching, S. and Feng, T. [2020]. The hourly rate of temperature change in these models could reflect a gradual change over the entire 60 minute period, meaning that per-minute changes are 1/60 of hourly changes. They also could occur instantaneously, and the per-minute change is exactly represented by the hourly rate of change. Therefore, comparing the hourly dT data here with prior research would result in these dT values or 1/60 of those values.

As an attempt to validate the various model inputs, I compare model inputs and results with previous measurements from field data [Eppes, M. C., Magi, B., Scheff, J., Warren, K., Ching, S. and Feng, T., 2020], keeping in mind the wide range of variability that hourly data presents when attempting to compare with per-minute measurements. This range is shown atop real acoustic emission data [proxy for rock cracking, represented by colors] with binned data for each dT and VP value [Fig. 4.7]. The full range of options are within the dashed bounds [hourly values being the daily dT divided by 24, shown in upper portion; lower values being 1/60th of the hourly dT, lower portion] and reasonably overlap the measured data from a rock in North Carolina [left] and New Mexico [right]. The climate of the New Mexico site most closely aligns with that of the Middle site with a Köppen-Geiger classification of Bsk [cold semi-arid]; both sites experience more rain in the winter than summer. The northernmost site is seasonally similar, but more temperature, with the cooler

summer temperatures leading to a lower VP. The comparison suggests that the full range of possible dT values – from per-minute to per-hour – are reasonable, but that cracking at the Northernmost site would require that this temperature change is quite rapid to overlap with the conditions during which significant cracking was measured by Eppes, M. C., Magi, B., Scheff, J., Warren, K., Ching, S. and Feng, T. [2020].

I also compare the model prediction with the field data collected at each site [Rasmussen et al., Ch. 2]. Due to the model constraints of only considering stresses between single mineral grains, the bulk rock cracking rates are not comparable. The most relevant metrics for understanding grain-grain stresses and grain-scale disaggregation are

1. the binary "presence of granular disintegration" [GD] metric that was marked for each boulder I measured in the field [based on the presence of loose grains atop the boulder surface],

2. the increased abundance of intergranular and shallow [single- to multi-grain thickness] surface-parallel cracks on the boulders, and

3. the increased abundance of small [cm-scale] clasts on the ground around the boulders.

The proportion of rocks experiencing active GD and the proportion of measured cracks that are parallel to the rock surface are both shown in Fig. 4.8 for all granitoid rocks at the three sites. The overall increase in the first ∼30 kyr of rock exposure age is clear in both figures and is consistent with trends presented by Rasmussen et al. [Ch. 2].

First, at the Southernmost site [dark red circles] where data are available for 0, 1, and 5 ka rocks, the presence of GD generally increases with rock exposure. By contrast, surface-parallel cracks are at their peak at 5 kyr. This may indicate that many clasts are removed from the rock surface between 5 - 10 kyr, or that the overall

increase in other modes of cracking [e.g., cracks that propagate through the middle of the rock] in this timeframe increase in abundance relative to the surface-parallel cracks. To investigate this I turn to my third metric: rock size on the surface [Figs. 4.9,4.10and Ch. 6]. Fig. 4.9 shows the Southernmost site granitoid clast intermediate axis length from modified Wolman pebble counts [Wolman, M. Gordon, 1954] performed on the alluvial surfaces. While the median clast length [black vertical line] slowly decreases over time, the histogram shows an abrupt increase in $\leq$2.0 cm clasts already appearing after 1 kyr. By 5 kyr, the smallest measured clast size is dominant, and by 10 kyr this is so prevalent that the median value begins to decrease.

I interpret the overall stabilization in the proportion of surface-parallel cracks as reflecting that the cracks are coalescing or disaggregating rock continuously after only 1 kyr. This may be happening at a faster rate, but this is the highest time resolution of available data. These observations are consistent with many of the models presented here.

At the Middle site, surface-parallel cracking is high by 6 kyr, and on the next-oldest 21 ka surface, the amount of observed *GD* reaches its peak. These metrics may be related, whereby the slight decrease in surface-parallel cracking proportion is reflected by loose clasts having been produced from the rock surface. By 33 kyr both metrics are down, and then they increase again by 76 kyr. Since this modeling is mostly focused on the younger rocks, I focus on the $\leq$21 kyr field data. The clast intermediate axis lengths for the Middle site [Fig. 4.10] portrays a different behavior than the Southernmost site. Here, the 6 ka surface shows a dramatic increase in $\leq$2.0 cm clasts, similar to the Southernmost site. However, the 21 ka surface has a higher median value and only a weak dominance in the smaller clasts. Additionally, the fracture number density and intensity of $\geq$2.0 cm clasts is still increasing at this time [Rasmussen et al., Ch. 2, Fig. 2.5]. Instead of indicating that smaller rocks are not disaggregating, I interpret this relative drop in surface-parallel cracks coupled

with increasing crack intensity and abundance of larger rocks to reflect a higher proportion of rocks that are cracking into two large, similarly sized pieces – in other words, through-going cracks are breaking the rocks in half instead of removing small pieces from the boulder surface. Like the Southernmost site, the observation that abundant clast disaggregation can occur in the first 6 kyr of exposure is consistent with modeling presented here.

At the Northernmost site, the presence of *GD* and abundance of surface-parallel cracks are both low until the 18 ka surface, at which time they increase. This would suggest that the modelled intergranular rock stresses are not dominant for the first ∼18 kyr. This appears to be inconsistent with the model results presented here. However, given the rapid crack growth predicted at the other sites by Rasmussen et al. [Ch.2], it is difficult to say with certainty that significant *GD* does not occur in the first ∼15 kyr of exposure, during which time data are not available. Additionally, recent construction at the Northernmost site made Wolman pebble counts at the modern deposit unreliable, so the clast size data have no "baseline" distribution against which to compare.

Cases where rocks can disaggregate grains in a matter of days are clearly unrealistic; if this could occur, all rocks would be experiencing active granular disaggregation, yet it is never observed on more than ∼60% of rocks.

4.6.4 Conclusion

Here I show that the oft-used *MAP/MAT* proxies for different climates within a climosequence approach are insufficient for understanding the influence of climate on rock subcritical cracking due to intergranular thermal stresses, unless the approach is coupled with the lowest measurements of compliance [high E] from laboratory analysis of rocks at these sites. At other sites where rock elasticity will undoubtedly be different, this factor may not be impactful; however, the inconsistencies between field observation and modeling at the Southernmost site emphasize the importance

of proper calibration of rock properties for modeling.

While modeling is highly sensitive to rock elastic and thermal properties, it consistently shows that growth occurs on high dT days, regardless of moisture and precipitation conditions that could influence crack tip processes independent of this stress driver, within the normal range of conditions at these sites. However, rain may cause an increase in daily dT, as it does in the Southernmost site. Additionally, by using a more detailed Köppen-Geiger climate classification for the sites, it is clear that what might be inferred from MAP and MAT to be a gradational climosequence actually represents two different seasonal regimes, with cracking occurring in the months of highest dT and low precipitation in the Northernmost and Middle sites, and cracking occurring during a moderate dT month overall, but alongside high precipitation.

Since this study shows that crack growth occurs as punctuated events on high stress days, as opposed to gradually every day, the model would greatly benefit from a longer weather record, or predictions of Köppen-Geiger paleoclimate and magnitudes of high stress days. Modeling sites of different Köppen-Geiger classifications would also greatly elucidate the main drivers of subcritical intergranular rock cracking around the world.

Further, full-scale models of an entire rock would provide a fuller picture of rock cracking by incorporating the whole-rock stress field. Thus far, these models have not been calibrated for Earth's surface, outside of minimal modeling by Shi, Jian [2011] which was included in Eppes, Martha Cary, Magi, Brian, Hallet, Bernard, Delmelle, Eric, Mackenzie-Helnwein, Peter, Warren, Kimberly and Swami, Suraj [2016] as validation. Calibration of a full-rock stress model like Molaro, J. L., Byrne, S. and Le, J. L. [2017] would help to understand whether daily weather conditions impact cracks driven by bulk rock radial stresses; however, such modeling is outside the scope of this study.

This study does not address bedrock fracture, but this type of model should directly

apply, since all rocks exposed at Earth's surface experience thermal cycling and the grain-grain stresses can exist in any rock greater than a few grains across. While bulk thermal modeling has been performed to understand spall removal from bedrock walls [e.g., Collins, Brian D. and Stock, Greg M., 2016; Marmoni, G. M. and Fiorucci, M. and Grechi, G. and Martino, S., 2020], this approach has not been implemented to add the removal of rock mass from the surface caused by grain-grain thermal stresses. This addition could help constrain cosmogenic dating and models that rely upon and erosion rate corrections can be linear over time. If rock surface removal is truly dependent on daily events, it would be highly sensitive to paleoclimate, and thus will vary over time. Indeed, implementing a new approach for understanding rock weathering – that of seasonal, daily weather in addition to long-term climate – may help close the gap between theoretical predictions of weathering and the behavior we observe.

4.7 Tables

Table 4.1: Weather station record data alongside [1]1991-2020 30-year means from PRISM Climate Group, Oregon State University [2024]. Site weather stations from Miller [2020], Western Regional Climate Center: WRCC [2023], and Kelson and Amundson [2023]. 'Site' *MAT* and *MAP* calculated from weather stations.

Site	Weather record total [yr.]	Dates of record	30-year *MAT*[1] [°C]	Site *MAT* [°C]	30-year *MAP*[1] [mm]	Site *MAP* [mm]
Northernmost	13.9	10/15/2005 - 7/12/2010, 12/4/2010 - 4/20/2017, 1/12/2018 - 9/16/2019 9/21/2019 - 10/12/2020	7.2	7.4	390	296
Middle	27.8	1/11/1994 - 12/31/1994 1/3/1995 - 3/9/1996 3/28/1996 - 9/1/1997 9/4/1997 - 11/9/2000 11/11/2000 - 12/15/2000 2/2/2001 - 2/25/2005 4/3/2008 - 7/12/2008 9/16/2008 - 11/30/2008 12/13/2008 - 2/28/2023	15.2	15.7	177	177
Southernmost	4.9	3/17/2017 - 4/11/2017 4/14/2017 - 11/24/2019 3/21/2021 - 5/21/2023	18.9	20.2	156	134

Table 4.2: Modeling scenario inputs. All scenarios used an initial crack length of 0.7 mm, grain size of 2.0 mm, and $/K_{IC}]$ of 1.7 MPa $\sqrt{m}$. All α values are from Eppes, Martha-Cary and Keanini, Russell [2017]. [Suppl. S4.1 [1]Miller [2020], S4.2 [2]Western Regional Climate Center: WRCC [2023], S4.3 [3]Kelson and Amundson [2023]]

Site	Scenario	E [GPa]	ν	α [per °C]	Rock sample for E, ν	Weather data source
Northernmost	Most compliant	23.6	0.2	$2.75*10^{-5}$	Modern rock	Private[1]
Northernmost	Least compliant	25.3	0.2	$5.06*10^{-5}$	Modern rock	Private[1]
Northernmost	Average compliance	24.4	0.2	$3.905*10^{-5}$	Modern rock	Private[1]
Northernmost	Least compliant weathered rock	23.19	0.25	$5.06*10^{-5}$	15 kyr rock	Private[1]
Northernmost	Least compliant, most weathered	22.5	0.25	$5.06*10^{-5}$	18 kyr rock	Private[1]
Middle	Most compliant	20.88	0.2	$2.75*10^{-5}$	Modern rock	Public[2]
Middle	Least compliant	47.28	0.4	$5.06*10^{-5}$	Modern rock	Public[2]
Middle	Average compliance	32.34	0.295	$3.905*10^{-5}$	Modern rock	Public[2]
Middle	Least compliant weathered rock	41.97	0.28	$5.06*10^{-5}$	6 kyr rock	Public[2]
Middle	Least compliant, most weathered	17.4	0.22	$5.06*10^{-5}$	21 kyr rock	Public[2]
Southernmost	Most compliant	20.88	0.2	$2.75*10^{-5}$	Modern rock	Private[2]
Southernmost	Least compliant	47.28	0.4	$5.06*10^{-5}$	Modern rock	Private[2]
Southernmost	Average compliance	32.34	0.295	$3.905*10^{-5}$	Modern rock	Private[2]
Southernmost	Least compliant weathered rock	41.97	0.28	$5.06*10^{-5}$	6 kyr rock	Private[2]
Southernmost	Least compliant, most weathered	17.4	0.22	$5.06*10^{-5}$	21 kyr rock	Private[2]

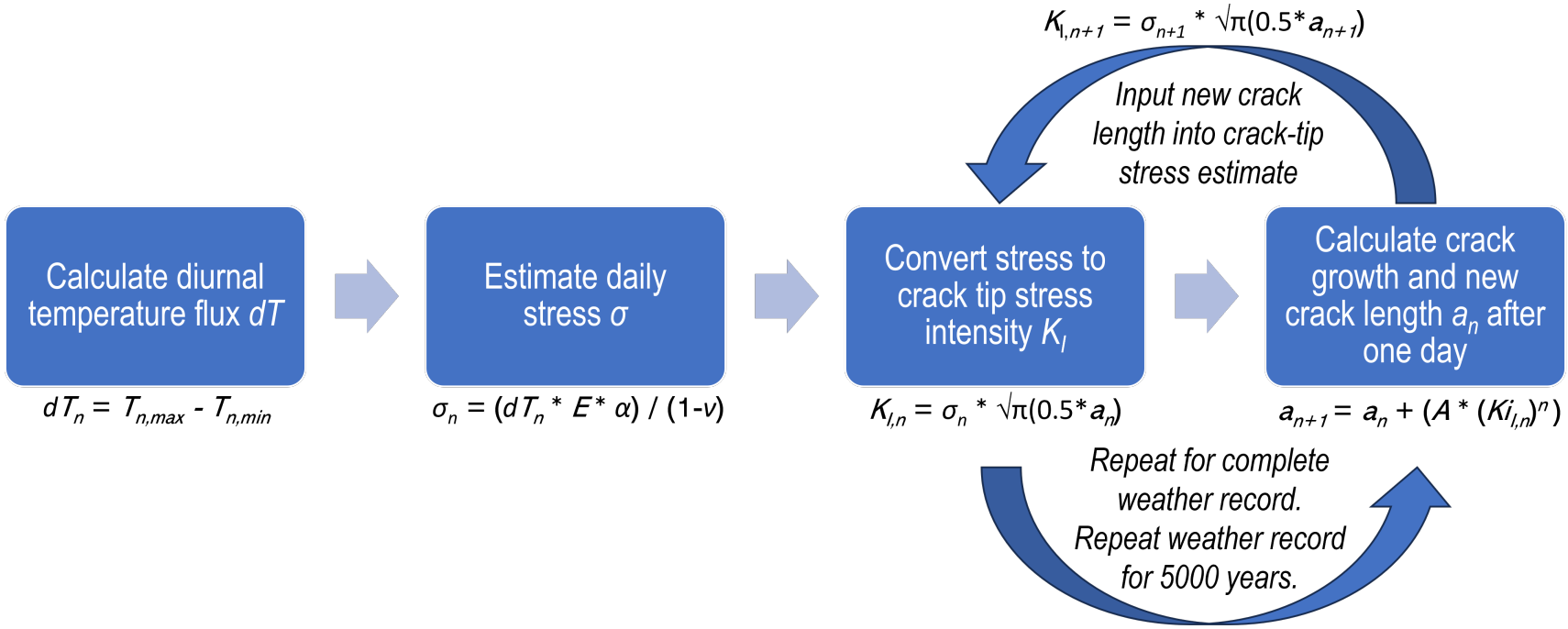

Figure 4.1: Crack growth calculation workflow.

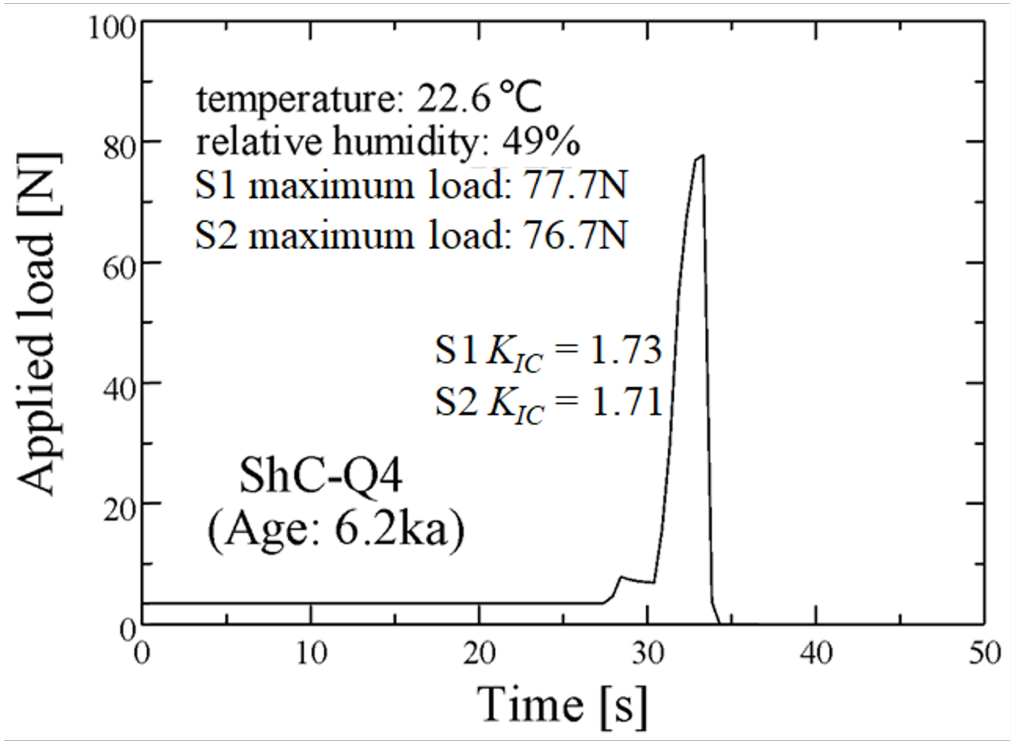

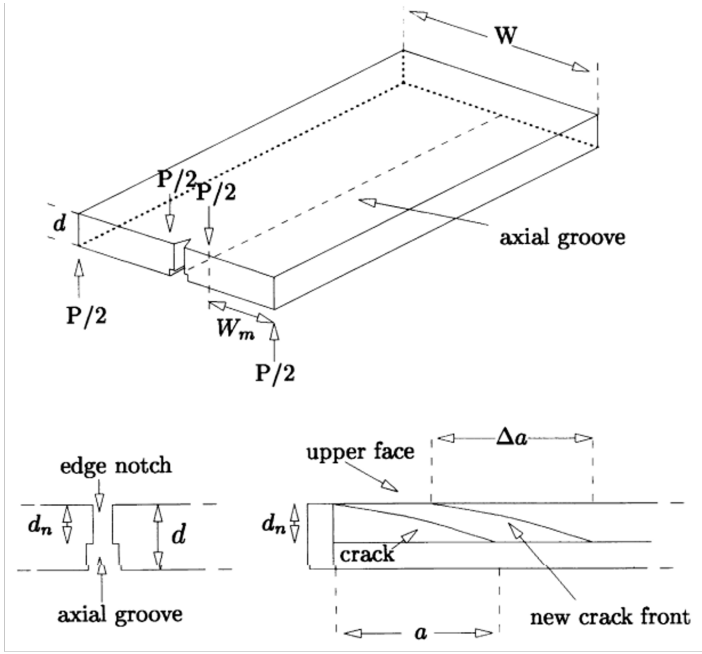

$$K_{IC} = P_{max} w_m \sqrt{\frac{3(1+\nu)}{W d^3 d_n}}$$

Figure 4.2: Applied load over time during double torsion testing on two samples from the same ~6 ka rock. K_{IC} was calculated using the equation below where $P_{\max}$ is the maximum applied load, w_{m} is the width of the billet on either side of the notch, ν is Poisson's ratio, W is the total width of the billet, d is the total thickness of the billet, and d_{n} is the thickness of the billet that is notched [see schematic to the right from Ciccotti, Matteo, Negri, N., Sassi, L., Gonzato, Guido and Mulargia, Francesco [2000], modified from Atkinson, B. K. [1979]].

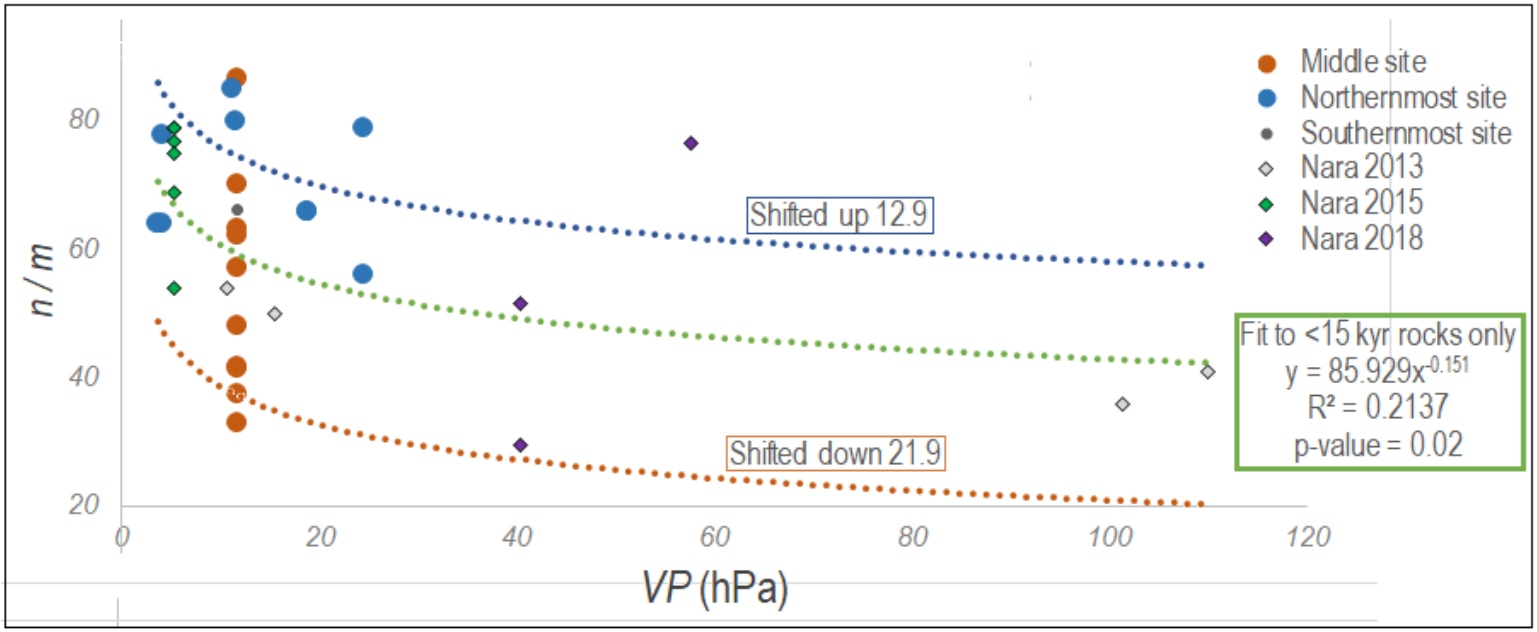

Figure 4.3: Derivation of n / m from VP using previously published data [Nara, Yoshitaka, Yamanaka, Hiroshi, Oe, Yuma and Kaneko, Katsuhiko, 2013; Nara, Y., 2015; Nara, Yoshitaka. Harui, Tomoki and Kashiwaya, Koki, 2018] and results from double torsion experiments [this study, Northernmost and Middle site]. All studied rock were granitoids and were tested using the same double torsion methods by the same researcher. The dashed blue line represents the vertically shifted 'high m' value for the Northernmost site and the dashed orange line represents the vertically shifted 'low m' value for the Middle site.

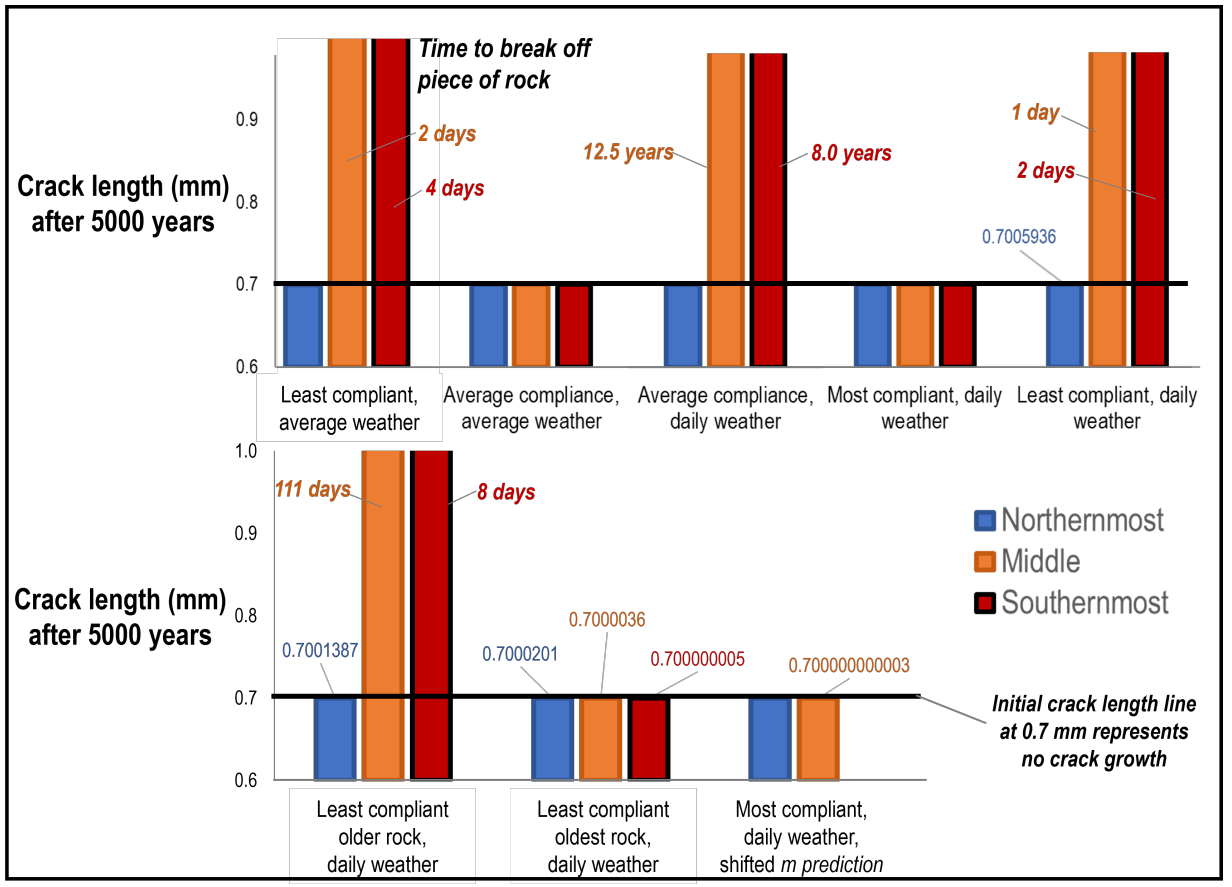

Figure 4.4: Calculated crack lengths after 5000 years of daily cycles for all scenarios. The upper panel shows the impact of changes in compliance [E, ν] and thermal expansion differential between grains, and the average scenario where the average daily dT and VP are repeated for 5000 years. The lower panel shows the impact of using the properties of weathered clasts, or the impact of shifting the prediction for m from VP. Solid black line at 0.7mm represents that there was no crack growth after 5000 years. Unlabeled scenarios experienced no crack growth. Scenarios where bars exceed the height of the graph indicate that the crack grows to grain size diameter and causes disaggregation at the time indicated adjacent to the bar.

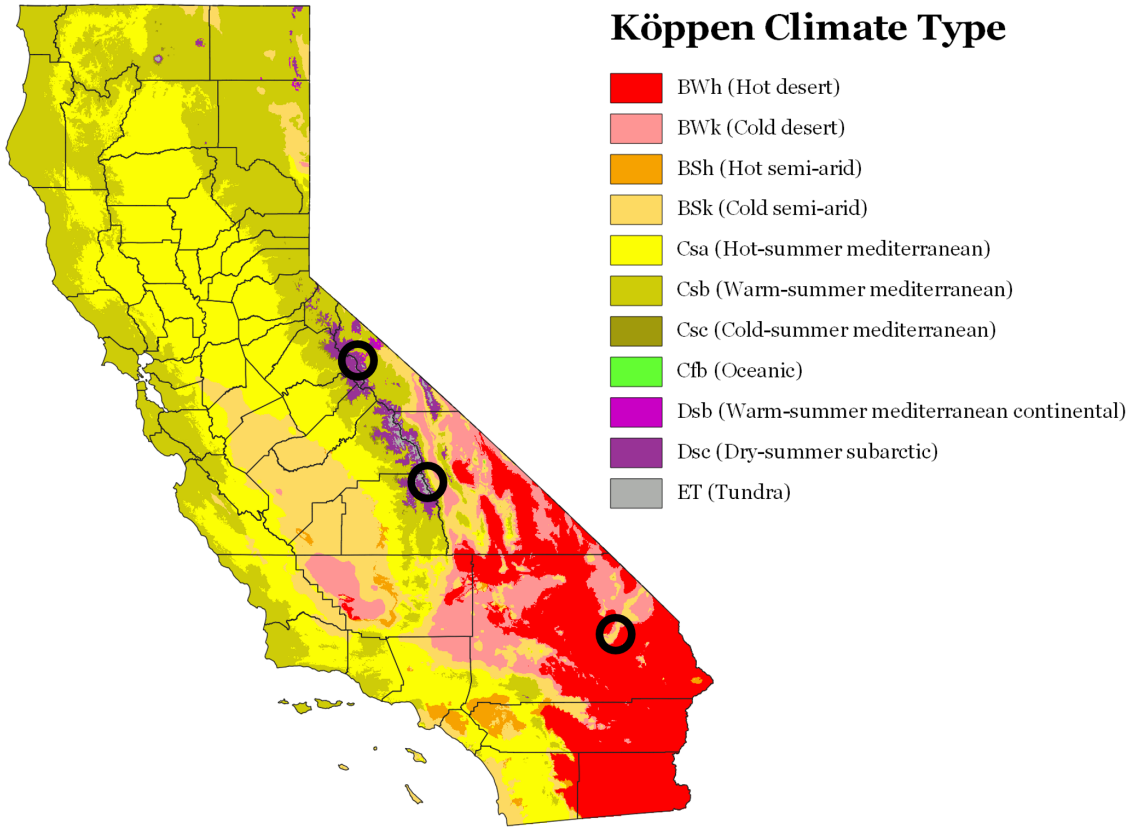

Figure 4.5: Köppen Climate Classification of study sites. Circles are enlarged beyond the study area for clarity; the study sites fall approximately in the center of the circles. Sites cover multiple climate zones because the depositional fans are directly adjacent to the Sierra Nevada to their west [Northernmost, Middle], the Providence Mountains to their east [Southernmost], and the Kelso Sand Dunes to their west [Southernmost]. Comparison with weather station data classifies the Northernmost site as Dsb, Middle site as Csa, and Southernmost site as Bwh. Figure from Peel, M. C., Finlayson, B. L. and McMahon, T. A. [2007] using PRISM Climate Group, Oregon State University [2024] 1990-2020 climate mean values. Map outline from US Census Bureau.

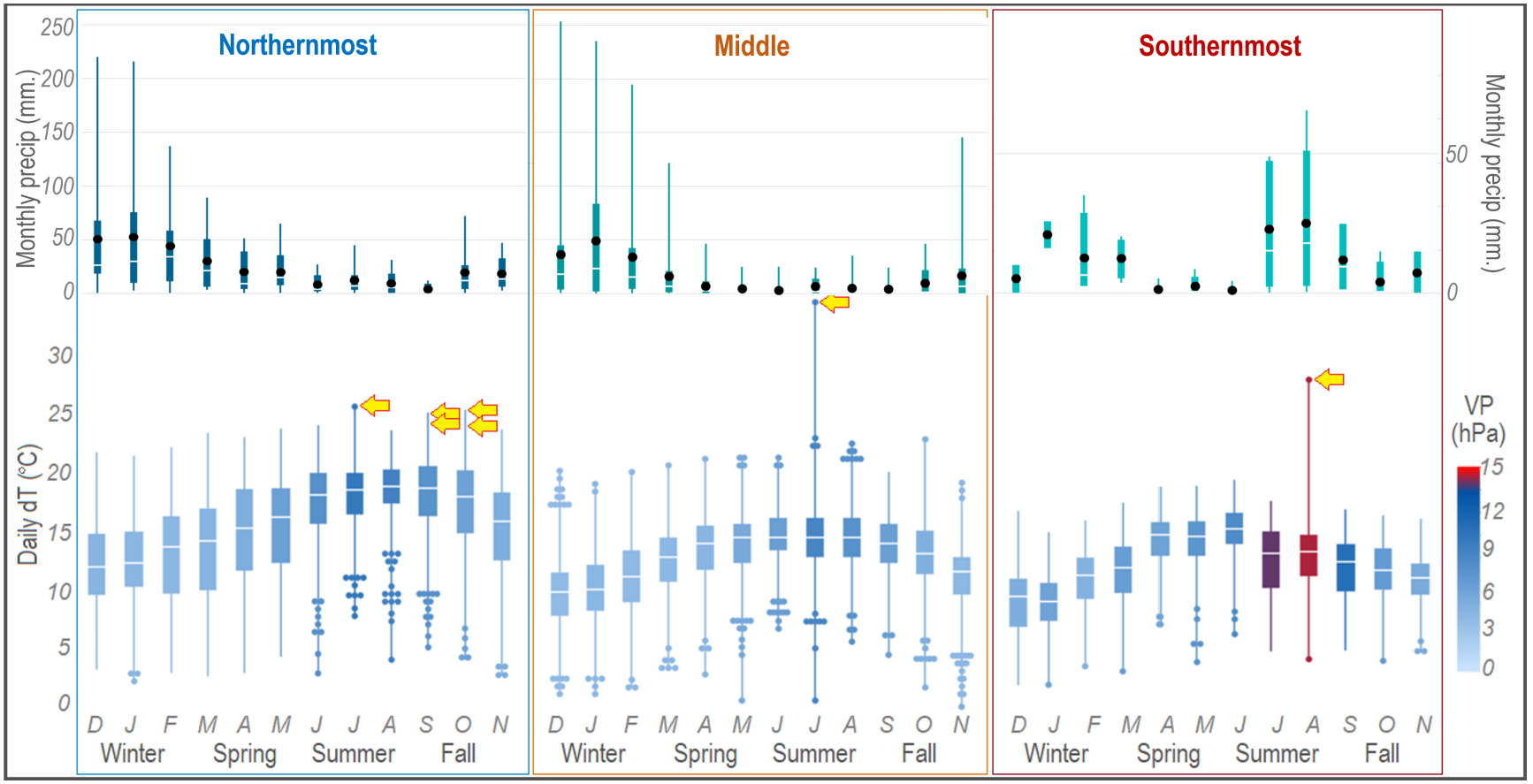

Figure 4.6: Monthly precipitation [upper] for the entire weather record from each site with black points representing monthly averages, and all daily dT values per month, colored by the monthly average value of daily maximum VP, the same parameters used in the modeling. Yellow arrows highlight the days on which significant crack growth occurred. Note that the precipitation values cannot be compared between sites due to the variable weather record lengths; however, the length of weather record for each site is capturing the same data in the lower and upper plots.

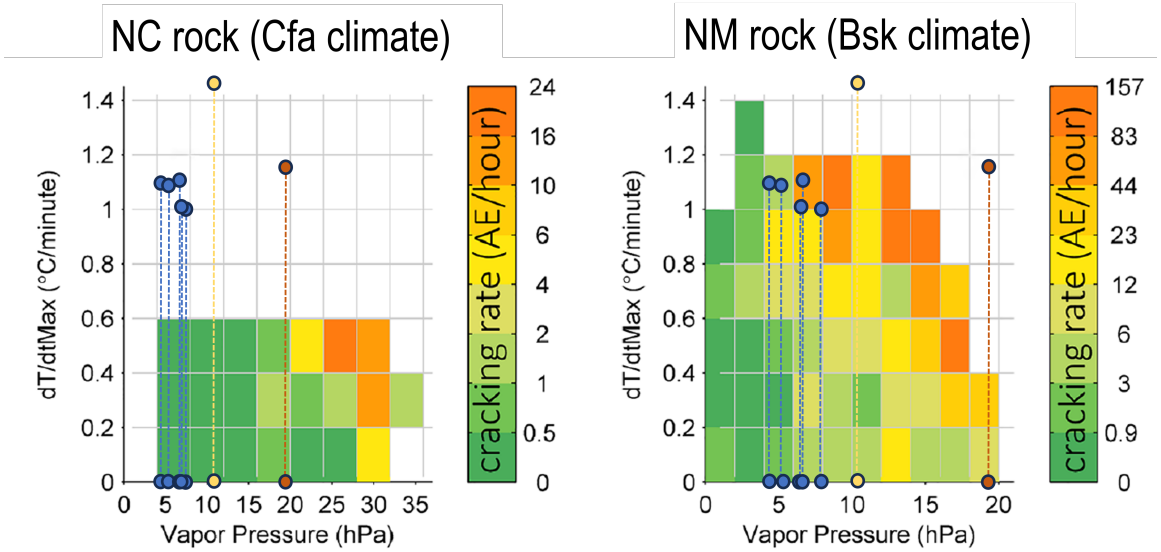

Figure 4.7: *VP* vs. dT plots from Eppes, M. C., Magi, B., Scheff, J., Warren, K., Ching, S. and Feng, T. [2020], with climate classifications of the Eppes et al. field site listed in titles. Classifications were derived using PRISM Climate Group, Oregon State University [2024] and Köppen [2011]. Circles represent the days on which cracking is predicted by the model, and are colored by site [blue represents the Northernmost site, orange the Middle site, and dark red the Southernmost site]. The dashed line between circles represents the range of possible conditions, using the hourly value [upper values, daily dT divided by 24] and per-minute values [lower values, hourly dT divided by 60] on the highest growth days indicated in Fig. 4.6.

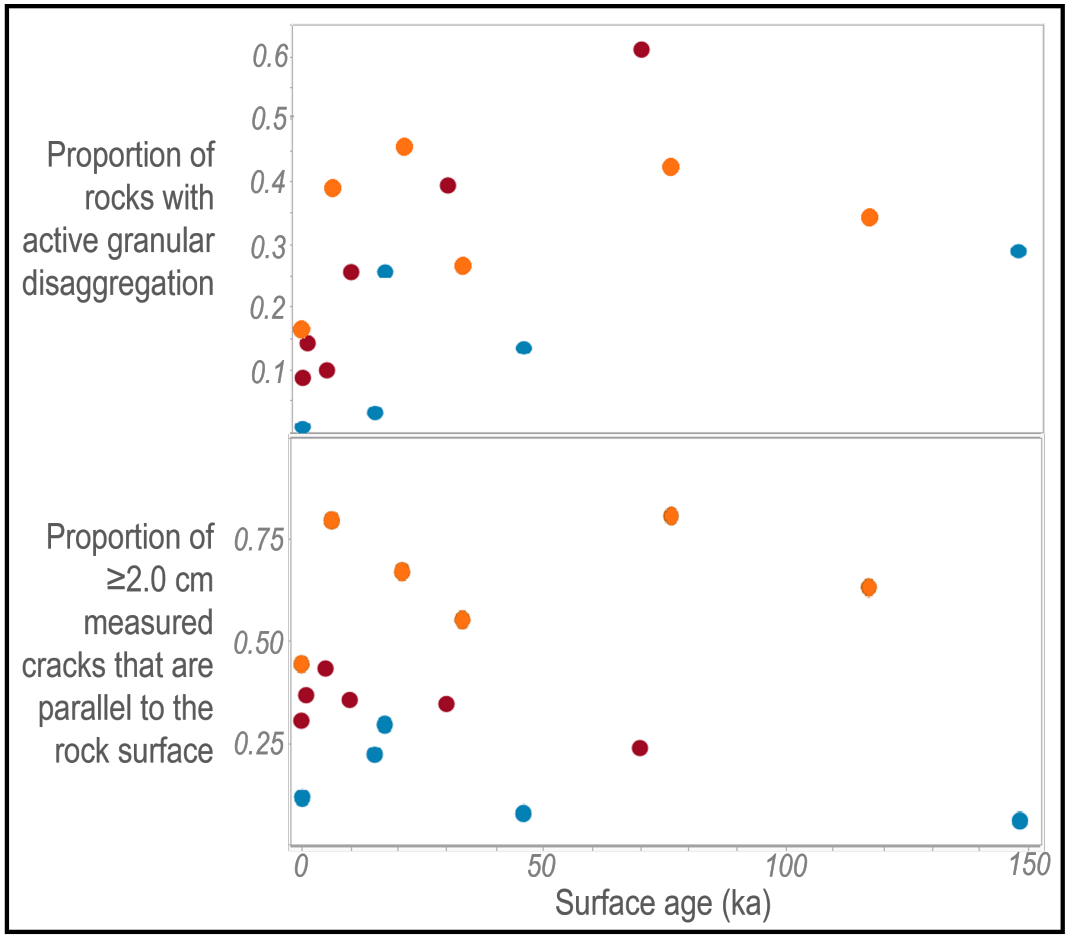

Figure 4.8: The proportion of granitoid rocks at all three sites with visible active granular disaggregation [upper] and the proportion of ≥2.0 cm cracks measured on the rocks which are parallel to the rock surface [lower]. Blue represents the Northernmost site, orange the Middle site, and dark red the Southernmost site.

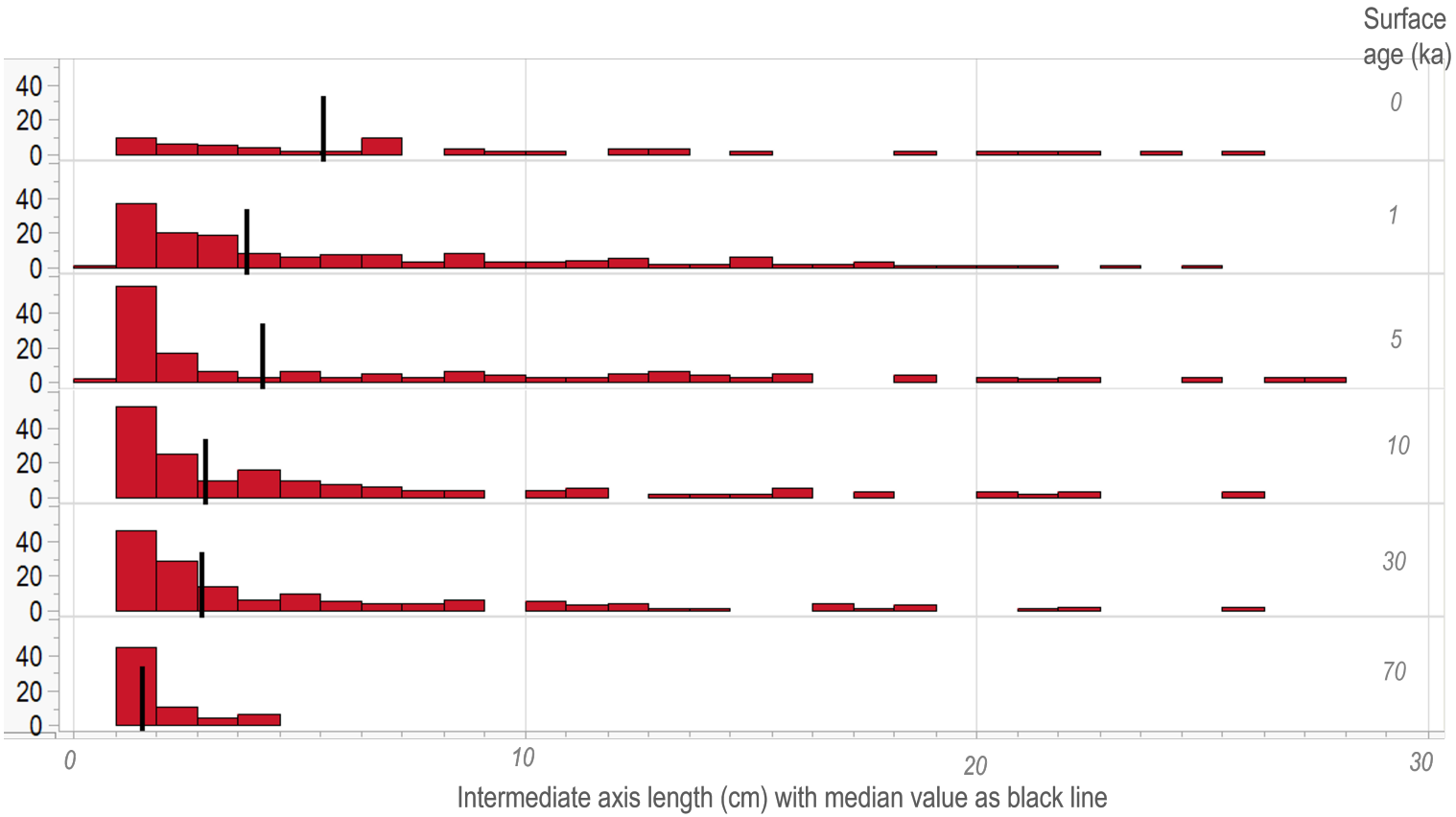

Figure 4.9: Wolman pebble count data for all clasts ≤30 cm in intermediate axis length at the Southernmost site, 1.0 cm bin width. Y-axis shows the percentage of all clasts that fall into that bin. Black vertical lines are the median values for each surface. Medians were selected over means due to the positive skew of the histograms that is apparent on all surfaces, and increases with age. Note that larger clasts exist but for ease of interpretation are not included in this figure.

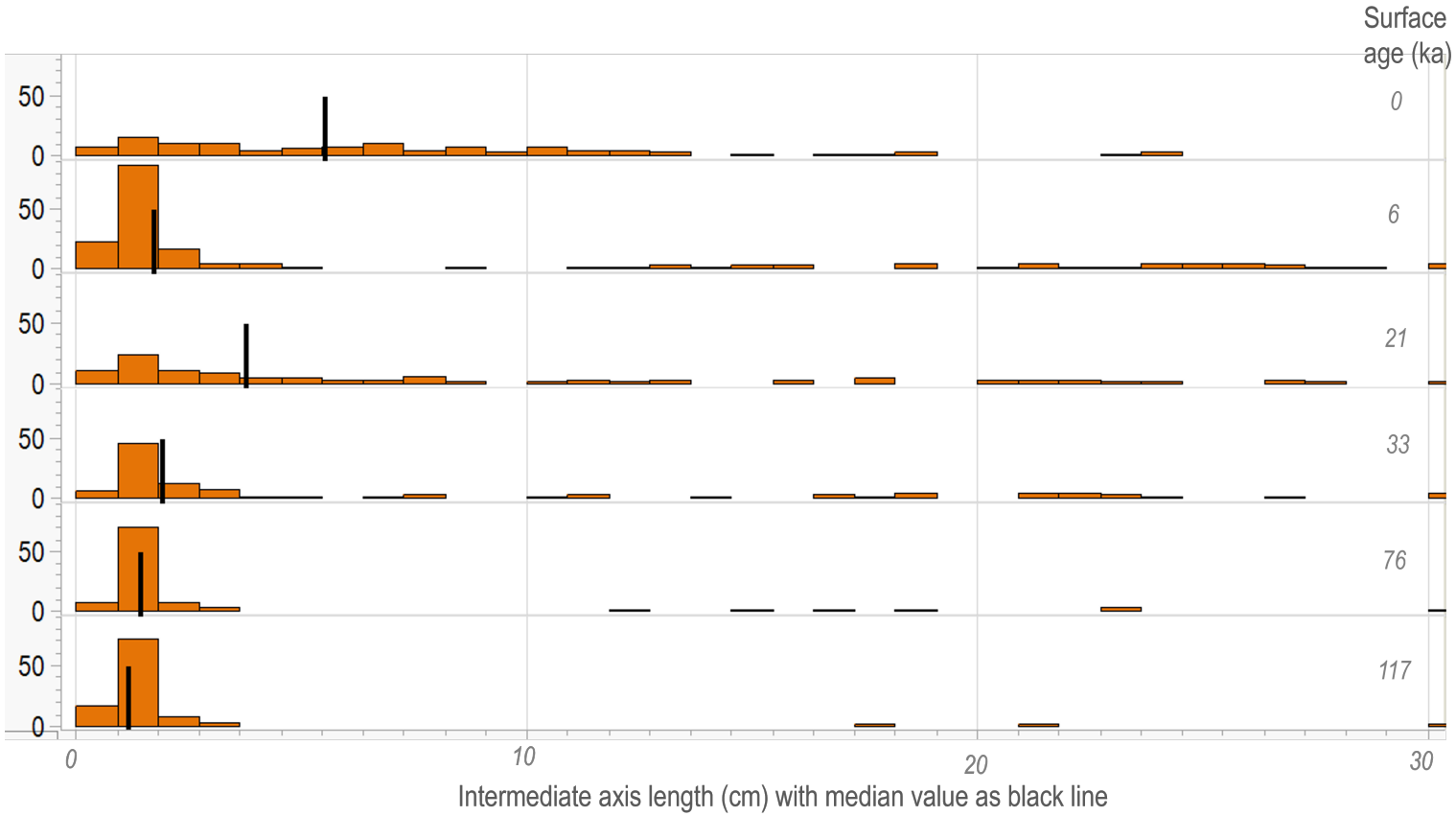

Figure 4.10: Wolman pebble count data for all clasts ≤30 cm in intermediate axis length at the Middle site, 1.0 cm bin width.

CHAPTER 5: WHAT CONTROLS MECHANICAL WEATHERING?

AUTHORS:

Monica Rasmussen and Martha Cary Eppes

5.1 Introduction

The rate and magnitude of rock mechanical weathering [cracking/fracturing] depends upon internal rock properties and external variables including grain size, mineralogy, rock elastic properties, environmental temperature and moisture conditions, and biological processes; causing weathering to progress non-linearly [e.g., Rasmussen et al., Ch. 2; Birkeland, Peter W., 1999]. When researchers isolate single environmental variables, their impact on rock cracking is often well-predicted by theoretical explanations. Under controlled environments, rock tensile strength decreases when temperature and/or relative humidity are increased [e.g., Nara, Yoshitaka, Yamanaka, Hiroshi, Oe, Yuma and Kaneko, Katsuhiko, 2013; Atkinson, Barry Kean and Meredith, Philip George, 1987b], and field data suggest that for a given stress magnitude, rock cracking due to ambient earth surface conditions is enhanced by higher temperatures and vapor pressures [Eppes, M. C., Magi, B., Scheff, J., Warren, K., Ching, S. and Feng, T., 2020]. Similarly, based on field observations, bedrock weathering increases alongside mean annual precipitation [Riebe, Clifford S., Callahan, Russell P., Granke, Sarah B. M., Carr, Bradley J., Hayes, Jorden L., Schell, Marlie S. and Sklar, Leonard S., 2021].

However, many lithological properties determined by rock formation, e.g., anisotropy, grain size, and amount of quartz, do not exhibit consistent impacts on rock cracking. Anisotropy controlled by bedding can dictate fracture spacing [Olson, Jon E., 1997] and lead to preferential fracture growth along layers with lower fracture toughness [Chandler, Michael R., Meredith, Philip G., Brantut, Nicolas and Crawford, Brian R., 2016]. Mechanical anisotropy is observed even in granitic rocks that are typically

considered isotropic in nature [Dai, F., Xia, K., Zuo, J. P., Zhang, R. and Xu, N. W., 2013], presumably due to stress conditions during and after rock formation. These anisotropic effects can lead to increases and/or decreases in rock cracking rates.

Higher amounts of quartz in granitic rock have been shown to increase linear thermal expansion [Janio de Castro Lima, José and Paraguassú, Antenor Braga, 2004] across grain sizes. Experimental studies show that linear thermal expansion can either be highest in finer-grained granitic rocks [Janio de Castro Lima, José and Paraguassú, Antenor Braga, 2004], or lowest in finer-grained granitic rock [Yin, Weitao, Feng, Zijun and Zhao, Yangsheng, 2021]. This may be due to grain size heterogeneity, where more heterogeneous grain size compositions have been shown to experience larger thermal expansion [Kang, Fangchao, Li, Yingchun and Tang, Chun'an, 2021]. Heterogeneous rocks may crack faster than homogeneous rocks due to more pre-existing weaknesses [Lu, Yinlong, Elsworth, Derek and Wang, Lianguo, 2014], but the increased compliance of cracked rocks could result in lower cracking rates over time [e.g., Rasmussen et al., Ch. 2-3]; so, this relationship is unclear. Additionally, phenocrysts within a rock can inhibit crack propagation [Gudmundsson, Agust and Brenner, Sonja L., 2001] by creating a physical barrier. Even within one "lithology", differences in grain size and porosity combined can impact how the rock responds to stress by an order of magnitude [e.g., Turowski, J. M., Pruß, G., Voigtländer, A., Ludwig, A., Landgraf, A., Kober, F. and Bonnelye, A., 2023].

The most direct controls on rock cracking, e.g., tensile strength, Young's modulus, and porosity, can vary over time as the rock is exposed to natural weathering conditions [Rasmussen et al., Ch. 3]. Experimentally, rock tensile strength for all lithologies correlates well with tensile fracture toughness [K_{IC}], which dictates the likelihood of rock fracture [e.g., Meredith, P. G. and Atkinson, B. K., 1985; Daoud, Ali, Browning, John, Meredith, Philip G. and Mitchell, Thomas M., 2020]. Tensile strength inversely correlates with erosion rates in experimental conditions, but so

do density, compressive strength, and Young's modulus [Turowski, J. M., Pruß, G., Voigtländer, A., Ludwig, A., Landgraf, A., Kober, F. and Bonnelye, A., 2023]. Isolating the impact of a single rock property is therefore challenging, and in practice, many properties will consistently covary due to rock physics relationships.

Biological and geochemical processes that occur due to natural weathering, herein termed 'secondary processes' further complicate the rock cracking prediction. The current research on the impact of lichen is not just limited, but contradictory, suggesting that lichen weaken and break rock [e.g., Burford, E. P. and Fomina, M. and Gadd, G. M., 2003; Scarciglia, Fabio, Saporito, Natalina, La Russa, Mauro F., Le Pera, Emilia, Macchione, Maria, Puntillo, Domenico, Crisci, Gino M. and Pezzino, Antonino, 2012], or reprecipitate minerals and strengthen rock [Burford, E. P. and Fomina, M. and Gadd, G. M., 2003]. Lichen connect pieces of rock, but release the hold when they die. It is currently unknown how their presence will impact cracking in the long-term. Varnish development on a rock's surface is a microbially-mediated process that occurs from the outside inward, and can strengthen rock while also enhancing the likelihood of rock cracking [e.g., Lamp, J. L., Marchant, D. R., Mackay, S. L. and Head, J. W., 2017; Thomachot, Céline and Jeannette, Daniel, 2004]. Further complicating these effects is timing: varnish development and lichen lifecycles may be independent of the rate of evolution of mechanical properties.

Geochemically, carbonate rocks dissolve under ambient surface conditions. Dissolution around crack edges can slowly lead to crack tip blunting, which decreases stress intensity [e.g., Chen, Xiaofeng, Eichhubl, Peter, Olson, Jon E. and Dewers, Thomas A., 2020]. Crack infilling processes, whereby minerals dissolve and reprecipitate, can strengthen cracks by physically reconnecting adjacent crack faces. The presence of this infilling is expected to increase over exposure age if it is indeed a secondary, post-depositional process, as opposed to a characteristic inherited from the rock's formation.

These primary and secondary properties change in tandem and frequently covary, so isolating a single influencing factor is difficult. This hinders our fundamental understanding of material physics, as well as all processes impacted by rock fracture, including building degradation [e.g., Sousa, Luís M. O., 2013], slope stability [e.g., Ballantyne, Colin K, Sandeman, Graeme F., Stone, John O. and Wilson, Peter, 2014], and landscape evolution [e.g., DiBiase, Roman A., Rossi, Matthew W. and Neely, Alexander B., 2018].

5.2 Methods

Here I present rock and fracture data from 2221 boulders that were deposited in random orientations and left exposed to natural conditions on Earth's surface for up to 148 kyr. Within this substantial dataset, I subdivided the data to isolate specific variables and determine where statistically significant trends exist for predicting rock fracture metrics. I also calculated the dependency of various properties on surface age to aid in interpreting whether rock fracture trends correlate with changing rock properties, or are driven by them.

5.2.1 Site selection

The data presented here are from the exact locations for which fracture and rock elastic property data were presented by Rasmussen et al. [Ch. 2, 3]. I analyzed surficial boulders in three Eastern California sites in different climates, including granitoid rocks at all three sites and volcanic and carbonate rocks at one site [see Fig. 4.5 for site locations and Köppen Climate Classification]. Sites were selected based on the similarity of granitoid bedrock lithology at all three sites [Bateman, P. C., 1992; Dohrenwend, J. C., 1982; Keith, W. J. and Seitz, J. F., 1981; Moore, J. G., 1981; Stone, Paul, Dunne, George C., Moore, James G. and Smith, George I., 2000], available surficial maps accompanied by surface age dating [Rood, Dylan H., Burbank, Douglas W. and Finkel, Robert C., 2011; D'Arcy, Mitch. Roda Boluda,

Duna C.. Whittaker, Alexander C. and Carpineti, Alfredo, 2015; McDonald, Eric V., McFadden, Leslie D., Wells, Stephen G., Enzel, Y. and Lancaster, N., 2003], and the abundance of boulders for analysis that are located atop stable, abandoned geomorphic surfaces. In addition to the dated surfaces, a modern active deposit [channel or wash] was identified per site, and data were collected from boulders in these deposits. These data, representing boulders that have been exposed to Earth surface conditions for varying amounts of time within one site, form a space-for-time or chronosequence study [Jenny, Hans, 1948; Birkeland, Peter W., 1999]. By including the rocks within modern deposits, properties of unweathered 'time-0' rocks can be compared with weathered rocks. The granitoid rocks on the Northernmost, Middle, and Southernmost sites form a climosequence of chronosequences, where temperature and aridity increase from North to South.

5.2.2 Field methods

Rock and fracture data were collected from 15-50 cm diameter clasts using a modified Wolman sampling methodology [Wolman, M. Gordon, 1954] to ensure random selection. For each clast, rock properties were recorded [Table 5.1], and all open planar cracks $\geq$2.0 cm were manually measured following Eppes, Martha Cary, Aldred, Jennifer, Berberich, Samantha, Dahlquist, Maxwell P., Evans, Sarah G., Keanini, Russell, Moser, Faye, Morovati, Mehdi, Porson, Steven and Rasmussen, Monica [2022] and were analyzed by Rasmussen et al. [Ch. 2] [Table 5.2].

5.2.3 Statistical approach

All statistical analyses were performed in JMP Pro software, v. 16.1.0 [SAS Institute Inc. JMP, 1989-2023]. The majority of rock property data collected are ordinal [see Table 5.3]; that is, to conserve time in collecting the data, metrics such as the percentage of clast surface covered by lichen were recorded in ranges, or by using visual reference charts for properties like rock shape [Krumbein, William Christian and

Sloss, Laurence Louis, 1963]. To represent overall rock cracking I use two metrics: crack/fracture intensity [$\sum$all $\geq$2.0 cm crack lengths / rock surface area, mm/m^2] and crack/fracture number density [$\sum$number of cracks / rock surface area, #/m^2], both continuous numerical values that were calculated for every boulder measured. Due to the highly skewed distribution of crack lengths in natural systems [e.g., Olson, Jon E., 1997], fracture intensity is log-transformed. Fracture number density is not log transformed. Detailed discussion of these fracture metrics are presented by Rasmussen et al. [Ch. 2].

I present statistics from analysis of variance [ANOVA] to determine how rock and environmental variables [ordinal data] drive rock fracture metrics [continuous data]. For rock surface ages, I use ordinal-ordinal matrix plots to understand how variables change over time. When comparing two continuous variables, e.g., clast intermediate axis length vs. fracture intensity, linear trends are fit to the data. For all approaches I present R^2 and two-tailed p-values.

5.3 Results

All results are summarized per site and lithology based on the ability to predict the fracture metrics [fracture intensity and fracture number density, Tables 5.4, 5.6, 5.8, 5.10, 5.12] and the ability for surface age to predict rock and fracture metrics [Tables 5.5, 5.7, 5.9, 5.11, 5.13], with R^2 of correlations and Pearson's p-values. Based on the field observation that both fracture intensity and fracture number density increase rapidly after rocks are initially deposited on the surface, then begin to stabilize beyond $\sim$40 ka [see Rasmussen et al., Ch.2], only clast and crack data from surfaces $<$40 ka are used to understand the relationships among rock characteristics and those two fracture metrics. For understanding the impact of surface age on rock characteristics, all available data are presented.

5.3.1 Rock and fracture property correlations, Northernmost site

At the Northernmost site, statistically significant correlations [p-value <0.05, bold in table] between rock properties and fracture metrics have R^2 values ranging from 0.04-0.36. The strongest variables that correlate with rock cracking are the percentage of mafic minerals negatively correlating with fracture intensity [R^2=0.14] and fracture number density [R^2=0.36, Fig. 5.1], clast size negatively correlating with fracture number density [R^2=0.10] and fracture intensity [R^2=0.15, Fig. 5.2], and clast roundness [R^2=0.09] and sphericity [R^2=0.15] negatively correlating with fracture number density [Fig. 5.3].

For these same rocks, when assessing the correlation between rock properties with surface age, all are statistically significant [Table 5.5] with R^2 values ranging from 0.04-0.27. The strongest correlations between surface age and clast properties are lichen coverage which increases with surface age [R^2=0.27, Fig. 5.4], clast sphericity which increases with surface age [R^2=0.14, Fig. 5.5], granular disintegration which increases with surface age [R^2=0.11, Fig. 5.6], and clast size which increases with surface age [R^2=0.11, Fig. 5.7].

5.3.2 Rock and fracture property correlations, Middle site

At the Middle Site, more rock property data were collected from clasts on differently aged surfaces, including crack infilling [the amount of cracks which have a visible, secondary infilling like carbonate minerals, varnish development, or immovable lichen] and the short crack density [number of cracks <2.0cm long that are present for every decimeter of rock surface]. Statistically significant correlations [p-value <0.05, bold in Table 5.6] with fracture metrics have R^2 values ranging from 0.01-0.18. The strongest variables that correlate with rock cracking are surface age driving increases in fracture intensity [R^2=0.15] and fracture number density [R^2=0.18, Fig. 5.8], the density of <2cm cracks positively correlating with fracture intensity [R^2=0.10] and fracture

number density [R^2=0.18, Fig. 5.9], and the amount of crack infilling negatively correlating with fracture number density [R^2=0.12, Fig. 5.10]. This implies that crack infilling is effectively decreasing the number of visible cracks on the rock surface.

For these same rocks, when assessing the correlation between rock properties with surface age, all are significant with R^2 values ranging from 0.03-0.15 [Table 5.7], except the presence of veins in the rocks. The strongest correlations between surface age and clast properties are clast size which decreases with surface age [R^2=0.15, opposite trend to Northernmost site, Fig. 5.11], and increases in both <2cm crack density and the amount of infilled cracks with surface age [R^2=0.10 for both, Fig. 5.12]. Since short crack density can continue to increase over time while infilling is also increasing, it is possible that the infilling itself is dividing measurable ($\geq$2.0 cm) cracks into shorter cracks.

5.3.3 Rock and fracture property correlations, Southernmost site

At the Southernmost site, fewer rocks were measured per lithology, but three lithologies were measured. For granitoid rocks, statistically significant correlations [p-value <0.05, bold in Table 5.8] with fracture metrics have R^2 values ranging from 0.03-0.25. The strongest variables that correlate with rock cracking are the density of <2cm cracks positively correlating with fracture intensity [R^2=0.22] and fracture number density [R^2=0.25, Fig. 5.13], the amount of crack infilling negatively correlating with fracture number density [R^2=0.12, Fig. 5.14], and surface age positively correlating with fracture intensity [R^2=0.10] and fracture number density [R^2=0.10, Fig. 5.15].

For these granitoid rocks, when assessing the correlation between rock properties with surface age, all are significant except the presence of veins in the rocks, observed pitting, and the amount of lichen coverage [Table 5.9] with R^2 values of significant variables ranging from 0.04-0.23. The strongest correlations between surface age and clast properties are the density of short cracks which increase alongside surface age

[R^2=0.23, Fig. 5.16], varnish development increasing with age [R^2=0.23, Fig. 5.17], roundness increasing [R^2=0.19] and sphericity decreasing [R^2=0.21] as age increases [Fig. 5.18], increasingly older rocks having larger mafic grain sizes [R^2=0.15, Fig [5.19], and an increase in granular disintegration over time [R^2=0.12, Fig. 5.20].

Unlike the granitoid rocks, the volcanic rocks at the Southernmost site show a strong correlation between fracture metrics and grain size. Statistically significant correlations [p-value <0.05, bold in Table 5.10] with fracture metrics have R^2 values ranging from 0.04-0.23. Felsic grain size correlates with both fracture intensity [R^2=0.23] and fracture number density [R^2=0.21, Fig. 5.21], with larger grain sizes correlating with more cracking. Surface age positively correlates with fracture intensity [R^2=0.13, Fig. 5.22]. The density of <2cm cracks only weakly positively correlates with fracture intensity [R^2=0.09] and fracture number density [R^2=0.07, Fig. 5.23].

The volcanic rock age trends are not significant as frequently as the granitoid rocks. Only grain size, varnish development, crack infilling, and clast size have a statistically significant relationship with surface age. However, varnish positively correlates with surface age relatively strongly [R^2=0.31, Fig. 5.24], alongside crack infilling [R^2=0.17, Fig. 5.25]. Mafic grain size decreases while felsic grain size increases with increasing age [R^2=0.23 and 0.15, respectively, Fig. 5.26], perhaps because of an increase in the amount of finer-grained volcanic rocks which included larger felsic phenocrysts [Stone, Paul, Miller, David M., Stevens, Calvin H., Rosario, Jose, Vazquez, Jorge A., Wan, Elmira, Priest, Susan S. and Valin, Zenon C., 2017].

For carbonate rocks at the Southernmost site, half of the clast and crack properties correlate significantly with fracture metrics, with R^2 values ranging from 0.04-0.43. The strongest correlations are with surface age, which positively correlates with both fracture intensity [R^2=0.43] and fracture number density [R^2=0.34, Fig. 5.27. Crack infilling presumably drives a decrease in fracture intensity [R^2=0.19] and fracture

number density [R^2=0.20, Fig. 5.28], and the density of <2 cm cracks positively correlates with fracture intensity [R^2=0.20] and fracture number density [R^2=0.31, Fig. 5.29].

Like granitoid rocks, most carbonate rock properties correlate significantly with surface age, with R^2 ranging between 0.05-0.27. The strongest correlations are for granular disintegration which increases with surface age [R^2=0.27, Fig. 5.30], an increase in lichen with age [R^2=0.24, Fig. 5.31], and increasing density of <2 cm cracks with increasing surface age [R^2=0.12, Fig. 5.32].

5.3.4 Trends between sites among granitoid rocks

Across all sites, rock properties of granitoid rocks vary significantly with surface age. This is unsurprising, given documented relative age dating techniques which leverage parameters like lichen cover and varnish [e.g., McFadden, Leslie D., Ritter, John B. and Wells, Stephen G., 1989; Peter W. Birkeland, 1973], clast size [McFadden, Leslie D., Ritter, John B. and Wells, Stephen G., 1989], and clast shape [Peter W. Birkeland, 1973]. Clast shape also correlates with fracture metrics at Lundy Canyon where lower sphericity correlates with more cracking, but lower sphericity at the other two sites more strongly correlates with surface age. Rock fracture that increases with surface age will change the shape of a clast by both removing irregularly shaped pieces of rocks from edges [e.g., corner cracks, Zhang, Bin and Guo, Wanlin, 2007] and breaking spherical rocks into two elongated rocks. Given this strong dependence of rock shape on prior fracture, it is impossible to disentangle rock shape changes over time, from fracture metrics increasing over time.

Varnish is expected to increase with rock exposure [surface] age [e.g., Ronald I. Dorn and Theodore M. Oberlander, 1982], which it does at Shepherd Creek and Providence Mountains; however, it remains about constant at Lundy Canyon. This varnish can act to infill and strengthen the surface of rocks [e.g., Lamp, J. L., Marchant, D. R., Mackay, S. L. and Head, J. W., 2017; Ronald I. Dorn and Theodore M. Oberlander,

1982]. Alternatively, the varnish can enhance spallation, [e.g., behavior proposed by Thomachot, Céline and Jeannette, Daniel, 2004]. To test which of these behaviors – either counteracting or instigating cracking – dominates over geologic time, I compare varnish development at all three sites with the amount of infilled cracks on the rock surface, and the preponderance of surface-parallel cracks which can lead to spallation [Fig. 5.33, left]. At Lundy Canyon, the correlation between varnish and crack infilling is insignificant, and varnish significantly but weakly correlates with crack infilling at Shepherd Creek and Providence Mountains [R^2=0.05 at both sites]. Surface-parallel cracking similarly only weakly correlates with the amount of rock varnish on granitic rocks. Taken together, this indicates that varnish coverage increases over exposure age, but is not having a strong impact on the amount of surface parallel rock spallation that is evident on the clasts.

Surprisingly, the density of short [<2 cm] cracks positively correlates with crack infilling at the Middle site, while it negatively correlates at the other two sites [Fig. 5.34]. This may represent the balance between the sealing of visible cracks through secondary varnish development, leading to less measurable cracks; and the infilling process occurring as bridges that turn one long crack into multiple shorter cracks, leading to a higher short crack density. Anecdotally, both full-crack infilling and bridge infilling was observed during field data acquisition.

5.3.5 Trends between rock types

To further understand the impacts of varnish development increasing with surface age at the Southernmost Providence Mountains site, I compare varnish development with surface-parallel crack abundance for all three rock types [Fig. 5.35]. Correlations are very weak [R^2=0.01] or insignificant, suggesting that varnish development does not seem to modify spallation for any rock type at this location over this time frame. For granitoid rocks, an increase in varnish coverage correlates with an increase in short cracks [R^2=0.13, Fig. 5.36] but the correlation is not significant for other rock

types, so this may simply reflect that both variables increase with age. Similarly, for volcanic rocks, the amount of crack infilling increases alongside varnish [R^2=0.16, Fig. 5.37], perhaps suggesting that the varnish itself is infilling and strengthening cracks.

The grain size of volcanic lithological units varies within the catchment and appears to provide a lithological control that leads to a bias in the availability of rocks remaining on the oldest surfaces. At the Providence Mountains, the wide range of 'volcanic' units range from relatively uniform, fine-grained rhyolite with a wavy foliation; to rhyolitic rock with a fine-grained mafic groundmass that has no visible fabric but contains larger felsic phenocrysts [Stone, Paul, Miller, David M., Stevens, Calvin H., Rosario, Jose, Vazquez, Jorge A., Wan, Elmira, Priest, Susan S. and Valin, Zenon C., 2017]. The overwhelming abundance of fine-grained mafic rocks on surfaces older than 5 ka [Fig. 5.26] suggests that perhaps, the finer-grained rocks are more resistant to cracking, leading to a 'survivor's bias' where the rocks remaining on the 10 ka surface are disproportionately represented by these stronger lithologies. The finer-grained rocks are again abundant on the oldest 70 ka surface, which could suggest that the rocks with large phenocrysts have also been significantly cracked by this time. Alternatively, the source material available for transport during the multiple depositional events may have changed slightly, causing different bedrock units to be more abundant on different surfaces.

For granitoid rocks, mafic grain sizes are larger on older rocks [R^2=0.15] and felsic grain size does not significantly change. This may indicate that the same 'survivor's bias' is impactful for granitoid rocks, especially given that the statistical correlation between age and fracture metrics [R^2=0.10 for both metrics] has a lower R^2 than the correlation between mafic grain sizes and surface age. This could suggest that granitoid rocks with larger mafic grain sizes are more resistant to cracking, and thus are able to 'survive' on older surfaces more than those with smaller-grained mafic minerals. This is in seeming opposition to experimental and theoretical studies showing

that larger-grained granitic rocks have consistently lower tensile strength [e.g., Yu, Miao, Wei, Chenhui, Niu, Leilei, Li, Shaohua and Yu, Yongjun, 2018]; therefore, these results may again be an issue of the source rock of clasts in the catchment differing among depositional events.

Grain size does not significantly change on carbonate rocks over time even though the catchment contains a range of fine-grained, bedded limestones, to dolostones with nodules, to coarse-grained marbles [Stone, Paul, Miller, David M., Stevens, Calvin H., Rosario, Jose, Vazquez, Jorge A., Wan, Elmira, Priest, Susan S. and Valin, Zenon C., 2017].

5.4 Discussion

5.4.1 Significant variables driving fracture

When focused on the first ∼40 ka, surface age is the most impactful variable I identified, positively correlating with the rock fracture metrics fracture intensity and fracture number density for all rock types at all sites. Time, more than any variable that has been tested in the laboratory, is strongly driving rock fracture, suggesting that rock fracture is predominantly progressive.

Rasmussen et al. [in prep, see Ch. 2] present strong evidence explaining why rocks accumulate cracks quickly when first exposed to environmental conditions, then cracking continues but cracking rates decrease over time. The nonlinear crack growth behavior (decreasing rate) occurs in the first ∼30-40 ka of rock exposure, and after this point, fracture metrics remain relatively steady. This nonlinear behavior may explain why fracture intensity and number density are not the strongest predictors of all surface ages, given that the fracture metrics evolve non-linearly over time and this statistical approach assumes linear relationships.

Other variables which impact rock fracture metrics but are less consistent among rock types and sites include:

1. Crack infilling by minerals, lichen, or varnish [negative correlation for granitoid rocks at all sites; and for only the granitoid and carbonate rocks at the arid Providence Mountains site]

2. Mafic mineral size [negative correlation for Lundy Canyon granitoid rocks, no correlation for Shepherd Creek granitoid rocks, positive correlation for Providence Mountains granitoid rocks, and no correlation for volcanic or carbonate rocks]

Our understanding of how lichen and varnish impact rock cracking is limited and often contradictory, showing that these variables can sometimes inhibit but sometimes initiate rock fracture [e.g., Burford, E. P. and Fomina, M. and Gadd, G. M., 2003; Lamp, J. L., Marchant, D. R., Mackay, S. L. and Head, J. W., 2017; Thomachot, Céline and Jeannette, Daniel, 2004]. Here, lichen coverage increases with surface age on the Northernmost granitoid [Table 5.5] and Southernmost carbonate rocks [Table 5.13], but only weakly correlates with fracture metrics. This suggests that for some rock types, lichen growth increases over geologic timescales, but that this growth does not impact rock cracking in a predictable way. If lichen were enhancing or counteracting cracking, its increased abundance on older surfaces would also significantly correlate with fracture metrics, which increase over time.

Similarly, varnish development has a higher positive R^2 correlation with surface age than with fracture metrics for all rock types at all sites. Varnish can infill cracks and reduce the number of countable cracks on the rock. Since both varnish and fracture metrics increase with surface age, it is possible that varnish is counteracting some crack growth; however, if this is the case, the increase in crack growth still dominates over the varnish development.

For carbonate rocks, the cracking increase with age has highest R^2 in the entire dataset, suggesting that the crack growth rate in the first $\sim$40 ka is fairly linear with these rocks. It is also possible that carbonate rocks can withstand more distributed

cracking before pieces of rock break off. Olson, Jon E. [2004] showed that fracture spacing is related to the subcritical cracking index n. Experimentally, carbonate rocks generally have a lower n than granitic and volcanic rocks [see review of laboratory results in Atkinson, Barry Kean and Meredith, Philip George, 1987b]. Olson, Jon E. [2004] predict a lower n would result in distributed microfracture growth, with multiple spaced cracks growing simultaneously. This would result in a high number of measurable cracks that are simultaneously growing, but have not yet broken the rock.

Mineralogy dictates cracking rates, and research has shown that the proportion of minerals matters, with a 'sweet spot' of high thermal stress existing even for a simple quartz-microcline mixture [Vázquez, Patricia, Shushakova, Victoria and Gómez-Heras, Miguel, 2015]. This mixture does not represent mostly quartz or mostly microcline, but an approximately equal mixture of both minerals. In the data presented here, I test statistical correlations of increases or decreases between two continuous or ordinal variables. However, if there is a mineralogical mixture in any of the rock types that enhances thermal stresses, the statistical tests will not reflect this unless it is at either the highest or lowest end of the mixture. This may explain the sometimes conflicting relationships among different rock types and sites when assessing the impact of grain size and mafic mineral percentage relative to fracture metrics.

The volcanic rocks which persist on older surfaces have a finer matrix than younger rocks, but more heterogeneity, with large felsic phenocrysts [Fig. 5.26]. The increased amount of these rocks may be due to finer-grained rocks having higher tensile strength [e.g., Yu, Qinglei, Zhu, Wancheng, Ranjith, PG and Shao, Shishi, 2018; Yu, Miao, Wei, Chenhui, Niu, Leilei, Li, Shaohua and Yu, Yongjun, 2018], or experiencing lower thermal expansion, like that observed by Yin, Weitao, Feng, Zijun and Zhao, Yangsheng [2021]. Experimental data show that heterogeneity could enhance cracking by providing areas of weakness [Lu, Yinlong, Elsworth, Derek and Wang, Lianguo,

2014], or phenocrysts themselves could provide a barrier that blocks crack growth [Gudmundsson, Agust and Brenner, Sonja L., 2001]. Here, the heterogeneity may be inhibiting fracture, or similar to other rock properties, this may simply reflect a slightly different assemblage of rocks that were deposited on this site initially.

5.4.2 Reliability of relative age dating

Visible, measurable field rock properties have been successfully employed as a relative age indicator for decades [e.g., McFadden, Leslie D., Ritter, John B. and Wells, Stephen G., 1989]. This study reconfirms that properties like varnish and lichen coverage and rock shape are reasonable predictors of surface age for granitoid rocks [see Tables 5.5, 5.7, 5.9]. Varnish is lithology-dependent, and may lead to crack infilling. For volcanic rocks, varnish development covaries with grain size and the amount of crack infilling, all of which increase with surface age and thus consequently positively correlate with fracture metrics. For carbonate rocks, lichen coverage is a strong age predictor, but lichen coverage was statistically insignificant for predicting the ages of both volcanic and granitoid rocks at the same Southernmost site. Like varnish, the species of lichen is dependent on lithology, so this may be expected; however, given the minimal studies on lichen species globally, the discrepancy in its ability to predict age makes it an unreliable metric across different rock types.

While it is not always the best predictor of age, rock fracture density [number of cracks normalized for surface area] of cracks $\geq$2.0 cm positively correlates with surface age to a statistically significant degree for all rock types and sites, within the first $\sim$40 ka of rock exposure. Additionally, short [$<$2.0 cm] crack density always positively correlates with $\geq$2.0 cm fracture density in a statistically significant way. This suggests that the most overall reliable semi-quantitative relative age metric is an easy type of data to collect: researchers can simply measure the length of the three primary axes of the clast, and count the visible cracks.

5.4.3 Conclusion

Overall, this analysis shows the complex interplay of rock physical properties, how they evolve, and how they may drive or limit cracking. This chapter provides a detailed analysis of a large dataset containing measurements from 2221 rocks yet the results show that the unknowns in rock cracking still greatly outweigh the known drivers. More data, and/or more detailed data, from field studies will be required to help us fully understand what has impacted rock cracking in the past, and how it may continue to evolve in the future. Most importantly, the age of the surface positively correlates with cracking in the first ∼40 ka of exposure across all sites and rock types.

For surface dating, by simply counting the number of cracks on a rock's surface, researchers may discover a new and broadly reliable relative age estimator. Compared with approaches like geochemical testing of rock varnish, this is a much faster and cheaper metric to test. By including crack density as a relative age dating metric collected in fieldwork, future research where surface ages are known can inform our understanding of how the complexities of natural materials drive rock cracking over time.

5.5 Tables

Table 5.1: Type of data collected from clasts, and surfaces for which data are available.

Site	Clast measurements	Surface ages available [ka]
Northernmost	primary axes length	0, 15, 18, 41, 148
Middle	primary axes length	0, 6, 21, 33, 76, 117
Southernmost	primary axes length	0, 1, 5, 10, 30, 70
Northernmost	roundness & angularity	0, 15, 18, 41, 148
Middle	roundness & angularity	0, 6, 21, 33, 76, 117
Southernmost	roundness & angularity	0, 1, 5, 10, 30, 70
Northernmost	presence of rock fabric	0, 15, 18, 41, 148
Middle	presence of rock fabric	0, 6, 21, 33, 76, 117
Southernmost	presence of rock fabric	0, 1, 5, 10, 30, 70
Northernmost	grain size/% mafic	18
Middle	grain size/% mafic	0, 6, 21, 33, 76, 117
Southernmost	grain size/% mafic	0, 1, 5, 10, 30, 70
Northernmost	granular disintegration	0, 15, 18, 41, 148
Middle	granular disintegration	0, 6, 21, 33, 76, 117
Southernmost	granular disintegration	0, 1, 5, 10, 30, 70
Northernmost	presence of pitting	18
Middle	presence of pitting	0, 6, 21, 33, 76, 117
Southernmost	presence of pitting	0, 1, 5, 10, 30, 70
Northernmost	amount of lichen coverage	0, 15, 18, 41, 148
Middle	amount of lichen coverage	0, 6, 21, 33, 76, 117
Southernmost	amount of lichen coverage	0, 1, 5, 10, 30, 70
Northernmost	amount of varnish coverage	0, 15, 18, 41, 148
Middle	amount of varnish coverage	0, 6, 21, 33, 76, 117
Southernmost	amount of varnish coverage	0, 1, 5, 10, 30, 70

Table 5.2: Data collected for each crack ≥2.0 cm in continuous, open surface length, and surfaces for which data are available.

Site	Rock type	Crack measurements	Surface ages available [ka]
Northernmost	granitoid	length, width, strike, dip	0, 15, 18, 41, 148
Middle	granitoid	length, width, strike, dip	0, 6, 21, 33, 76, 117
Southernmost	all	length, width, strike, dip	0, 1, 5, 10, 30, 70
Northernmost	granitoid	fracture intensity	0, 15, 18, 41, 148
Middle	granitoid	fracture intensity	0, 6, 21, 33, 76, 117
Southernmost	all	fracture intensity	0, 1, 5, 10, 30, 70
Northernmost	granitoid	fracture number density	0, 15, 18, 41, 148
Middle	granitoid	fracture number density	0, 6, 21, 33, 76, 117
Southernmost	all	fracture number density	0, 1, 5, 10, 30, 70
Northernmost	granitoid	density of <2.0 cm cracks	8
Middle	granitoid	density of <2.0 cm cracks	0, 6, 21, 33, 76, 117
Southernmost	granitoid	density of <2.0 cm cracks	0, 1, 5, 10, 30
Southernmost	volcanic	density of <2.0 cm cracks	0, 1, 5, 10, 70
Southernmost	carbonate	density of <2.0 cm cracks	0, 1, 5, 10, 30, 70
Northernmost	granitoid	degree of crack infilling	18
Middle	granitoid	degree of crack infilling	0, 6, 21, 33, 76
Southernmost	granitoid	degree of crack infilling	0, 1, 5, 10, 30
Southernmost	volcanic	degree of crack infilling	0, 1, 5, 10, 70
Southernmost	carbonate	degree of crack infilling	0, 1, 5, 10, 30, 70

Table 5.3: The type of data used for statistical correlation, based on how data were collected in the field.

Data	Categorical	Ordinal	Continuous
Rock type	X		
Surface age		X	
Clast width			X
Fracture intensity			X
Fracture number density			X
<2 cm crack density		X	
Mafic mineral percentage		X	
Mafic / felsic grain size		X	
Roundness / sphericity		X	
Granular disintegration		X	
Pitting		X	
Lichen		X	
Varnish		X	
Amount of crack infilling		X	
Presence of fabric/veins		X	

Table 5.4: Statistical parameters for fracture metric prediction at the Northernmost Lundy Canyon site. Note that only surfaces <40 ka are used here [41 and 148 ka surfaces excluded].

Independent variable	Dependent variable	R^2	p-value
Surface age	fracture intensity	0.02	0.29
Surface age	**fracture # density**	**0.08**	**0.00**
Mafic percentage	**fracture intensity**	**0.14**	**0.02**
Mafic percentage	**fracture # density**	**0.36**	**0.00**
Mafic/felsic grain size	fracture intensity	0.03/0.18	0.90/0.29
Mafic/felsic grain size	fracture # density	0.09/0.11	0.58/0.62
Roundness/sphericity	fracture intensity	0.09/0.08	0.06/0.09
Roundness/sphericity	**fracture # density**	**0.09/0.15**	**0.04/0.00**
Granular disintegration	fracture intensity	0.00	0.50
Granular disintegration	fracture # density	0.00	0.59
Lichen	**fracture intensity**	**0.04**	**0.05**
Lichen	fracture # density	0.02	0.26
Varnish	fracture intensity	0.01	0.75
Varnish	fracture # density	0.04	0.23
<2 cm crack # density	fracture intensity	0.00	0.77
<2 cm crack # density	fracture # density	0.02	0.41
Crack infilling	fracture intensity	0.07	0.67
Crack infilling	fracture # density	0.23	0.28
Fabric/veins	fracture intensity	0.00	0.45
Fabric/veins	fracture # density	0.02	0.08
Clast size	**fracture intensity**	**0.10**	**0.00**
Clast size	**fracture # density**	**0.15**	**0.00**

Table 5.5: Statistical parameters predicting rock and crack parameters from surface age at the Northernmost Lundy Canyon site. All surface ages included.

Independent variable	Dependent variable	R^2	p-value
Surface age	**Roundness/sphericity**	**0.07/0.14**	**0.00/0.00**
Surface age	**Granular disintegration**	**0.11**	**0.00**
Surface age	**Pitting**	**0.04**	**0.02**
Surface age	**Lichen**	**0.27**	**0.00**
Surface age	**Varnish**	**0.06**	**0.00**
Surface age	**Fabric/veins**	**0.04**	**0.02**
Surface age	**Clast size**	**0.11**	**0.00**

Table 5.6: Statistical parameters for fracture metric prediction at the Middle Shepherd Creek site. Note that only surfaces <40 ka are used here [76 and 117 ka surfaces excluded].

Independent variable	Dependent variable	R^2	p-value
Surface age	**fracture intensity**	**0.15**	**0.00**
Surface age	**fracture # density**	**0.18**	**0.00**
Mafic percentage	fracture intensity	0.00	0.80
Mafic percentage	fracture # density	0.01	0.63
Mafic/felsic grain size	fracture intensity	0.04/0.04	0.33/0.30
Mafic/felsic grain size	fracture # density	0.03/0.04	0.40/0.20
Roundness/**sphericity**	**fracture intensity**	0.01/**0.06**	0.80/**0.00**
Roundness/**sphericity**	**fracture # density**	0.02/**0.05**	0.13/**0.00**
Granular disintegration	fracture intensity	0.01	0.09
Granular disintegration	**fracture # density**	**0.01**	**0.02**
Pitting	fracture intensity	0.00	1.00
Pitting	fracture # density	0.00	0.80
Lichen	fracture intensity	0.01	0.53
Lichen	fracture # density	0.01	0.24
Varnish	**fracture intensity**	**0.06**	**0.00**
Varnish	**fracture # density**	**0.07**	**0.00**
<2 cm crack # density	**fracture intensity**	**0.10**	**0.00**
<2 cm crack # density	**fracture # density**	**0.18**	**0.00**
Crack infilling	**fracture intensity**	**0.09**	**0.00**
Crack infilling	**fracture # density**	**0.12**	**0.00**
Fabric/veins	fracture intensity	0.00	0.25
Fabric/veins	fracture # density	0.00	0.12
Clast size	**fracture intensity**	**0.01**	**0.03**
Clast size	fracture # density	0.00	0.54

Table 5.7: Statistical parameters predicting rock and crack parameters from surface age at the Middle Shepherd Creek site. All surface ages included.

Independent variable	Dependent variable	R^2	p-value
Surface age	**Mafic percentage**	**0.03**	**0.00**
Surface age	**Mafic/felsic grain size**	**0.06/0.06**	**0.00/0.00**
Surface age	**Roundness/sphericity**	**0.08/0.07**	**0.00/0.00**
Surface age	**Granular disintegration**	**0.05**	**0.00**
Surface age	**Pitting**	**0.11**	**0.00**
Surface age	**Lichen**	**0.08**	**0.00**
Surface age	**Varnish**	**0.09**	**0.00**
Surface age	**<2 cm crack # density**	**0.10**	**0.00**
Surface age	**Crack infilling**	**0.10**	**0.00**
Surface age	Fabric/veins	0.03	0.31
Surface age	**Clast size**	**0.15**	**0.00**

Table 5.8: Statistical parameters for fracture metric prediction at the Southernmost Providence Mountains granitoid rocks. Note that only surfaces <40 ka are used here [70 ka surface excluded].

Independent variable	Dependent variable	R^2	p-value
Surface age	**fracture intensity**	**0.10**	**0.00**
Surface age	**fracture # density**	**0.10**	**0.00**
Mafic percentage	**fracture intensity**	**0.06**	**0.03**
Mafic percentage	**fracture # density**	**0.07**	**0.00**
Mafic/felsic grain size	fracture intensity	0.02/0.06	0.46/0.24
Mafic/felsic grain size	fracture # density	0.03/0.01	0.21/0.93
Roundness/sphericity	fracture intensity	0.02/0.05	0.53/0.11
Roundness/sphericity	fracture # density	0.02/0.05	0.38/0.06
Granular disintegration	**fracture intensity**	**0.07**	**0.00**
Granular disintegration	**fracture # density**	**0.03**	**0.02**
Lichen	fracture intensity	0.03	0.12
Lichen	fracture # density	0.00	0.66
Varnish	fracture intensity	0.03	0.10
Varnish	**fracture # density**	**0.05**	**0.03**
<2 cm crack # density	**fracture intensity**	**0.22**	**0.00**
<2 cm crack # density	**fracture # density**	**0.25**	**0.00**
Crack infilling	fracture intensity	0.03	0.09
Crack infilling	**fracture # density**	**0.12**	**0.00**
Fabric/veins	fracture intensity	0.01	0.15
Fabric/veins	fracture # density	0.00	0.56
Clast size	**fracture intensity**	**0.03**	**0.01**
Clast size	**fracture # density**	**0.06**	**0.00**

Table 5.9: Statistical parameters predicting granitoid rock and crack parameters from surface age at the Southernmost Providence Mountains site. All surface ages included.

Independent variable	Dependent variable	R^2	p-value
Surface age	**Mafic percentage**	**0.08**	**0.01**
Surface age	**Mafic**/felsic grain size	**0.15**/0.08	**0.00**/0.07
Surface age	**Roundness/sphericity**	**0.19/0.21**	**0.00/0.00**
Surface age	**Granular disintegration**	**0.12**	**0.00**
Surface age	Pitting	0.25	0.20
Surface age	Lichen	0.07	0.33
Surface age	**Varnish**	**0.23**	**0.00**
Surface age	**<2 cm crack # density**	**0.23**	**0.00**
Surface age	**Crack infilling**	**0.07**	**0.00**
Surface age	Fabric/veins	0.02	0.32
Surface age	**Clast size**	**0.04**	**0.00**

Table 5.10: Statistical parameters for fracture metric prediction at the Southernmost Providence Mountains volcanic rocks. Note that only surfaces <40 ka are used here [70 ka surface excluded].

Independent variable	Dependent variable	R^2	p-value
Surface age	**fracture intensity**	**0.13**	**0.00**
Surface age	**fracture # density**	**0.08**	**0.00**
Mafic percentage	fracture intensity	0.15	0.09
Mafic percentage	fracture # density	0.03	0.83
Grain size	**fracture intensity**	**0.23**	**0.04**
Grain size	**fracture # density**	**0.21**	**0.00**
Roundness/sphericity	fracture intensity	0.07/0.05	0.12/0.57
Roundness/sphericity	fracture # density	0.05/0.02	0.19/0.79
Lichen	fracture intensity	0.04	0.31
Lichen	fracture # density	0.06	0.06
Varnish	fracture intensity	0.03	0.15
Varnish	fracture # density	0.02	0.33
<2 cm crack # density	**fracture intensity**	**0.09**	**0.05**
<2 cm crack # density	**fracture # density**	**0.07**	**0.03**
Crack infilling	fracture intensity	0.08	0.33
Crack infilling	fracture # density	0.07	0.12
Fabric/veins	fracture intensity	0.01	0.10
Fabric/veins	fracture # density	0.01	0.08
Clast size	**fracture intensity**	**0.04**	**0.00**
Clast size	**fracture # density**	**0.08**	**0.00**

Table 5.11: Statistical parameters predicting volcanic rock and crack parameters from surface age at the Southernmost Providence Mountains site. All surface ages included.

Independent variable	Dependent variable	R^2	p-value
Surface age	**Mafic/felsic grain size**	**0.23/0.15**	**0.00/0.01**
Surface age	Roundness/sphericity	0.07/0.05	0.14/0.40
Surface age	Granular disintegration	0.17	0.62
Surface age	Pitting	0.11	0.80
Surface age	Lichen	0.05	0.34
Surface age	**Varnish**	**0.31**	**0.00**
Surface age	<2 cm crack # density	0.04	0.67
Surface age	**Crack infilling**	**0.17**	**0.00**
Surface age	Fabric/veins	0.03	0.08
Surface age	**Clast size**	**0.07**	**0.00**

Table 5.12: Statistical parameters for fracture metric prediction at the Southernmost Providence Mountains carbonate rocks. Note that only surfaces <40 ka are used here [70 ka surface excluded].

Independent variable	Dependent variable	R^2	p-value
Surface age	**fracture intensity**	**0.43**	**0.00**
Surface age	**fracture # density**	**0.34**	**0.00**
Grain size	fracture intensity	0.00	0.91
Grain size	fracture # density	0.00	0.98
Roundness/sphericity	fracture intensity	0.05/0.02	0.07/0.45
Roundness/sphericity	fracture # density	0.04/0.02	0.09/0.19
Granular disintegration	fracture intensity	0.00	0.64
Granular disintegration	fracture # density	0.00	0.90
Pitting	fracture intensity	0.00	0.59
Pitting	fracture # density	0.01	0.11
Lichen	**fracture intensity**	**0.09**	**0.00**
Lichen	**fracture # density**	**0.11**	**0.00**
Varnish	fracture intensity	0.03	0.34
Varnish	fracture # density	0.01	0.52
<2 cm crack # density	**fracture intensity**	**0.20**	**0.00**
<2 cm crack # density	**fracture # density**	**0.31**	**0.00**
Crack infilling	**fracture intensity**	**0.19**	**0.00**
Crack infilling	**fracture # density**	**0.20**	**0.00**
Bedding	**fracture intensity**	**0.05**	**0.00**
Bedding	**fracture # density**	**0.04**	**0.00**
Clast size	**fracture intensity**	**0.05**	**0.00**
Clast size	fracture # density	0.01	0.26

Table 5.13: Statistical parameters predicting carbonate rock and crack parameters from surface age at the Southernmost Providence Mountains site. All surface ages included.

Independent variable	Dependent variable	R^2	p-value
Surface age	Grain size	0.08	0.08
Surface age	Roundness/**sphericity**	0.06/**0.05**	0.6/**0.03**
Surface age	**Granular disintegration**	**0.27**	**0.01**
Surface age	**Pitting**	**0.09**	**0.00**
Surface age	**Lichen**	**0.24**	**0.00**
Surface age	**Varnish**	**0.10**	**0.00**
Surface age	**<2 cm crack # density**	**0.12**	**0.00**
Surface age	**Crack infilling**	**0.09**	**0.00**
Surface age	**Bedding**	**0.09**	**0.00**
Surface age	Clast size	0.02	0.34

5.6 Figures

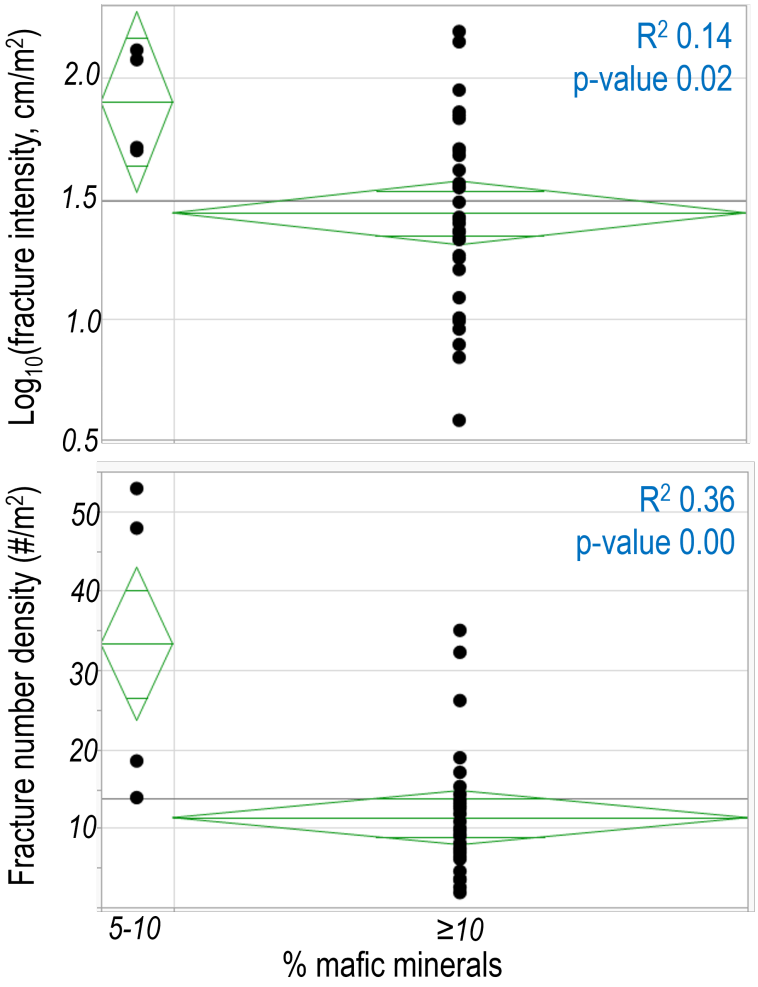

Figure 5.1: Fracture metrics as a function of the amount of mafic minerals present, Lundy Canyon.

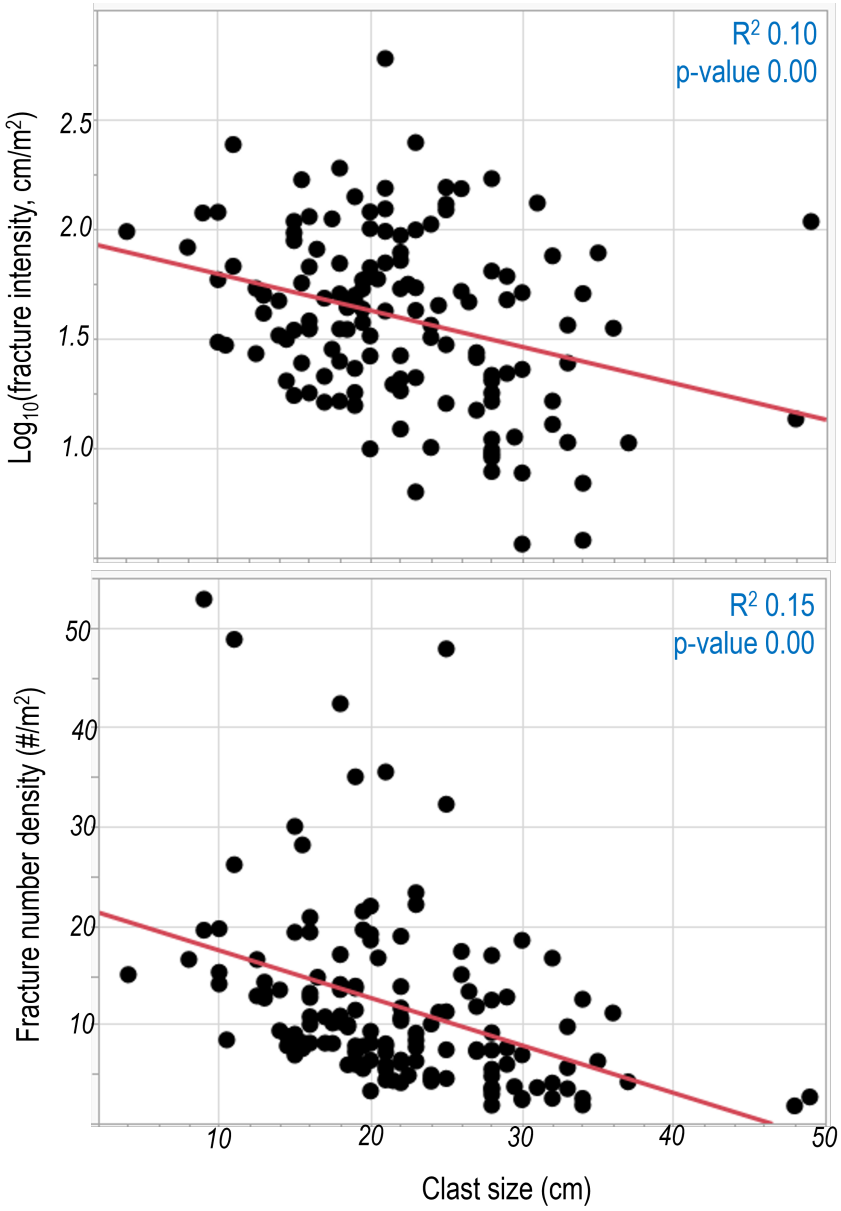

Figure 5.2: Fracture metrics as a function of clast intermediate axis length, Lundy Canyon.

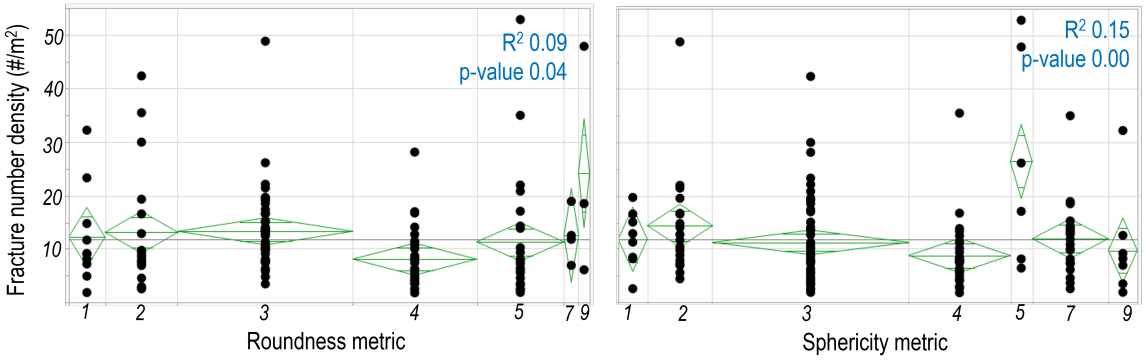

Figure 5.3: Fracture number density as a function of clast roundness and sphericity, Lundy Canyon.

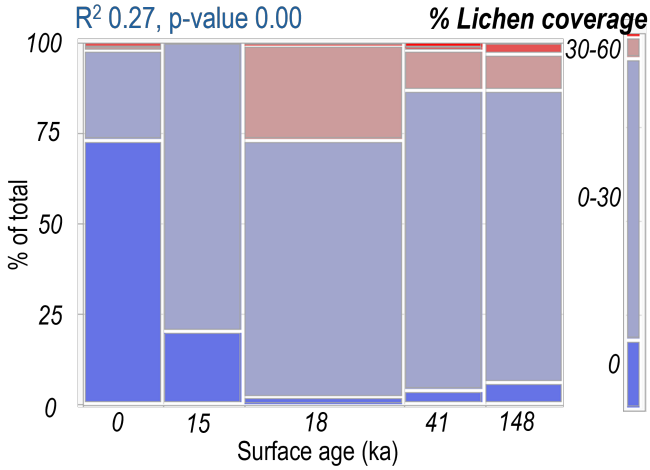

Figure 5.4: The percentage of rock covered by lichen as a function of surface age, Lundy Canyon.

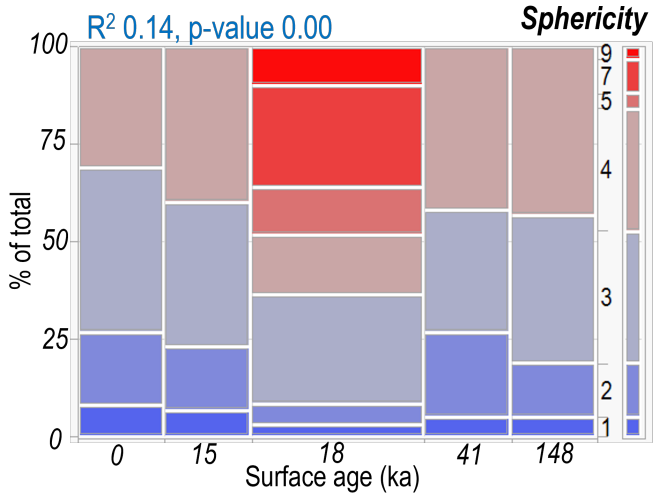

Figure 5.5: Clast sphericity as a function of surface age, Lundy Canyon.

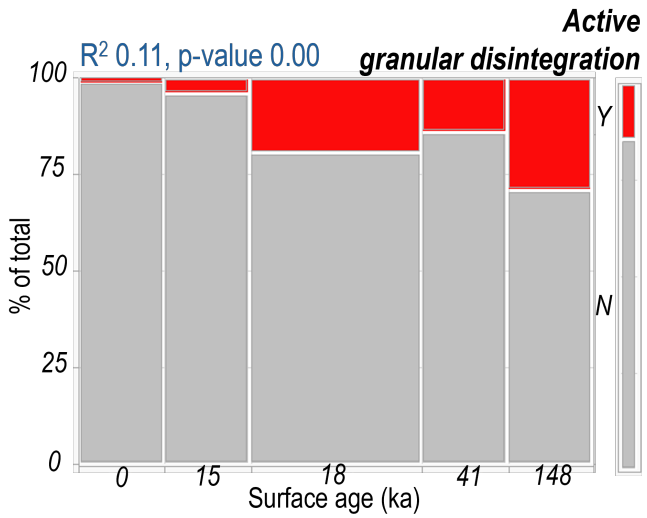

Figure 5.6: Active granular disintegration as a function of surface age, Lundy Canyon.

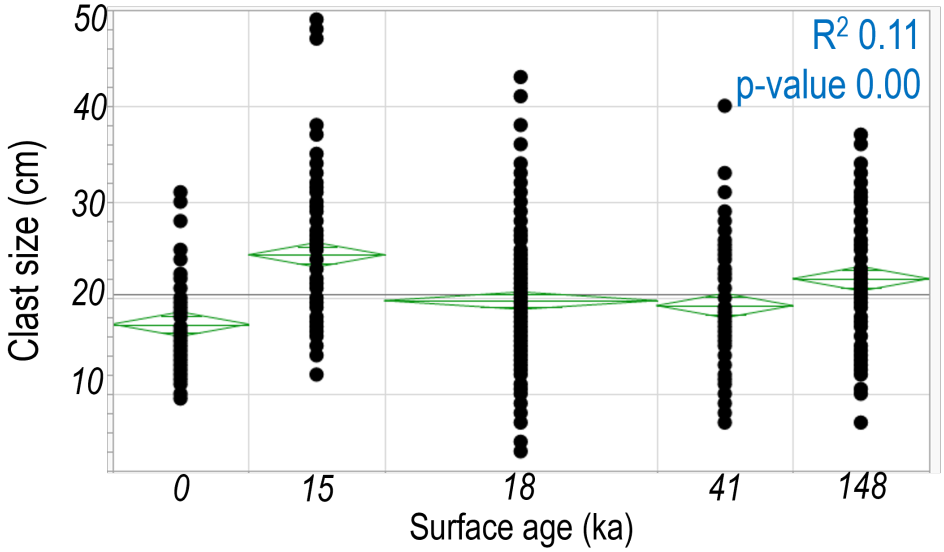

Figure 5.7: Clast intermediate axis length as a function of surface age, Lundy Canyon.

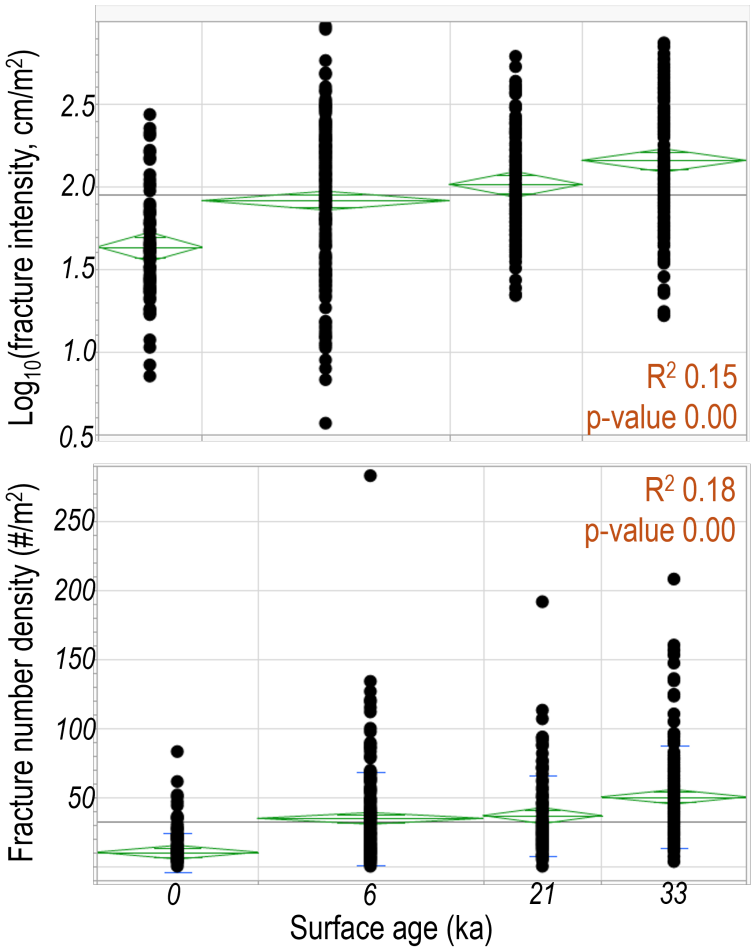

Figure 5.8: Fracture intensity and fracture number density as a function of surface age, Shepherd Creek.

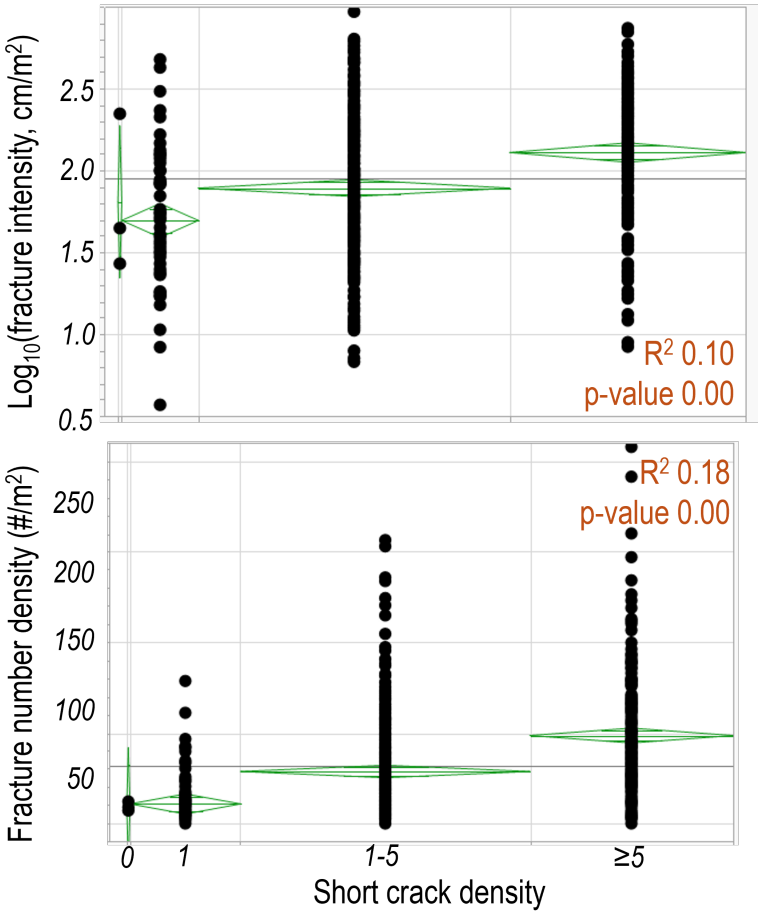

Figure 5.9: Fracture intensity and fracture number density as a function of density of <2 cm cracks, Shepherd Creek.

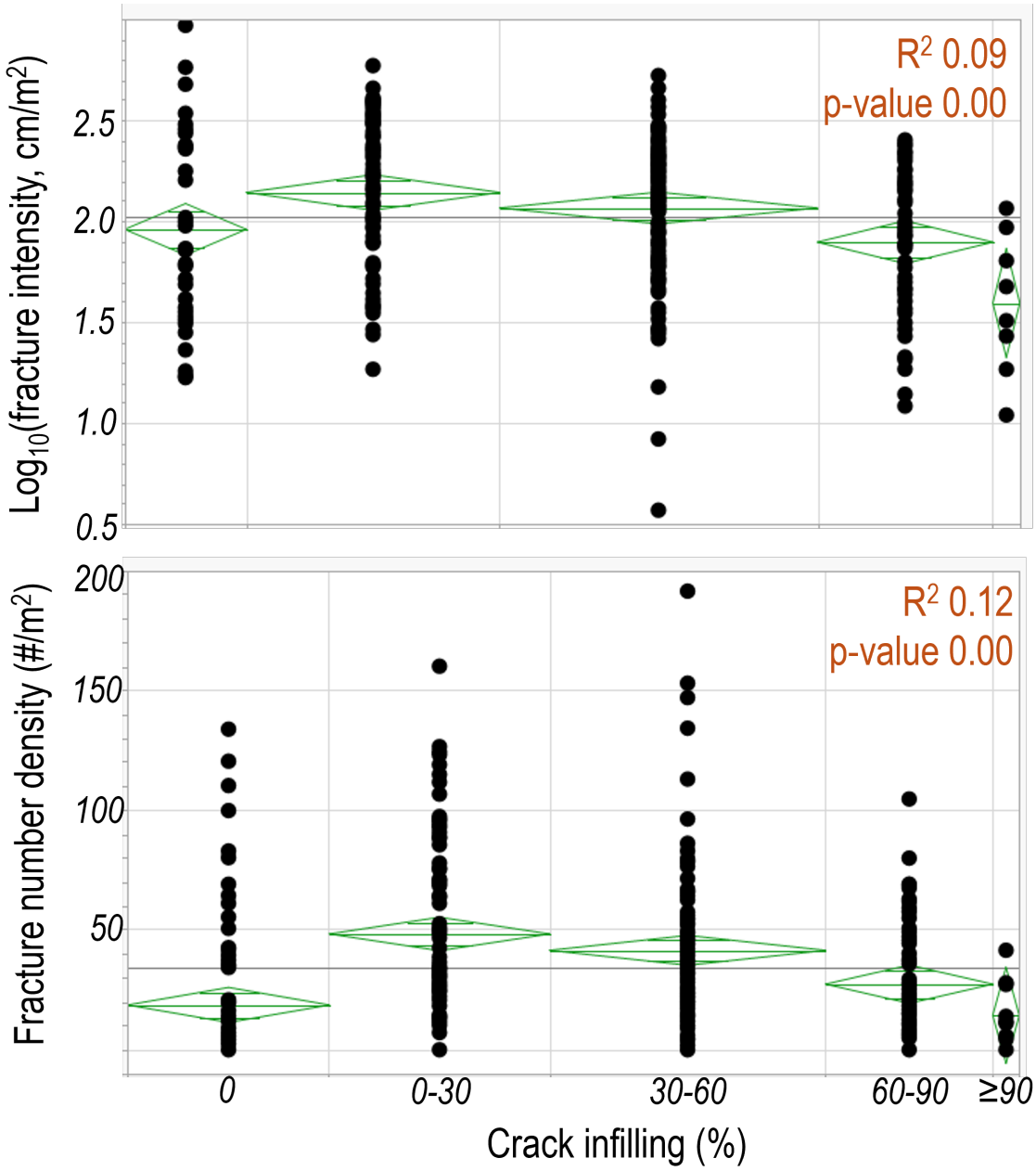

Figure 5.10: Fracture intensity and fracture number density as a function of the percentage of infilled cracks, Shepherd Creek.

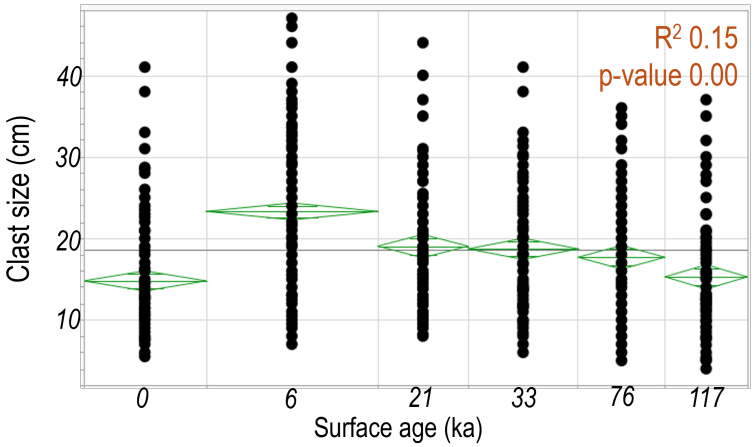

Figure 5.11: Clast intermediate axis length as a function of surface age, Shepherd Creek.

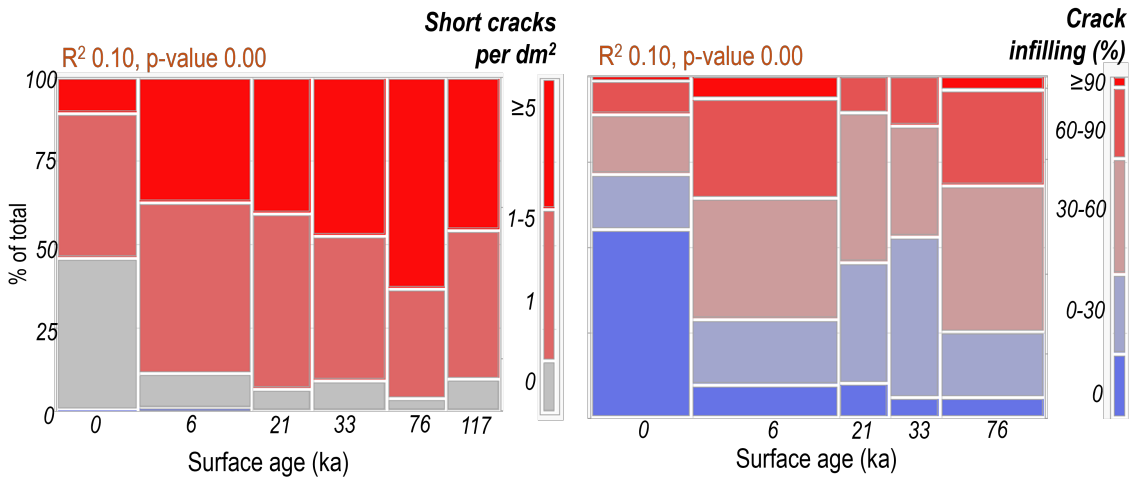

Figure 5.12: The amount of short cracks and infilled cracks as a function of surface age, Shepherd Creek.

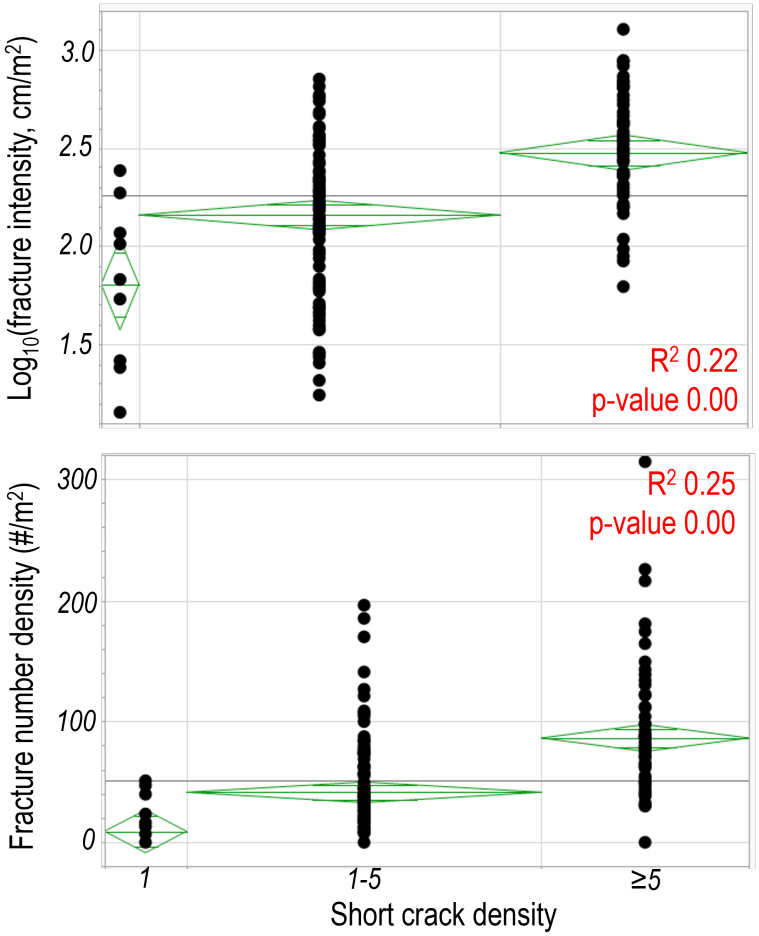

Figure 5.13: The number of short cracks as a function of fracture intensity and fracture number density, Providence Mountains granitoid rocks.

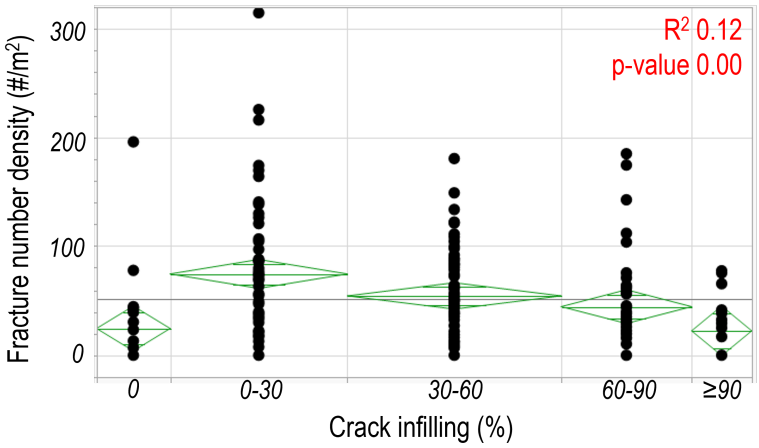

Figure 5.14: The amount of crack infilling as a function of fracture number density, Providence Mountains granitoid rocks.

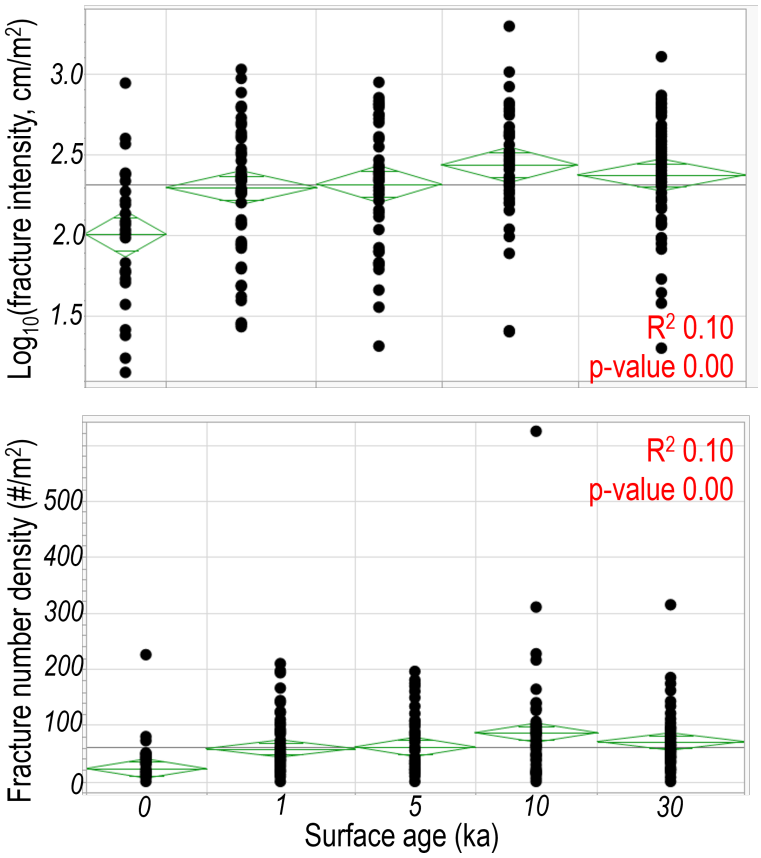

Figure 5.15: Fracture intensity and fracture number density as a function of surface age, Providence Mountains granitoid rocks.

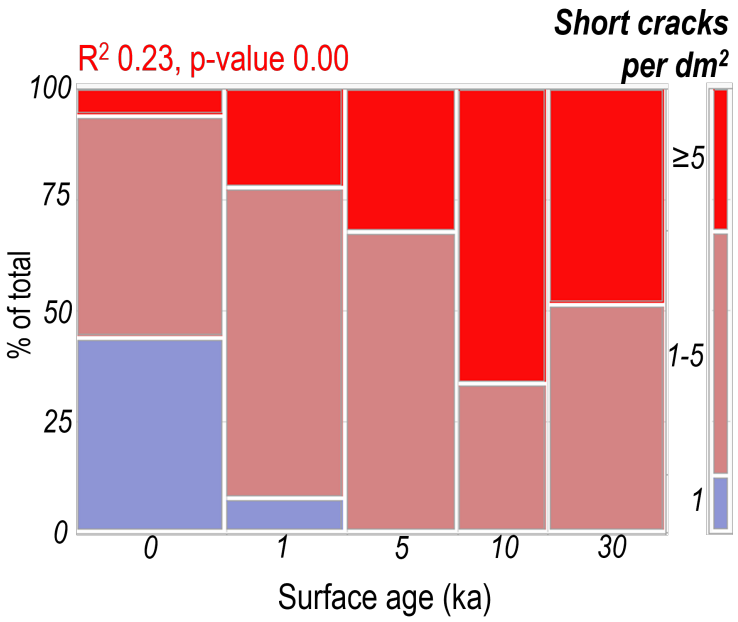

Figure 5.16: The number of short cracks as a function of surface age, Providence Mountains granitoid rocks.

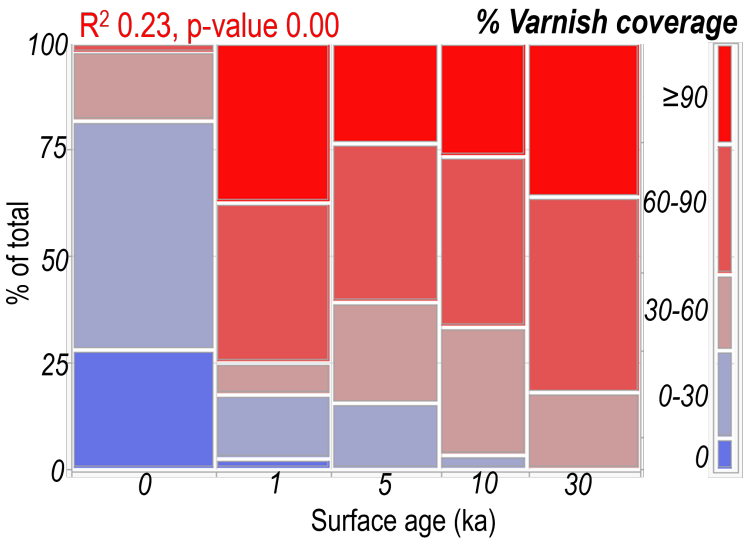

Figure 5.17: The percentage of rock covered in varnish as a function of surface age, Providence Mountains granitoid rocks.

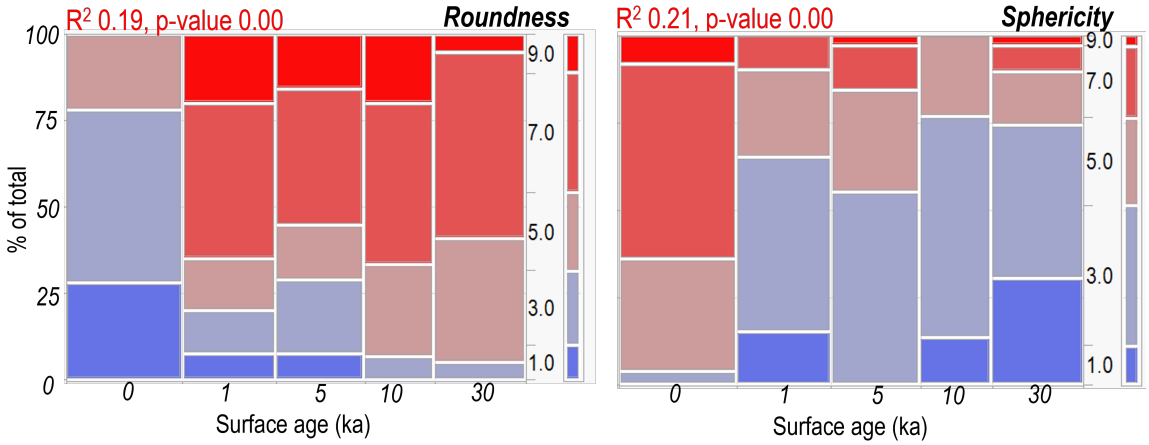

Figure 5.18: Roundness and sphericity as a function of surface age, Providence Mountains granitoid rocks.

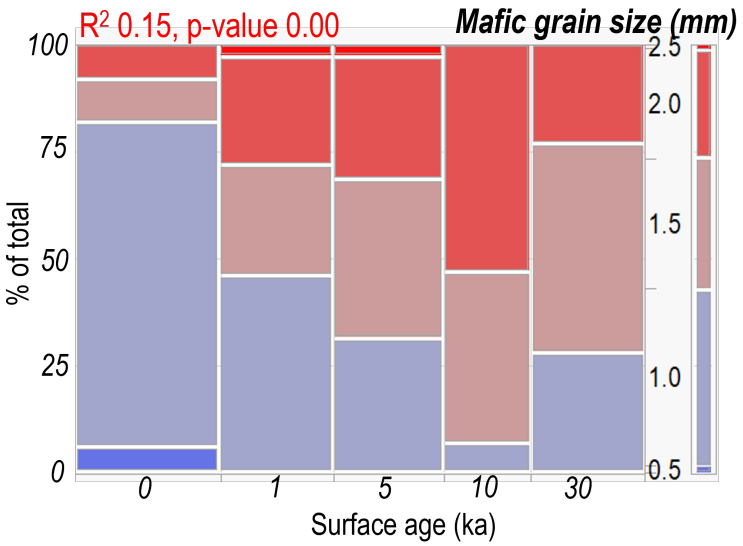

Figure 5.19: Mafic grain size as a function of surface age, Providence Mountains granitoid rocks.

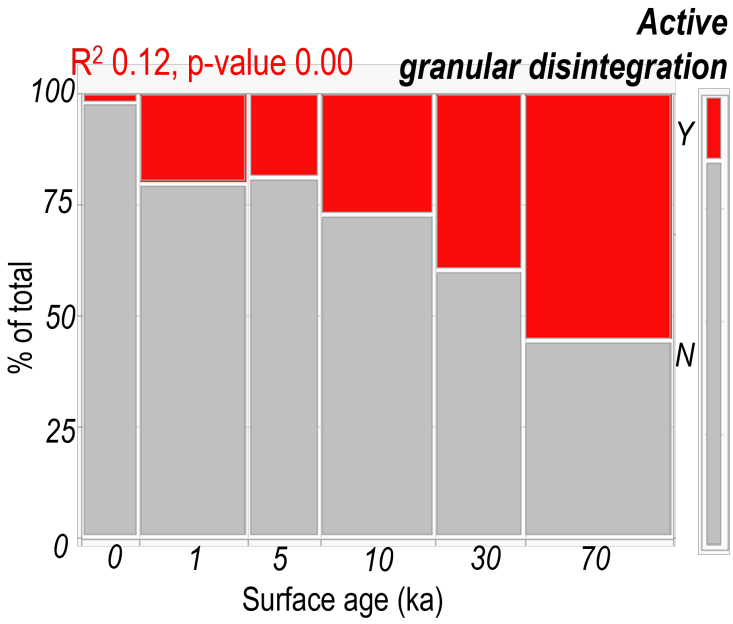

Figure 5.20: Granular disintegration as a function of surface age, Providence Mountains granitoid rocks.

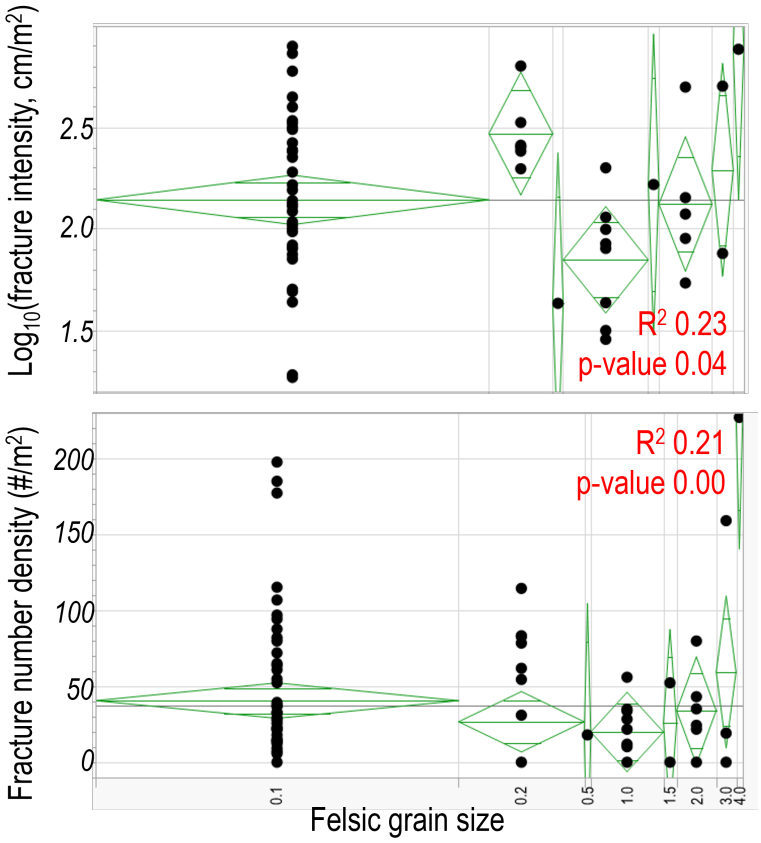

Figure 5.21: Fracture metrics as a function of as a function of felsic grain size, Providence Mountains volcanic rocks.

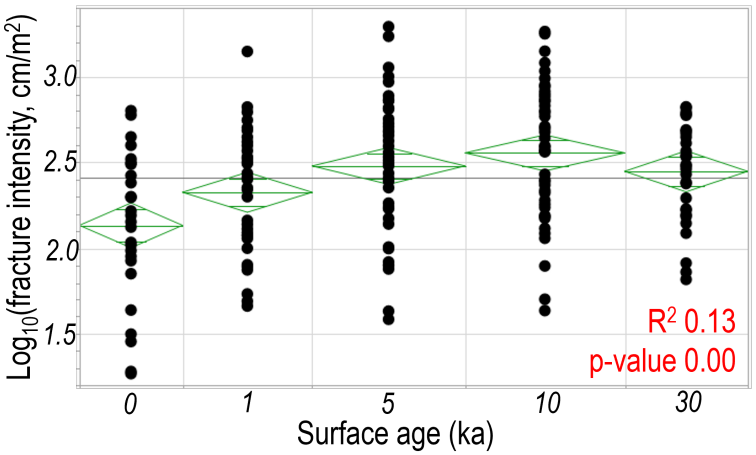

Figure 5.22: Fracture intensity as a function of surface age, Providence Mountains volcanic rocks.

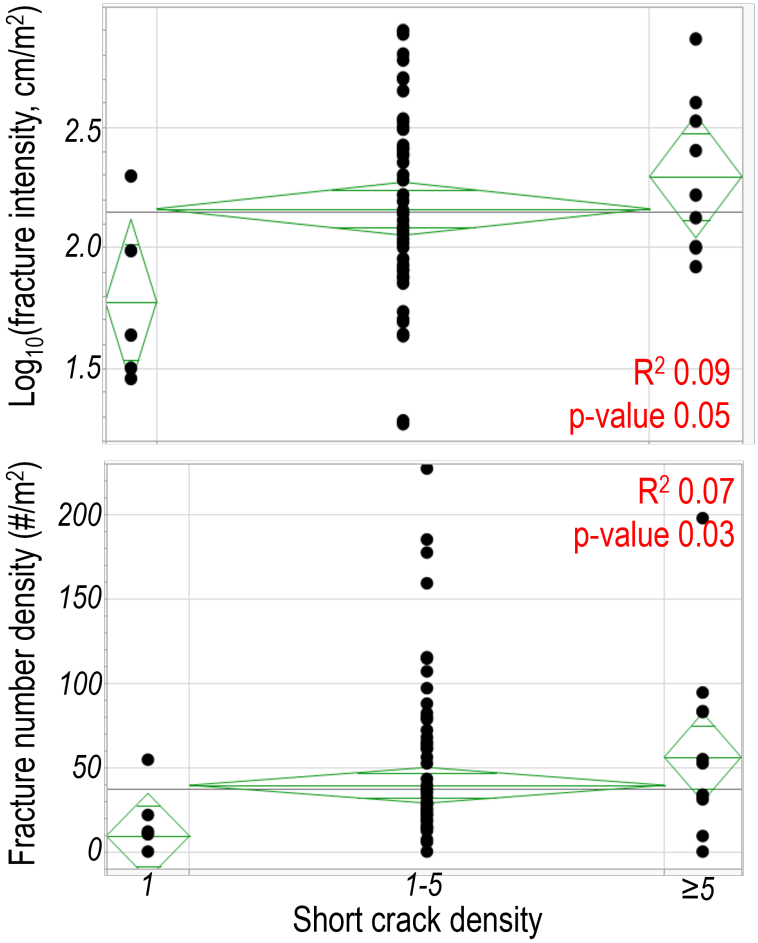

Figure 5.23: Fracture intensity and fracture number density as a function of short crack density, Providence Mountains volcanic rocks.

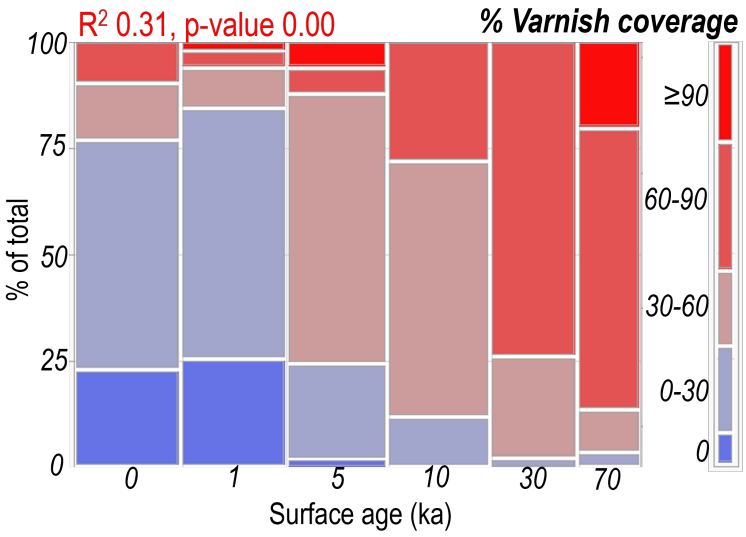

Figure 5.24: Varnish as a function of surface age, Providence Mountains volcanic rocks.

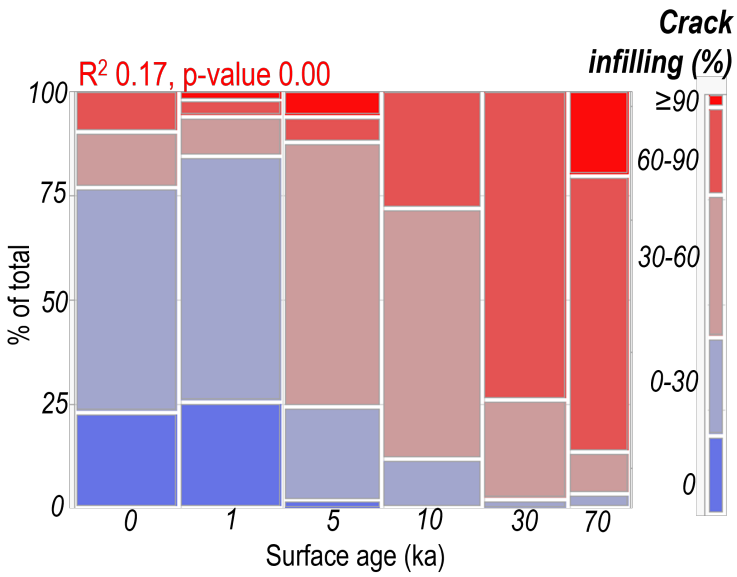

Figure 5.25: Amount of cracking infilling as a function of surface age, Providence Mountains volcanic rocks.

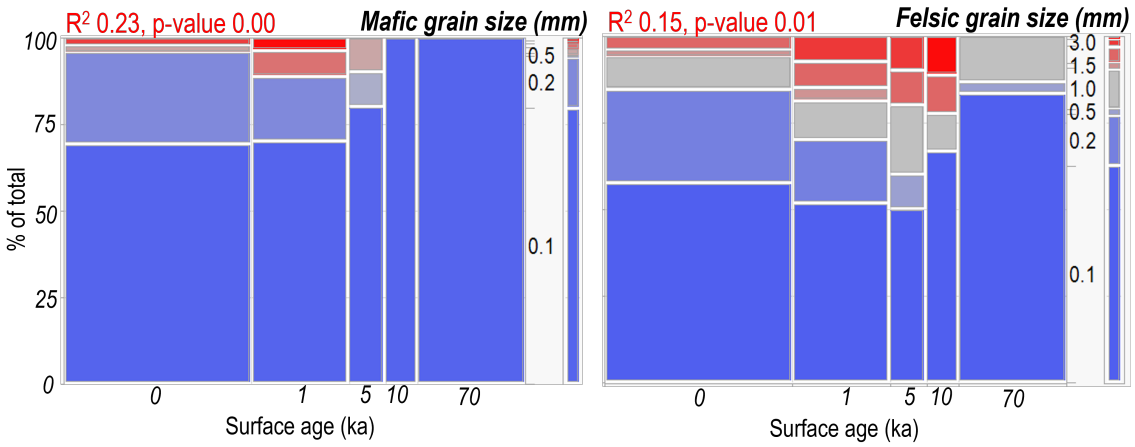

Figure 5.26: Grain size as a function of surface age, Providence Mountains volcanic rocks.

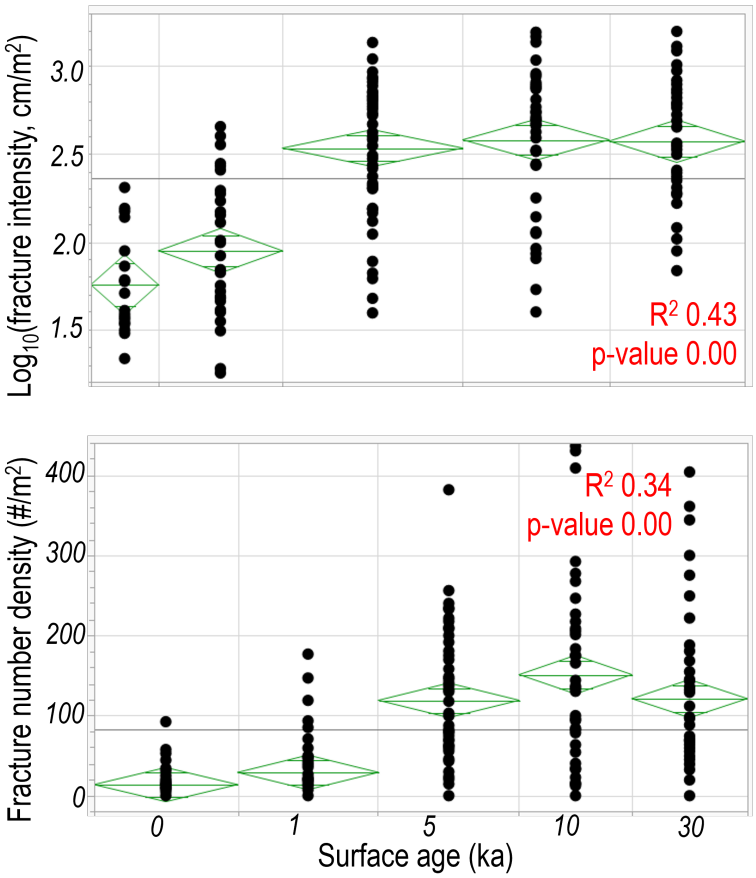

Figure 5.27: Fracture intensity and fracture number density as a function of surface age, Providence mountains carbonate rocks.

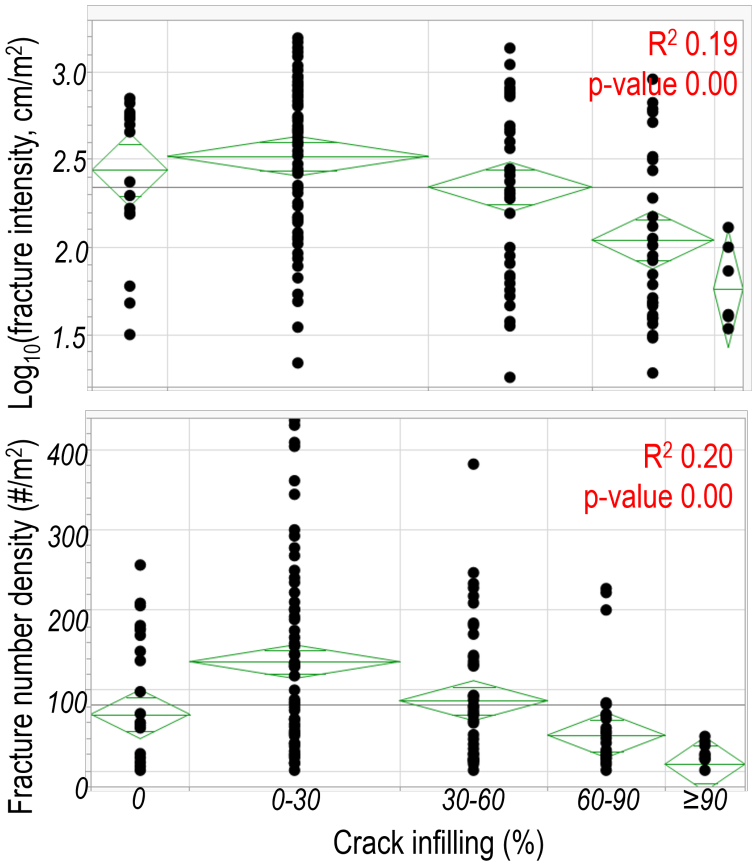

Figure 5.28: Fracture metrics as a function of infilling, Providence mountains carbonate rocks.

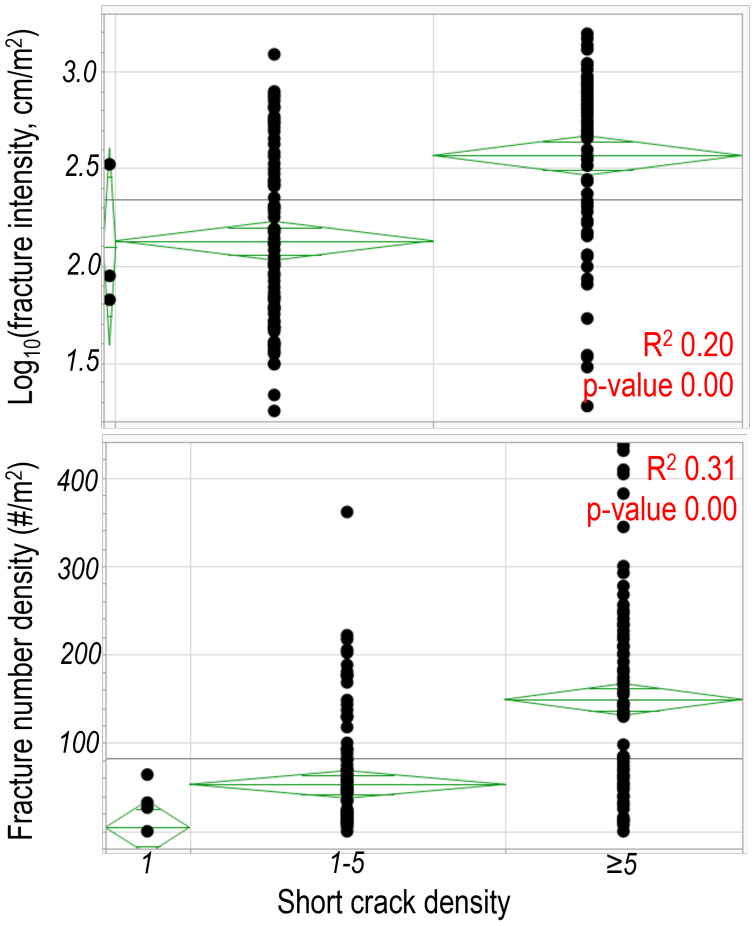

Figure 5.29: Fracture metrics as a function of short crack density, Providence mountains carbonate rocks.

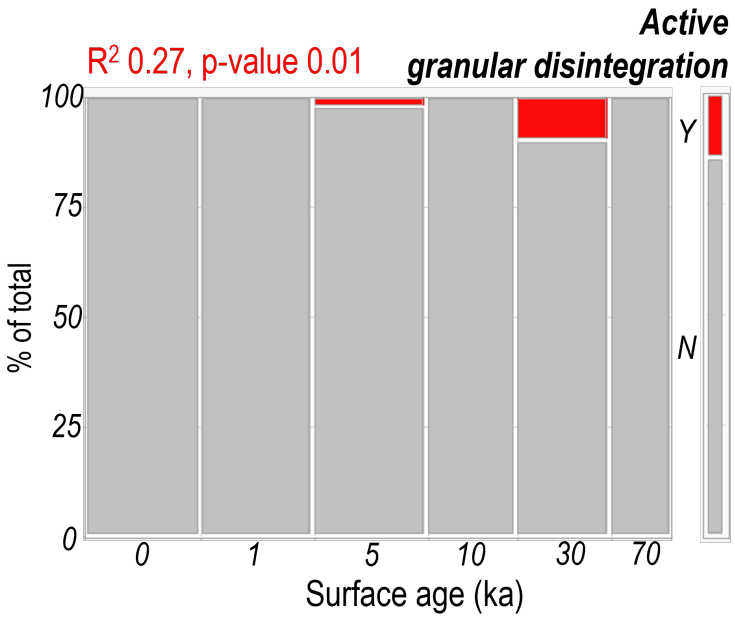

Figure 5.30: Granular disintegration as a function of surface age, Providence mountains carbonate rocks.

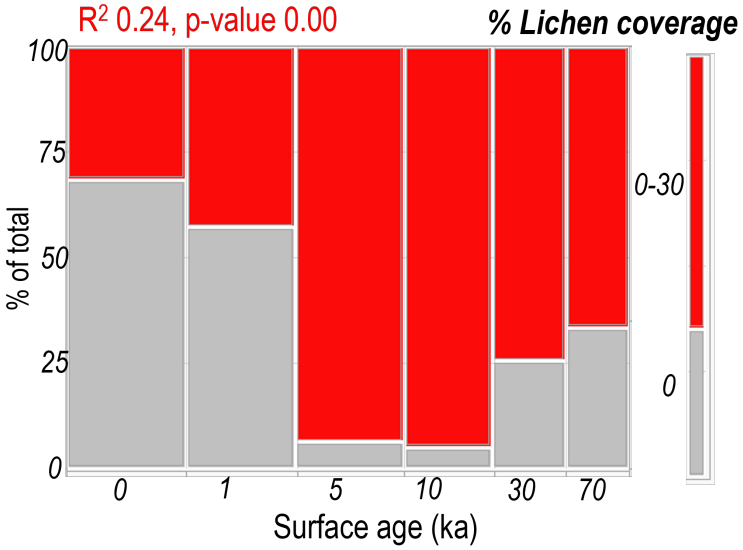

Figure 5.31: Lichen coverage as a function of surface age, Providence mountains carbonate rocks.

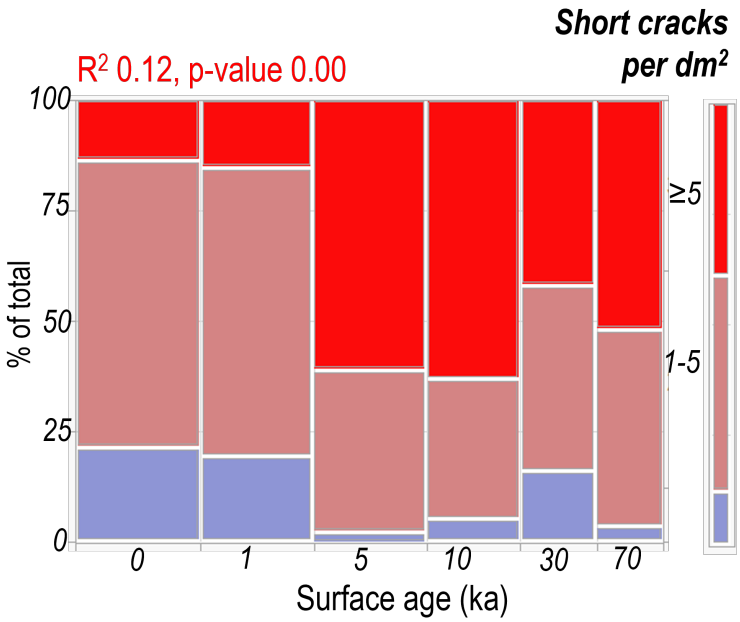

Figure 5.32: Short crack density as a function of surface age, Providence Mountains carbonate rocks.

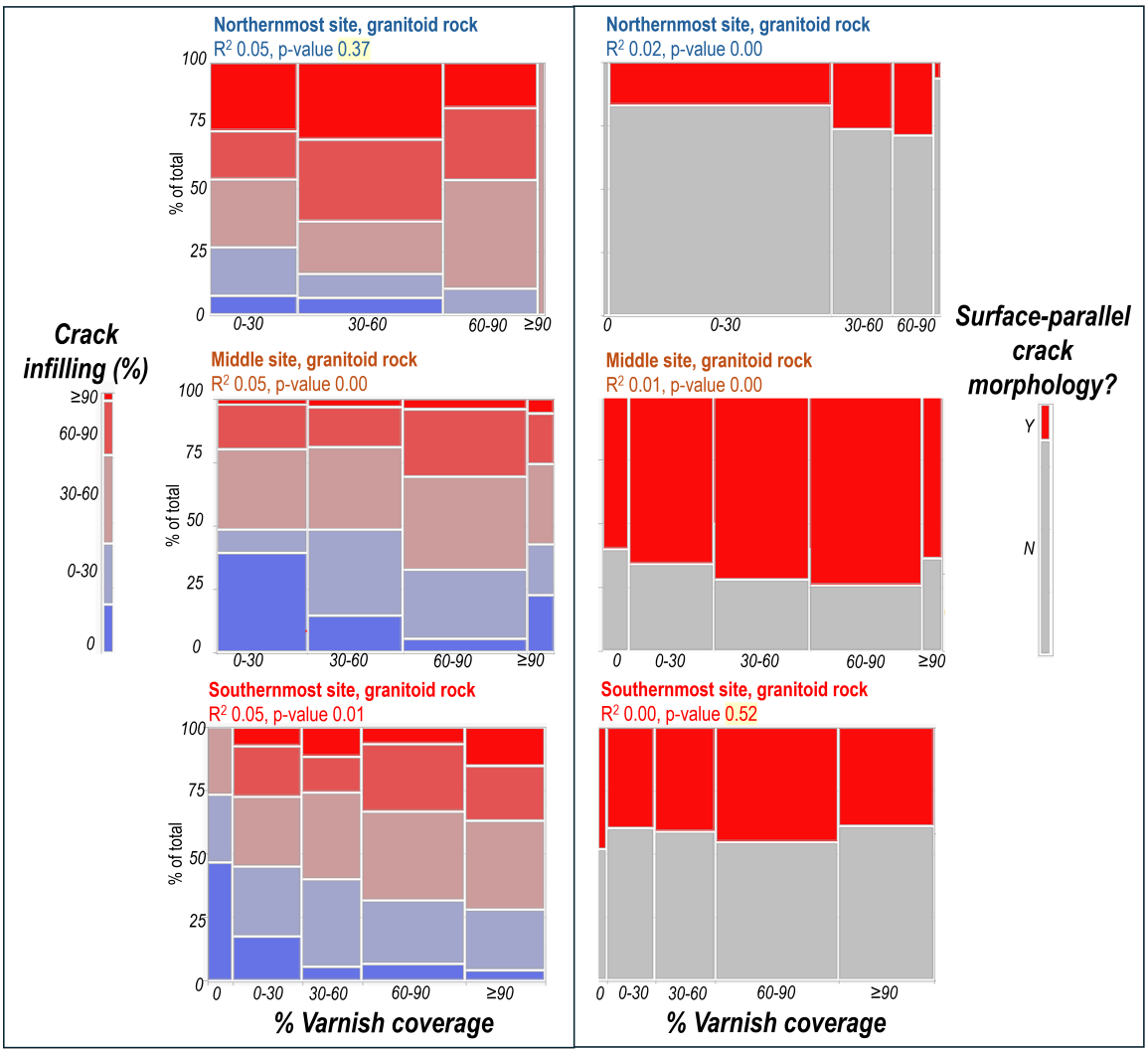

Figure 5.33: With increasing varnish coverage on granitoid rocks, there is a slight increase in crack infilling at the Shepherd Creek and Providence Mountains sites crack infilling [left], and a very weak correlation with increasing surface-parallel cracks at the Lundy Canyon and Shepherd Creek sites.

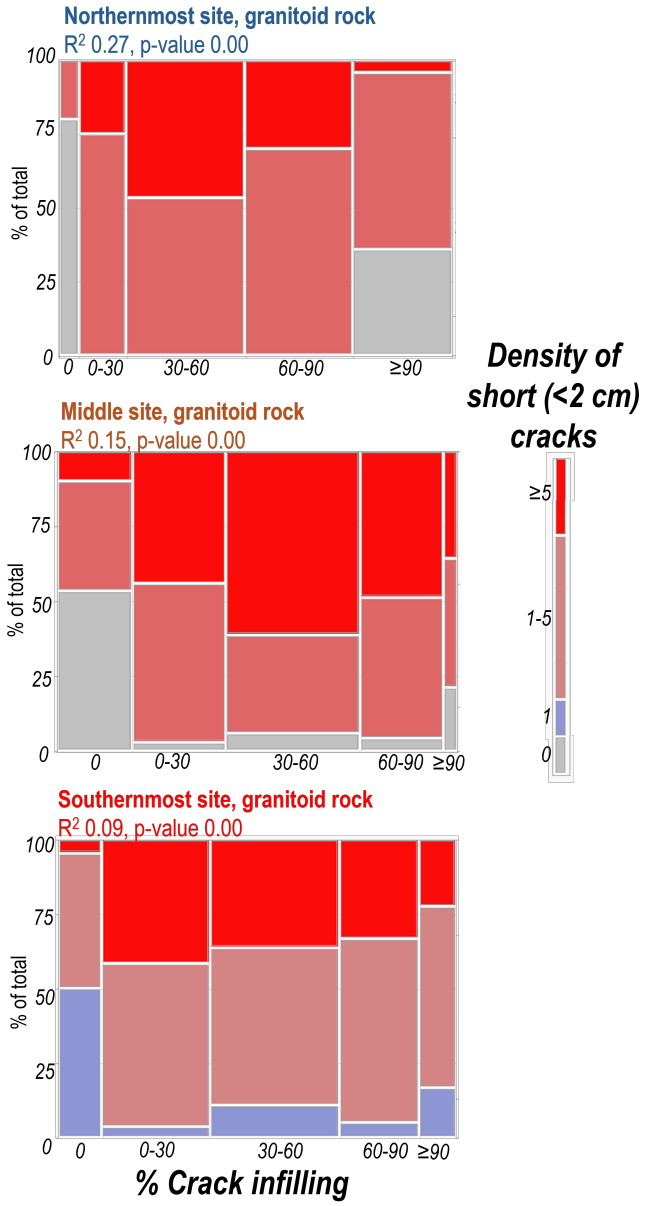

Figure 5.34: Short crack density as a function of crack infilling is one of the stronger correlations observed in granitoid rocks at all three sites.

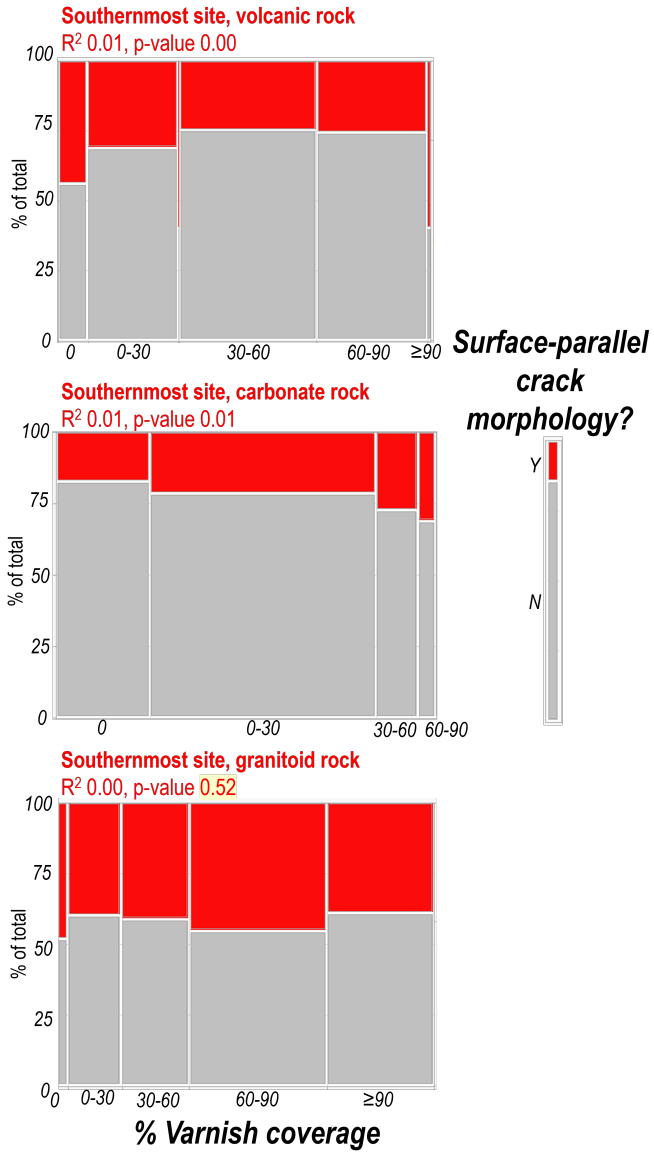

Figure 5.35: Varnish coverage insignificantly impacts the amount of surface-parallel cracks on rocks at the Southernmost Providence Mountains site.

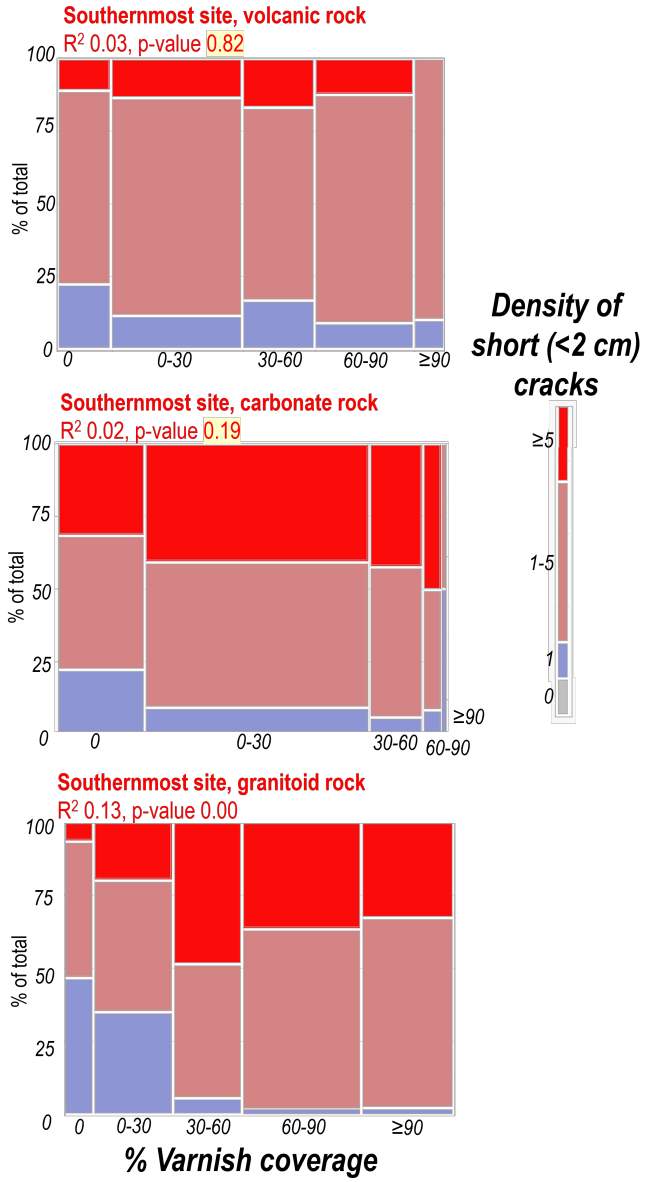

Figure 5.36: Short crack density shows no correlation with varnish development for volcanic and carbonate rocks, but positively correlates for granitoid rocks.

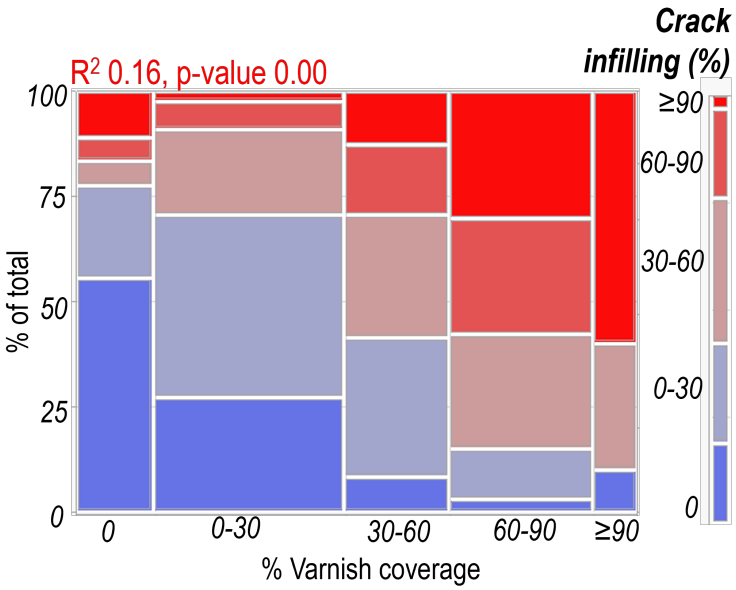

Figure 5.37: Crack infilling as a function of varnish coverage, Providence Mountains volcanic rocks.

CHAPTER 6: IMPACTS OF CRACKING GEOMETRIES AND RATES ON SEDIMENT PRODUCTION

AUTHORS:

Monica Rasmussen and Martha Cary Eppes

6.1 Introduction

The size and shape of clasts on abandoned geomorphic landforms evolves as weathering ensues, modifying chemistry and mechanical properties, and causing fractures to propagate through the rock. These changes dictate erodibility of soils [Li, Xinli, Fu, Suhua, Hu, Yaxian and Liu, Baoyuan, 2022; Becker, K. and Gronz, O. and Wirtz, S. and Seeger, Manuel and Brings, C. and Iserloh, T. and Casper, M. C. and Ries, Johannes B., 2015] and bedrock [Glade, Rachel C., Shobe, Charles M., Anderson, Robert S. and Tucker, Gregory E., 2019], sediment production [Neely, Alexander B. and DiBiase, Roman A., 2020], and thus the sediment which is subsequently redeposited into fluvial networks [Sklar, Leonard S., Riebe, Clifford S., Marshall, Jill A., Genetti, Jennifer, Leclere, Shirin, Lukens, Claire L. and Merces, Viviane, 2017]. However, the rates and processes of clast shape and size evolution on exposed natural rock are scantly constrained [e.g., Johnstone, Samuel A. and Hudson, Adam M. and Nicovich, Sylvia and Ruleman, Chester A. and Sare, Robert M. and Thompson, Ren A., 2018; Mushkin, Amit, Sagy, Amir, Trabelci, Eran, Amit, Rivka and Porat, Naomi, 2014] and the impacts of rock mechanical weathering on sediment shape over time have been minimally studied [e.g., McGrath, Gavan S., Nie, Zhengyao, Dyskin, Arcady, Byrd, Tia, Jenner, Rowan, Holbeche, Georgina and Hinz, Christoph, 2013; Ehlmann, Bethany L., Viles, Heather A. and Bourke, Mary C., 2008; Eppes, Martha Cary and Griffing, David, 2010]. To my knowledge, clast shapes and quantitative crack measurements have not been combined as a means of interpreting cracking behavior in the geologic record, nor have cracking data been applied to interpretations

of clast size and shape.

Sedimentologists and soil scientists depend upon clast size data to interpret sedimentary deposits [e.g., Felton, E. Anne, 2002; Bluck, Brian J., 2011; McCubbin, Francis M., Boyce, Jeremy W., Novák-Szabó, Tímea, Santos, Alison R., Tartèse, Romain, Muttik, Nele, Domokos, Gabor, Vazquez, Jorge, Keller, Lindsay P., Moser, Desmond E., Jerolmack, Douglas J., Shearer, Charles K., Steele, Andrew, Elardo, Stephen M., Rahman, Zia, Anand, Mahesh, Delhaye, Thomas and Agee, Carl B., 2016], clast reworking [e.g., Cox, Rónadh, Lopes, Ward A. and Jahn, Kalle L., 2018; Caballero, Lizeth, Sarocchi, Damiano, Borselli, Lorenzo and Cárdenas, Angel I., 2012; Lukas, Sven, Benn, Douglas I., Boston, Clare M., Brook, Martin, Coray, Sandro, Evans, David J.A., Graf, Andreas, Kellerer-Pirklbauer, Andreas, Kirkbride, Martin P., Krabbendam, Maarten, Lovell, Harold, Machiedo, Martin, Mills, Stephanie C., Nye, Kate, Reinardy, Benedict T.I., Ross, Fionna H. and Signer, Michael, 2013], erosional dynamics [e.g., Glade, Rachel C., Shobe, Charles M., Anderson, Robert S. and Tucker, Gregory E., 2019; Naylor, Larissa A., Stephenson, Wayne J., Smith, Helen C. M., Way, Oliver, Mendelssohn, James and Cowley, Andrew, 2016] paleoclimate [e.g., D'Arcy, Mitch, Roda-Boluda, Duna C. and Whittaker, Alexander C., 2017; Howard, Jeffrey L., 1992], and infer transport regimes [e.g., Boulton, G. S., 1978; McCarroll, Nicholas R. and Temme, Arnaud J. A. M., 2022], presuming that the size distribution of clasts in the geologic record or surface accurately reflects the size of clasts which were initially deposited. However, post-depositional in situ cracking reduces overall grain size and produces new, smaller sediment within a few thousand years of rock exposure [Rasmussen et al., in prep, Ch. 2]. Here, I investigate the change in clast sizes and shapes over time, and compare these data alongside cracking geometries to understand the direct impact of rock cracking on clast sizes and shapes.

Crack morphologies will necessarily modify the distribution of clast sizes and shapes on and within a geomorphic surface over time [Eppes, Martha-Cary Missy, 2022].

When a crack propagates through the center of a rock, it can cut the rock into two semi-equal smaller rocks. If a crack instead propagates along a plane parallel to the rock surface, it can cause pieces to spall off the surface, including grain-scale clasts and flat, elongated clasts. Therefore, the current size and shape distribution of clasts on abandoned geomorphic surfaces may be used to interpret cracking that has occurred in the past. Alternatively, the morphology of cracks can be used to infer the size and shape of sediment which will be produced if the crack continues to propagate through the rock.

Here, I analyze clast size and shape changes over time alongside crack morphologies measured at the exact same sites, to test how specific cracking geometries could produce certain sediment shapes and sizes. I utilized clast intermediate axis lengths determined through modified Wolman pebble counts [Wolman, M. Gordon, 1954] and Zingg shape classification [Zingg, Theodor, 1935] to analyze sedimentary deposits. I assessed the feasibility of interpreting clast size and shape changes due to weathering by comparing the subsurface clast size and shape distributions among differently aged abandoned sedimentary deposits. Presumably, if different subsurface deposits are similar to each other in clast size composition, then the differences on their exposed depositional surfaces are primarily due to weathering. After determining that clast size distribution in the subsurface was initially similar for various surfaces, I compared the subsurface shape and size of clasts on each subsurface deposit with those of the surface. I conclude that the clast size and shapes on exposed surfaces change over time as a function of rock mechanical weathering; that granitoid rocks produce abundant grain-scale clasts [grus], as previously described in other field studies [e.g., Eppes, Martha Cary and McFadden, Leslie, 2008; Riber, L., Le Pera, E., Conforti, M., Ietto, F., Dypvik, H. and others, 2020]; and that finer-grained volcanic and carbonate lithologies exhibit a relationship between a sudden decrease in surface-parallel cracking, and an increase in flattened, elongated sediment shapes on the

surface.

6.2 Methods

This clast size/shape methodology incorporates cutting-edge rock fracture data [Rasmussen et al., Ch. 2] and data processing for statistical comparison [ANOVA in JMP SAS Institute Inc. JMP, 1989-2023] with traditional surface processes and sedimentological analysis [modified Wolman pebble counts, Wolman, M. Gordon, 1954] and clast shape classification [Zingg, Theodor, 1935].

6.2.1 Rock fracture data

To interpret cracking geometries alongside clasts size and shapes, I leverage crack measurements acquired during field analysis of 2221 15-50 cm boulders at three Eastern California sites, all collected by Rasmussen et al. [Ch. 2-4]. The three sites have different climates representing a 'climosequence' and are composed of geomorphic surfaces that have been dated and mapped [Rood, Dylan H., Burbank, Douglas W. and Finkel, Robert C., 2011; D'Arcy, Mitch. Roda Boluda, Duna C.. Whittaker, Alexander C. and Carpineti, Alfredo, 2015; Dühnforth, Miriam, Anderson, Robert S., Ward, Dylan and Stock, Greg M., 2010; Blisniuk, Kimberly Diem Chi, 2011; McDonald, Eric V., McFadden, Leslie D., Wells, Stephen G., Enzel, Y. and Lancaster, N., 2003; Wang, Yang, McDonald, Eric, Amundson, Ronald, McFadden, Leslie and Chadwick, Oliver, 1996; Stone, Paul, Miller, David M., Stevens, Calvin H., Rosario, Jose, Vazquez, Jorge A., Wan, Elmira, Priest, Susan S. and Valin, Zenon C., 2017], representing sequences of progressively older surfaces or 'chronosequences' per site which can be interpreted for understanding the impact of exposure time on weathering [Jenny, Hans, 1948; Birkeland, Peter W., 1999]. The sites include a warm-summer mediterranean continental climate at the Northernmost Lundy Canyon site, hot-summer mediterranean climate at the Middle Shepherd Creek site, and hot desert climate at the Southernmost Providence Mountains site [Fig. 4.5, Köppen, 2011]. Surfaces at the Lundy

Canyon site include a modern creek deposit and moraines and outwash terraces extending back to 148 ka; at the Shepherd Creek site, alluvial deposits from modern to 117 ka, and the Providence Mountains site, alluvial deposits from modern to 70 ka [Fig. 2.4]. At all three sites, granitoid rocks were measured, and at the Southernmost Providence Mountains site, volcanic and carbonate rocks were also measured. At regular intervals along surficial boulder bar deposits, all visible, planar, open cracks $\geq$2.0 cm long were measured per boulder. Crack length, opening width, and strike and dip were recorded. For each measured crack per boulder, the authors also noted morphological characteristics including whether the crack was aligned parallel to foliation or veins or bedding ['fabric-parallel cracks'], and when the crack was parallel to the boulder's surface and at a depth of $\leq$10% of the boulder diameter ['surface-parallel cracks']. Additionally, the number of cracks $<$2.0 cm long that are visible in a representative 10*10 cm [dm^2] of rock surface area ['short crack density'] was recorded for each boulder, and the presence of active granular disintegration/disaggregation was also noted when observed on the rock surface.

6.2.2 Modified Wolman pebble counts

All surface and subsurface clast size data are available in Supplement S6.1. Clast count data for each surface was collected along the same transects laid out for collecting boulder crack data [Rasmussen et al., in prep] following a modified Wolman pebble count methodology [Wolman, M. Gordon, 1954]. Every 25 cm, the long, short, and intermediate axes lengths were measured for the clast closest to the transect that was $\geq$1.0 cm intermediate axis length. The three axes were measured orthogonally, relative to the long axis orientation. A total of 100 clasts were counted for each surface, along as many transects or plots needed to reach 100. At the Providence Mountains site where many rock types are present, the rock type [granitoid, carbonate, or volcanic] was recorded, and I collected at least 25-30 clast measurements per rock type. Data were collected from two surfaces at the Northernmost site, six surfaces at the

Middle site, and six surfaces at the Southernmost site.

6.2.2.1 Subsurface clast sizes

I measured clast sizes within pits, cutbanks, or road cuts for each abandoned surface, where permitted. No subsurface counts were performed on the 0 ka deposits because presumably they are fresh and relatively unweathered, so the surface and subsurface should be equivalent. The surface distribution of 0 ka deposits is displayed alongside the subsurface distributions, for comparison.

Subsurface sampling was accomplished for granitoid clasts in the 18 and 148 ka dated geomorphic surfaces at Lundy Canyon [Rood, Dylan H., Burbank, Douglas W. and Finkel, Robert C., 2011], granitoid clasts in the 6, 21, 33, 76, and 117 ka dated geomorphic surfaces at Shepherd Creek [D'Arcy, Mitch. Roda Boluda, Duna C.. Whittaker, Alexander C. and Carpineti, Alfredo, 2015], and for granitoid, volcanic, and carbonate clasts in the 1, 5, 10, and 30 ka dated geomorphic surfaces at Providence Mountains [McDonald, Eric V., McFadden, Leslie D., Wells, Stephen G., Enzel, Y. and Lancaster, N., 2003]. At Lundy Canyon, subsurface clasts in the 15, 46, and 101 ka depositional surfaces were not measured because digging pits was not permitted and there were no accessible exposed banks. At Providence Mountains, the well-developed calcic soils of the 70 ka surface formed a calcrete in the subsurface, making clast removal impossible.

Subsurface clasts were sampled using a grid system where a vertical tape was lain and every clast $\geq$ 1.0cm in diameter was measured when encountered along a 10cm grid. If no clast met the size criteria at the sampling location, the location was skipped. At least 30 $\geq$ 1.0 cm clasts were measured per subsurface exposure.

For pits at Shepherd Creek, during digging, clasts $\geq$15 cm long-axis diameter were separated into one pile and the remaining clasts were isolated on a tarp. The pit was dug to at least 30 cm depth. The long, short, and intermediate axes of clasts $\geq$15 cm long-axis diameter were measured to the nearest 0.5 cm, then clasts were returned to

the pit. From the smaller sediment pile, 1 gallon of sediment was transferred from the middle of the sediment pile to a bucket using a shovel, capturing a representative distribution of smaller sediments.

After the 1-gallon bucket of sediment was separated from the pile, the remaining sediment was returned to infill the pit. The 1 gallon of sediment was sieved through 0.25 inch hardware cloth to remove the fine fraction and gravels, then from the remaining clasts, every clast with intermediate axis $\geq$1.0 cm was measured. Due to these differences in sampling procedures among sites, and the physical limitation of moving or accessing larger rocks, clast size distributions may vary slightly from one site to another. However, within each site, the methods used were uniform.

6.2.3 Data processing

I compared clast size distributions among all subsurface data for each site and rock type using Analysis of Variance tests [ANOVA] of clast intermediate axis lengths, to determine if the initial particle size distributions at each dated surface were statistically similar to each other when they were initially deposited. Clast sizes of the subsurface [Figs. 6.1, 6.2, 6.4, 6.5, and 6.3 with ANOVA atop the histograms] and surface [Figs. 6.1, 6.2, 6.4, 6.5, 6.3, 6.6, 6.7, 6.9, 6.10, and 6.8] were analyzed by plotting the intermediate axis length of all clasts as histograms binned every 1.0 cm, with medians added to the plots for comparison among surfaces of different depositional ages.

The degree of surface-parallel cracking is presented as the percentage of all cracks per surface that exhibited surface-parallel morphology during field data collection [Fig. 6.11A, B]. The degree of fabric-parallel cracks is presented as the percentage of rocks exhibiting any measurable fabric, and the percentage of all cracks which are parallel to fabric [Fig. 6.11C, D]. For granitoid rocks, the amount of rocks with any fabric, including veins, never exceeds 10%, so only carbonate and volcanic rocks are included in fabric-parallel analysis.

6.2.4 Zingg classification of sediment shape

The Wolman pebble count data are next leveraged to understand the clast shapes both on the depositional surface, and in the subsurface, according to the Zingg classification [Fig. 6.12, Drake, Lon D., 1970; Zingg, Theodor, 1935]. The following assessments of clast shape uses the three orthogonal axes measurements of a [long-axis length], b [intermediate-axis length], and c [short-axis length]:

1. Rod: $b/a < 2/3$ and $c/b > 2/3$
2. Blade: $b/a < 2/3$ and $c/b < 2/3$
3. Disk: $b/a > 2/3$ and $c/b < 2/3$
4. Sphere: $b/a > 2/3$ and $c/b > 2/3$

6.3 Results

6.3.1 Clast sizes

While the general clast size distribution will be determined by bedrock fracture spacing in the sloping parts of the catchment from which the clasts originally eroded [e.g., Neely, Alexander B. and DiBiase, Roman A., 2020], the initial/subsurface clast size distribution may be dissimilar between deposits due to varying amounts of energy required to transport the clasts. At the Lundy Canyon site, the deposits include a modern creek, glacial moraines, and glacial outwash [Rood, Dylan H., Burbank, Douglas W. and Finkel, Robert C., 2011]. All dated deposits at the Providence Mountains and Shepherd Creek site appear to be a result of debris flow events [McDonald, Eric V., McFadden, Leslie D., Wells, Stephen G., Enzel, Y. and Lancaster, N., 2003; D'Arcy, Mitch. Roda Boluda, Duna C.. Whittaker, Alexander C. and Carpineti, Alfredo, 2015], and the modern surfaces are in dry creek beds which presumably flow during flooding events. Since I am trying to compare the impact of post-depositional rock cracking on clast sizes, I must know if the deposits started in the same state;

if not, their current distribution may not be related to weathering processes. To determine if the overall distribution is similar, I present ANOVA of all subsurface clast size distributions together, atop each histogram [Figs. 6.1, 6.2, 6.4, 6.5, and 6.3]. The ANOVA report [SAS Institute Inc. JMP, 1989-2023] provides Student's t tests of all pair combinations; where p-value of Student's t is <0.05, the variance of that surface from other surfaces is statistically significant, and is indicated as "surface different" atop the ANOVA diagram in the figures.

At the middle Shepherd Creek and southernmost Providence Mountains sites [Figs. 6.2, 6.3, 6.4, and 6.5] the modern deposits have significantly larger medians and a more distributed range of clast sizes. This may be a result of the deposition type since these deposits are fluvial; however, surface clast counts for both the fluvial and alluvial deposits were performed on distinct, relatively linear boulder bar deposits, with mostly dm-scale boulders in a pile. By contrast, in the subsurface, a vertical face or entire pit is sampled, increasing the likelihood that smaller clasts exist as a finer-grained fill around the larger clasts. Additionally, although the subsurface deposits were located underneath boulder bars, they are not definitively from bar deposits, making their abundance of smaller clasts more likely.

At the Northernmost Lundy Canyon site [Fig. 6.1], only two subsurface clast counts are available, and they are dissimilar; this is not enough data to make any judgments on the surface data, especially given the range of depositional environments represented here [glacial moraine, outwash, fluvial]. At the Middle Shepherd Creek site [Fig. 6.2], the 33 ka deposit contains statistically larger clasts in its subsurface than the other deposits, although this is not reflected in the surface clast size distribution [Fig. 6.7]. This may be due to an unusually high energy transport event that was able to deposit larger clasts. While this would lead to larger clasts also existing on the surface, the surface clast count is mostly dominated by <2.0 cm clasts. Either the initial clast size of this surface was different than its subsurface counterpart, or the

impact of mechanical weathering is significant enough that no unusually large clasts are left on the surface.

At the Southernmost Providence Mountains site, trends are less clear, possibly due to the smaller datasets per rock type [∼30 clasts per rock type here vs. 100 at Shepherd Creek). For all rock types [Figs. 6.4, 6.5], and 6.3 the surficial clasts in the modern deposit are statistically larger than all subsurface clasts. For granitic rocks [Fig. 6.3], all other subsurface distributions are similar; and for carbonate [Fig. 6.4] and volcanic [Fig. 6.5] rocks, the modern and 1 ka surfaces are dissimilar from the others.

For surficial clasts, it is apparent from Figs. 6.6, 6.7, 6.9, 6.10, and 6.8 that the younger surfaces have a wider range of clast sizes than the older deposits, and the distribution becomes more positively skewed over exposure time as smaller [<3 cm] clasts dominate. Unlike the subsurface deposits, the surficial deposits were measured along similar bars to the 0 ka deposit, so there should not be a discrepancy due to depositional dynamics.

At Lundy Canyon [Fig. 6.6] and for volcanic clasts at Providence Mountains [Fig. 6.10], the modern wash does not have the highest median clast size. This seems counter-intuitive, however it likely reflects how energetic the transport event must have been leading up to deposition. On the abandoned surfaces, these deposits may have resulted from transport during extreme precipitation and flooding events, or during glacial processes. The modern deposits are creek or wash deposits, presumably transported and reworked during typical annual floods. Therefore, the largest boulders are smaller, and the median is lower.

In the Providence Mountains, the Southernmost site, the time span required for different rock types to produce small clast sizes varies. For the carbonate rocks [Fig. 6.9], small clasts are not dominant until 30 ka, at which point the median clast size drops from 3.0 cm on the 10 ka surface to 1.7 cm on the 30 ka surface. For volcanic

rocks [Fig. 6.10], the smallest clasts are not dominant until the oldest surface, but the skewed clast size distribution becomes apparent starting at the 10 ka surface. For these rocks, the median value decreases more steadily than for the carbonates.

For the granitoid rocks at Providence Mountains [Fig. 6.8], the small clast size dominance begins the earliest, already apparent on the 5 ka surface. Beyond this point, the median decreases by 25% from the previous surface and is 1.5-2.5 cm on the three oldest surfaces. This trend is also observed at Shepherd Creek, the middle site [Fig. 6.7], where the small clast dominance starts at 6 ka when median clast size is 1.7 cm. At Lundy Canyon, the northernmost site [Fig. 6.6], the youngest available surface is the 15 ka fluvial terrace, which already has a low median of 2.7 cm. There is a wide distribution of clast sizes on the 18 ka glacial outwash deposit, then the clast size distribution and medians follow similar trends as the other sites, with small clasts slowly increasing in abundance on older deposits.

6.3.1.1 Clast size differences between subsurface and surface over time

At the Northernmost Lundy Canyon site, too few subsurface clast counts are available for meaningful comparison with the surface. At the Middle Shepherd Creek and Southernmost Providence Mountains sites, both the subsurface and surface granitoid clasts on dated surfaces are predominantly <2.0 cm clasts. This may imply that cracking is not producing these sediments, and they existed during initial sediment deposition. However, active granular disintegration is observed on these clasts [Rasmussen et al., Ch. 5], so small sediments are certainly being produced. The abundance of small clasts in the subsurface may still be weathering-related, since even solid bedrock weathering can occur in the upper few meters of the subsurface [e.g., Eppes, Martha Cary and Griffing, David, 2010]. However, the stresses to which these buried clasts are exposed will most likely be minimal compared with their surface counterparts due to thermal insulation by surrounding clasts [e.g., Bruce, Robert Russell and Stelly, Matthias and others, 1973]. Therefore, I assume that the subsurface clast size

distribution reflects the initially deposited clasts.

Interestingly, the volcanic and carbonate rocks at the Southernmost Providence Mountains site have consistently smaller clasts in the subsurface than they do on the surface of dated deposits. However, given the difficulty of removing larger clasts from the calcified soils, this may reflect a sampling bias.

6.3.2 Surface-parallel cracking

The percentage of cracks that are surface-parallel, relative to the entire crack assemblage per surface and per lithology, is shown separated by location, lithology, and age in panels A and B of Fig. 6.11. At the southernmost Providence Mountains site, all three rock types exhibit an increase in the abundance of surface-parallel cracks upon initial exposure. Carbonate rocks have the lowest percentage overall, never exceeding 30%. On carbonates, surface-parallel cracks increase in abundance until 10 ka, stabilize until 30 ka, then by 70 ka are less dominant. The volcanic rocks initially have the highest percentage of surface-parallel cracks at this site, an even larger proportion on the 1 ka surface, then the percentage of surface-parallel cracks is lower on older surfaces. The granitoid rocks follow a similar pattern to carbonates with a gradual increase in the percentage of surface-parallel cracks until 5 ka, then slightly less on older surfaces, with the lowest proportion on its oldest surface.

At the middle Shepherd Creek site, the granitoid rock surface-parallel cracks are more abundant than at the southernmost site, but the pattern is similar, with a peak in the abundance of surface-parallel cracks around 6 ka then a slight decrease or stabilization on older surfaces. At the northernmost Lundy Canyon site, the highest value is at the youngest site. However, without any data between 0 and 15 ka, it is impossible to determine if the Lundy Canyon rocks are exhibiting a different pattern than the granitoid rocks at other sites.

6.3.3 Fabric-parallel cracking

The percentage of carbonate and volcanic rocks that have any fabric-parallel character is shown in panel C of Fig. 6.11, and the percentage of cracks that are bedding-, vein-, or foliation-parallel, relative to the entire crack assemblage per surface and per lithology, is shown in panel D of Fig. 6.11. Carbonate rocks show the highest overall occurrence of fabric with 22-65% of rocks per surface having visible fabric, which consisted of bedding, veins, or foliation. Volcanic foliation is slightly less common, with 11-48% of rocks having visible foliation. In both cases, the rocks with the highest prevalence of fabric were observed on the 5 ka surface.

It is therefore unsurprising that the amount of cracks parallel to rock fabric is highest on the 5 ka surface for both rock types. Carbonate rocks exhibit an increase of 3 to 21% in fabric-parallel cracks from 0 to 5 ka, after which time their presence decreases to 8% at 10 ka, then down to 4% on the 70 ka surface. Volcanic rocks have overall fewer fabric-parallel cracks, ranging from 1-7% of all cracks. Both the 1 and 70 ka surface have the fewest rocks with fabric, and the fewest fabric-parallel cracks; overall, the amount of fabric-parallel cracks on volcanic rocks parallels the availability of rocks with visible fabric, and has no particular age trend.

6.3.4 Clast shape evolution

The proportions of different clast shapes on surface deposits are presented in Figs. 6.13, 6.14, 6.16, 6.17, and 6.15 according to the Zingg classification. The data are subdivided into larger [$>$2.5 cm intermediate axis length] and smaller clasts [$\leq$2.5 cm intermediate axis length]. The separation at 2.5 cm was chosen to represent a clast size of about 10 2-3mm long grains. In granitoid rocks, these smaller clasts are presumed to be the sediment produced from the grain-grain stresses modeled by Rasmussen, et al. [Ch. 4], disaggregating from the rock's surface. They are also small enough that they may originate from larger pieces breaking when falling off of the

boulder, so their shapes may be less informative than larger clasts. Additionally, the smaller clasts may be over-represented in the subsurface deposits, but their separation will remove this potential bias. The subsurface clast size distributions are also shown as bar graphs with the percentage of each shape per distribution per surface age [Figs. 6.18, 6.19, 6.20, 6.21, and 6.22].

Most clasts at the Northernmost Lundy Canyon site [Fig. 6.13] are disks and spheres, with very few rods and blades making up the smaller clast category. For large clasts, blades broadly increase in abundance until 101 ka. Rods are unusually dominant for large clasts on the oldest surface here. Like the Northernmost site, at the middle Shepherd Creek site [Fig. 6.14] disks and spheres dominate the smaller clasts, with spheres being unusually common on the 76 ka surface. Initially, larger clasts are mostly disks and spheres, then disks dominate until the oldest surface which has mostly blades. Larger spheres decrease in abundance over time, and overall rod shaped clasts are minimal.

The granitoid rocks at Providence Mountains [Fig. 6.15] are mostly disk and sphere shaped. Both clast size categories exhibit an increasing number of blades until 30 ka, then the proportion stabilizes or decreases on the oldest surface. There are nearly uniform amounts of small and large rods on all surfaces until 30 ka, and fewer on the oldest surface. The amount of small spheres is highest on the 0 ka surface, then remains relatively stable until a slight increase on the older surface. By contrast, larger spheres are progressively less likely, but also increase in abundance again on the oldest surface.

For Providence Mountains carbonates [Fig. 6.16], the smaller clasts are of all four clast shapes, with disk shapes dominating at 0, 5, and 30 ka, spheres dominating at 1 ka, blades and rods at 10 ka, and blades at 70 ka. For the larger clasts, rod shapes increase in abundance until 10 ka then nearly disappear, and disk shapes are relatively dominant throughout. Spherical clasts are most abundant on the two

youngest surfaces, and on the two oldest surfaces, blades and disks dominate. On the oldest surface, a developed desert pavement, the larger clasts are all blades and disks.

The smaller volcanic clasts [Fig. 6.17] are predominantly disk-shaped, except for the oldest surface where most clasts are spherical. Other shapes do not exhibit consistent trends over time. The larger clasts, by contrast, are predominantly spherical on the two youngest surfaces, then at 5 ka and beyond, disk shapes dominate.

In addition to comparing surface-to-surface clast shapes, here I compare the surface shapes with their subsurface counterparts, presenting the data as an increase or decrease in the percentage of each shape [Figs. 6.23 and 6.24]. Comparisons for the 0 ka surfaces are unavailable, because the surface and subsurface were presumed to be the same [unweathered]. At the southernmost Providence Mountains site [6.23], carbonate rocks are more spherical and less blade shaped on the 1 ka surface when compared with the subsurface. By 10 ka, there are more blades and rods on the surface, and less disks. Interestingly, by 30 ka, the subsurface and surface shape distributions are very similar.

The volcanic rocks similarly are more spherical and less blade shaped on the 1 ka surface when compared with the subsurface. The distributions are fairly similar between surface and subsurface, although surface spheres become less common on older surfaces. For granitoid rocks, the difference from subsurface to surface shows that as surfaces get older, there are more rods and blades on the surface, and less spheres, than the unweathered clasts in the subsurface.

Compared with the southernmost site, the clast shape changes at the Middle site Shepherd Creek and Northernmost Lundy Canyon sites [Fig. 6.24] are minimal, although the dominance in non-spherical clasts on the older surface is evident at the Middle Shepherd Creek site.

6.4 Clast shapes and sizes relative to surface-parallel cracks

If the clast shapes on weathered surfaces is connected to the prior cracks which divided the initial clasts [Fig. 6.11A and B], I expect that surface-parallel cracks will produce flattened sediments [blades and disks] either when surface-parallel cracking is at its peak, or following its peak, after the surface-parallel cracks have eroded pieces of rock. For the larger sized carbonate rocks [Fig. 6.16], blades and disks are the only shapes on the 70 ka surface, which correlates with a decrease in the abundance of surface-parallel cracks. Similarly, for volcanic rocks, surface-parallel cracking is at its peak at 1 ka, then beyond 1 ka, disk shapes dominate the larger clasts.

For granitoid rocks in the southernmost site [Fig. 6.15], rocks are less spherical over time, and blades become slightly more dominant. Only at the oldest site, after which time surface-parallel cracks decrease [Fig. 6.11A], is there a significant dominance of disk shapes. At the middle site [Fig. 6.14], the increase in flattened blades and disks is apparent for larger clasts starting at 6 ka, the time when surface-parallel cracking is at its peak [Fig. 6.11A]. At the northernmost site, the lack of clast size data at 0 ka and lack of surface-parallel fracture metrics for the first 15 ka of exposure make this analysis inconclusive.

To more easily assess the overall trends of surface-parallel cracking vs. clast shape, I combined blades and disks to represent flattened clasts, and compared their dominance on all surface and sites [Fig. 6.25]. Fig. 6.25A shows that granitoid rocks do not follow a single pattern, although flattened clasts they do increase in abundance upon initial exposure. However, for the volcanic rocks, where presumably the fine grain size increases the likelihood that eroded pieces of rock maintain their shape when falling to the ground, the peak in surface-parallel cracking [1 ka, Fig. 6.11] corresponds to the lowest proportion of flat clasts [Fig. 6.25B] , and when the surface-parallel cracking drops off at 5 ka, flat clasts increase in abundance. Similarly, for carbonate rocks, the highest number of flattened clasts are on the oldest surface; by this time,

surface-parallel cracking has decreased from younger surfaces [1 ka, Fig. 6.11B].

The fabric-parallel crack morphology peaks in carbonate and volcanic rocks at 5 ka, then decreases [Fig. 6.11D]. Neither of these trends appear to have any impact on the abundance of blades and disks (flattened clasts) on the surfaces.

6.5 Discussion and conclusion

It has long been known that granitoid rocks weather to produce grus [e.g., Riber, L., Le Pera, E., Conforti, M., Ietto, F., Dypvik, H. and others, 2020; Eppes, Martha Cary and Griffing, David, 2010; Eppes, Martha Cary and McFadden, Leslie, 2008; Hoskin, Charles M. and Sundeen, Daniel A., 1985], and Rasmussen et al. [Ch. 4] predict this happens relatively quickly at these exact sites. This may explain why surface-parallel crack morphologies do not result in a particular granitoid clast shape being produced. If granitoid clasts are only composed of a few dozen mineral grains [e.g., 1-2 cm long clasts] their shape is likely unrelated to fracture type. In other words, a thin blade can easily split into a collection of rods, spheres, and disks when it drops from the larger rock to the ground surface. However, surface-parallel cracks may be the reason why fewer granitoid rocks are spherical on older surfaces for all sites. While grus is the product of this cracking, the rock that is left behind has experienced asymmetrical surface removal and is thus a different shape. Alternatively, this may be the result of cracks propagating through the center of the rock, splitting the rock into semi-equal sizes [e.g., shattering behavior posited by Mushkin, Amit, Sagy, Amir, Trabelci, Eran, Amit, Rivka and Porat, Naomi, 2014], which would make the two remaining rocks less spherical.

For the predominantly fine-grained carbonate and volcanic rocks which are less likely to produce small, rounded $<$2.0 cm clasts as grus, early surface-parallel cracking appears to result in a higher proportion of flattened clasts existing on older surfaces. While rocks with foliation or bedding do contain cracks that follow those planes, the amount of cracks following those planes does not appear to dominate over other

types of cracks [Fig. 6.11D]. Therefore, it is unlikely that the rhyolitic foliation; and carbonate bedding, metamorphic foliation, and veins; are specifically driving rock cracking. Additionally, the peak in fabric-parallel cracking has no relation to the shape of clasts produced [Fig. 6.11D].

It is important to note that when surface-parallel cracking peaks, this does not necessarily mean that there is a net increase in surface-parallel cracks. This effect could also be a result of non-surface-parallel cracks, those which propagate through the center of the rock, increasing in their own abundance. This would decrease the percentage of cracks that are surface-parallel, even though their actual number could increase. Subdividing the dataset into rocks with/without surface-parallel cracks and recreating the cracking chronofunctions presented by Rasmussen et al. [in prep, see Ch. 2] may provide some insights into this issue.

For finer-grained rocks, clast sizes and shapes can be used to help infer when different modes of cracking are dominating. When surface-parallel cracks are observed to dominate for a particular lithology, this can be used to infer the likelihood that elongated clasts are being produced. Using clast sizes and shapes thus provides an easier, faster way to begin to understand the impact of fractures on sediment production, without requiring the meticulous and time-consuming analysis of cracking data presented in this Dissertation. Perhaps, similar to how clast-sized granitoid sediments are called 'grus', the product of surface-parallel cracking of volcanic and carbonate rocks could be considered 'blades', 'disks', or 'shards'.

When using geomorphic surface roughness as a proxy for surface age [e.g., Mushkin, Amit, Sagy, Amir, Trabelci, Eran, Amit, Rivka and Porat, Naomi, 2014], clast lithology must be used to interpret the rate and shape of clast evolution. Surfaces composed of many rock types may need to be analyzed in terms of percentages of different lithologies, depending on the size of sediments involved. Grus is produced from granitoid rocks within thousands of years, and is predominantly disk and sphere shaped;

this leads to a predominantly small clast size within ∼15 ka at all sites. However, in most cases, spherical granitoid clasts ≥2.5 cm intermediate axis length decrease in abundance on older surfaces, and may be a better indicator of surface age over longer timescales.

The differences in rate and style of comminution of clasts based on lithology provide a glimpse into the importance of understanding rock fracture and its implication on sediment evolution. The shape of boulder-sized clasts will dictate surface stability and potential erosive power of the sediment. Taking the entire fractured rock as a whole, any fracture that propagates into fresh rock provides a surface on which chemical weathering may begin anew. This impacts not only the carbon cycle through natural weathering-induced CO_2 sequestration, but the availability of nutrients within soils. Not only does the lithology dictate which minerals the rock contributes to the ecosystem, but it also dictates the rate and magnitude of fresh surface availability due to its fracture characteristics. Extending this study to bedrock would provide significant insight into regolith production at the soil-rock interface, help us predict where and how steady-state soil profiles can evolve [e.g., Heimsath, Arjun M., Dietrich, William E., Nishiizumi, Kunihiko and Finkel, Robert C., 1997], and allow better planning for preservation of soil as a natural resource necessary for life on Earth.

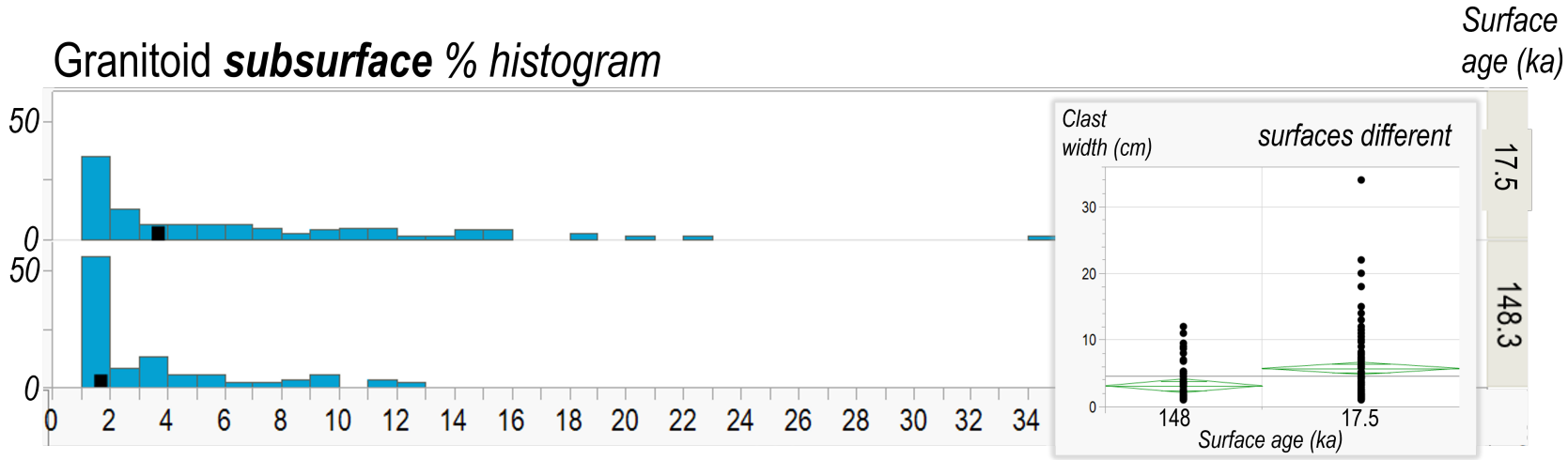

Figure 6.1: Percentage histogram of subsurface intermediate clast lengths (cm) at Lundy Canyon, with median values shown as black bars. The limited subsurface data available at the Lundy Canyon site exhibit dissimilar clast size distributions, as shown through the Analysis of Variance [ANOVA] plot.

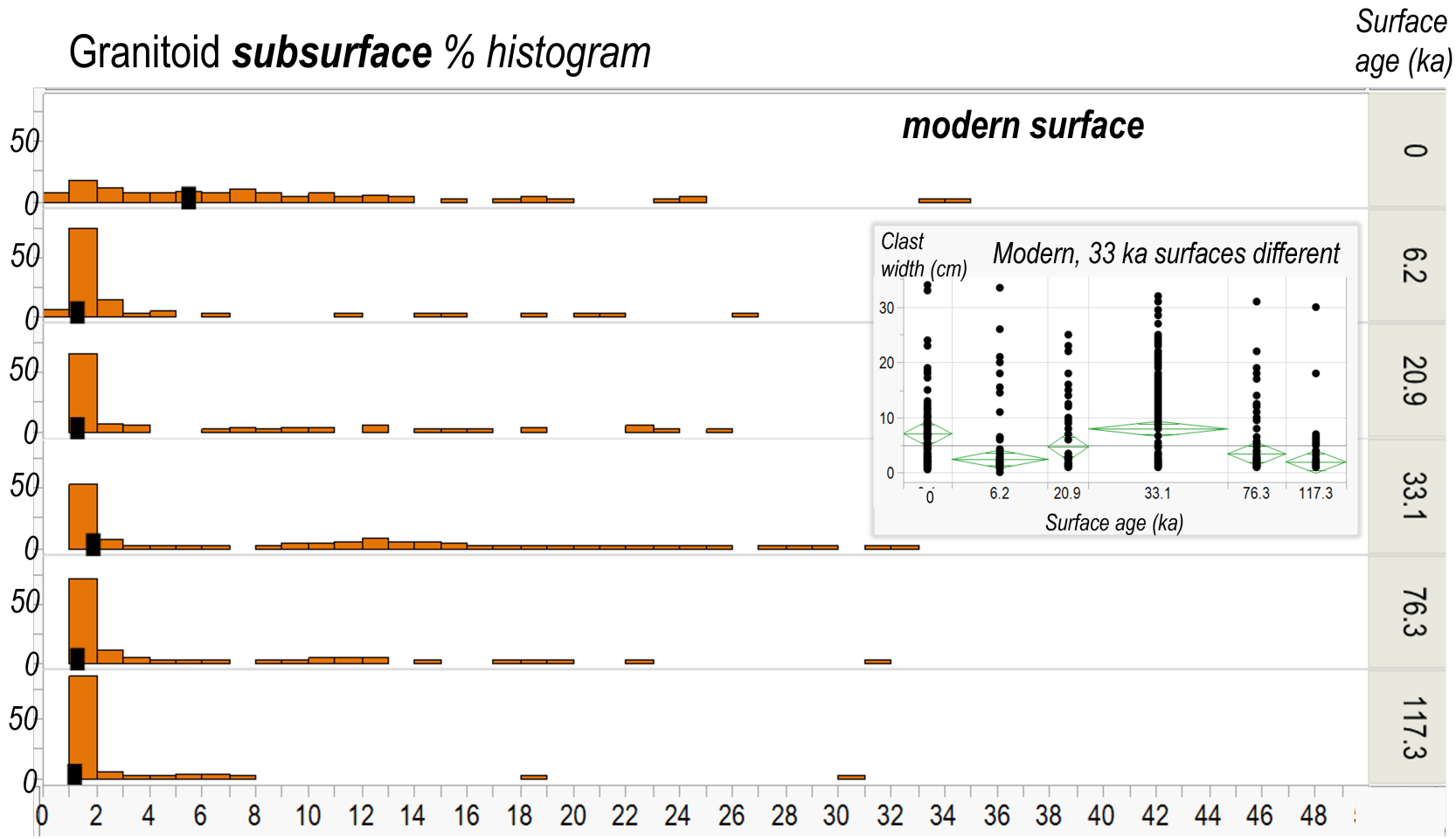

Figure 6.2: Percentage histogram of subsurface intermediate clast lengths (cm) at Shepherd Creek, with median values shown as black bars. All clast distributions in the subsurface are simlar, except the 33 ka subsurface which contained larger clasts.

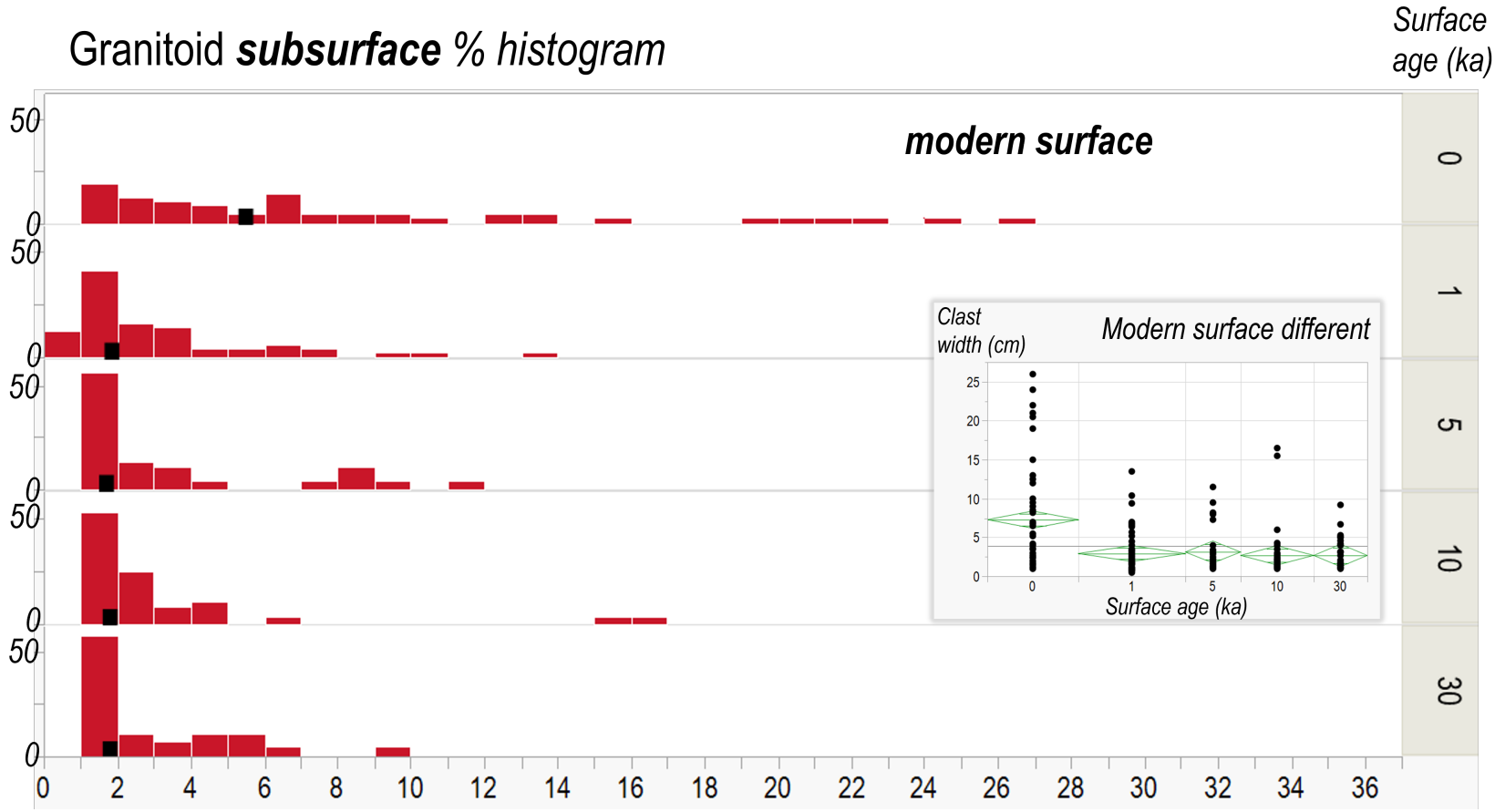

Figure 6.3: Percentage histogram of subsurface intermediate granitoid clast lengths (cm) at Providence Mountains, with median values shown as black bars. The clast size distribution in all subsurface exposures are similar, suggesting that the 1, 5, 10, and 30 ka surfaces started with statistically similar clast size distributions.

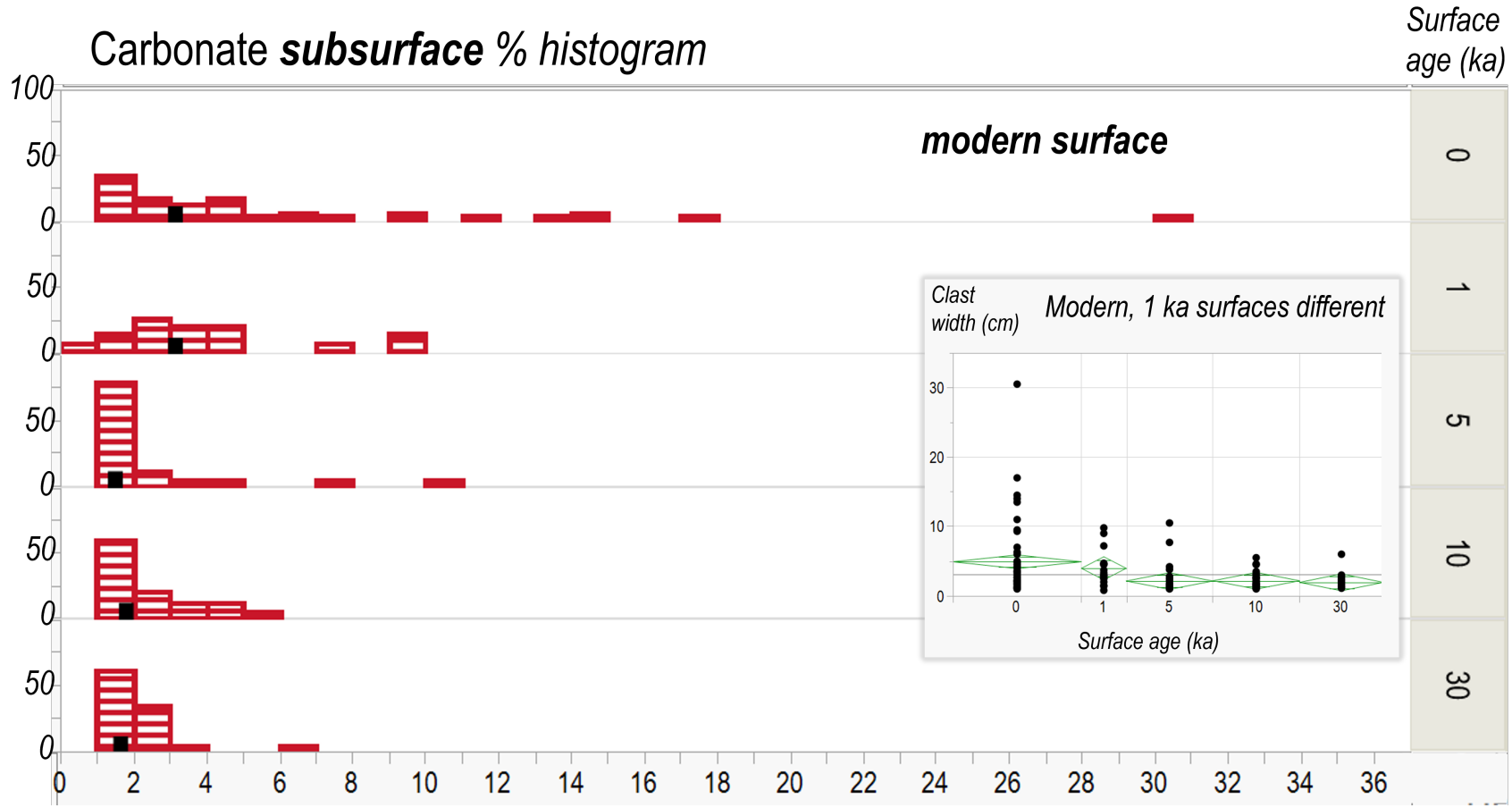

Figure 6.4: Percentage histogram of subsurface intermediate carbonate clast lengths (cm) at Providence Mountains, with median values shown as black bars. The carbonate clasts in the subsurface were statistically larger in the 1 ka subsurface, while the 5, 10, and 30 ka surfaces were similar.

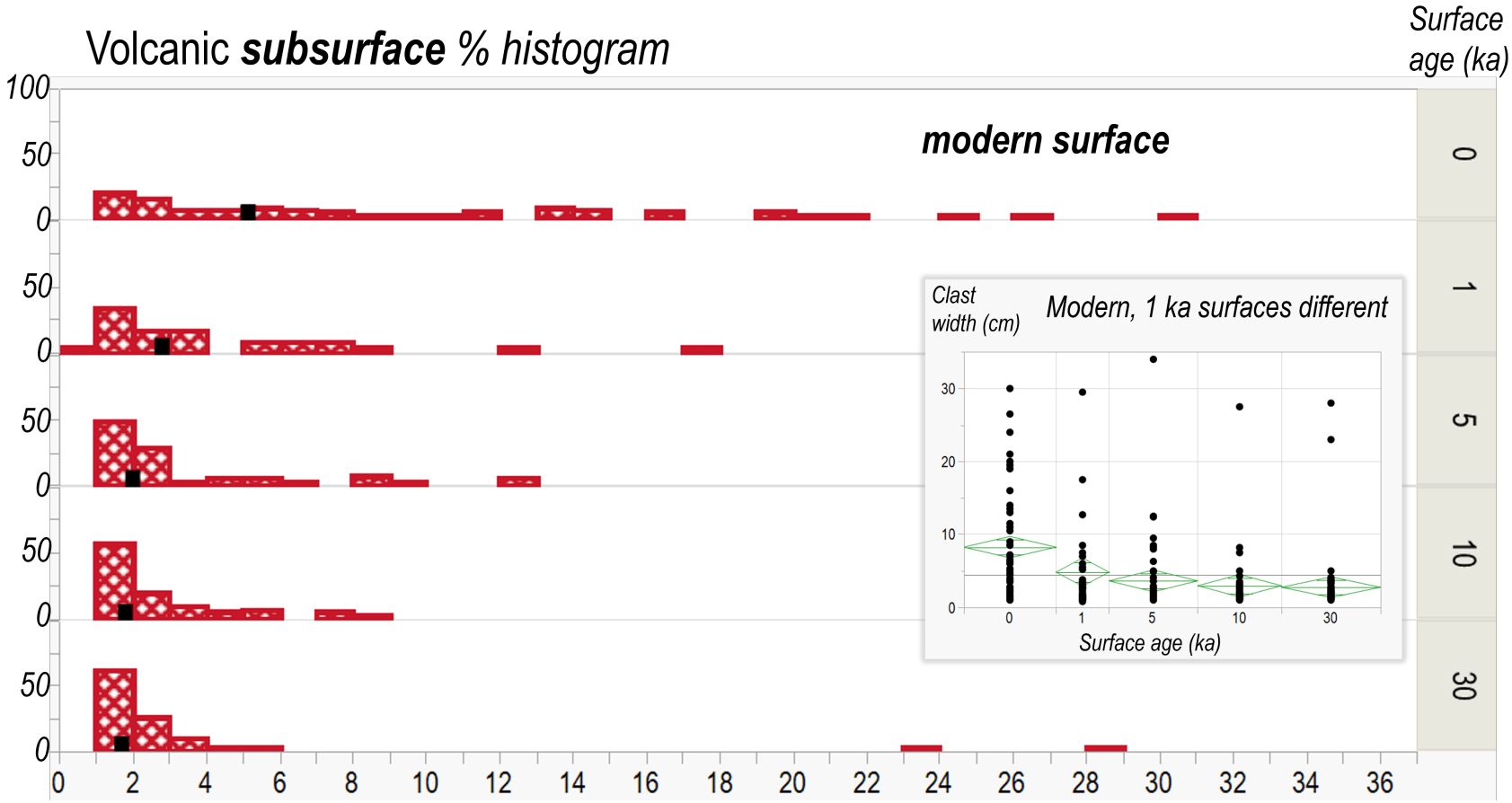

Figure 6.5: Percentage histogram of subsurface intermediate volcanic clast lengths (cm) at Providence Mountains, with median values shown as black bars. The volcanic clast size distribution in the subsurface exposures is similar, suggesting that the 1, 5, 10, and 30 ka surfaces started with statistically similar clast size distributions.

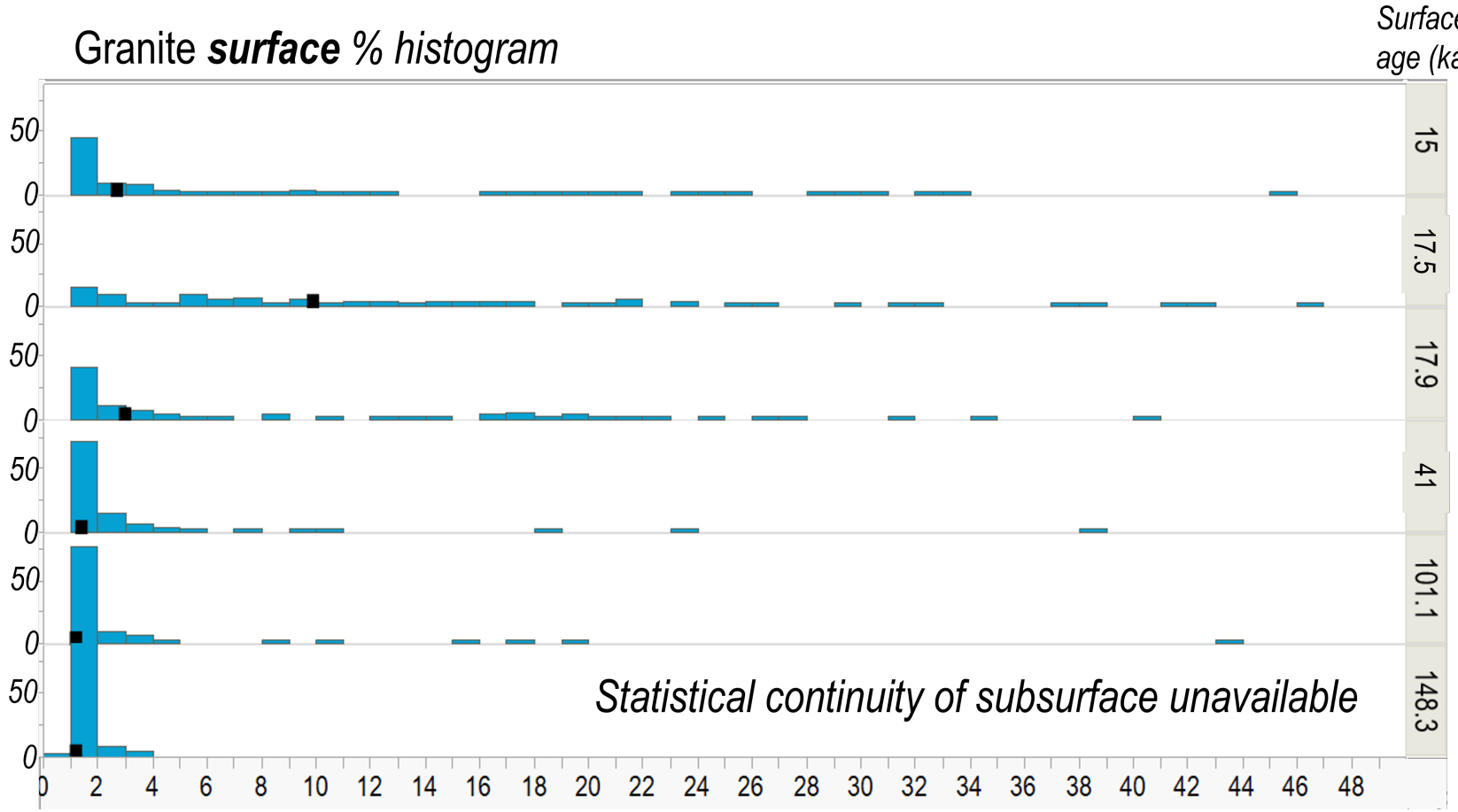

Figure 6.6: Percentage histogram of surficial intermediate clast lengths (cm) at Lundy Canyon, with median values shown as black bars. Note that the youngest modern surface is missing, so the 'time-zero' comparison is not possible.

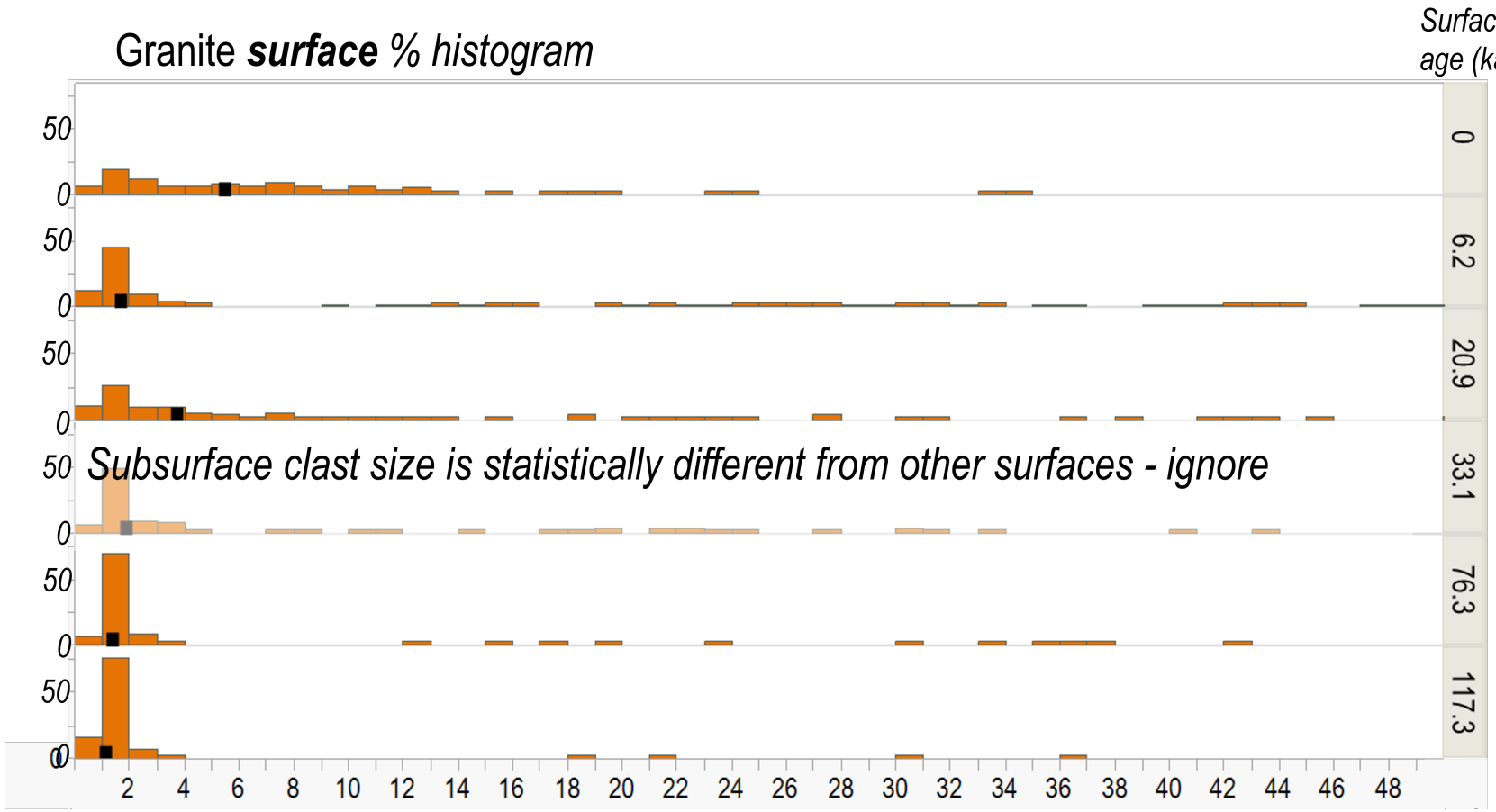

Figure 6.7: Percentage histogram of surficial intermediate clast lengths (cm) at Shepherd Creek, with median values shown as black bars. The 33 ka subsurface was shown to be statistically dissimilar from the other surfaces, however its surface clast sizes are similar to the next oldest 76 ka surface.

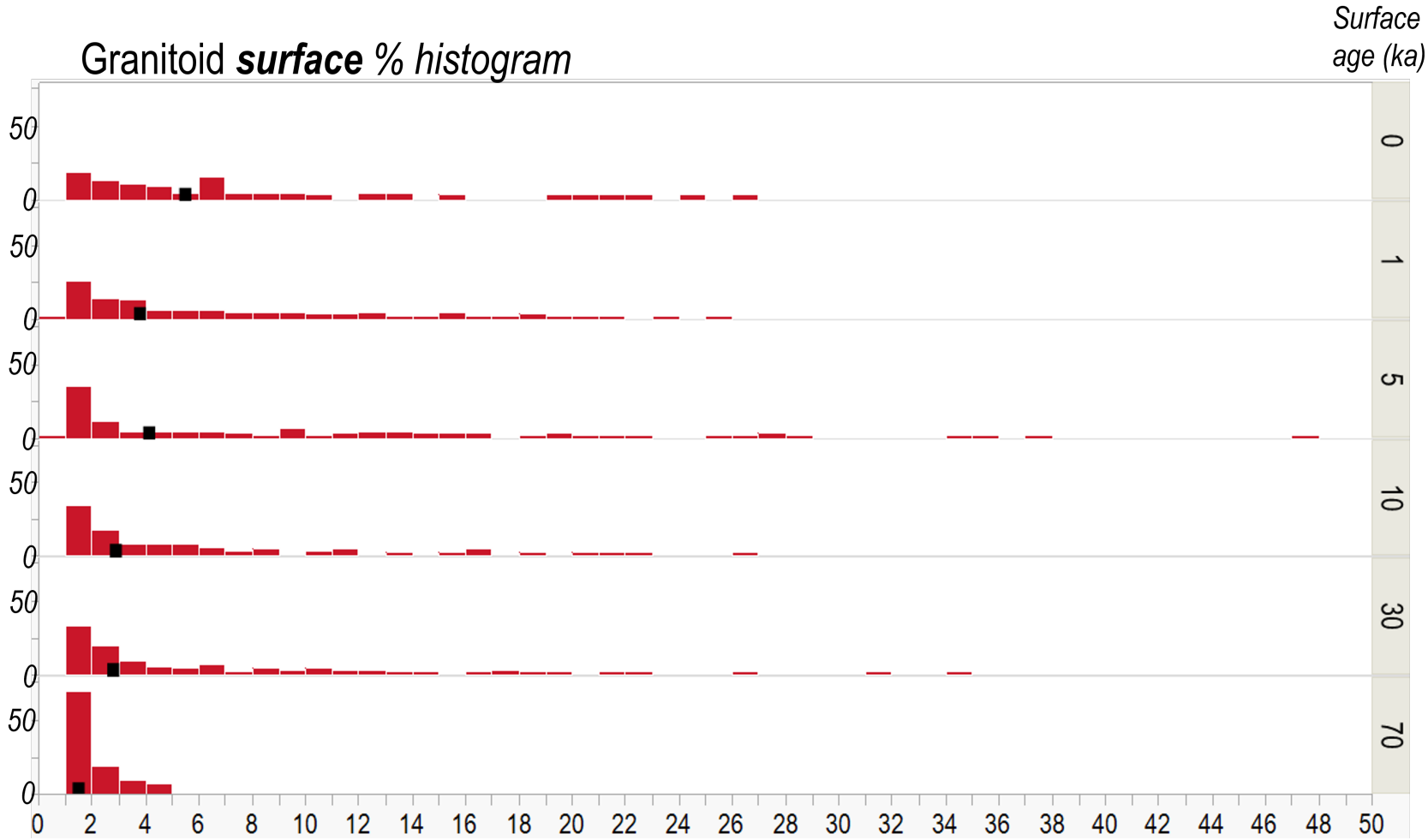

Figure 6.8: Percentage histogram of surficial intermediate granitoid clast lengths (cm) at Providence Mountains, with median values shown as black bars.

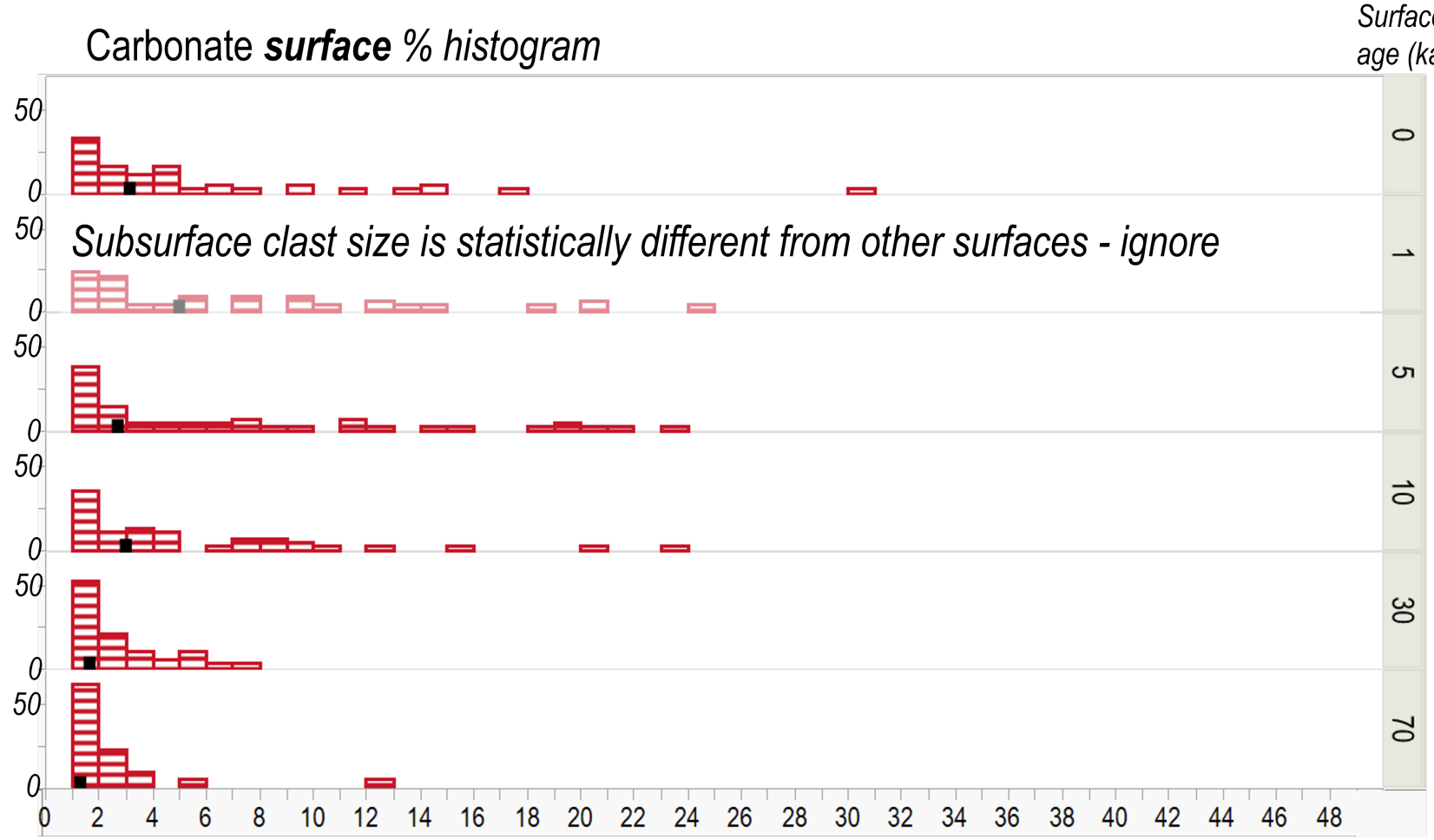

Figure 6.9: Percentage histogram of surficial intermediate carbonate clast lengths (cm) at Providence Mountains, with median values shown as black bars. The 1 ka subsurface clast size distribution was statistically dissimilar with unusually large clasts; this is reflected in a larger overall clast size on the 1 ka surface than the 5 ka surface, and the highest median clast size.

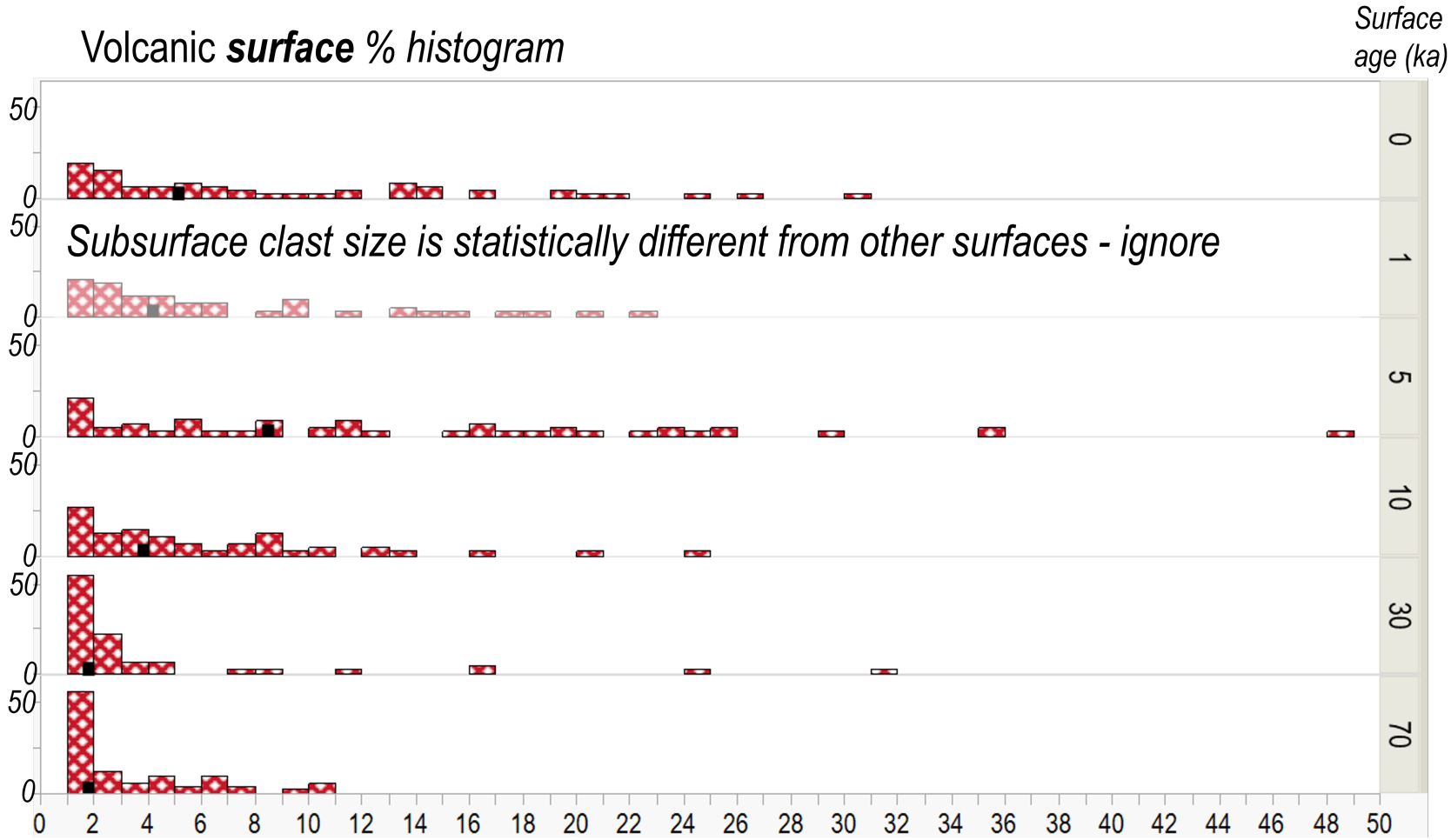

Figure 6.10: Percentage histogram of surficial intermediate volcanic clast lengths (cm) at Providence Mountains, with median values shown as black bars.

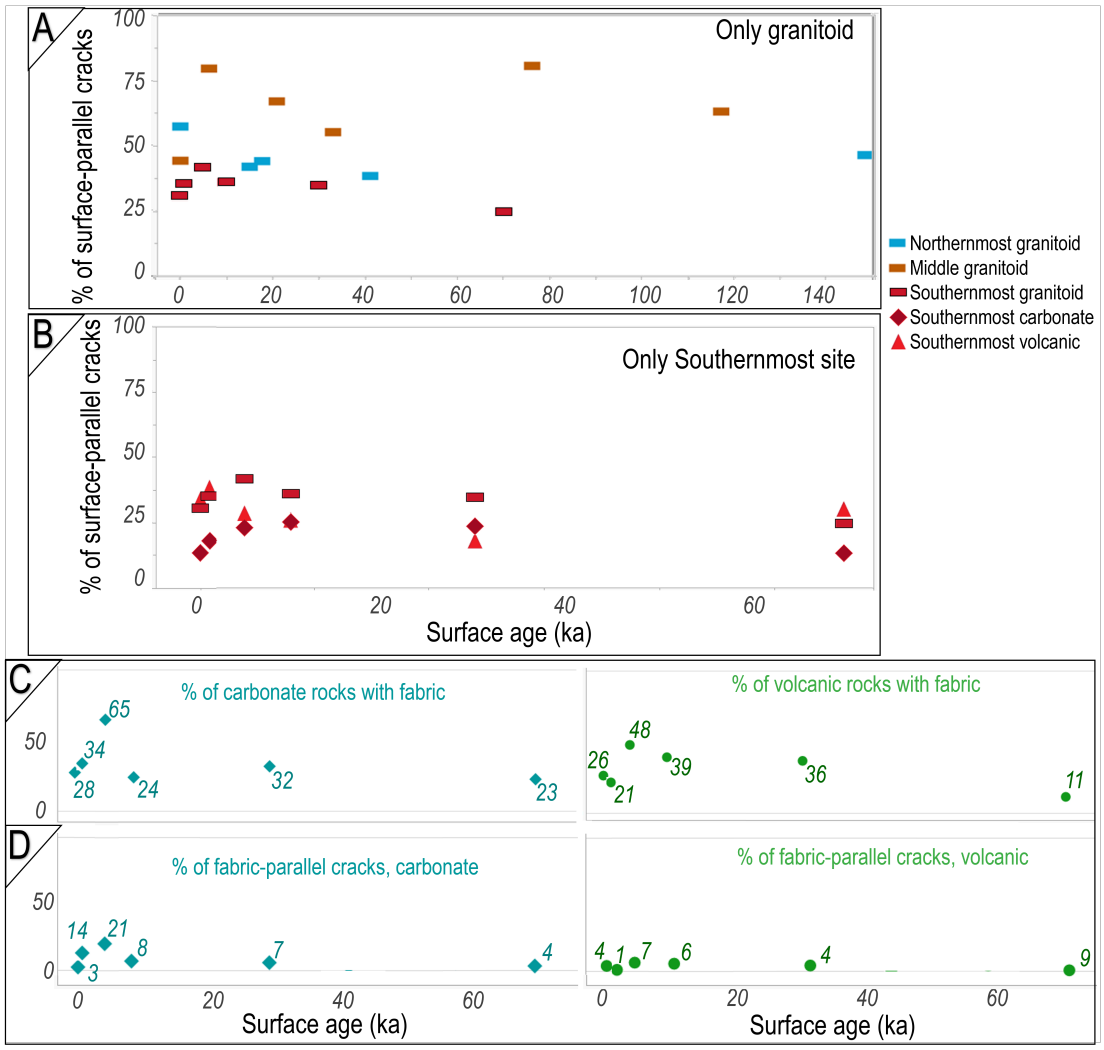

Figure 6.11: The amount of surface-parallel cracks presented as a percentage of all cracks for granitoid rocks only [A] and rocks at the Southernmost site [B]. In the lower panels, granitoid rocks are emitted because fabric is rarely encountered. The left panels show the amount of carbonate rocks that have a visible fabric, as a percentage of all rocks per surface [C] and the percentage of all measured cracks on that surface which are aligned parallel to that fabric [D]. The right panels display the same statistics for volcanic rocks.

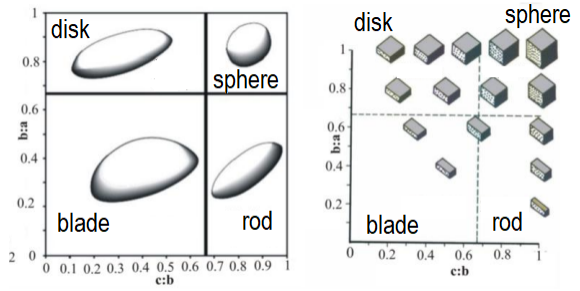

Figure 6.12: Zingg classification modified from Zingg, Theodor [1935] and Dumitriu, Dan, Niculiţă and Condorachi.

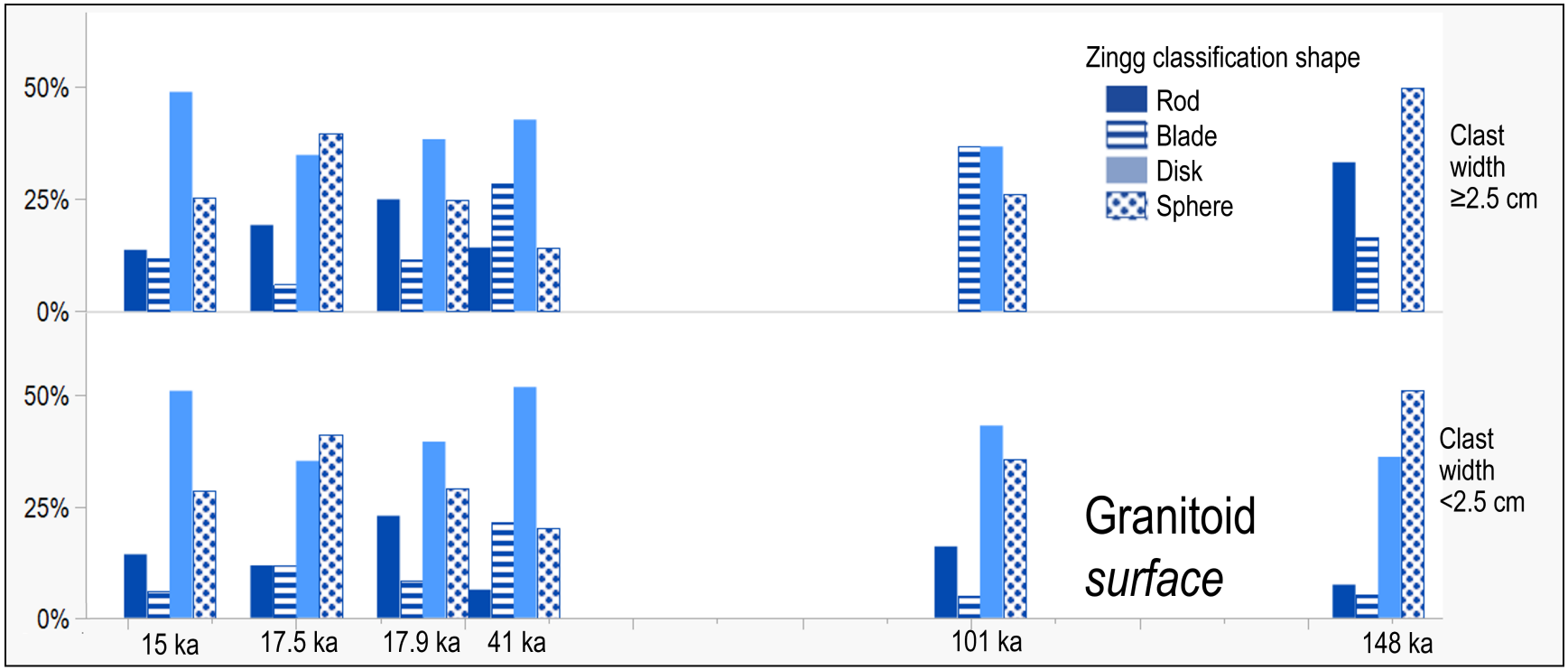

Figure 6.13: The percentage of clasts that are classified as Zingg rods, blades, disks, and spheres, per surface, at Lundy Canyon. The upper plot shows larger clasts, and the lower plot shows smaller clasts. Note that the surfaces have been shifted horizontally to display all four shape per surface.

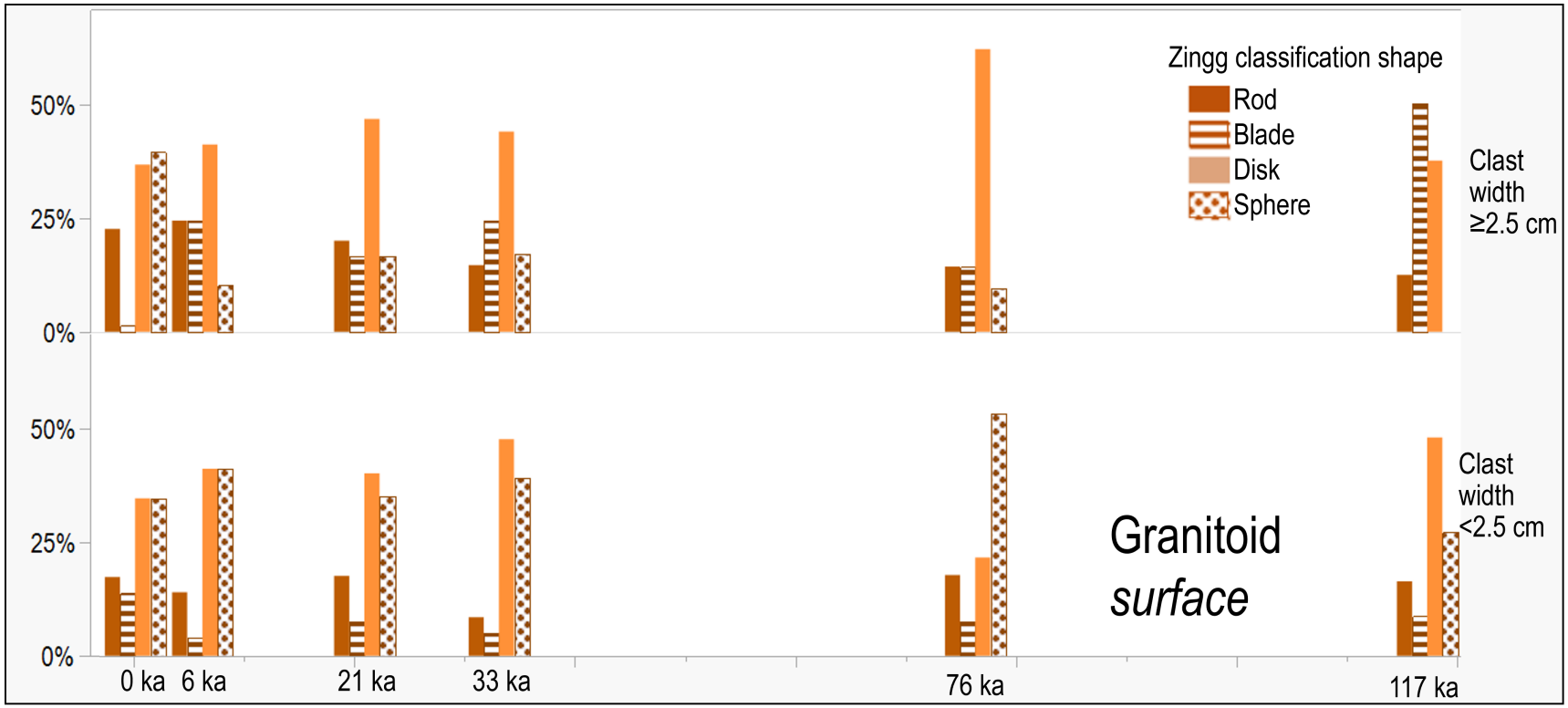

Figure 6.14: The percentage of clasts that are classified as Zingg rods, blades, disks, and spheres, per surface, at Shepherd Creek. The upper plot shows larger clasts, and the lower plot shows smaller clasts.

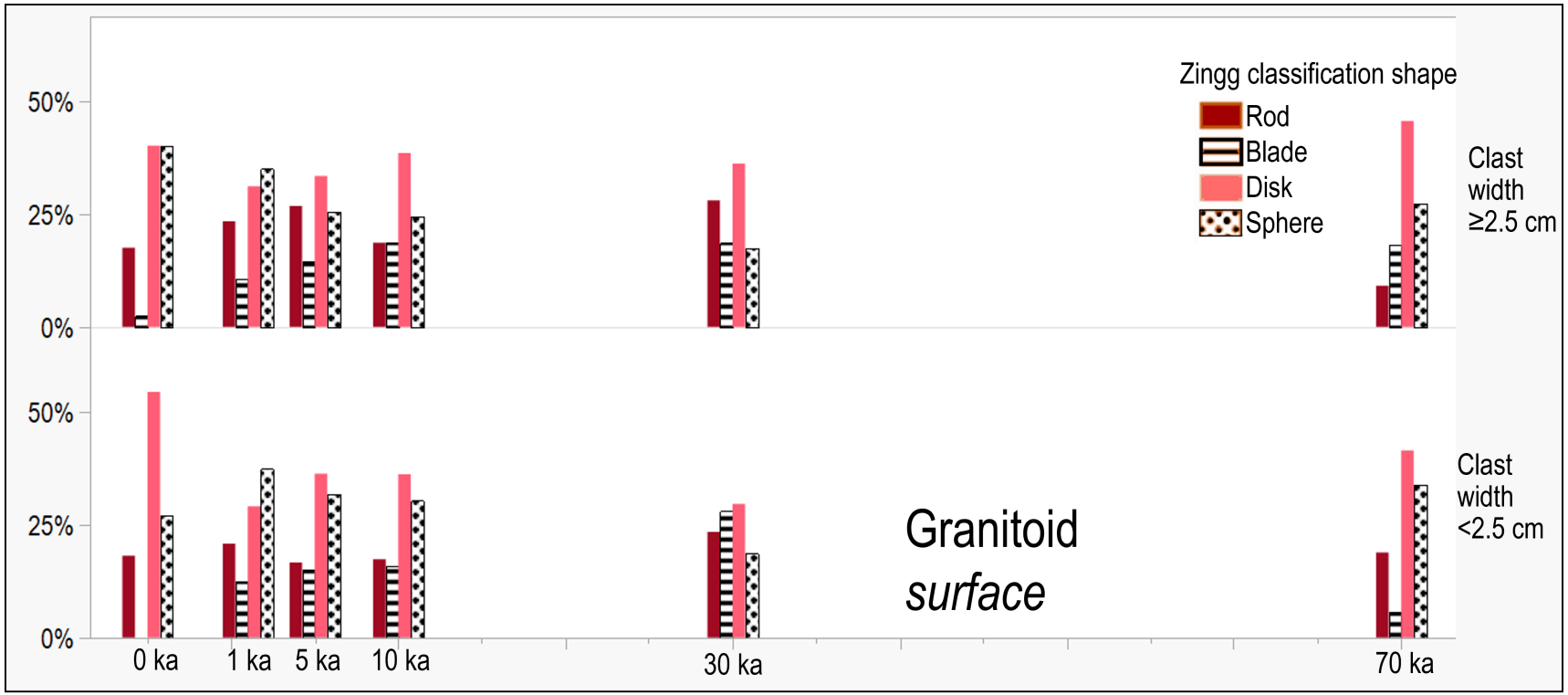

Figure 6.15: The percentage of granitoid clasts that are classified as Zingg rods, blades, disks, and spheres, per surface, at Providence Mountains The upper plot shows larger clasts, and the lower plot shows smaller clasts. Note that the surfaces have been shifted horizontally to display all four shape per surface.

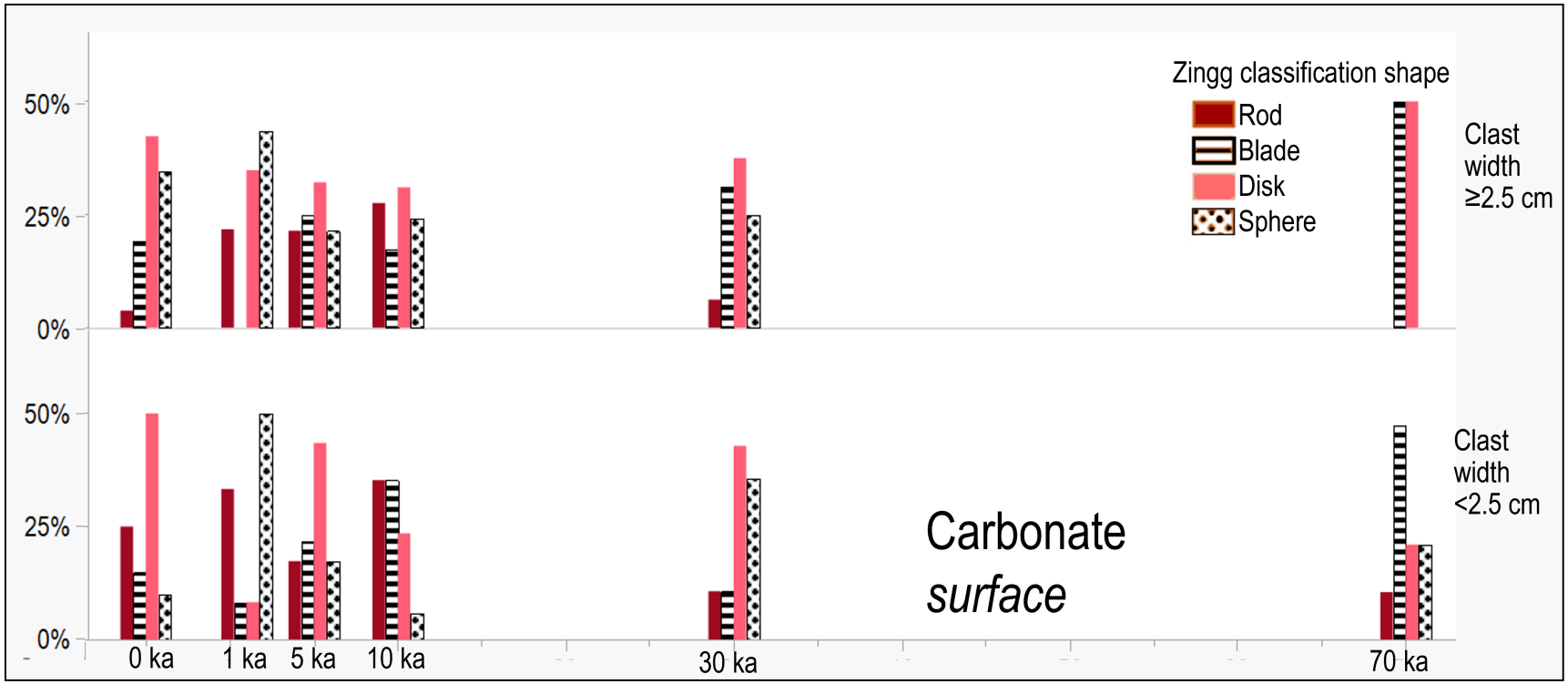

Figure 6.16: The percentage of carbonate clasts that are classified as Zingg rods, blades, disks, and spheres, per surface, at Providence Mountains The upper plot shows larger clasts, and the lower plot shows smaller clasts. Note that the surfaces have been shifted horizontally to display all four shape per surface.

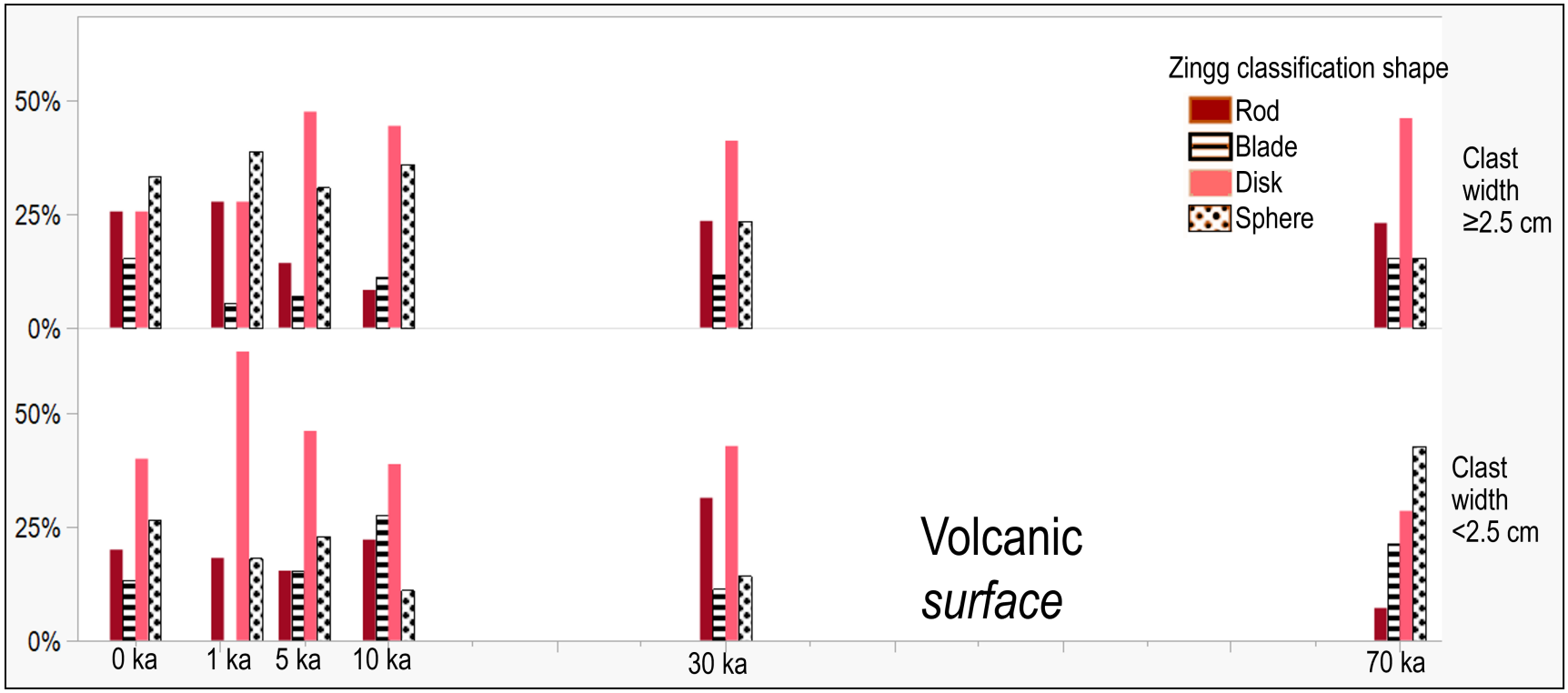

Figure 6.17: The percentage of carbonate clasts that are classified as Zingg rods, blades, disks, and spheres, per surface, at Providence Mountains The upper plot shows larger clasts, and the lower plot shows smaller clasts. Note that the surfaces have been shifted horizontally to display all four shape per surface.

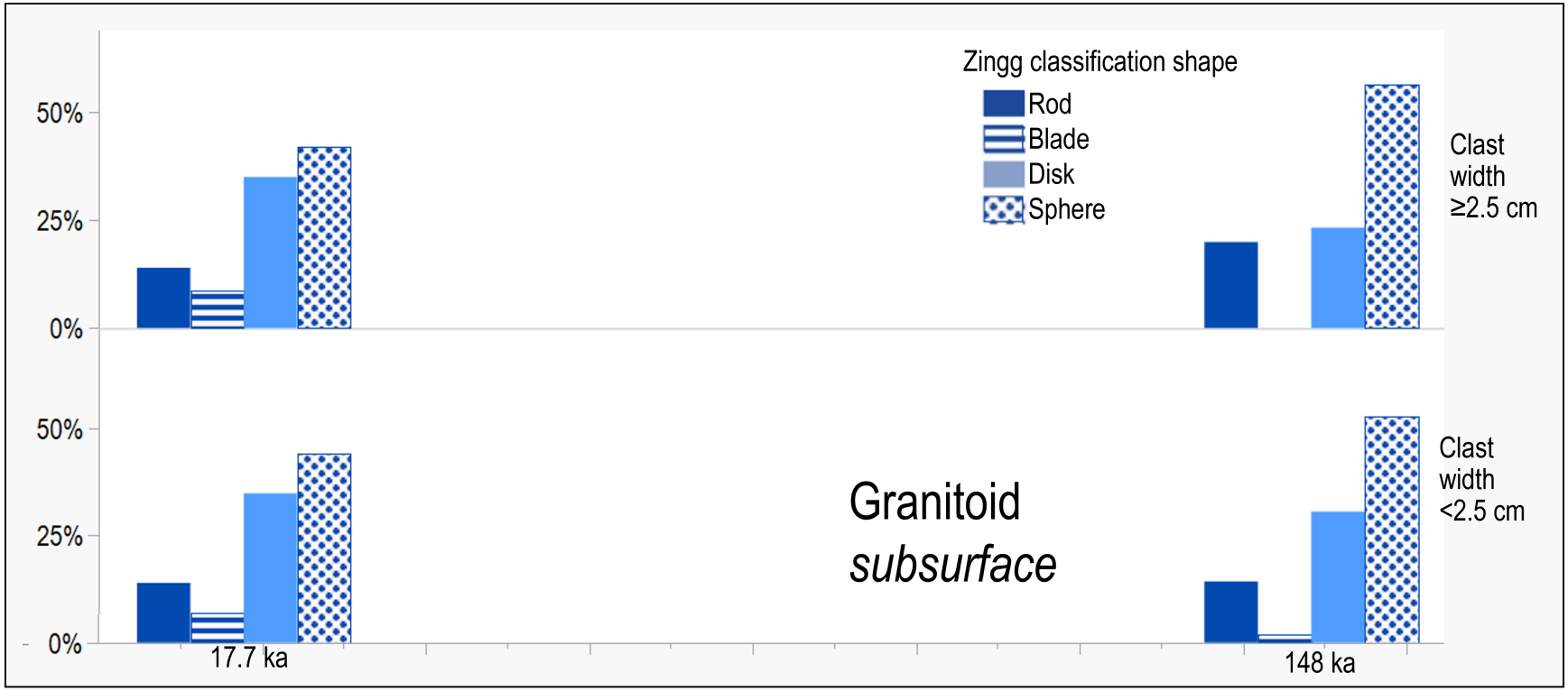

Figure 6.18: Zingg shape classification of subsurface clasts at Lundy Canyon. The upper plot shows larger clasts, and the lower plot shows smaller clasts.

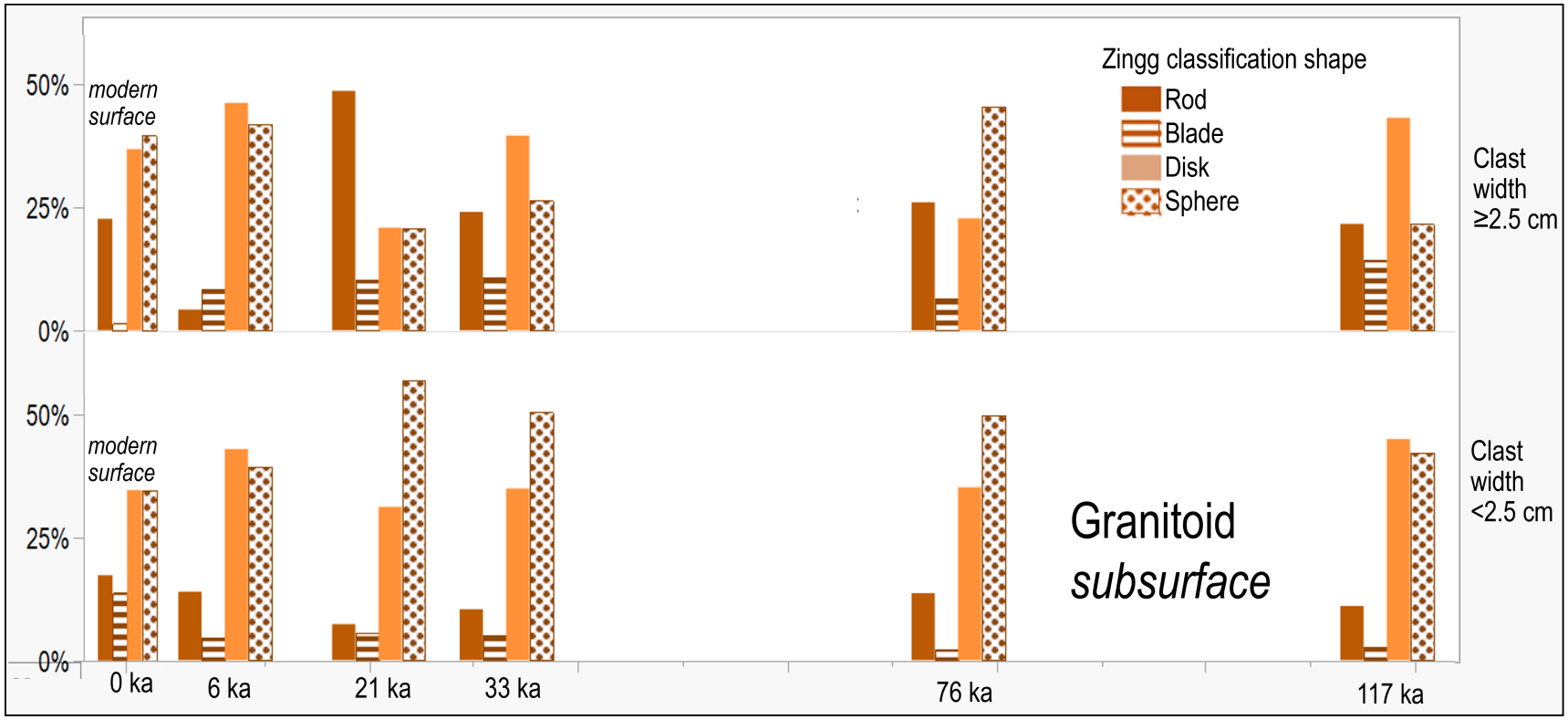

Figure 6.19: Zingg shape classification of subsurface clasts at Shepherd Creek. The upper plot shows larger clasts, and the lower plot shows smaller clasts.

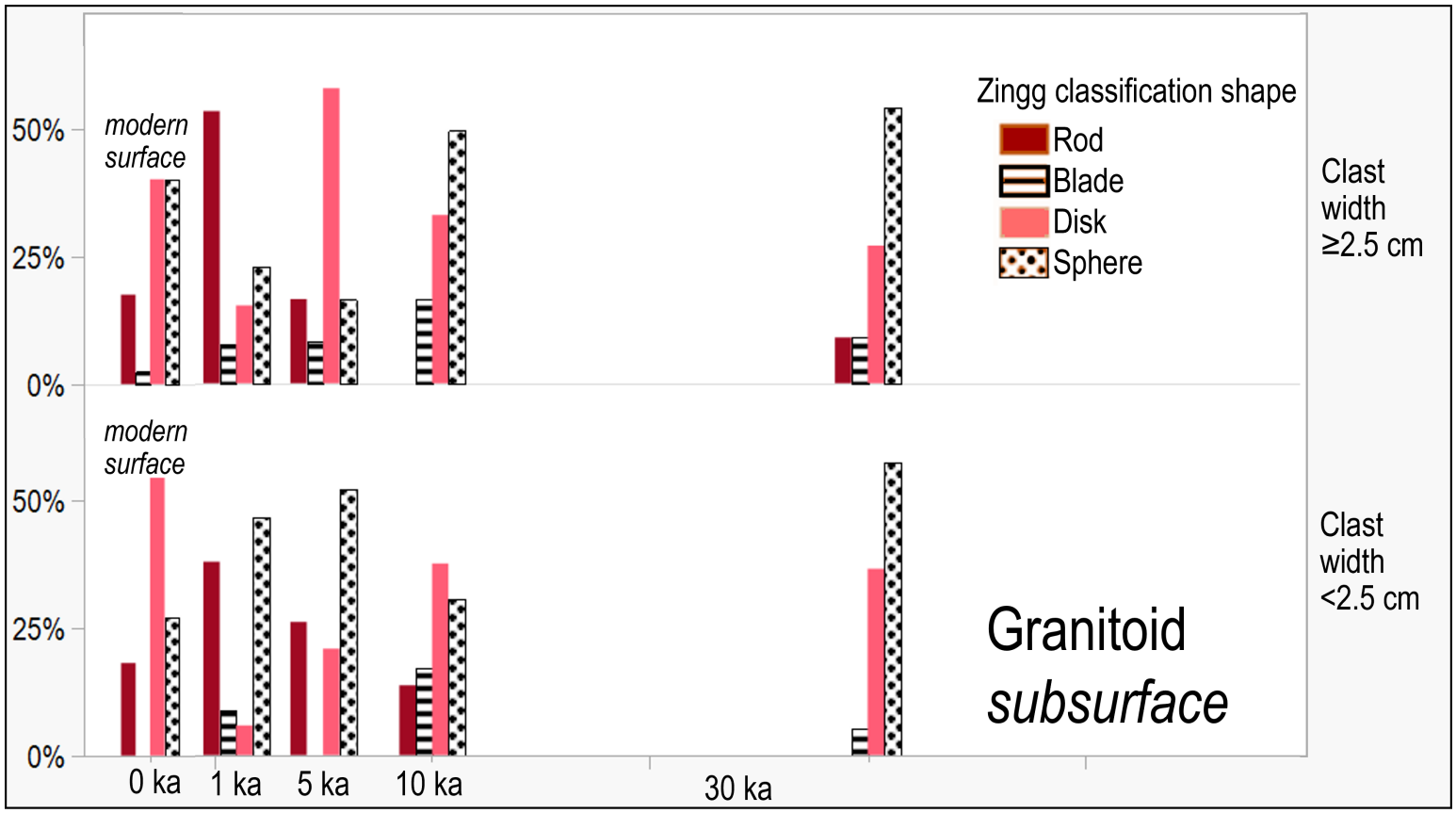

Figure 6.20: Zingg shape classification of subsurface granitoid clasts at Providence Mountains. The upper plot shows larger clasts, and the lower plot shows smaller clasts. Note that the surfaces have been shifted horizontally to display all four shape per surface.

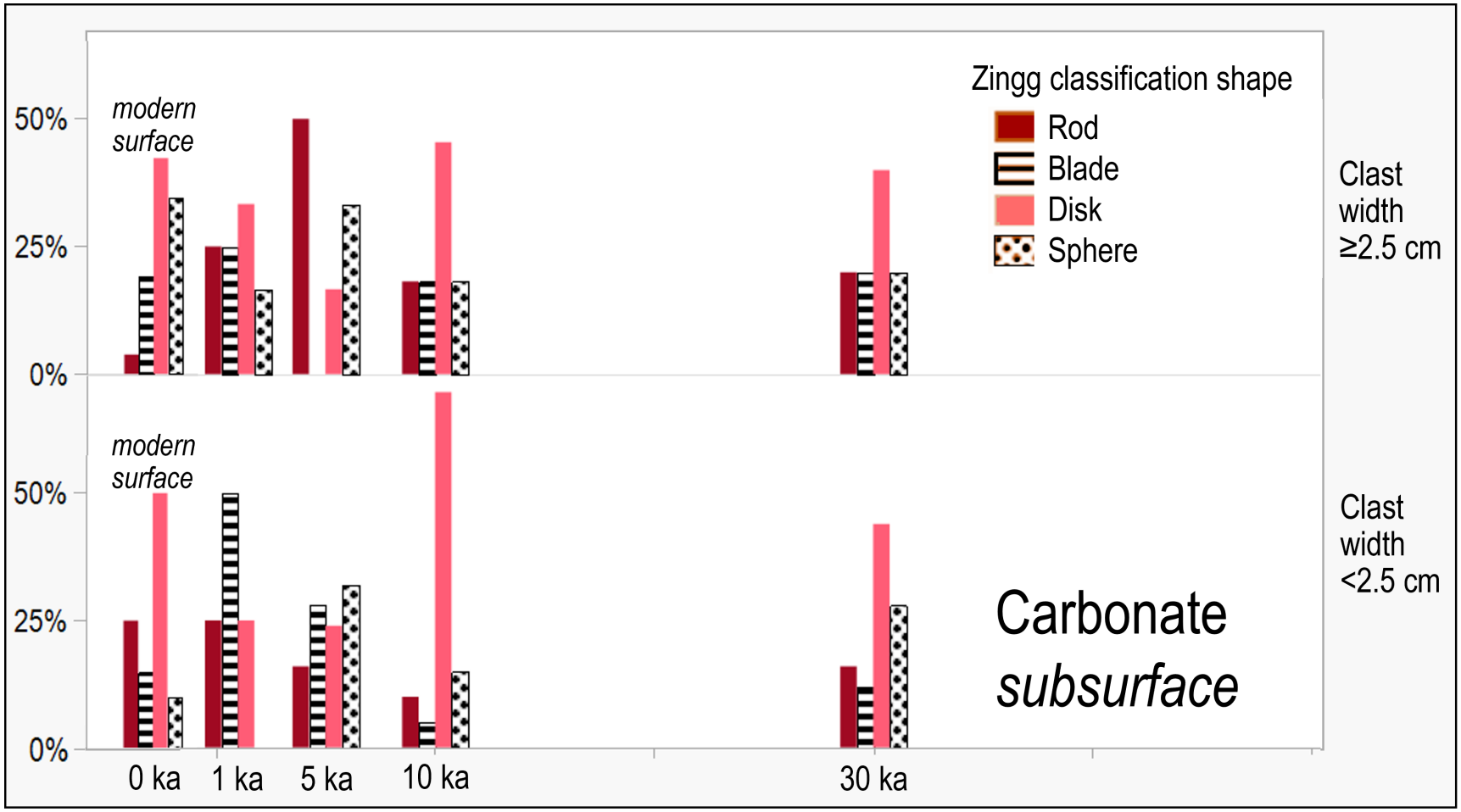

Figure 6.21: Zingg shape classification of subsurface carbonate clasts at Providence Mountains. The upper plot shows larger clasts, and the lower plot shows smaller clasts. Note that the surfaces have been shifted horizontally to display all four shape per surface.

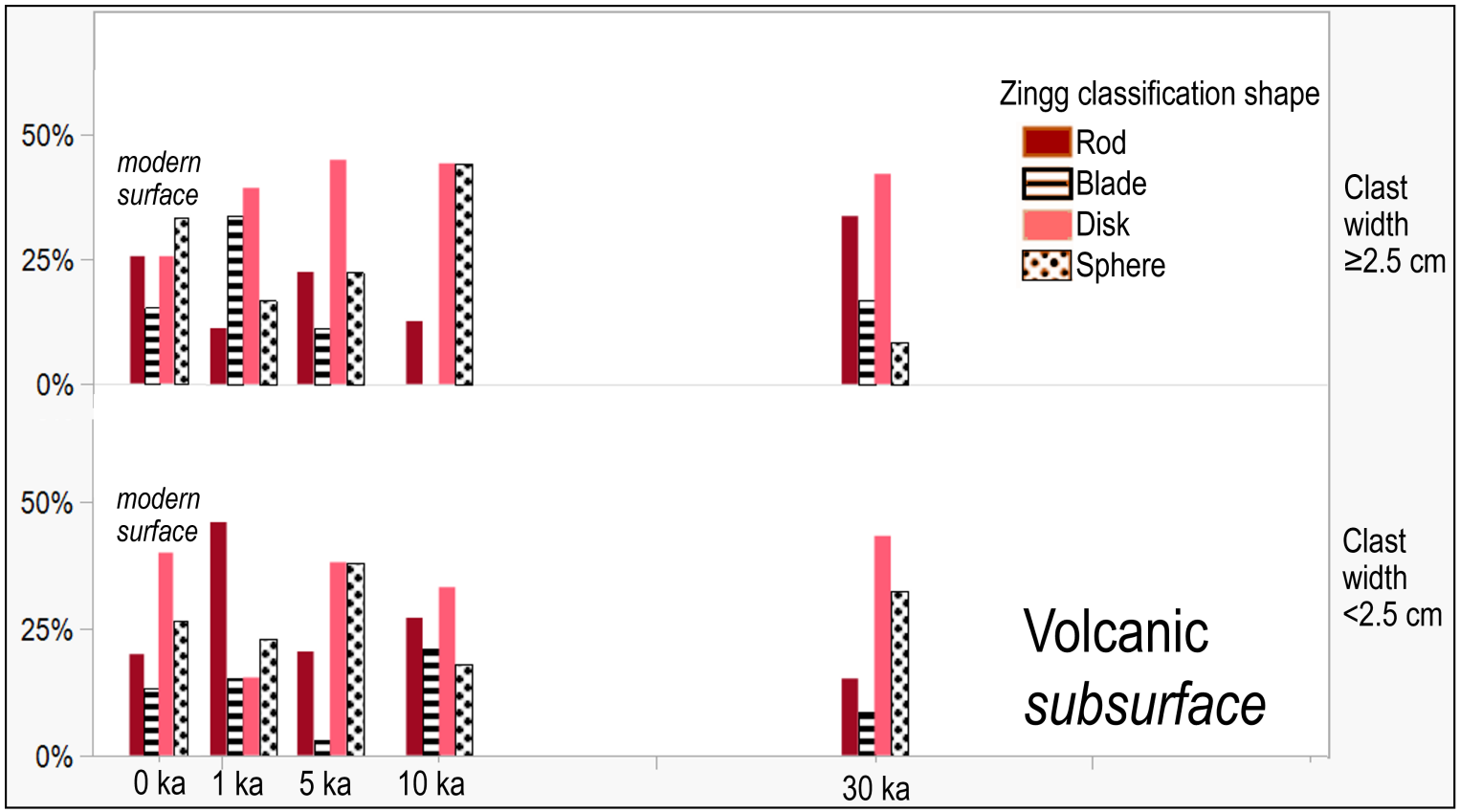

Figure 6.22: Zingg shape classification of subsurface volcanic clasts at Providence Mountains. The upper plot shows larger clasts, and the lower plot shows smaller clasts. Note that the surfaces have been shifted horizontally to display all four shape per surface.

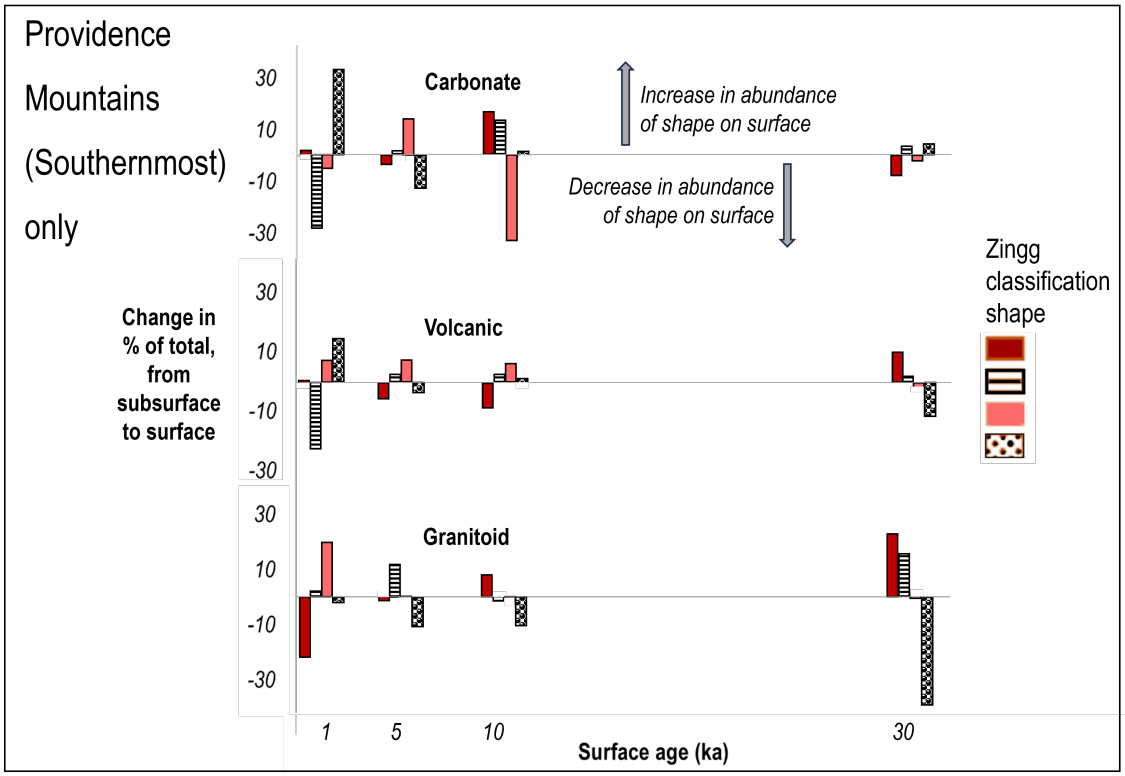

Figure 6.23: The change in clast shapes from subsurface to surface for various rock types at Providence Mountains, where a positive number represents that there are more of that shape on the surface than the subsurface, and a negative number represents that there are less of that shape on the surface. For example, there are about 30% more carbonate spheres on the 1 ka surface than there are in the subsurface.

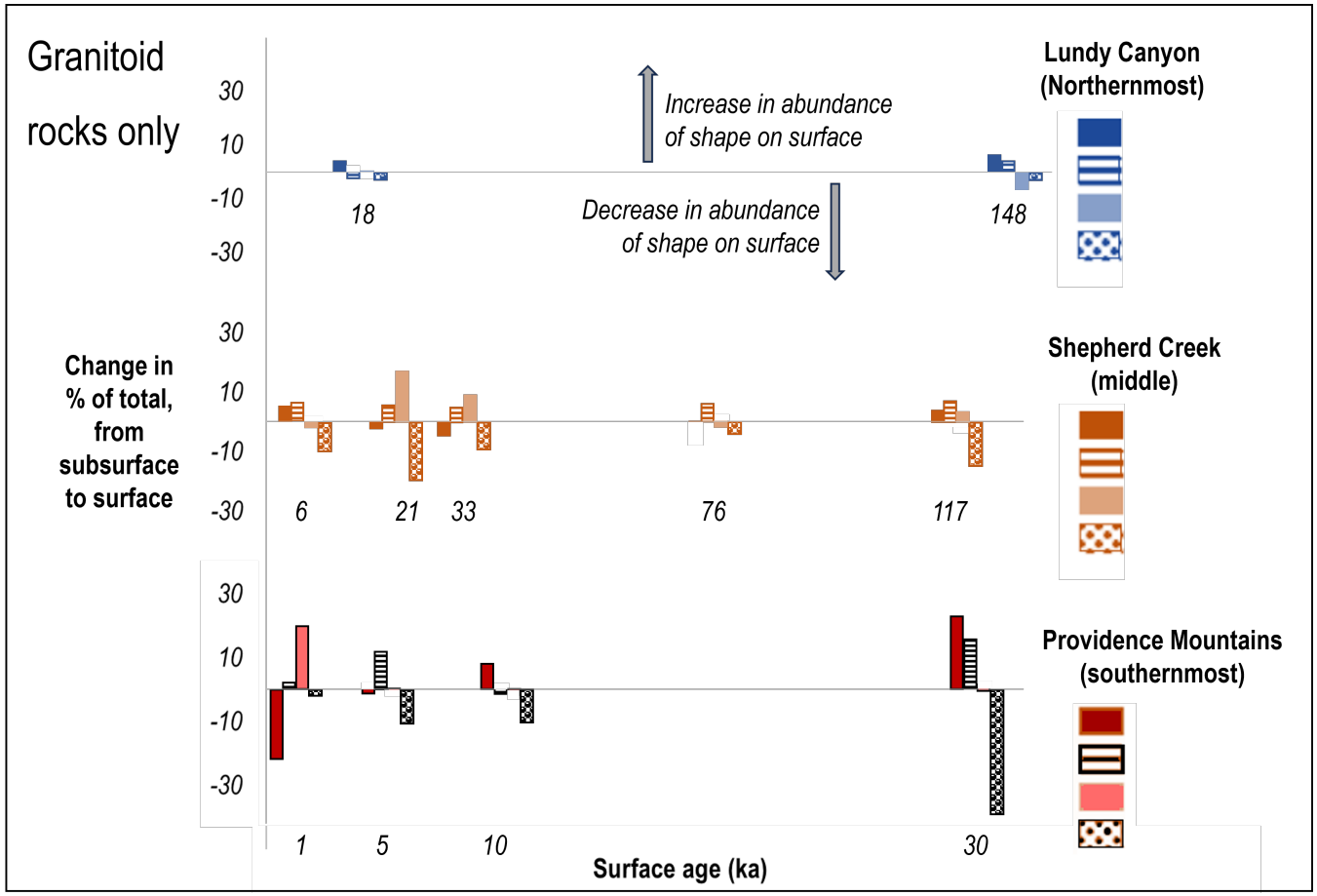

Figure 6.24: The change in clast shapes from subsurface to surface for granitoid rocks, where a positive number represents that there are more of that shape on the surface than the subsurface, and a negative number represents that there are less of that shape on the surface. For example, there are about 10% less spheres on the 6 ka surface at Shepherd Creek than there are in the subsurface.

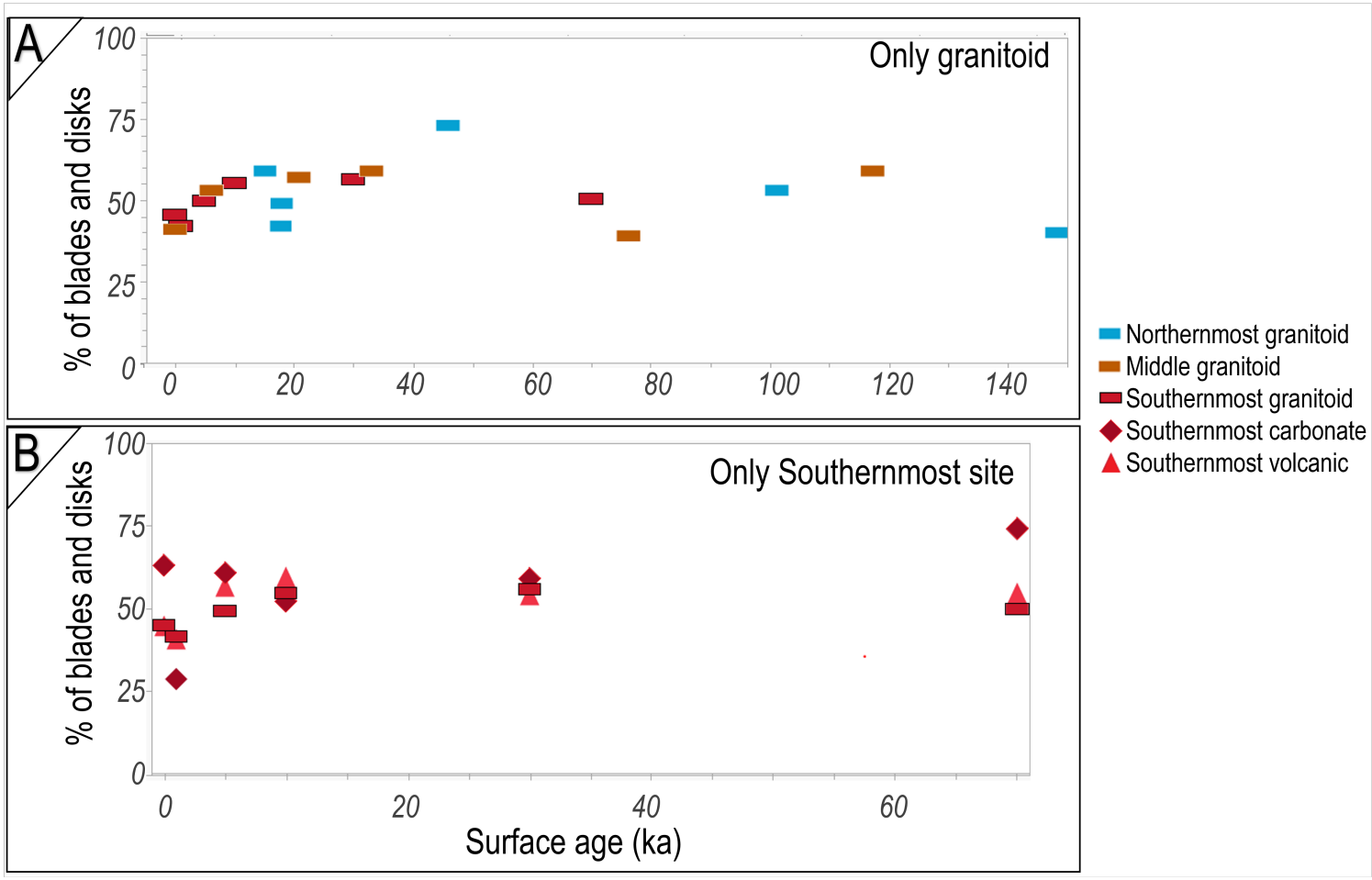

Figure 6.25: By adding together the percentage of all clasts that are blade or disk shape, here I display the proportion of clasts which are flat, or their short-axis length is $<2/3$ the length of the intermediate axis length. Granitoid rocks are shown in panel A and all Southernmost site rocks are shown in panel B.

CHAPTER 7: CONCLUSIONS AND FUTURE WORK

My Dissertation presents abundant evidence that boulders exposed to arid and semi-arid conditions on Earth's surface experience non-linear mechanical weathering, or rock cracking. Upon initial exposure and for the first 6 kyr, macroscale cracking occurs most rapidly. After this time, macroscale cracking begins to slow down [Ch. 2] as the rock compliance increases due to the new abundance of cracks throughout the rock body [Ch. 3]. The decreasing rate in macroscale cracking over time occurs for granitoid, volcanic, and carbonate rocks, across three Eastern California sites.

Unsurprisingly, the climatic conditions across sites impact the magnitude of cracking, with higher fracture intensity and fracture number density observed in the hot, arid site, and decreasing in the progressively cooler/semi-arid climates. However, the traditional approach to climate is not appropriate for rock cracking studies. In previous climosequence studies, the sites were chosen based on mean annual temperature and precipitation. I found in Ch. 4 that by assessing climatic differences due to extreme events instead of long-term means, our sequence of cool-wet climates to hot-dry climates does not capture the correct variables, nor does the sequence gradually change from one site to the next. Instead, the elastic properties of rocks and seasonality of weather events are important factors driving long-term intergranular rock cracking.

Expectations from laboratory behavior of which particular rock properties drive cracking [Ch. 5] do not show statistically significant or strong predictability, suggesting that the properties we think drive cracking may be interconnected with other properties that limit cracking. However, rock fracture metrics correlate with surface age, so cracking information is useful for relative age dating. Further research is needed in understanding the complex impacts of grain size and lithology on stress distribution and subsequent cracking.

The implications of this work are broad, relevant most immediately to geologists

working with clasts on Earth's surface. When attempting to understand "erodibility", rock properties should be used with caution, as shown by the inconsistent impacts of different field metrics on rock cracking behavior. Rock shape and size evolution modifies how sedimentological deposits are interpreted, and dictate how rivers flow, erode, and deposit sediment. Production of fresh rock surfaces through cracking dictates the rates of chemical reactions, thus constraining rates of nutrient availability and soil production, plus carbon sequestration. Currently, chemical weathering studies either assume linear cracking rates or ignore cracking completely.

The novel data presented in this Dissertation highlights the interdependencies of drivers of rock cracking in natural conditions, which result in nonlinear cracking rates. As with many underrepresented fields of research, there are even more questions about mechanical weathering that have arisen from this work. If we only have data points at 0 and 1 kyr, how quickly does cracking happen? Are individual cracks growing primarily as punctuated, short growth events, or are the bonds holding rocks together breaking daily? How do nonlinear cracking rates change our understanding of the carbon cycle? What else might we learn about the fundamental physics of fracture through studying natural materials?

Here, I suggest that cracking neither uniquely speeds up as cracks grow, nor slows down as compliance increases, but some balance of the two processes that evolve together. This behavior is likely expressed in bedrock, other climates, and various lithologies, but understanding how these processes balance each other and when one process dominates requires data from more sites. Future research must include detailed fracture analysis alongside elasticity measurements. This can include similar studies that apply my techniques to other rock types and sites, or modified studies that assess the same properties on bedrock for similar lithologies and sites. In other words, gradually adding more complexity to this dataset will show its broad applicability and continue to reveal the nuances and drivers of rock cracking.

The balance of cracking as two competing processes represents a paradigm shift in fracture mechanics of rocks. This new approach combines previous theories while offering a mechanism to explain material fatigue, the Kaiser effect, and the persistence of seemingly unstable rock bodies like cliffs and large boulders over hundreds of thousands of years or more. Beyond theory, these concepts can help explain tectonic behavior, rockfall hazards, and earthquake cycling. Engineering geologists can better predict the stability of the ground as well as their materials, depending on the exposure age of the rock. Further bedrock studies will allow surface process geoscientists to incorporate their knowledge into the subsurface, connecting our understanding of the surface to the lower Critical Zone, and into the realm of natural resources like groundwater, oil and gas, and geothermal energy.

As we transition to cleaner energy options, the world needs long-term solutions. Understanding the slow progression of cracking will help us store carbon, hydrogen, and nuclear waste in subsurface rocks in a more stable and predictable way. Now more than ever, this advancement in the understanding of the drivers and rates of rock mechanical weathering are critical to our development of a cleaner, safer future for the world.

REFERENCES

Adelsberger, Katherine A. and Smith, Jennifer R. Desert pavement development and landscape stability on the Eastern Libyan Plateau, Egypt. *Geomorphology*, 107(3):178–194, 2009. ISSN 0169-555X. doi: https://doi.org/10.1016/j.geomorph.2008.12.005.

Aldred, Jennifer, Eppes, Martha Cary, Aquino, Kimberly, Deal, Rebecca, Garbini, Jacob,. The influence of solar-induced thermal stresses on the mechanical weathering of rocks in humid mid-latitudes. *Earth Surface Processes and Landforms*, 41 (5):603–614, 2016. ISSN 0197-9337. doi: 10.1002/esp.3849.

Andričević, P., Sellwood, E. L., Freiesleben, T., Hidy, A. J., Kook, M., Eppes, M. C. and Jain, M. Dating fractures using luminescence. *Earth and Planetary Science Letters*, 624:118461, 2023.

Andričević, Pavao, Sellwood, Elaine L., Eppes, Martha-Cary, Kook, Myungho and Jain, Mayank. Passive atomic-scale optical sensors for mapping light flux in ultrasmall cavities. *Scientific Reports*, 13(1):5309, 2023.

Apuzzo, A., Frigeri, A., Salvini, F., Brossier, J., De Sanctis, M. C, Schmidt, G. W. and Ma MISS Team. Fractured Regions of Exomars 2022 Landing Site: Mapping of the Fractured Regions. In *53rd Lunar and Planetary Science Conference*, volume 2678, page 2115, 2022.

Ashby, M. F. and Sammis, C. G. The damage mechanics of brittle solids in compression. *Pure and Applied Geophysics*, 133:489–521, 1990.

Atkinson, B. K. Fracture toughness of Tennessee sandstone and Carrara marble using the double torsion testing method. In *International journal of rock mechanics and mining sciences & geomechanics abstracts*, volume 16, pages 49–53. Elsevier, 1979.

Atkinson, Barry Kean. Subcritical crack propagation in rocks: theory, experimental results and applications. *Journal of Structural Geology*, 4(1):41–56, 1982. ISSN 0191-8141. doi: https://doi.org/10.1016/0191-8141(82)90005-0.

Atkinson, Barry Kean. Subcritical crack growth in geological materials. *Journal of Geophysical Research: Solid Earth*, 89(B6):4077–4114, 1984. ISSN 2156-2202.

Atkinson, Barry Kean and Meredith, Philip George. Stress corrosion cracking of quartz: a note on the influence of chemical environment. *Tectonophysics*, 77(1-2): T1–T11, 1981. ISSN 0040-1951.

Atkinson, Barry Kean and Meredith, Philip George. The theory of subcritical crack growth with applications to minerals and rocks. *Fracture Mechanics of Rock*, 2: 111–166, 1987a.

Atkinson, Barry Kean and Meredith, Philip George. Experimental fracture mechanics data for rocks and minerals. *Fracture Mechanics of Rock*, page 477, 1987b. ISSN 0123822386.

Bacon, Steven N., Jayko, Angela S., Owen, Lewis A., Lindvall, Scott C., Rhodes, Edward J., Schumer, Rina A. and Decker, David L. A 50,000-year record of lake-level variations and overflow from Owens Lake, eastern California, USA. *Quaternary Science Reviews*, 238:106312, 2020. ISSN 0277-3791. doi: https://doi.org/10.1016/j.quascirev.2020.106312.

Baker, Victor R. Catastrophism and uniformitarianism: logical roots and current relevance in geology. *Geological Society, London, Special Publications*, 143(1):171–182, 1998.

Balco, Greg, Stone, John O., Lifton, Nathaniel A. and Dunai, Tibor J. A complete and easily accessible means of calculating surface exposure ages or erosion rates

from 10Be and 26Al measurements. *Quaternary Geochronology*, 3(3):174–195, 2008. ISSN 1871-1014. doi: https://doi.org/10.1016/j.quageo.2007.12.001.

Ballantyne, Colin K, Sandeman, Graeme F., Stone, John O. and Wilson, Peter. Rock-slope failure following Late Pleistocene deglaciation on tectonically stable mountainous terrain. *Quaternary Science Reviews*, 86:144–157, 2014. ISSN 0277-3791.

Bateman, P. C. Pre-Tertiary bedrock geologic map of the Mariposa 1 degree by 2 degrees Quadrangle, Sierra Nevada, California; Nevada. Report, 1992.

Bažant, Zdenek P., Le, Jia-Liang and Salviato, Marco. *Quasibrittle fracture mechanics and size effect: A first course*. Oxford University Press, 2021. ISBN 0192661388.

Baynes, J. and Dearman, W. The microfabric of a chemically weathered granite. *Bulletin of Engineering Geology & the Environment*, 18(1), 1978.

Beck, Hylke E., Zimmermann, Niklaus E., McVicar, Tim R., Vergopolan, Noemi, Berg, Alexis and Wood, Eric F. Present and future Köppen-Geiger climate classification maps at 1-km resolution. *Scientific Data*, 5(1):180214, 2018. ISSN 2052-4463. doi: 10.1038/sdata.2018.214.

Becker, K. and Gronz, O. and Wirtz, S. and Seeger, Manuel and Brings, C. and Iserloh, T. and Casper, M. C. and Ries, Johannes B. Characterization of complex pebble movement patterns in channel flow–a laboratory study. *Cuadernos de investigación geográfica: Geographical Research Letters*, 41:63–85, 2015.

Bellprat, Omar, Guemas, Virginie, Doblas-Reyes, Francisco and Donat, Markus G. Towards reliable extreme weather and climate event attribution. *Nature communications*, 10(1):1732, 2019.

Berberich, Samantha. *A Chronosequence of Cracking in Mill Creek, California*. M.S. Thesis, The University of North Carolina at Charlotte, 2020.

Birkeland, Peter W. *Soils and geomorphology.* Oxford University Press, 3 edition, 1999. ISBN 0195033981.

Blackwelder, Eliot. Exfoliation as a phase of rock weathering. *The Journal of Geology*, 33(8):793–806, 1925.

Blisniuk, Kimberly Diem Chi. *Testing for Quaternary fault slip rate variability on the southern San Jacinto fault zone, California.* Ph.D., University of California, Davis, 2011.

Bluck, Brian J. Structure of gravel beaches and their relationship to tidal range. *Sedimentology*, 58(4):994–1006, 2011. doi: https://doi.org/10.1111/j.1365-3091.2010.01192.x.

Bonnet, Eric, Bour, Olivier, Odling, Noelle E., Davy, Philippe, Main, Ian, Cowie, Patience and Berkowitz, Brian. Scaling of fracture systems in geological media. *Reviews of Geophysics*, 39(3):347–383, 2001.

Boulton, G. S. Boulder shapes and grain-size distributions of debris as indicators of transport paths through a glacier and till genesis. *Sedimentology*, 25(6):773–799, 1978.

Brantley, S. L., Shaughnessy, Andrew, Lebedeva, Marina I. and Balashov, Victor N. How temperature-dependent silicate weathering acts as Earth's geological thermostat. *Science*, 379(6630):382–389, 2023. doi: doi:10.1126/science.add2922.

Brantley, Susan L., Buss, H. and Lebedeva, M., Fletcher, R. C. and Ma, Lin. Investigating the complex interface where bedrock transforms to regolith. *Applied Geochemistry*, 26:S12–S15, 2011. ISSN 0883-2927.

Brantley, Susan L., Evans, Brian, Hickman, Stephen H. and Crerar, David A. Healing of microcracks in quartz: Implications for fluid flow. *Geology*, 18(2):136–139, 1990. ISSN 0091-7613. doi: 10.1130/0091-7613(1990)018<0136:HOMIQI>2.3.CO;2.

Brantut, Nicolas and Baud, Patrick and Heap, M. J. and Meredith, P. G. Micromechanics of brittle creep in rocks. *Journal of Geophysical Research: Solid Earth*, 117 (B8), 2012.

Brice, Tim and Hall, Todd. Vapor Pressure Calculator. *https* : *//www.weather.gov/epz/wxcalc*$_v$*aporpressure*, 2024. Accessed 2024-01-13.

Bruce, Robert Russell and Stelly, Matthias and others. Field soil water regime. 1973.

Burford, E. P. and Fomina, M. and Gadd, G. M. Fungal involvement in bioweathering and biotransformation of rocks and minerals. *Mineralogical Magazine*, 67(6):1127–1155, 2003. ISSN 1471-8022.

Buss, Heather L., Sak, Peter B., Webb, Samuel M. and Brantley, Susan L. Weathering of the Rio Blanco quartz diorite, Luquillo Mountains, Puerto Rico: Coupling oxidation, dissolution, and fracturing. *Geochimica et Cosmochimica Acta*, 72(18): 4488–4507, 2008. ISSN 0016-7037. doi: https://doi.org/10.1016/j.gca.2008.06.020.

Byerlee, James D. Frictional characteristics of granite under high confining pressure. *Journal of Geophysical Research*, 72(14):3639–3648, 1967.

Caballero, Lizeth, Sarocchi, Damiano, Borselli, Lorenzo and Cárdenas, Angel I. Particle interaction inside debris flows: Evidence through experimental data and quantitative clast shape analysis. *Journal of Volcanology and Geothermal Research*, 231-232:12–23, 2012. ISSN 0377-0273. doi: https://doi.org/10.1016/j.jvolgeores.2012.04.007.

Canady, Wyatt. A method for full-range Young's modulus correction. In *SPE Unconventional Resources Conference/Gas Technology Symposium*, pages SPE–143604. SPE, 2011.

Caricchi, Luca, Townsend, Meredith, Rivalta, Eleonora and Namiki, Atsuko. The build-up and triggers of volcanic eruptions. *Nature Reviews Earth 'I&' Environment*, 2(7):458–476, June 2021. ISSN 2662-138X. doi: 10.1038/s43017-021-00174-8.

Carter, N. E. A. and Viles, H. A. Bioprotection explored: the story of a little known earth surface process. *Geomorphology*, 67(3-4):273–281, 2005.

Chandler, Michael R., Mecklenburgh, Julian, Rutter, Ernest and Lee, Peter. Fluid injection experiments in shale at elevated confining pressures: Determination of flaw sizes from mechanical experiments. *Journal of Geophysical Research: Solid Earth*, 124(6):5500–5520, 2019.

Chandler, Michael R., Meredith, Philip G., Brantut, Nicolas and Crawford, Brian R. Fracture toughness anisotropy in shale. *Journal of Geophysical Research: Solid Earth*, 121(3):1706–1729, 2016.

Chandler, Mike, Meredith, Philip, Brantut, Nicolas and Crawford, Brian. Effect of temperature on the fracture toughness of anisotropic shale and other rocks. *Geological Society, London, Special Publications*, 454:SP454.6, 2017. doi: 10.1144/SP454.6.

Charles, R. J. Static fatigue of glass. I. *Journal of Applied Physics*, 29(11):1549–1553, 1958. ISSN 0021-8979.

Chen, Xiaofeng, Eichhubl, Peter, Olson, Jon E. and Dewers, Thomas A. Salinity, pH, and temperature controls on fracture mechanical properties of three shales and their implications for fracture growth in chemically reactive fluid environments. *Geomechanics for Energy and the Environment*, 21:100140, 2020. ISSN 2352-3808. doi: https://doi.org/10.1016/j.gete.2019.100140.

Ciccotti, Matteo, Negri, N., Sassi, L., Gonzato, Guido and Mulargia, Francesco. Elastic and fracture parameters of Etna, Stromboli, and Vulcano lava rocks. *Journal of volcanology and geothermal research*, 98(1-4):209–217, 2000.

Collins, Brian D. and Sitar, Nicholas. Processes of coastal bluff erosion in weakly lithified sands, Pacifica, California, USA. *Geomorphology*, 97(3-4):483–501, 2008.

Collins, Brian D. and Stock, Greg M. Rockfall triggering by cyclic thermal stressing of exfoliation fractures. *Nature Geoscience*, 9(5):395–400, 2016. ISSN 1752-0908.

Collins, Brian D., Stock, Greg M., Eppes, Martha-Cary, Lewis, Scott W., Corbett, Skye C. and Smith, Joel B. Thermal influences on spontaneous rock dome exfoliation. *Nature Communications*, 9(1):762, 2018. ISSN 2041-1723. doi: 10.1038/s41467-017-02728-1.

Cowie, S. and Walton, G. The effect of mineralogical parameters on the mechanical properties of granitic rocks. *Engineering Geology*, 240:204–225, 2018.

Cox, Rónadh, Lopes, Ward A. and Jahn, Kalle L. Quantitative roundness analysis of coastal boulder deposits. *Marine Geology*, 396:114–141, 2018. ISSN 0025-3227. doi: https://doi.org/10.1016/j.margeo.2017.03.003.

Dai, F., Xia, K., Zuo, J. P., Zhang, R. and Xu, N. W. Static and Dynamic Flexural Strength Anisotropy of Barre Granite. *Rock Mechanics and Rock Engineering*, 46 (6):1589–602, 2013. ISSN 0723-2632. doi: 10.1007/s00603-013-0390-y.

Damjanac, Branko and Fairhurst, Charles. Evidence for a long-term strength threshold in crystalline rock. *Rock Mechanics and Rock Engineering*, 43:513–531, 2010.

Daoud, Ali, Browning, John, Meredith, Philip G. and Mitchell, Thomas M. Microstructural controls on thermal crack damage and the presence of a temperature-

memory effect during cyclic thermal stressing of rocks. *Geophysical Research Letters*, 47(19):e2020GL088693, 2020.

D'Arcy, Mitch, Roda-Boluda, Duna C. and Whittaker, Alexander C. Glacial-interglacial climate changes recorded by debris flow fan deposits, Owens Valley, California. *Quaternary Science Reviews*, 169:288–311, 2017. ISSN 0277-3791. doi: https://doi.org/10.1016/j.quascirev.2017.06.002.

D'Arcy, Mitch. Roda Boluda, Duna C.. Whittaker, Alexander C. and Carpineti, Alfredo. Dating alluvial fan surfaces in Owens Valley, California, using weathering fractures in boulders. *Earth Surface Processes and Landforms*, 40(4):487–501, 2015. ISSN 0197-9337.

de Vilder, S. J. and Brain, M. J. and Rosser, N. J. Controls on the geotechnical response of sedimentary rocks to weathering. *Earth Surface Processes and Landforms*, 44(10):1910–1929, 2019. ISSN 0197-9337. doi: https://doi.org/10.1002/esp.4619.

DeGraff, Jerome, Wagner, David L., Gallegos, Alan J., DeRose, Margie, Shannon, Casey and Ellsworth, Todd. The remarkable occurrence of large rainfall-induced debris flows at two different locations on July 12, 2008, Southern Sierra Nevada, CA, USA. *Landslides*, 8(3):343–353, 2011.

Delbo, Marco, Libourel, Guy, Wilkerson, Justin, Murdoch, Naomi, Michel, Patrick, Ramesh, K. T., Ganino, Clément, Verati, Chrystele and Marchi, Simone. Thermal fatigue as the origin of regolith on small asteroids. *Nature*, 508(7495):233–236, 2014. ISSN 1476-4687.

Delbo, Marco, Walsh, Kevin J., Matonti, Christophe, Wilkerson, Justin, Pajola, Maurizio, Al Asad, Manar M., Avdellidou, Chrysa, Ballouz, Ronald-Louis, Bennett, Carina A., Connolly Jr., Harold C. and others. Alignment of fractures on Bennu's

boulders indicative of rapid asteroid surface evolution. *Nature Geoscience*, 15(6): 453–457, 2022.

Delonca, A., Gunzburger, Y. and Verdel, T. Statistical correlation between meteorological and rockfall databases. *Natural Hazards and Earth System Sciences*, 14(8): 1953–1964, 2014. doi: 10.5194/nhess-14-1953-2014.

Dexing, Li, Enyuan, Wang, Xiangguo, Kong, Haishan, Jia, Dongming, Wang and Muhammad, Ali. Damage precursor of construction rocks under uniaxial cyclic loading tests analyzed by acoustic emission. *Construction and Building Materials*, 206:169–178, 2019. ISSN 0950-0618. doi: https://doi.org/10.1016/j.conbuildmat.2019.02.074.

DiBiase, Roman A., Rossi, Matthew W. and Neely, Alexander B. Fracture density and grain size controls on the relief structure of bedrock landscapes. *Geology*, 46 (5):399–402, 2018. ISSN 0091-7613.

Dohrenwend, J. C. Surficial geologic map of the Walker Lake 1 degree by 2 degrees Quadrangle, Nevada-California. Report, 1982.

Drake, Lon D. Rock texture: an important factor for clast shape studies. *Journal of Sedimentary Research*, 40(4):1356–1361, 1970. ISSN 1527-1404. doi: 10.1306/74D721B2-2B21-11D7-8648000102C1865D.

Dühnforth, Miriam, Anderson, Robert S., Ward, Dylan and Stock, Greg M. Bedrock fracture control of glacial erosion processes and rates. *Geology*, 38(5):423–426, 2010. ISSN 0091-7613. doi: 10.1130/G30576.1.

Mihai Dumitriu, Dan, Niculiţă and Daniel Condorachi. Downstream Variation in the Pebble Morphometry of the Trotuş River, Eastern Carpathians (Romania).

East, Amy E. and Sankey, Joel B. Geomorphic and sedimentary effects of modern climate change: current and anticipated future conditions in the western United States. *Reviews of Geophysics*, 58(4):e2019RG000692, 2020. ISSN 8755-1209.

Ehlmann, Bethany L., Viles, Heather A. and Bourke, Mary C. Quantitative morphologic analysis of boulder shape and surface texture to infer environmental history: A case study of rock breakdown at the Ephrata Fan, Channeled Scabland, Washington. *Journal of Geophysical Research: Earth Surface*, 113(F2), 2008.

Eppes, M. C., Magi, B., Scheff, J., Warren, K., Ching, S. and Feng, T. Warmer, wetter climates accelerate mechanical weathering in field data, independent of stress-loading. *Geophysical Research Letters*, n/a(n/a):e2020GL089062, 2020. ISSN 0094-8276. doi: https://doi.org/10.1029/2020GL089062.

Eppes, Martha Cary, Aldred, Jennifer, Berberich, Samantha, Dahlquist, Maxwell P., Evans, Sarah G., Keanini, Russell, Moser, Faye, Morovati, Mehdi, Porson, Steven and Rasmussen, Monica. Standardized field methods for fracture-focused surface processes research. *Earth Surface Dynamics Discussions*, pages 1–41, 2022.

Eppes, Martha Cary and Griffing, David. Granular disintegration of marble in nature: A thermal-mechanical origin for a grus and corestone landscape. *Geomorphology*, 117(1-2):170–180, 2010. ISSN 0169-555X.

Eppes, Martha-Cary and Keanini, Russell. Mechanical weathering and rock erosion by climate-dependent subcritical cracking. *Reviews of Geophysics*, 55(2):470–508, 2017. ISSN 87551209. doi: 10.1002/2017rg000557.

Eppes, Martha Cary and McFadden, Leslie. The influence of bedrock weathering on the response of drainage basins and associated alluvial fans to Holocene climates, San Bernardino Mountains, California, USA. *The Holocene*, 18(6):895–905, 2008.

Eppes, Martha Cary, Magi, Brian, Hallet, Bernard, Delmelle, Eric, Mackenzie-Helnwein, Peter, Warren, Kimberly and Swami, Suraj. Deciphering the role of solar-induced thermal stresses in rock weathering. *Geological Society of America Bulletin*, 128(9-10):1315–1338, 2016. ISSN 0016-7606 1943-2674. doi: 10.1130/b31422.1.

Eppes, Martha Cary, McFadden, Leslie D., Wegmann, Karl W. and Scuderi, Louis A. Cracks in desert pavement rocks: Further insights into mechanical weathering by directional insolation. *Geomorphology*, 123(1-2):97–108, 2010. ISSN 0169-555X.

Eppes, Martha-Cary Missy. 3.03 Mechanical Weathering: A Conceptual Overview. *Treatise on Geomorphology*, 2022.

Eppes, Martha-Cary, Willis, Andrew, Molaro, Jamie, Abernathy, Stephen and Zhou, Beibei. Cracks in Martian boulders exhibit preferred orientations that point to solar-induced thermal stress. *Nature Communications*, 6(1):6712, 2015. ISSN 2041-1723. doi: 10.1038/ncomms7712.

Espinosa-Marzal, Rosa M., Hamilton, Andrea, McNall, Megan, Whitaker, Kathryn and Scherer, George W. The chemomechanics of crystallization during rewetting of limestone impregnated with sodium sulfate. *Journal of Materials Research*, 26 (12):1472–1481, 2011. ISSN 0884-2914. doi: 10.1557/jmr.2011.137.

Fairbairn, H. W. *A Cooperative Investigation of Precision and Accuracy in Chemical, Spectrochemical and Modal Analysis of Silicate Rocks*. U.S. Government Printing Office, 1951. URL `https://books.google.com/books?id=KOLmOR-QYLcC`.

Felton, E. Anne. Sedimentology of rocky shorelines: 1. A review of the problem, with analytical methods, and insights gained from the Hulopoe Gravel and the modern rocky shoreline of Lanai, Hawaii. *Sedimentary Geology*, 152(3-4):221–245, 2002.

Fink, David, McKelvey, Barrie, Hambrey, Michael J., Fabel, Derek and Brown, Roderick. Pleistocene deglaciation chronology of the Amery Oasis and

Radok Lake, northern Prince Charles Mountains, Antarctica. *Earth and Planetary Science Letters*, 243(1):229–243, 2006. ISSN 0012-821X. doi: https://doi.org/10.1016/j.epsl.2005.12.006.

Fiorucci, Matteo, Marmoni, Gian Marco, Martino, Salvatore and Mazzanti, Paolo. Thermal response of jointed rock masses inferred from infrared thermographic surveying (Acuto test-site, Italy). *Sensors*, 18(7):2221, 2018.

Flandes, Nicol E., Villalobos, Felipe A. and King, Robert. The effect of weathering on the variation of geotechnical properties of a granitic rock from Chile. *Quarterly Journal of Engineering Geology and Hydrogeology*, pages qjegh2023–022, 2023. ISSN 1470-9236. doi: 10.1144/qjegh2023-022.

Flatt, Robert J. Salt damage in porous materials: how high supersaturations are generated. *Journal of Crystal Growth*, 242(3):435–454, 2002. ISSN 0022-0248. doi: https://doi.org/10.1016/S0022-0248(02)01429-X.

Fookes, P. G., Gourley, C. S. and Ohikere, C. Rock weathering in engineering time. *Quarterly Journal of Engineering Geology and Hydrogeology*, 21(1):33–57, 1988. ISSN 1470-9236. doi: 10.1144/GSL.QJEG.1988.021.01.03.

Fort, Rafael, Alvarez de Buergo, Monica and Perez-Monserrat, Elena M. Non-destructive testing for the assessment of granite decay in heritage structures compared to quarry stone. *International Journal of Rock Mechanics and Mining Sciences*, 61:296–305, 2013. ISSN 1365-1609. doi: https://doi.org/10.1016/j.ijrmms.2012.12.048.

Freire-Lista, David Martín, Fort, Rafael and Varas-Muriel, María José. Freeze-thaw fracturing in building granites. *Cold Regions Science and Technology*, 113:40–51, 2015. ISSN 0165-232X.

Glade, Rachel C., Shobe, Charles M., Anderson, Robert S. and Tucker, Gregory E. Canyon shape and erosion dynamics governed by channel-hillslope feedbacks. *Geology*, 47(7):650–654, 05 2019. ISSN 0091-7613. doi: 10.1130/G46219.1.

Goodfellow, Bradley W., Hilley, George E., Webb, Samuel M., Sklar, Leonard S., Moon, Seulgi and Olson, Christopher A. The chemical, mechanical, and hydrological evolution of weathering granitoid. *Journal of Geophysical Research: Earth Surface*, 121(8):1410–1435, 2016. ISSN 2169-9003. doi: https://doi.org/10.1002/2016JF003822.

Goodman, Richard E. *Introduction to rock mechanics*, volume 2. Wiley New York, 1989.

Griffith, Alan Arnold. VI. The phenomena of rupture and flow in solids. *Philosophical transactions of the royal society of london. Series A, containing papers of a mathematical or physical character*, 221(582-593):163–198, 1921. ISSN 0264-3952.

Gudmundsson, Agust and Brenner, Sonja L. How hydrofractures become arrested. *Terra Nova*, 13(6):456–462, 2001. ISSN 0954-4879. doi: https://doi.org/10.1046/j.1365-3121.2001.00380.x.

Gunzburger, Yann and Merrien-Soukatchoff, Véronique. Near-surface temperatures and heat balance of bare outcrops exposed to solar radiation. *Earth Surface Processes and Landforms*, 36(12):1577–1589, 2011. ISSN 0197-9337. doi: https://doi.org/10.1002/esp.2167.

Harnois, Luc. The CIW index: A new chemical index of weathering. *Sedimentary Geology*, 55(3):319–322, 1988. ISSN 0037-0738. doi: https://doi.org/10.1016/0037-0738(88)90137-6.

Healy, David, Rizzo, Roberto E., Cornwell, David G., Farrell, Natalie J. C., Watkins, Hannah, Timms, Nick E., Gomez-Rivas, Enrique and Smith, Michael. FracPaQ:

A MATLAB^{TM} toolbox for the quantification of fracture patterns. *Journal of Structural Geology*, 95:1–16, 2017.

Heap, M. J., Vinciguerra, S. and Meredith, P. G. The evolution of elastic moduli with increasing crack damage during cyclic stressing of a basalt from Mt. Etna volcano. *Tectonophysics*, 471(1):153–160, 2009. ISSN 0040-1951. doi: https://doi.org/10.1016/j.tecto.2008.10.004.

Heimsath, Arjun M. and DiBiase, Roman A. and Whipple, Kelin X. Soil production limits and the transition to bedrock-dominated landscapes. *Nature Geoscience*, 5 (3):210–214, 2012.

Heimsath, Arjun M., Dietrich, William E., Nishiizumi, Kunihiko and Finkel, Robert C. The soil production function and landscape equilibrium. *Nature*, 388(6640): 358–361, 1997. ISSN 1476-4687.

Hillis, Richard R. Pore pressure/stress coupling and its implications for rock failure. *Geological Society, London, Special Publications*, 216(1):359–368, 2003.

Hirschwald, Julius. *Die Prüfung der natürlichen Bausteine auf ihre Wetterfeständigkeit*. W. Ernst and Sohn, 1908.

Hoek, E. and Martin, C. D. Fracture initiation and propagation in intact rock - a review. *Journal of Rock Mechanics and Geotechnical Engineering*, 6(4):287–300, 2014. ISSN 1674-7755.

Holbrook, W. Steven, Marcon, Virginia, Bacon, Allan R., Brantley, Susan L., Carr, Bradley J., Flinchum, Brady A., Richter, Daniel D. and Riebe, Clifford S. Links between physical and chemical weathering inferred from a 65-m-deep borehole through Earth's critical zone. *Scientific Reports*, 9(1):4495, 2019. ISSN 2045-2322. doi: 10.1038/s41598-019-40819-9.

Hooker, J. N., Laubach, S. E. and Marrett, R. A universal power-law scaling exponent for fracture apertures in sandstones. *GSA Bulletin*, 126(9-10):1340–1362, 2014. ISSN 0016-7606. doi: 10.1130/B30945.1.

Hoskin, Charles M. and Sundeen, Daniel A. Grain size of granite and derived grus, Enchanted Rock pluton, Texas. *Sedimentary geology*, 42(1-2):25–40, 1985.

Howard, Jeffrey L. An evaluation of shape indices as palaeoenvironmental indicators using quartzite and metavolcanic clasts in Upper Cretaceous to Palaeogene beach, river and submarine fan conglomerates. *Sedimentology*, 39(3):471–486, 1992. doi: https://doi.org/10.1111/j.1365-3091.1992.tb02128.x.

Hutton, James. *Theory of the Earth: With proofs and illustrations*, volume 111. Geological society, 1899.

Irwin, George R. Analysis of stresses and strains near the end of a crack traversing a plate. 1957.

Janio de Castro Lima, José and Paraguassú, Antenor Braga. Linear thermal expansion of granitic rock: influence of apparent porosity, grain size and quartz content. *Bulletin of engineering geology and the environment*, 63(3):215–220, 2004. ISSN 1435-9529. doi: 10.1007/s10064-004-0233-x.

Jenny, Hans. Great soil groups in the equatorial regions of Colombia, South America. *Soil Science*, 66(1):5–28, 1948.

Jimerson, Cole Robert. *Environmental Influences on Tree-driven Karst Bedrock Physical Weathering*. University of Arkansas, 2020.

Johnstone, Samuel A. and Hudson, Adam M. and Nicovich, Sylvia and Ruleman, Chester A. and Sare, Robert M. and Thompson, Ren A. Establishing chronologies for alluvial-fan sequences with analysis of high-resolution topographic data: San

Luis Valley, Colorado, USA. *Geosphere*, 14(6):2487–2504, 2018. ISSN 1553-040X. doi: 10.1130/GES01680.1. URL https://doi.org/10.1130/GES01680.1.

Jones, E.C. Vann, Rosser, N. J., Brain, M. J. and Petley, D. N. Quantifying the environmental controls on erosion of a hard rock cliff. *Marine Geology*, 363:230–242, 2015.

Kachanov, Mark L. Microcrack model of rock inelasticity part III: Time-dependent growth of microcracks. *Mechanics of Materials*, 1(2):123–129, 1982.

Kang, Fangchao, Li, Yingchun and Tang, Chun'an. Grain size heterogeneity controls strengthening to weakening of granite over high-temperature treatment. *International Journal of Rock Mechanics and Mining Sciences*, 145:104848, 2021.

Kang, Jian-Qi, Zhu, Jian-Bo and Zhao, Jian. A review of mechanisms of induced earthquakes: from a view of rock mechanics. *Geomechanics and Geophysics for Geo-Energy and Geo-Resources*, 5(2):171–196, January 2019. ISSN 2363-8427. doi: 10.1007/s40948-018-00102-z.

Keith, W. J. and Seitz, J. F. Geologic map of the Hoover Wilderness and adjacent study area. *Mono and Tuolumne counties, California: US Geological Survey Map MF1101-A, scale*, 1(62,500), 1981.

Kelly, Meredith A., Lowell, Thomas V., Applegate, Patrick J., Phillips, Fred M., Schaefer, Joerg M., Smith, Colby A., Kim, Hanul, Leonard, Katherine C. and Hudson, Adam M. A locally calibrated, late glacial 10Be production rate from a low-latitude, high-altitude site in the Peruvian Andes. *Quaternary Geochronology*, 26(1):70–85, 2015. ISSN 1871-1014. doi: 10.1016/j.quageo.2013.10.007.

Julia Kelson and Ronald Amundson. Personal communication, 2023.

Klos, P. Zion, Goulden, Michael L., Riebe, Clifford S., Tague, Christina L., O'Geen, A. Toby, Flinchum, Brady A., Safeeq, Mohammad, Conklin, Martha H., Hart, Stephen C., Berhe, Asmeret Asefaw, Hartsough, Peter C., Holbrook, W. Steven and Bales, Roger C. Subsurface plant-accessible water in mountain ecosystems with a Mediterranean climate. *WIREs Water*, 5(3):e1277, 2018. doi: https://doi.org/10.1002/wat2.1277.

Ko, Tae Young and Lee, Sean Seungwon. Characteristics of Crack Growth in Rock-Like Materials under Monotonic and Cyclic Loading Conditions. *Applied Sciences*, 10(2):719, 2020. ISSN 2076-3417. URL `https://www.mdpi.com/2076-3417/10/2/719`.

Kohl, C. P. and Nishiizumi, Kunihiko. Chemical isolation of quartz for measurement of in-situ-produced cosmogenic nuclides. *Geochimica et Cosmochimica Acta*, 56(9): 3583–3587, 1992.

Wladimir Köppen. The thermal zones of the earth according to the duration of hot, moderate and cold periods and to the impact of heat on the organic world. *Meteorologische Zeitschrift*, 20(3):351–360, 06 2011. doi: 10.1127/0941?2948/2011/105.

Krumbein, William Christian and Sloss, Laurence Louis. Stratigraphy and sedimentation. Report, 1963.

Kumar, R., Kook, M., Murray, A. S. and Jain, M. Towards direct measurement of electrons in metastable states in K-feldspar: do infrared-photoluminescence and radioluminescence probe the same trap? *Radiation Measurements*, 120:7–13, 2018.

Lajtai, E. Z., Duncan, E. J. Scott and Carter, B. J. The effect of strain rate on rock strength. *Rock Mechanics and Rock Engineering*, 24(2):99–109, 1991. ISSN 1434-453X. doi: 10.1007/BF01032501.

Lamp, J. L., Marchant, D. R., Mackay, S. L. and Head, J. W. Thermal stress weathering and the spalling of Antarctic rocks. *Journal of Geophysical Research: Earth Surface*, 122(1):3–24, 2017. ISSN 2169-9003.

Laubach, Stephen E., Lander, R. H., Criscenti, Louise J., Anovitz, Lawrence M., Urai, J. L., Pollyea, R. M., Hooker, John N., Narr, Wayne, Evans, Mark A. and Kerisit, Sebastien N. The role of chemistry in fracture pattern development and opportunities to advance interpretations of geological materials. *Reviews of Geophysics*, 57 (3):1065–1111, 2019. ISSN 8755-1209.

Leith, Kerry, Moore, Jeffrey R., Amann, Florian and Loew, Simon. In situ stress control on microcrack generation and macroscopic extensional fracture in exhuming bedrock. *Journal of Geophysical Research: Solid Earth*, 119(1):594–615, 2014. ISSN 2169-9313. doi: https://doi.org/10.1002/2012JB009801.

Leith, Kerry, Perras, Matthew, Siren, Topias, Rantanen, Tuomas, Heinonen, Suvi and Loew, Simon. Dynamic fracture development in response to extreme summer temperatures: 27/7/2014, Långören Island, Finland. In *EGU General Assembly Conference Abstracts*, page 16387, 2017.

Li, Xinli, Fu, Suhua, Hu, Yaxian and Liu, Baoyuan. Effects of rock fragment coverage on soil erosion: Differ among rock fragment sizes? *Catena*, 214:106248, 2022.

Lindqvist, J. E., Åkesson, U. and Malaga, K. Microstructure and functional properties of rock materials. *Materials Characterization*, 58(11):1183–1188, 2007. ISSN 1044-5803. doi: https://doi.org/10.1016/j.matchar.2007.04.012.

Lu, Yinlong, Elsworth, Derek and Wang, Lianguo. A dual-scale approach to model time-dependent deformation, creep and fracturing of brittle rocks. *Computers and Geotechnics*, 60:61–76, 2014. ISSN 0266-352X.

Lukas, Sven, Benn, Douglas I., Boston, Clare M., Brook, Martin, Coray, Sandro, Evans, David J.A., Graf, Andreas, Kellerer-Pirklbauer, Andreas, Kirkbride, Martin P., Krabbendam, Maarten, Lovell, Harold, Machiedo, Martin, Mills, Stephanie C., Nye, Kate, Reinardy, Benedict T.I., Ross, Fionna H. and Signer, Michael. Clast shape analysis and clast transport paths in glacial environments: A critical review of methods and the role of lithology. *Earth-Science Reviews*, 121:96–116, 2013. ISSN 0012-8252. doi: https://doi.org/10.1016/j.earscirev.2013.02.005.

Lyakhovsky, Vladimir, Reches, Ze'ev, Weinberger, Ram and Scott, Thurman E. Non-linear elastic behaviour of damaged rocks. *Geophysical Journal International*, 130 (1):157–166, 1997. ISSN 1365-246X.

Madoff, Risa D. and Putkonen, Jaakko. Climate and hillslope degradation vary in concert; 85 ka to present, eastern Sierra Nevada, CA, USA. *Geomorphology*, 266: 33–40, 2016. ISSN 0169-555X.

Marmoni, G. M. and Fiorucci, M. and Grechi, G. and Martino, S. Modelling of thermo-mechanical effects in a rock quarry wall induced by near-surface temperature fluctuations. *International Journal of Rock Mechanics and Mining Sciences*, 134:104440, 2020.

Marshall, Jill A. From ice to trees, surprising insights into past and present processes that sculpt our earth. *AGUFM*, 2018:EP44A–01, 2018.

Marshall, Jill A., Roering, Joshua J., Bartlein, Patrick J., Gavin, Daniel G., Granger, Darryl E., Rempel, Alan W., Praskievicz, Sarah J. and Hales, Tristram C. Frost for the trees: Did climate increase erosion in unglaciated landscapes during the late Pleistocene? *Science Advances*, 1(10):e1500715, 2015. ISSN 2375-2548.

Matsuoka, Norikazu and Murton, Julian. Frost weathering: recent advances and

future directions. *Permafrost and Periglacial Processes*, 19(2):195–210, 2008. ISSN 1045-6740.

Mavko, Gary, Mukerji, Tapan and Dvorkin, Jack. *The rock physics handBook*. Cambridge university press, 2020. ISBN 1108420265.

Mazurier, Arnaud, Sardini, Paul, Rossi, Ann M., Graham, Robert C., Hellmuth, Karl-Heinz, Parneix, Jean-Claude, Siitari-Kauppi, Marja, Voutilainen, Mikko and Caner, Laurent. Development of a fracture network in crystalline rocks during weathering: Study of Bishop Creek chronosequence using X-ray computed tomography and 14C-PMMA impregnation method. *GSA Bulletin*, 128(9-10):1423–1438, 2016. ISSN 0016-7606. doi: 10.1130/B31336.1.

McCarroll, Nicholas R. and Temme, Arnaud J. A. M. Transport and Weathering of Large Limestone Blocks on Hillslopes in Heterolithic Sedimentary Landscapes. *Journal of Geophysical Research: Earth Surface*, 127(9):e2022JF006609, 2022. doi: https://doi.org/10.1029/2022JF006609.

McCubbin, Francis M., Boyce, Jeremy W., Novák-Szabó, Tímea, Santos, Alison R., Tartèse, Romain, Muttik, Nele, Domokos, Gabor, Vazquez, Jorge, Keller, Lindsay P., Moser, Desmond E., Jerolmack, Douglas J., Shearer, Charles K., Steele, Andrew, Elardo, Stephen M., Rahman, Zia, Anand, Mahesh, Delhaye, Thomas and Agee, Carl B. Geologic history of Martian regolith breccia Northwest Africa 7034: Evidence for hydrothermal activity and lithologic diversity in the Martian crust. *Journal of Geophysical Research: Planets*, 121(10):2120–2149, 2016. doi: https://doi.org/10.1002/2016JE005143.

McDonald, Eric V., McFadden, Leslie D., Wells, Stephen G., Enzel, Y. and Lancaster, N. Regional response of alluvial fans to the Pleistocene-Holocene climatic

transition, Mojave Desert, California. *Special Papers-Geological Society of America*, pages 189–206, 2003. ISSN 0072-1077.

McFadden, L. D., Eppes, M. C., Gillespie, A. R. and Hallet, B. Physical weathering in arid landscapes due to diurnal variation in the direction of solar heating. *GSA Bulletin*, 117(1-2):161–173, 2005. ISSN 0016-7606. doi: 10.1130/B25508.1.

McFadden, Leslie D., McDonald, Eric V., Wells, Stephen G., Anderson, Kirk, Quade, Jay and Forman, Steven L. The vesicular layer and carbonate collars of desert soils and pavements: formation, age and relation to climate change. *Geomorphology*, 24(2):101–145, 1998. ISSN 0169-555X. doi: https://doi.org/10.1016/S0169-555X(97)00095-0.

McFadden, Leslie D., Ritter, John B. and Wells, Stephen G. Use of Multiparameter Relative-Age Methods for Age Estimation and Correlation of Alluvial Fan Surfaces on a Desert Piedmont, Eastern Mojave Desert, California. *Quaternary Research*, 32(3):276–290, 1989. doi: 10.1016/0033-5894(89)90094-X.

McGrath, Gavan S., Nie, Zhengyao, Dyskin, Arcady, Byrd, Tia, Jenner, Rowan, Holbeche, Georgina and Hinz, Christoph. In situ fragmentation and rock particle sorting on arid hills. *Journal of Geophysical Research: Earth Surface*, 118(1):17–28, 2013. ISSN 2169-9003. doi: https://doi.org/10.1029/2012JF002402.

Veronika Menéndez, Beatriz and Petráňová. Effect of mixed vs single brine composition on salt weathering in porous carbonate building stones for different environmental conditions. *Engineering Geology*, 210:124–139, 2016. ISSN 0013-7952. doi: https://doi.org/10.1016/j.enggeo.2016.06.011.

Meredith, P. G. and Atkinson, B. K. Fracture toughness and subcritical crack growth during high-temperature tensile deformation of Westerly granite and Black gabbro.

Physics of the Earth and Planetary Interiors, 39(1):33–51, 1985. ISSN 0031-9201. doi: https://doi.org/10.1016/0031-9201(85)90113-X.

Bartshe Miller. Personal communication, 2020.

Miller, David M., Schmidt, Kevin M., Mahan, Shannon A., McGeehin, John P., Owen, Lewis A., Barron, John A., Lehmkuhl, Frank and Löhrer, Rene. Holocene landscape response to seasonality of storms in the Mojave Desert. *Quaternary International*, 215(1-2):45–61, 2010.

Mitchell, T. M. and Faulkner, D. R. Experimental measurements of permeability evolution during triaxial compression of initially intact crystalline rocks and implications for fluid flow in fault zones. *Journal of Geophysical Research: Solid Earth*, 113(B11), 2008. ISSN 0148-0227.

Mohr, Otto. Welche Umstände bedingen die Elastizitätsgrenze und den Bruch eines Materials. *Zeitschrift des Vereins Deutscher Ingenieure*, 46(1524-1530):1572–1577, 1900.

Mohr, Otto. *Abhandlungen aus dem Gebiete der technischen Mechanik*. Ripol Classic, 1928.

Molaro, J. L., Byrne, S. and Le, J. L. Thermally induced stresses in boulders on airless body surfaces, and implications for rock breakdown. *Icarus*, 294:247–261, 2017. ISSN 0019-1035. doi: https://doi.org/10.1016/j.icarus.2017.03.008.

Molaro, J. L., Hergenrother, C. W., Chesley, S. R., Walsh, K. J., Hanna, R. D., Haberle, C. W., Schwartz, S. R., Ballouz, R. L., Bottke, W. F., Campins, H. J. and Lauretta, D. S. Thermal Fatigue as a Driving Mechanism for Activity on Asteroid Bennu. *Journal of Geophysical Research: Planets*, 125(8):e2019JE006325, 2020. ISSN 2169-9097. doi: https://doi.org/10.1029/2019JE006325.

Molaro, Jamie L., Byrne, Shane and Langer, Stephen A. Grain-scale thermoelastic stresses and spatiotemporal temperature gradients on airless bodies, implications for rock breakdown. *Journal of Geophysical Research: Planets*, 120(2):255–277, 2015. ISSN 2169-9097. doi: https://doi.org/10.1002/2014JE004729.

Molnar, Peter, Anderson, Robert S., Anderson, Suzanne Prestrud. Tectonics, fracturing of rock, and erosion. *Journal of Geophysical Research: Earth Surface*, 112 (F3), 2007. ISSN 0148-0227. doi: https://doi.org/10.1029/2005JF000433.

Montgomery, David R. Observations on the role of lithology in strath terrace formation and bedrock channel width. *American Journal of Science*, 304(5):454–476, 2004. ISSN 0002-9599.

Moon, S., Perron, J. T., Martel, S. J., Holbrook, W. S. and St. Clair, J. A model of three-dimensional topographic stresses with implications for bedrock fractures, surface processes, and landscape evolution. *Journal of Geophysical Research: Earth Surface*, 122(4):823–846, 2017. ISSN 2169-9003. doi: https://doi.org/10.1002/2016JF004155.

Moon, Seulgi, Perron, J. Taylor, Martel, Stephen J., Goodfellow, Bradley W., Mas Ivars, Diego, Hall, Adrian, Heyman, Jakob, Munier, Raymond, Näslund, Jens-Ove, Simeonov, Assen and Stroeven, Arjen P. Present-Day Stress Field Influences Bedrock Fracture Openness Deep Into the Subsurface. *Geophysical Research Letters*, 47(23):e2020GL090581, 2020. ISSN 0094-8276. doi: https://doi.org/10.1029/2020GL090581.

Moore, J. G. Geologic map of the Mount Whitney quadrangle. *Inyo and Tulare Counties, California: US Geological Survey Geologic Quadrangle Map GQ-1545, scale*, 1(62,500), 1981.

Moore, Jeffrey R., Gischig, Valentin, Katterbach, Maren and Loew, Simon. Air

circulation in deep fractures and the temperature field of an alpine rock slope. *Earth Surface Processes and Landforms*, 36(15):1985–1996, 2011.

Moore, Jeffrey R., Sanders, Johnny W., Dietrich, William E. and Glaser, Steven D. Influence of rock mass strength on the erosion rate of alpine cliffs. *Earth Surface Processes and Landforms*, 34(10):1339–1352, 2009.

Moore, Oliver W., Buss, Heather L. and Dosseto, Anthony. Incipient chemical weathering at bedrock fracture interfaces in a tropical critical zone system, Puerto Rico. *Geochimica et Cosmochimica Acta*, 252:61–87, 2019. ISSN 0016-7037. doi: https://doi.org/10.1016/j.gca.2019.02.028.

Mushkin, Amit, Sagy, Amir, Trabelci, Eran, Amit, Rivka and Porat, Naomi. Measuring the time and scale-dependency of subaerial rock weathering rates over geologic time scales with ground-based lidar. *Geology*, 42(12):1063–1066, 2014. ISSN 1943-2682 0091-7613. doi: 10.1130/g35866.1.

Nara, Y. Effect of anisotropy on the long-term strength of granite. *Rock Mechanics and Rock Engineering*, 48(3):959–69, 2015. ISSN 0723-2632. doi: 10.1007/s00603-014-0634-5.

Nara, Yoshitaka. Harui, Tomoki and Kashiwaya, Koki. Influence of calcium ions on subcritical crack growth in granite. *International Journal of Rock Mechanics and Mining Sciences*, 102:71–77, 2018. ISSN 1365-1609.

Nara, Yoshitaka. Kashiwaya, Koki. Nishida, Yuki and Ii, Toshinori. Influence of surrounding environment on subcritical crack growth in marble. *Tectonophysics*, 706:116–128, 2017. ISSN 0040-1951.

Nara, Yoshitaka, Morimoto, Kazuya, Yoneda, Tetsuro, Hiroyoshi, Naoki and Kaneko, Katsuhiko. Effects of humidity and temperature on subcritical crack growth in

sandstone. *International Journal of Solids and Structures*, 48(7):1130–1140, 2011. ISSN 0020-7683. doi: https://doi.org/10.1016/j.ijsolstr.2010.12.019.

Nara, Yoshitaka, Yamanaka, Hiroshi, Oe, Yuma and Kaneko, Katsuhiko. Influence of temperature and water on subcritical crack growth parameters and long-term strength for igneous rocks. *Geophysical Journal International*, 193(1):47–60, 2013. ISSN 1365-246X.

Naylor, Larissa A., Stephenson, Wayne J., Smith, Helen C. M., Way, Oliver, Mendelssohn, James and Cowley, Andrew. Geomorphological control on boulder transport and coastal erosion before, during and after an extreme extratropical cyclone. *Earth Surface Processes and Landforms*, 41(5):685–700, 2016. doi: https://doi.org/10.1002/esp.3900.

Neely, Alexander B. and DiBiase, Roman A. Drainage Area, Bedrock Fracture Spacing, and Weathering Controls on Landscape-Scale Patterns in Surface Sediment Grain Size. *Journal of Geophysical Research: Earth Surface*, 125(10):e2020JF005560, 2020. ISSN 2169-9003. doi: https://doi.org/10.1029/2020JF005560.

Nesbitt, H. W. and Young, G. M. Early Proterozoic climates and plate motions inferred from major element chemistry of lutites. *Nature*, 299(5885):715–717, 1982. ISSN 1476-4687. doi: 10.1038/299715a0.

Olsen, Lars. A method for determining total clast roundness in sediments. *Boreas*, 12(1):17–21, 1983. ISSN 0300-9483. doi: https://doi.org/10.1111/j.1502-3885.1983.tb00355.x.

Olsen, Telemak, Borella, Josh and Stahl, Timothy. Clast transport history influences Schmidt hammer rebound values. *Earth Surface Processes and Landforms*, 45(6): 1392–1400, 2020.

Olson, Jon E. Natural fracture pattern characterization using a mechanically-based model constrained by geologic data—Moving closer to a predictive tool. *International Journal of Rock Mechanics and Mining Sciences*, 34(3):171.e1–171.e12, 1997. ISSN 1365-1609. doi: https://doi.org/10.1016/S1365-1609(97)00227-X.

Olson, Jon E. Predicting fracture swarms-The influence of subcritical crack growth and the crack-tip process zone on joint spacing in rock. *Geological Society, London, Special Publications*, 231(1):73–88, 2004. ISSN 0305-8719.

Ouchterlony, Finn. Review of fracture toughness testing of rock. *SM archives*, 7: 131–211, 1982.

Page, M. J., Trustrum, N. A. and DeRose, R. C. A high resolution record of storm-induced erosion from lake sediments, New Zealand. *Journal of paleolimnology*, 11: 333–348, 1994.

Paris, P. C. and Erdogan, Fazil. A critical analysis of crack propagation laws. *J. Basic Eng.*, 1963. ISSN 0021-9223.

Pawlik, Łukasz, Phillips, Jonathan D. and Šamonil, Pavel. Roots, rock, and regolith: Biomechanical and biochemical weathering by trees and its impact on hillslope - A critical literature review. *Earth-Science Reviews*, 159:142–159, 2016. ISSN 0012-8252. doi: https://doi.org/10.1016/j.earscirev.2016.06.002.

Peel, M. C., Finlayson, B. L. and McMahon, T. A. Updated world map of the Köppen-Geiger climate classification. *Hydrol. Earth Syst. Sci.*, 11(5):1633–1644, October 2007.

Penman, Donald E., Caves Rugenstein, Jeremy K., Ibarra, Daniel E. and Winnick, Matthew J. Silicate weathering as a feedback and forcing in Earth's climate and carbon cycle. *Earth-Science Reviews*, 209:103298, 2020. ISSN 0012-8252. doi: https://doi.org/10.1016/j.earscirev.2020.103298.

Peter W. Birkeland. Use of Relative Age-Dating Methods in A Stratigraphic Study of Rock Glacier Deposits, Mt. Sopris, Colorado. *Arctic and Alpine Research*, 5(4): 401–416, 1973. doi: 10.1080/00040851.1973.12003748.

Phillips, Fred M. and Argento, David C. and Balco, Greg and Caffee, Marc W. and Clem, John and Dunai, Tibor J. and Finkel, Robert and Goehring, Brent and Gosse, John C. and Hudson, Adam M. and Jull, A. J. Timothy and Kelly, Meredith A. and Kurz, Mark and Lal, Devendra and Lifton, Nathaniel and Marrero, Shasta M. and Nishiizumi, Kunihiko and Reedy, Robert C. and Schaefer, Joerg and Stone, John O. H. The CRONUS-Earth Project: A synthesis. *Quaternary Geochronology*, 31:119–154, 2016. ISSN 1871-1014. doi: 10.1016/j.quageo.2015.09.006.

Phillips, Jonathan D. Weathering instability and landscape evolution. *Geomorphology*, 67(1-2):255–272, 2005.

Prasad, Amit Kumar, Poolton, Nigel R. J., Kook, Myungho, Jain, Mayank. Optical dating in a new light: A direct, non-destructive probe of trapped electrons. *Scientific Reports*, 7(1):12097, 2017.

PRISM Climate Group, Oregon State University. `https://prism.oregonstate.edu`, 2024. Map created 2023-12-12.

Ravaji, Babak, Alí-Lagoa, Víctor, Delbo, Marco and Wilkerson, Justin W. Unraveling the Mechanics of Thermal Stress Weathering: Rate-Effects, Size-Effects, and Scaling Laws. *Journal of Geophysical Research: Planets*, 124(12):3304–3328, 2019. ISSN 2169-9097. doi: https://doi.org/10.1029/2019JE006019.

Reheis, Marith C., Adams, Kenneth D., Oviatt, Charles G. and Bacon, Steven N. Pluvial lakes in the Great Basin of the western United States—a view from the outcrop. *Quaternary Science Reviews*, 97:33–57, 2014. ISSN 0277-3791. doi: https://doi.org/10.1016/j.quascirev.2014.04.012.

Riber, L., Le Pera, E., Conforti, M., Ietto, F., Dypvik, H. and others. The formation of grus from granites, Sila Mountains, Calabria, Italy. In *34th Nordic Geological Winter Meeting 2020*, 2020.

Riebe, Clifford S., Callahan, Russell P., Granke, Sarah B. M., Carr, Bradley J., Hayes, Jorden L., Schell, Marlie S. and Sklar, Leonard S. Anisovolumetric weathering in granitic saprolite controlled by climate and erosion rate. *Geology*, 2021. ISSN 0091-7613. doi: 10.1130/G48191.1.

Riebe, Clifford S., Kirchner, James W. and Finkel, Robert C. Long-term rates of chemical weathering and physical erosion from cosmogenic nuclides and geochemical mass balance. *Geochimica et Cosmochimica Acta*, 67(22):4411–4427, 2003. ISSN 0016-7037. doi: https://doi.org/10.1016/S0016-7037(03)00382-X.

Riebe, Clifford S., Kirchner, James W. and Finkel, Robert C. Erosional and climatic effects on long-term chemical weathering rates in granitic landscapes spanning diverse climate regimes. *Earth and Planetary Science Letters*, 224(3):547–562, 2004. ISSN 0012-821X. doi: https://doi.org/10.1016/j.epsl.2004.05.019.

Ronald I. Dorn and Theodore M. Oberlander. Rock varnish. *Progress in Physical Geography: Earth and Environment*, 6(3):317–367, 1982. doi: 10.1177/030913338200600301.

Rood, Dylan H., Burbank, Douglas W. and Finkel, Robert C. Chronology of glaciations in the Sierra Nevada, California, from 10Be surface exposure dating. *Quaternary Science Reviews*, 30(5):646–661, 2011. ISSN 0277-3791. doi: https://doi.org/10.1016/j.quascirev.2010.12.001.

Sadler, Peter M. and Jerolmack, Douglas J. Scaling laws for aggradation, denudation and progradation rates: the case for time-scale invariance at sediment sources and sinks. *Geological Society, London, Special Publications*, 404(1):69–88, 2015.

SAS Institute Inc. JMP. JMP® Version 16.1.0, 1989-2023.

Sato, Masato and Hattanji, Tsuyoshi. A laboratory experiment on salt weathering by humidity change: salt damage induced by deliquescence and hydration. *Progress in Earth and Planetary Science*, 5(1):84, 2018. ISSN 2197-4284. doi: 10.1186/s40645-018-0241-2.

Saunders, M. K. and Fookes, P. G. A review of the relationship of rock weathering and climate and its significance to foundation engineering. *Engineering Geology*, 4(4): 289–325, 1970. ISSN 0013-7952. doi: https://doi.org/10.1016/0013-7952(70)90021-9.

Scarciglia, Fabio, Saporito, Natalina, La Russa, Mauro F., Le Pera, Emilia, Macchione, Maria, Puntillo, Domenico, Crisci, Gino M. and Pezzino, Antonino. Role of lichens in weathering of granodiorite in the Sila uplands (Calabria, southern Italy). *Sedimentary Geology*, 280:119–134, 2012. ISSN 0037-0738.

Scherer, George W. *Internal stress and cracking in stone and masonry*, pages 633–641. Springer, 2006.

Schijve, Jaap. Fatigue of structures and materials in the 20th century and the state of the art. *International Journal of fatigue*, 25(8):679–702, 2003.

Shaanan, Uri, Mushkin, Amit, Rasmussen, Monica, Sagy, Amir, Meredith, Philip, Nara, Yoshitaka, Keanini, Russell and Eppes, Martha-Cary. Progressive fracturing in alluvial clasts. *GSA Bulletin*, 07 2023. ISSN 0016-7606. doi: 10.1130/B36670.1.

Shi, Jian. *Study of thermal stresses in rocks due to diurnal solar exposure*. PhD thesis, University of Washington, 2011.

Shobe, Charles M., Hancock, Gregory S., Eppes, Martha C. and Small, Eric E. Field evidence for the influence of weathering on rock erodibility and channel form in

bedrock rivers. *Earth Surface Processes and Landforms*, 42(13):1997–2012, 2017. ISSN 0197-9337.

Simon H. Brocklehurst and Kelin X. Whipple. Glacial erosion and relief production in the Eastern Sierra Nevada, California. *Geomorphology*, 42(1):1–24, 2002. ISSN 0169-555X. doi: https://doi.org/10.1016/S0169-555X(01)00069-1.

Sklar, Leonard S., Riebe, Clifford S., Marshall, Jill A., Genetti, Jennifer, Leclere, Shirin, Lukens, Claire L. and Merces, Viviane. The problem of predicting the size distribution of sediment supplied by hillslopes to rivers. *Geomorphology*, 277:31–49, 2017. ISSN 0169-555X. doi: https://doi.org/10.1016/j.geomorph.2016.05.005.

Song, J. F., Ru, J. X., Liu, X. P. and Cui, X. Y. Oxalic Acid and Succinic Acid Mediate the Weathering Process of Granite in the Cold-Temperate Forest Regions of Northeast China. *Eurasian Soil Science*, 52(8):903–915, 2019. ISSN 1556-195X.

Sousa, Luís M. O. The influence of the characteristics of quartz and mineral deterioration on the strength of granitic dimensional stones. *Environmental earth sciences*, 69(4):1333–1346, 2013. ISSN 1866-6280.

Sousa, Luís, Siegesmund, Siegfried and Wedekind, Wanja. Salt weathering in granitoids: an overview on the controlling factors. *Environmental Earth Sciences*, 77 (13):502, 2018. ISSN 1866-6299. doi: 10.1007/s12665-018-7669-y.

St. Clair, J., Moon, S., Holbrook, W. S., Perron, J. T., Riebe, C. S., Martel, S. J., Carr, B., Harman, C., Singha, K. and Richter, D. deB. Geophysical imaging reveals topographic stress control of bedrock weathering. *Science*, 350(6260):534–538, 2015. doi: 10.1126/science.aab2210.

Stephen G. Smith, Karl W. Wegmann, Elana L. Leithold and Delwayne R. Bohnenstiehl. A 4000-year record of hydrologic variability from the Olympic

Mountains, Washington, USA. *The Holocene*, 29(8):1273–1291, 2019. doi: 10.1177/0959683619846975.

Stock, Greg M., Anderson, Robert S. and Finkel, Robert C. Rates of erosion and topographic evolution of the Sierra Nevada, California, inferred from cosmogenic 26Al and 10Be concentrations. *Earth Surface Processes and Landforms: The Journal of the British Geomorphological Research Group*, 30(8):985–1006, 2005.

Stock, Greg M., Collins, Brian D., Santaniello, David J., Zimmer, Valerie L., Wieczorek, Gerald F. and Snyder, James B. *Historical Rock Falls in Yosemite National Park, California (1857-2011)*. US Department of the Interior, US Geological Survey Menlo Park, CA, USA, 2013.

Stone, Paul, Dunne, George C., Moore, James G. and Smith, George I. *Geologic Map of the Lone Pine 15'Quadrangle, Inyo County, California*. The Survey, 2000. ISBN 060795258X.

Stone, Paul, Miller, David M., Stevens, Calvin H., Rosario, Jose, Vazquez, Jorge A., Wan, Elmira, Priest, Susan S. and Valin, Zenon C. Geologic Map of the Providence Mountains in Parts of the Fountain Peak and Adjacent 7.5' Quadrangles, San Bernardino County, California. Report 2329-132X, US Geological Survey, 2017.

Sumner, P. D., Nel, W. and Hedding, D. W. Thermal attributes of rock weathering: zonal or azonal? A comparison of rock temperatures in different environments. *Polar Geography*, 28(2):79–92, 2004.

Terzaghi, Karl. *Theoretical soil mechanics*. 1943.

Tesson, P. A., Conway, S. J., Mangold, N., Ciazela, J., Lewis, S. R. and Mège, D. Evidence for thermal-stress-induced rockfalls on Mars impact crater slopes. *Icarus*, 342: 113503, 2020. ISSN 0019-1035. doi: https://doi.org/10.1016/j.icarus.2019.113503.

Thomachot, Céline and Jeannette, Daniel. Effects of iron black varnish on petrophysical properties of building sandstone. *Environmental Geology*, 47(1):119–131, 2004.

Tsytovich, Nikolai Aleksandrovich. The mechanics of frozen ground. 1975.

Turowski, J. M., Pruß, G., Voigtländer, A., Ludwig, A., Landgraf, A., Kober, F. and Bonnelye, A. Geotechnical controls on erodibility in fluvial impact erosion. *Earth Surface Dynamics*, 11(5):979–994, 2023. doi: 10.5194/esurf-11-979-2023.

Ündül, Ömer and Tuğrul, Atiye. The Influence of Weathering on the Engineering Properties of Dunites. *Rock Mechanics and Rock Engineering*, 45(2):225–239, 2011. ISSN 0723-2632 1434-453X. doi: 10.1007/s00603-011-0174-1.

Vasile, Mirela and Vespremeanu-Stroe, Alfred. Thermal weathering of granite spheroidal boulders in a dry-temperate climate, Northern Dobrogea, Romania. *Earth Surface Processes and Landforms*, 42(2):259–271, 2017. ISSN 0197-9337. doi: https://doi.org/10.1002/esp.3984.

Vázquez, Patricia, Shushakova, Victoria and Gómez-Heras, Miguel. Influence of mineralogy on granite decay induced by temperature increase: Experimental observations and stress simulation. *Engineering Geology*, 189:58–67, 2015. ISSN 0013-7952. doi: https://doi.org/10.1016/j.enggeo.2015.01.026.

Viles, Heather A. Can stone decay be chaotic? In *Stone Decay in the Architectural Environment*. Geological Society of America, 01 2005. ISBN 9780813723907. doi: 10.1130/0-8137-2390-6.11.

Viles, Heather, Messenzehl, Karoline, Mayaud, Jerome, Coombes, Martin and Bourke, Mary. Stress histories control rock-breakdown trajectories in arid environments. *Geology*, 46(5):419–422, 2018. ISSN 0091-7613. doi: 10.1130/G39637.1.

von Blanckenburg, Friedhelm, Belshaw, N. S. and O'Nions, R.K. Separation of 9Be and cosmogenic 10Be from environmental materials and SIMS isotope dilution analysis. *Chemical Geology*, 129(1-2):93–99, 1996.

Vosteen, Hans-Dieter and Schellschmidt, Rüdiger. Influence of temperature on thermal conductivity, thermal capacity and thermal diffusivity for different types of rock. *Physics and Chemistry of the Earth, Parts A/B/C*, 28(9):499–509, 2003. ISSN 1474-7065. doi: https://doi.org/10.1016/S1474-7065(03)00069-X.

Walder, Joseph and Hallet, Bernard. A theoretical model of the fracture of rock during freezing. *GSA Bulletin*, 96(3):336–346, 1985. ISSN 0016-7606. doi: 10.1130/0016-7606(1985)96<336:ATMOTF>2.0.CO;2.

Wang, Juntao, Kreslavsky, Mikhail A., Liu, Jianzhong, Head, James W., Zhang, Ke, Kolenkina, Maria M. and Zhang, Li. Quantitative Characterization of Impact Crater Materials on the Moon: Changes in Topographic Roughness and Thermophysical Properties With Age. *Journal of Geophysical Research: Planets*, 125(10):e2019JE006091, 2020. ISSN 2169-9097. doi: https://doi.org/10.1029/2019JE006091.

Wang, Yang, McDonald, Eric, Amundson, Ronald, McFadden, Leslie and Chadwick, Oliver. An isotopic study of soils in chronological sequences of alluvial deposits, Providence Mountains, California. *GSA Bulletin*, 108(4):379–391, 1996. ISSN 0016-7606. doi: 10.1130/0016-7606(1996)108<0379:AISOSI>2.3.CO;2.

Warke, P. A. Complex weathering in drylands: Implications of 'stress' history for rock debris breakdown and sediment release. *Geomorphology*, 85(1):30–48, 2007. ISSN 0169-555X. doi: https://doi.org/10.1016/j.geomorph.2006.03.038.

Watanabe, Masaru, Saito, Masashi, Toda, Kenichiro and Shirasawa, Hiroaki. Rain-

Driven Failure Risk on Forest Roads around Catchment Landforms in Mountainous Areas of Japan. *Forests*, 14(3):537, 2023.

Western Regional Climate Center: WRCC. Oak Creek California. `https://raws.dri.edu/cgi-bin/rawMAIN.pl?caCOCR`, 2023. Accessed 2023-03-01.

Westoby, Matthew, Lim, Michael, Hogg, Michelle, Dunlop, Lesley, Pound, Matthew, Strzelecki, Mateusz and Woodward, John. Decoding Complex Erosion Responses for the Mitigation of Coastal Rockfall Hazards Using Repeat Terrestrial LiDAR. *Remote Sensing*, 12(16), 2020. ISSN 2072-4292. doi: 10.3390/rs12162620.

Wolman, M. Gordon. A method of sampling coarse riverbed material. *Eos, Transactions American Geophysical Union*, 35(6):951–956, 1954. ISSN 0002-8606. doi: 10.1029/TR035i006p00951.

Yellen, Brian, Woodruff, Jonathan D., Cook, Timothy L., Newton, Robert M. Historically unprecedented erosion from Tropical Storm Irene due to high antecedent precipitation. *Earth Surface Processes and Landforms*, 41(5):677–684, 2016.

Yin, Weitao, Feng, Zijun and Zhao, Yangsheng. Effect of grain size on the mechanical behaviour of granite under high temperature and triaxial stresses. *Rock Mechanics and Rock Engineering*, 54:745–758, 2021.

Young, Adam P., Guza, R. T., Flick, R. E., O'Reilly, W. C. and Gutierrez, R. Rain, waves, and short-term evolution of composite seacliffs in southern California. *Marine Geology*, 267(1-2):1–7, 2009.

Young, Holly H. and Hilley, George E. Millennial-scale denudation rates of the Santa Lucia Mountains, California: Implications for landscape evolution in steep, high-relief, coastal mountain ranges. *GSA Bulletin*, 130(11-12):1809–1824, 2018. ISSN 0016-7606. doi: 10.1130/B31907.1.

Yu, Miao, Wei, Chenhui, Niu, Leilei, Li, Shaohua and Yu, Yongjun. Calculation for tensile strength and fracture toughness of granite with three kinds of grain sizes using three-point-bending test. *PLOS ONE*, 13(3):e0180880, 2018. doi: 10.1371/journal.pone.0180880.

Yu, Qinglei, Zhu, Wancheng, Ranjith, PG and Shao, Shishi. Numerical simulation and interpretation of the grain size effect on rock strength. *Geomechanics and Geophysics for Geo-energy and Geo-resources*, 4:157–173, 2018.

Zhang, Bin and Guo, Wanlin. Three-dimensional stress state around quarter-elliptical corner cracks in elastic plates subjected to uniform tension loading. *Engineering Fracture Mechanics*, 74(3):386–398, 2007. ISSN 0013-7944. doi: https://doi.org/10.1016/j.engfracmech.2006.05.011. URL `https://www.sciencedirect.com/science/article/pii/S0013794406001895`.

Zingg, Theodor. *Beitrag zur schotteranalyse*. Thesis, 1935.

APPENDIX A: ^{10}BE METHODS

We calculated the surface age of the Lundy Canyon terrace deposit, previously undated. Geomorphically, this fluvial terrace is inset into the Tioga Outwash surface [dated ∼18 ka], and the modern Mill Creek is inset into the terrace by 1-3 meters. We collected the ∼30 cm diameter LC-HT1-RT-1 boulder from the surface of a flat, central portion of the terrace at WGS84 38.0315033, -119.1747511 at an altitude of 2186 m. We recorded the surrounding mountain heights using a Brunton compass before moving the boulder, to calculate topographic shielding when inputting the ^{10}Be data into the Washington CRONUS Calculator version 3 [Balco, Greg, Stone, John O., Lifton, Nathaniel A. and Dunai, Tibor J., 2008, http://hess.ess.washington.edu/math/].

The northern half of the top ∼3 cm of the boulder was removed for sampling [Fig. A.1]. Dr. Alan Hidy performed ^{10}Be dating by crushing, dry sieving, and manually removing the non-quartz minerals. The sample was chemically treated following Kohl, C. P. and Nishiizumi, Kunihiko [1992] to obtain the pure quartz, then beryllium was isolated following von Blanckenburg, Friedhelm, Belshaw, N. S. and O'Nions, R.K. [1996]. The ^{10}Be/^{9}Be ratios in the samples were measured by accelerator mass spectrometry, ion ratios were determined using an ICN revised ^{10}Be standard [07KNSTD, Nishiizumi et al., 2007], and the data were processed in the Washington CRONUS Calculator version 3 [Balco, Greg, Stone, John O., Lifton, Nathaniel A. and Dunai, Tibor J., 2008, http://hess.ess.washington.edu/math/]. Variables that were input into the calculator are available in Supplement SA1.

A.1 Figures

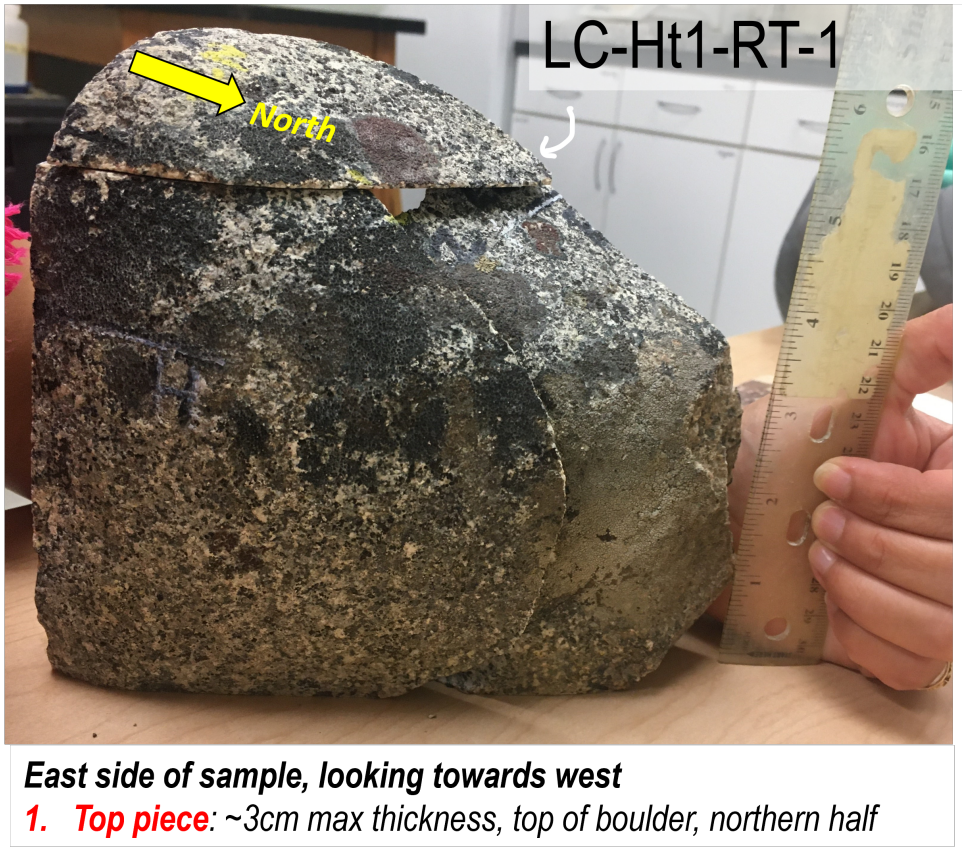

Figure A.1: The upper ∼3 cm of the northern half of the LC-Ht1-RT1 boulder was processed for ^{10}Be dating.